TRIPHENYL ETHER AND TRIPHENYL AMINE AS CHEMICAL SENSORS FOR TRANSITION METAL IONS USING ELECTROCHEMICAL AND SPECTROSCOPIC TECHNIQUES

A

Thesis submitted in

fulfillment of the requirement for the degree of

Doctor of Philosophy

Submitted by

Shivali Gupta

(901609013)

Under the supervision

of

Dr. Susheel Mittal CChem FRSC
Senior Professor

Dr. Manmohan Chhibber
Professor

School of Chemistry and Biochemistry

Thapar Institute of Engineering and Technology

Patiala-147004, India

August, 2021

Certificate

Certified that the thesis entitled "**TRIPHENYL ETHER AND TRIPHENYL AMINE AS CHEMICAL SENSORS FOR TRANSITION METAL IONS USING ELECTROCHEMICAL AND SPECTROSCOPIC TECHNIQUES**" which is submitted by Ms. Shivali Gupta in partial fulfillment of the requirements for the award of the Degree in philosophy in the School of Chemistry and Biochemistry, Thapar Institute of Engineering and Technology, Patiala is a record of candidate's original and independent research work carried out by her under our supervision and guidance. The material embodied in this thesis has not been submitted in part or full to any other university or institute for the award of any degree in India and abroad.

(Supervisors)

Susheel Mittal

Dr. Susheel Mittal CChem FRSC

Senior Professor

School of Chemistry and Biochemistry

Thapar Institute of Engineering and Technology, Patiala-147004

Dr. Manmohan Chhibber

Professor

School of Chemistry and Biochemistry

Thapar Institute of Engineering and Technology, Patiala-147004

(Head)

Dr. Satnam Singh

Head & Professor

School of Chemistry and Biochemistry

Thapar Institute of Engineering and Technology, Patiala-147004

Candidate's Declaration

I, hereby declare that the work presented in the thesis entitled "**TRIPHENYL ETHER AND TRIPHENYL AMINE AS CHEMICAL SENSORS FOR TRANSITION METAL IONS USING ELECTROCHEMICAL AND SPECTROSCOPIC TECHNIQUES**" in partial fulfillment of the requirements for the award of the degree of Doctor of Philosophy at School of Chemistry and Biochemistry, Thapar Institute of Engineering and Technology, Patiala, is an authentic record of my own work carried out under the joint supervision of Dr. Susheel Mittal, Senior Professor, and Dr. Manmohan Chhibber, Professor, School of Chemistry and Biochemistry, Thapar Institute of Engineering and Technology, Patiala, India. The matter embodied in this thesis has not been submitted in part or full to any other university and institute for the award of any degree in India or abroad.

Shivali Gupta.

Shivali Gupta
(901609013)

Acknowledgments

To God the father of all, I am thankful for the strength that keeps me standing and for the hope that keeps me believing. He helped me to reach the position that I could thank those that walked beside me and helped along the way. Undertaking this PhD has been a truly life-changing experience for me and the work presented in this would not have been possible without any close association with many people. I take this opportunity to thanks all those who have helped make my life what it is today.

My earnest gratitude to my Supervisors Dr. Susheel Mittal CChem FRSC, Senior Professor, and Dr. Manmohan Chhibber, Professor, School of Chemistry and Biochemistry, Thapar Institute of Engineering and Technology, Patiala for guiding me through this journey. During our course of interaction, I have learned extensively from them, including how to be brave at difficult times, be optimistic in every situation, how to approach a problem by systematic thinking and exploiting serendipity. It is through their constant guidance, expertise, and fruitful advice, cooperation, and support that I gained and grown.

I express my gratitude to the Director, Thapar Institute of Engineering and Technology, Patiala. I extend my thanks to my doctoral committee members Dr. Satnam Singh, Dr. Soumen Basu, and Dr. Puneet Sharma for their fruitful discussion and endless encouragement, constructive criticism, and inspiration.

I am highly thankful to all the faculty members of School of Chemistry and Biochemistry, for providing necessary guidance during my research work. I am thankful to Mr. Chandar Thakur, Mr. Hemant, Mr. Mayank, and other non-teaching staff of the department for the constant official help and cooperation.

I owe a debt of gratitude and heartfelt thanks to my seniors Dr. Manisha, Dr. Sonia Rana, Dr. Sanjeev Kumar, Dr. Iqbal Singh, Dr. Gulshan Kumar. This journey would not have been smooth without my companions Parmandeep Kaur, Vanshita, Pawan, Fatima Bhadra, Sonam Rani, Nisha Malik, Ruhi Mehta, Gagan, Ashok Kumar, Adil Bathala, and other lab mates. They all have been with me in my ups and downs. I am thankful to them for their kind concern, critical observations in designing and planning experiments, and above all their support, which always helped me endure hard times and to accomplish all my goals.

The help from different institutes and laboratories like SAI lab, Thapar Institute of Engineering and Technology, SAIF lab, Punjab University, Chandigarh, IIT, Roorkee.

I find no rhetorical gems from the ocean of words to express my heartfelt gratitude to my Father, Sh. Sanjeev Kumar, Mother, Sunita Rani, who instead of their serious concerns supported me for the higher education, with spring of inspiration and sacrifice since I saw the light on this earth. Both of them not only been a fathomless ocean of knowledge and wisdom to me most of all, their love, intellectual answers, words of care, and hands of blessing influenced and enriched me a lot. Words fail to express my gratitude from the depth of my heart for my loving brother Sachin, Gupta, Raghav Garg, loving sister Anu Kansal, Neha Garg and Sister-in-law, Rishu Gupta, and all my family members who provided me relentless encouragement, prayers, pure love, and unmatched affection that made this work to reach its destination.

A huge token of love and thanks to my little bundle of joy Shanaya Gupta and Arnika for giving me unconditional love and making me realize that there is life beyond work.

Shivali Gupta

List of content

Abstract

This doctoral thesis provides an insight into the synthesis, characterization, and development of triphenyl derivatives for the colorimetric and voltammetric sensing of metal ions and anions. Synthesized molecules were characterized by NMR, mass, and FT-IR spectroscopy. They were studied for their analytical applications as chemical sensors as well as for their biological applications. Naked eye detection of probes has modified their practical application. Experimental results were also compared with results obtained from theoretical calculations using DFT software. Furthermore, detection of amino acids, antibacterial activity, and preparation of molecular logic gate were some of the useful applications of our work.

A triphenyl ether derivative having amine linkage (TPEA), 1,1'-((((1,3-phenylene bis (oxy)) bis(2,1-phenylene))bis(azanediyl))bis(methylene))bis(naphthalene-2-ol), was synthesized as a customized receptor for cyanide ions. In the presence of a variety of competitive anions such as HSO_4^-, $H_2PO_4^-$, ClO_4^-, OAc^-, and halides, TPEA was selective for CN^- ions. With a detection limit of 0.4 μM and a binding constant of $4.16x10^7$ M^{-1}, the proposed receptor reacts linearly to CN^- ions up to a concentration of 400 μM. The colorimetric response of TPEA towards CN^- ions was confirmed by voltammetric technique. TPEA has also been tested as a water-detection probe in acetonitrile. For practical application, paper strips were prepared for naked-eye detection of CN^-.

A triphenyl ether amide (TPEAM) derivative, N,N'-((1,3-phenylene bis(oxy))bis(2,1-phenylene))bis(2-hydroxy-1-naphthamide), was developed as a probe for electrochemical and optical sensing of copper, cyanide ions and arginine. Among various cations and anions, the ionophore is selective for copper and cyanide ions, with detection limits of 40 nM and 0.4 μM, respectively. Sharp anodic and cathodic peaks in the differential pulse voltammograms of TPEAM-Cu(II) complex suggested a strong ligand ion complexing tendency, which was verified by spectrofluorimetry and ^1H NMR titrations. TPEAM-Cu(II) complex also detected arginine, a semi-essential amino acid, in an aqueous medium with a lower detection limit of 4 μM. As potential mechanisms for sensing respective ions, host-guest interactions between TPEAM and Cu(II) ions and intramolecular charge transfer interactions (ICT) for CN^- ions have been suggested. The use of TPEAM as a Cu(II) ion probe has also been validated on food samples, with the findings compared to those obtained using atomic absorption

spectroscopy. Following the response of TPEAM towards Cu(II) and CN^- ions, the molecular logic gate was designed with truth table values.

A diimine benzene and naphthaldehyde based molecular architecture (PDI) was synthesized, namely, 1,1'-((1E,1'E)-(1,2-phenylene bis(azanylylidene))bis(methanylylidene)) bis (naphthalene-2-ol), and its sensing behavior was found selective for Al^{+3} ions with a detection limit of $6.7x10^{-7}$ M. The binding event was signaled by the probe forming an absorption band at 406 nm and a new emission band at 504 nm. The mechanism is thought to be the chelation-induced enhanced fluorescence (CHEF) effect and limiting PET phenomena. Electrochemical tests of the probe for Al(III) ions backed up the photophysical results. Probe detected CN^- and F^- ions selectively using a new absorption band at 412 nm and a "turn-on" fluorescence band at 460 nm, with a detection limit of $1x10^{-7}$ M. ^1H NMR titrations confirmed the mechanism of anion detection. The experimental results were confirmed using DFT calculations. The presence of water as an impurity in acetonitrile was observed to the degree of 0.4 percent using the PDI-Al(III) complex as a sensor. PDI and its aluminium complex were also tested for antibacterial activity against non-pathogenic *E. coli*. The successful antibacterial activity of Probe and its aluminium complex was confirmed by fluorescence imaging and SEM analysis.

Chapter 1

Introduction

Sensor applications can be identified as an unavoidable part of daily living and the surroundings. Any chemical or physical property of any item or process can be detected and measured with a sensor. Even a smartphone has a slew of sensors that track the apparatus's location, the user's appearance, the intensity of the environment, and a variety of other parameters. Sensors function similarly to sense organs in the body. In reality, the word sensor comes from the Latin word *sentire*[1], which means "to feel." A sensor may detect and transform measurable physical and chemical quantities into electrical signals that an observer can evaluate. A chemical sensor can be linked to an artificial tongue or ear since it can provide chemical information about the environment. As a result, chemical sensors have become an integral feature of analytical chemistry teaching in recent decades. Chemosensor research is significant not only for chemistry students, but also for researchers in other subjects such as engineering science, medicine, biology, and other disciplines.

1.1 Chemical Sensors

According to IUPAC definition "a chemical sensor is a device that transforms chemical information like composition, presence of particular element or ion, concentration or chemical activity into an analytically useful signal". The information obtained from the chemical sensor may have come from the analyte's chemical reaction or changes in its physical properties such as length, weight, pressure, electricity, etc.[2] This chemical reaction between the analyte and the target species (metal ion, anion, and biological species) established a new age in chemical sensing. After sensing the presence of energy or matter, a chemical sensor contains ionophore derived from abiotic components, which brighten the signal. In reality, a sensor should be in direct contact with the object under inquiry, respond frequently, convert non-electric data into an electric signal, and respond quickly.[3, 4]

Chemical sensors are made up of two parts- the receptor and a transducer. These two components form the chemical sensor's foundation and are linked in sequence. The receptor interacts with the analyte and causes a physical or chemical transition, which is reported by an integrated transducer that generates the output signal in the majority of chemical sensors

(Fig. 1).[5] The receptor component transfers chemical information to the transducer in the form of energy, which is then converted into an analytical signal.

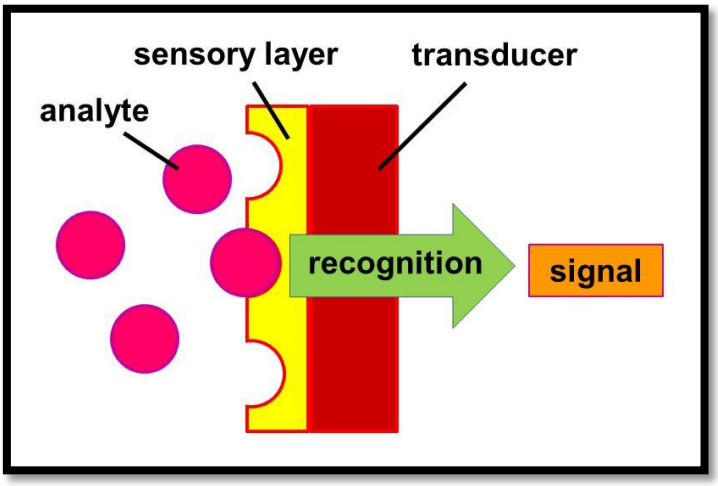

Fig. 1 Schematic presentation of chemical sensor

Various methods, such as UV-VIS spectroscopy, fluorescence spectroscopy, voltammetry, and potentiometry, are used to record these analytical signals.[6-10] When it comes to chemical sensors, several important factors play a role in making the job worthwhile. Selectivity, precision, solution nature, response time, working life span, and sensitivity are all important factors in designing a sensor. A sensor's selectivity is its ability to differentiate between various substances. The results within acceptable limit define accuracy which should be greater than 5%. The temperature, pH, and ionic strength of a solution determine the nature of the solution. In real-time applications, response time and life span are critical parameters that define the stability of the selective material.[11-16]

Sensors have been categorized into different groups based on the application of analytes. Following three classes have been discussed in the section below.

(1) Optical Sensors
(2) Electrochemical Sensors
(3) Biosensors

An **optical sensor** transforms light rays into an electronic signal that can be analyzed. Both internal and external optical sensors are available. The physical quantity of light is measured using an optical sensor and then transformed into a signal that can be read by an integrated

measuring system (Fig. 2). Chemical and biological molecules interact with the target species to generate the data that interprets concentration, mass, and temperature.[17-19]

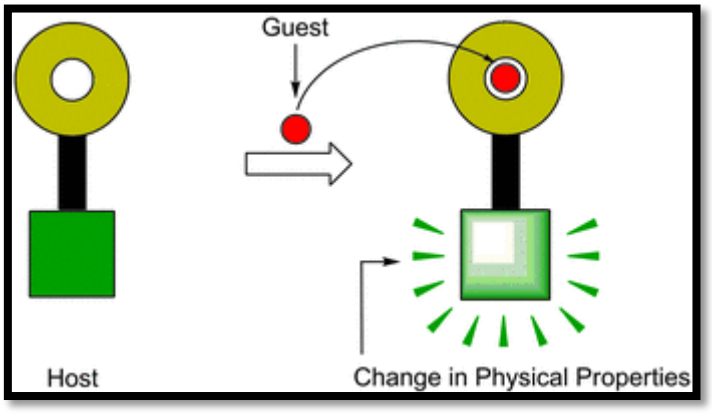

Fig. 2 Schematic presentation of optical sensor

Electrochemical sensors are also made up of the receptor and the transducer. The receptor unit in these sensors transforms chemical data into an analytical signal, which can then be interpreted by the transducer (Fig. 3). An electrochemical sensor is a small device that measures concentration, chemical composition, reaction speed, and other physical properties of an analyte.[20, 21]

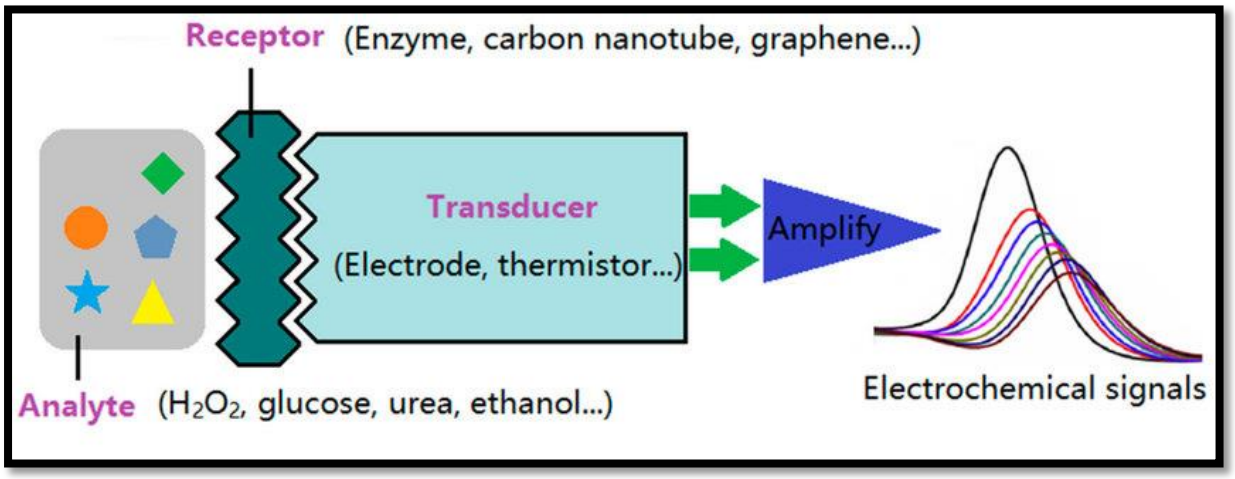

Fig. 3 Schematic presentation of electrochemical sensor

The analyte of interest in a **biosensor** is a biological species such as tissue, antibodies, enzymes, or nucleic acid (Fig. 4). Biosensors assist us in determining analyte biological parameters such as time, concentration, and pH effect.[22, 23]

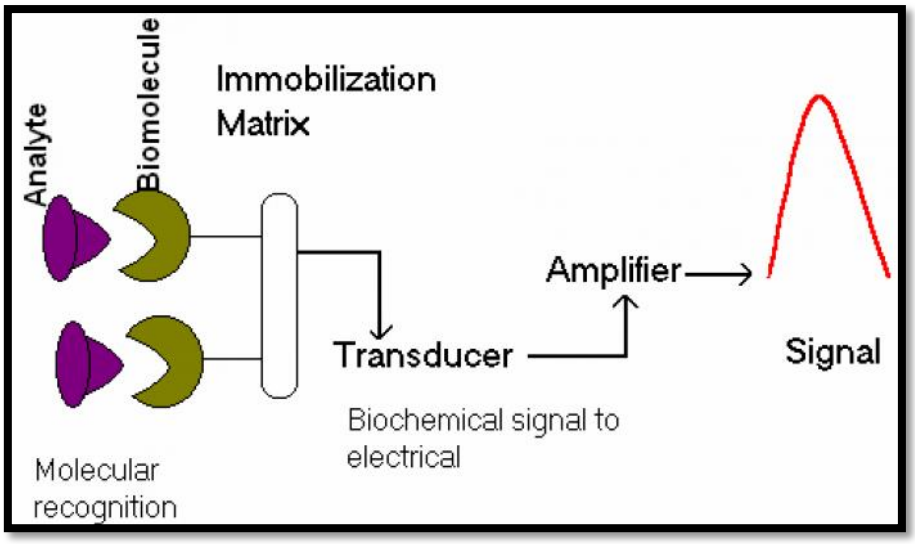

Fig. 4 Schematic presentation of biosensor

1.2 Methods of chemical sensing

For successful chemical sensing, the availability of various instruments and techniques has made it possible to design sensors that rely on the concept of physical, biological, and chemical changes. Chemical sensing is often divided into two groups, as follows:

(i) Receptor unit

(ii) Transducer unit

1.2.1 Classification of chemical sensors based on recognition unit

The main component of a sensor is the receptor unit/ recognition feature, which imparts selectivity so that the sensor can respond to a specific analyte without interference from other species. Various types of interactions between the receptor unit and analytes have been documented in the literature, including non-covalent bonds, electrostatic interactions, hard-soft acid-base interactions, and so on.[24-26] Receptors are organic building blocks that can bind several analytes, including cations, anions, and neutral molecules. In the solution process, receptor molecules arrange themselves to create a cavity wide enough to accommodate an analyte. Some analytes, such as sodium, calcium, potassium, and magnesium, are biologically essential. In terms of biologically important analytes, various kinds of metal cations such as Cu(II), Mn(II), Zn(II), and others play an important role in the proper functioning of metalloenzymes and proteins.[27] Apart from these, various toxic metals (Hg(II), Cd(II), Cr(VI)) must be detected by the receptor unit in addition to critical ions. As a result, the receptor unit must be able to detect or remove these metal ions selectively and easily. To fulfill these needs, different kinds of receptors are synthesized. Some of the important

receptor categories are Schiff base[28, 29], rhodamine derivatives[30, 31], benzocoumarin[32, 33], and quinolone[34, 35] derivatives that show specific behavior towards metal ions. Selectivity majorly depends on the structure of the receptor.

Complexation of the receptors with target species is caused by a variety of factors such as chirality, form, geometry, and size of the ion.[36] Besides these factors, the coordination sphere is ideal for ion detection due to the proper arrangement of the donor atoms and their flexibility. The solvent medium and its polarity play an important role in imparting stability to the formed complex.[37] Considering all these factors, Crown ethers, spherands, cyptands, and podands are proved to be the most prominent receptors in coordination or host-guest chemistry (Fig. 5). These receptors have a stereoelectronic arrangement of binding sites that are complementary to the size of the target species. They are capable of detecting both cations and anions. Depending on the shape of ionophore, they may be categorized into cyclic, acyclic, hemispherical, and ring-shaped ionophores.[38, 39]

Crown ethers are polyethers that contain ethyleneoxy as repeating units, i.e. $–CH_2CH_2O$, as discovered by Pederson in 1967.[40] Since it has a proper arrangement of 12 carbons and 6 oxygen atoms, 18-crown 6 is a perfect example of the crown ether category.

Podands are acyclic open chained analogs of crown ethers. They are also known as multidentate organic ligands because they come in a wide range of chains from single chained to multi-armed ligands.[41] Because of their low stability constant, podands are called poor ligands. Their binding efficiency can be increased by adjusting their conformation to a more ordered state.

Crpytands are macro heterocycles that are three-dimensional bi- and polycyclic. They are made by replacing the oxygen atom with a nitrogen atom in the monocyclic crown ethers structure. They have excellent selective behavior against a specific target species due to the rigidity of the structure.[42]

Spherands are made up of six donor oxygen atoms arranged in an octahedral pattern. They have high binding energy and can form complexes with metal ions. Besides ether linkage, the -NH fragment in the receptor backbone is also essential. In supramolecular self-assembly, it induces intramolecular hydrogen bonding interactions.

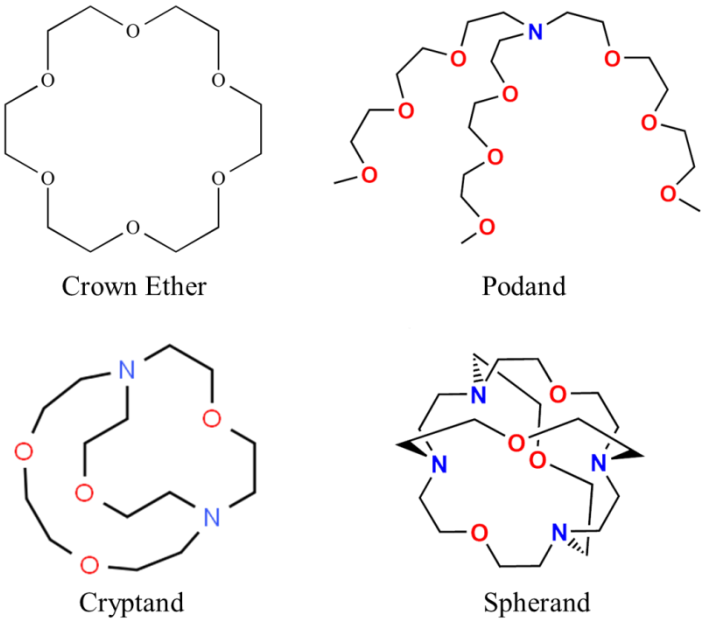

Fig. 5 Structure of aromatic receptors

1.2.2 Classification of chemical sensors based on transducer unit

The response signal produced by the interaction between receptor and metal ions is captured by a transducer device. Several devices are used to process signals such as potentiometric, voltammetric, thermal, and optical transducers. As a result, the productions of transducers that can detect physical, chemical, and biological signals are important. Transducers can be divided into the following categories based on their operating theory.

(1) Optical transducers: They are the instruments that turn the analyte-receptor interaction into an optical signal. More versatility and miniaturization are possible with these devices. They are further divided into subcategories based on the optical properties used in chemical sensors.

(a) Absorbance: It is calculated in a clear solution. It is triggered by the analyte's absorptivity or by its reaction with an indicator.

(b) Fluorescence: The analyte is irradiated with a suitable wavelength, which causes it. It is determined by the positive emission effect and, in some cases, fluorescence quenching, which is the foundation of such devices.

(c) Reflectance: It is normally tested in a non-transparent medium with an immobilized indicator.

(d) Light Scattering: These instruments are focused on the effects of particle size in the sample solution.

(e) Optothermal effect: It is based on a sample's absorption of light and then results in thermal effects.

(f) Refractive index: This allows for the measurement of changes in the solution's composition. Surface plasmon resonance effect may be one of them.

(g) Luminescence: It works by measuring the intensity of light released by a chemical reaction in the receptor system.

(2) Electrochemical transducers: These are used to convert an analyte's interaction with the target species into an electrochemical useful signal. Electrochemical transducers have been used in the development of most analytical sensors because they are inexpensive and easy to construct. Electrochemical techniques include the following subgroups:

(a) Potentiometric: At zero current, the emf or potential of a cell is determined. The emf that is measured is proportional to the substance's logarithmic concentration.[43]

(b) Voltammetric: Current is calculated by varying the potential with this tool. The potential is applied before the sample's oxidation/reduction is determined. The height of the current peak can be used to assess the analyte's concentration.[44]

(c) FET-based transducers: It is miniaturization of the said techniques on a field-effect transistor based on a silicon chip. It's often used in potentiometric sensors, but it won't work with voltammetric ones.[45]

(d) Conductometric: The changes in electrical conductivity of the solution are measured using this technique. Charges in electrical conductivity are caused by changes in the sample's composition.[45]

(3) Thermal sensor: When any chemical or biochemical process occurs, the change in heat (absorption/release) is registered. Sensitive thermistors are used for this, and the volume of analyte to be analyzed could be linked to them.

(4) Pizo-electric devices: This system is linked to surface acoustic waves. Electric current is produced by vibrating crystals in these devices. If mass of the material is adsorbed on the device's surface, the frequency of vibration changes, which is determined by the device.

Among all the above mentioned techniques, our work is mainly based on the optical and voltammetric techniques. Therefore, these techniques are discussed in details in next section.

1.3 Techniques used for chemical sensing

1.3.1 Spectrophotometry

Spectrophotometry is a technique for determining the quantitative composition of a chemical substance. It is used in chemistry, physics, clinical, materials, and chemical engineering, among other areas. It gives us quantitative information about how much a chemical material absorbs light by calculating the strength of light corresponding to the beam of light passing through the solution. The concentration of a known compound in a solution is determined by this calculation. Over a certain wavelength range, any compound exhibits absorbance and transmittance.

Single beam and double beam devices are the two main types of devices. A double beam spectrophotometer analyses the light intensity of two light channels, one of which contains a reference sample and the other of which contains a test sample. Before and after a test sample is introduced, a single-beam spectrophotometer detects the relative light intensity of the beam. Single-beam instruments can have a higher dynamic range and are optically simpler and more compact, even though comparison measurements from double-beam instruments are easier and more stable. Furthermore, due to practical reasons, some specialist instruments, such as spectrophotometers incorporated into microscopes or telescopes, are single-beam instruments.

1.3.2 Spectrofluorimetry

The spectrofluorimetry technique, which is a form of electromagnetic spectroscopy, is used to analyze the fluorescence of a sample. In this procedure, a sample containing solution is first excited from its ground state by absorbing a photon, and then de-excited by colliding with another molecule, returning to the ground state. The Jablonski diagram depicts the entire operation. The light source used in spectrofluorimetry is usually ultraviolet light, which is responsible for electron excitation and emission of visible light; however, this is not always the case.

The physics of fluorescence is complicated by the various electronic and vibrational states in which fluorophores might dwell. Multiple vibrational states can be found in an electrical state. Photons with energy in the ultraviolet to blue-green spectrum can cause an electronic transition from the ground state's lowest vibration to one of the vibrational levels of a higher electronic excited state. The fluorophore molecule relaxes into the lowest vibrational level of the excited electronic state as soon as the energy input from the photon (in other words,

excitation) stops. The fluorophore stays in this state for a short period (about 10 nanoseconds, or the fluorescence lifetime) before returning to the electronic ground state. Fluorescence emission is a release of energy linked with this return to the ground state.

1.3.3 Electroanalytical sensing

Different characteristics such as electric current, resistance, and potential are used to monitor the electric responses in analytical procedures. The electrochemical analysis is primarily divided into two categories.

Interfacial methods: They produce a signal in response to phenomena that occur at the electrode surface/solution contact. Essentially, it shows the presence of a secondary unit, such as analyte, at the electrode surface, either directly or indirectly. Based on current fluctuation, this method might be dynamic or static. The static interfacial approach is used to study events that occur when there is no electric current. The redox reaction is noticed in the dynamic approach due to the electron transfer process.

Non-interfacial approach: This method provides data on the properties of the entire solution. Conductometric measurement, for example, is a non-interfacial approach since it measures the concentration of the entire solution.

The electroanalytical determination of analyte using sensors can be accomplished using the interfacial dynamic approach. Importantly, depending on the regulated and measured parameters employed throughout the mode of operation, the interfacial approach can be related to coulometric, potentiometric, conductometric, and voltammetric determination. Current and potentiometry sensors, as well as potential measurement, are used in conductometric sensors. Current is measured as a function of voltage applied to the electrode surface in a voltammetric sensor. As a result, the voltammetric method is the most appropriate because current-potential characteristics reveal the analyte's redox behavior. Voltammetric determination is a highly selective, sensitive method that may also be used on the go. So, in our research, we primarily looked towards voltammetric sensors for ion sensing.

Voltammetry

Voltammetry is a technique for calculating current at the electrode surface at a constant or changing potential.[44] It is made up of a three-electrode setup. It entails the investigation of an analyte’s oxidation and reduction potential to determine its electrochemical activity. It offers

qualitative and quantitative information about the analyte in addition to redox activity. It aids in determining the number of electrons involved in each step, as well as mechanistic and kinetic parameters and the adsorption process on the electrode's surface.

The potential is changed freely, either step by step or continuously, with the current value as the dependent variable. Amperometry, on the other hand, is conceivable but uncommon. The curves' shape is determined by the rate of potential variation (the driving force) and whether the solution is agitated or not (mass transfer). Most studies measure the current produced by controlling the voltage (volts) of an electrode in contact with the analyte (amperes).

Electrochemical cell

It is a three-electrode device with working electrode, counter electrode, and reference electrode used in this setup (Fig. 6). The three electrodes are connected to an energy source that contains a potentiostat, which is a specially designed circuit.[46, 47]

The potential between the working electrode and the reference electrode is pulsed from an initial potential to an interlevel potential, where it stays for around 5 to 100 milliseconds before changing to a final potential that is distinct from the starting potential. The pulse is repeated, changing the end potential, and the initial and interlevel potentials are preserved at a constant difference. Before and after the pulse, the current between the working electrode and the auxiliary electrode is measured, and the differences are shown against potential.

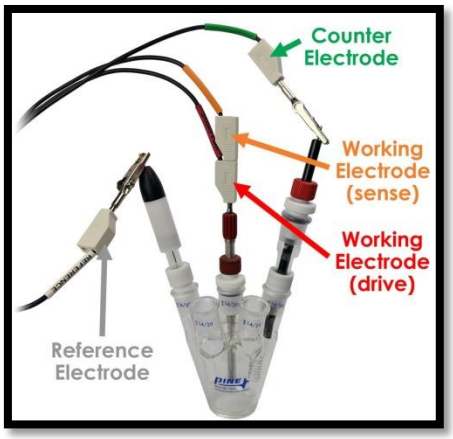

Fig. 6 Three electrode system

Working electrode

The working electrode in an electrochemical system is the electrode on which the reaction of interest is taking place. In a three-electrode system, the working electrode is frequently utilized in conjunction with an auxiliary electrode and a reference electrode. The working

electrode is classified as cathodic or anodic depending on whether the reaction on the electrode is a reduction or oxidation. Both organic and inorganic materials are analyzed using chemically modified electrodes.

It is a polarised electrode that conducts an electrochemical reaction. The reaction takes place at a constant potential concerning the reference electrode. The working electrode is made of redox-inert material and should be kept as clean as possible. Inert metals such as gold, silver, or platinum, inert carbons such as glassy carbon, boron-doped diamond, or pyrolytic carbon, and mercury drop and film electrodes are all common working electrodes. Mechanical polishing with alumina slurry is a common method for cleaning platinum and gold electrode surfaces.[48, 49]

Reference electrode

The potential of the reference electrode remains constant throughout the experiment. Commercially available reference electrodes include saturated calomel electrode, standard hydrogen electrode, and Ag/AgCl electrode. Non-aqueous solution using silver electrode dipped in solution is called Ag/Ag^{+}.[50]

A redox system with constant (buffered or saturated) concentrations of each redox reaction participant is frequently used to achieve excellent electrode potential stability. Reference electrodes can be utilized in a variety of ways. The easiest method is to employ the reference electrode as a half-cell in the construction of an electrochemical cell. This enables the other half cell's potential to be determined. It is yet to be created an accurate and feasible method for measuring an electrode's potential in isolation (absolute electrode potential).

Counter electrode

The electric circuit of electrochemical cell is completed by adding a counter electrode to the device. It allows current to flow between the working and counter electrodes and acts as a source of electron flow. Because of its inert nature, platinum wire is used as a counter electrode.[51]

When electroanalytical chemistry is performed with a three-electrode cell, the auxiliary electrode, along with the working electrode, forms a circuit over which current is either applied or measured. The auxiliary electrode's voltage is normally not measured and is changed to balance the reaction occurring at the working electrode. This design allows the working electrode's potential to be compared to a known reference electrode without jeopardizing the reference electrode's stability by flowing current through it.

A glass frit can be used to separate the auxiliary electrode from the working electrode. By isolating the auxiliary electrode from the main test solution, any byproducts generated at the auxiliary electrode are prevented from contaminating the main test solution. For example, if a reduction is performed at the working electrode in an aqueous solution, oxygen may be released from the auxiliary electrode. During the bulk electrolysis of a species with reversible redox activity, such separation is critical.

Supporting electrolyte

Supporting electrolyte, also known as inert electrolyte, is made up of non-electroactive chemical compounds. It functions within the context of possibilities. It has a high ionic strength relative to electroactive species, and its concentration is a hundred times higher, allowing it to fully suppress migration effects.[52]

Inert electrolyte or inactive electrolyte are other terms for supporting electrolytes. When controlling electrode potentials, supporting electrolytes are commonly utilized in electrochemical experiments. This is done to boost the solution's conductivity, reduce electroactive species movement via ion migration in the electric field, maintain consistent ionic strength, and maintain stable pH, among other things.

Many direct electrochemical procedures are not only costly and time-intensive, but also necessitate the use of specialized instruments, laborious sample preparation, and dexterous handling. Linear sweep voltammetry, cyclic voltammetry, and differential pulse voltammetry are the most widely used voltammetry techniques (DPV). All of these methods use a three-electrode device to calculate current with a fixed or variable potential.

We majorly focused on the differential pulse voltammetry selective and sensitive detection of the target species. This is also useful for the onsite detection of the analyte and more importantly for metal ions that are involved in biological samples. Since DPV is the technique used in the analysis, it will be addressed in depth.

Differential pulse voltammetry

Differential pulse voltammetry is used to assess the number of electroactive species present at a trace level in an organic or inorganic sample. Potential is screened using this method, which uses a series of periodic pulses superimposed on a linear potential ramp (Fig. 7). Current is measured at two points: when the pulse starts and when the pulse finishes. The actual difference between these two points is calculated and plotted against the potential. Peak-shaped voltammograms are observed due to double sampling. The distance of the peak is

used to calculate electron stoichiometry.[53] Half-wave potential ($E_{1/2}$) is utilized in DPV to determine peak potential (E_p). Peak potential deviates from $E_{1/2}$ as the peak base broadens and the height of the peak diminishes. The difference between measured current and applied base potential is displayed. The advantage is that even at concentrations as low as 0.05 µM, an observer may detect analyte.

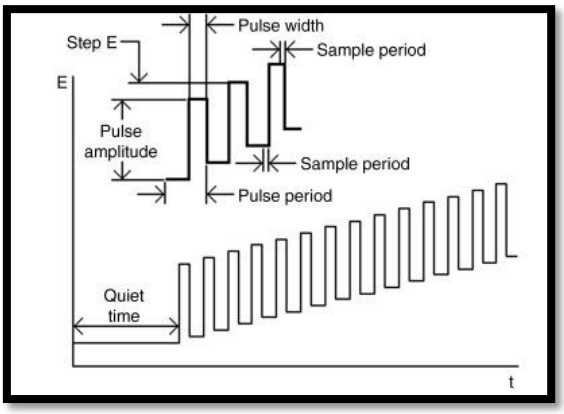

Fig.7 Voltage-time graph for differential pulse polarography

1.4 Need for chemical sensor

Identification of environmentally and biologically significant organisms has gotten a lot of attention because accurate detection of these analytes offers crucial details on how they should be disposed of in the ecosystem.[54-56] The employment of multiple ionic species has increased in diverse disciplines such as biology, medicine, catalysis, physiological processes, mining, and agriculture as the modern period progressed. Indeed, they play an important role in physio-chemical processes in living organisms as well as industrial activities. Many items that make life easier can also be associated with hazardous ingredients that have negative consequences for the living world. VOCs as a component of petroleum products, formaldehyde in paints, and heavy metal ions such as lead, copper, and zinc are just a few examples of potentially dangerous materials. In terms of anions, chlorides, fluorides, nitrites, etc. are used in clinical treatments, environmental samples, and fertilizers, etc. As a result of daily use of harmful element-containing materials, these compounds may be released into the ecosystem, causing contamination in both aquatic and terrestrial habitats. Furthermore, the above-mentioned contaminants can come into touch with living beings through industrial processes, food chains, occupational disclosure, and water sources.

Focusing on metal ions, certain metals (Hg (II), Pb (II), Cd (II), and others) are highly dangerous to mankind and the environment, and are referred to as heavy metal ions, while others (Cu (II), Zn (II), and Mn (II)) are essential for human growth but only up to a certain

concentration. Metals are essential not only for human survival but also for the growth of plants and aquatic animals also. Some metal ions' functions are summarised below. Aluminium is a stable metal that does not affect biological processes. In acidic conditions, it is easily absorbed by plants and animals in the soluble form produced by rocks and soil. Furthermore, an abnormally high level of aluminium in the body can lead to a variety of disorders, including Parkinson's disease, pulmonary dysfunction, renal failure, inflammation, and bone softening. Aluminium intake is roughly 7 mg/kg of body weight per week. According to the World Health Organization, daily intake for an average human should not exceed 3-10 mg.[57, 58]

Zinc is an essential component of numerous biological processes, including DNA synthesis, gene transcription, microtubule polymerization, and serving as a cofactor in metalloproteins. An imbalance in zinc concentration, on the other hand, can lead to a variety of problems, including neurological problems, immunological weakness, and growth retardation. Zinc is also utilized in paints, pharmaceutical industries, electroplating, chemical manufacture, and other applications. If these industries' waste is released into the environment, it can have phytotoxic consequences by reducing microbial activity.[59] Copper is required for a variety of biological functions, including the synthesis and release of enzymes and proteins, the development of the heart, kidneys, and brain, and the formation of red blood cells, among others. It also aids the immune system's optimal functioning. A high copper content, on the other hand, can lead to significant disorders such as Wilson's disease, leucopenia, and myelodysplasia.[60] Cobalt, an essential component of vitamin B12, aids nerve cell function and the production of genetic components. Cobalt toxicity, on the other hand, can harm the lungs, impair the cardiovascular and gastrointestinal systems, and increase thyroid activity.[61]

On the other hand, anions also have functions and significance in biological, environmental, and chemical processes. Because fluoride ions are beneficial to dental health, they are found in toothpaste and drinking water. It's also used to treat osteoporosis, and Teflon, a fluoride-based compound, is a common component of household and industrial items. However, higher fluoride concentrations can produce fluorosis or an increase in bone density.[62] Chloride is mostly used to trace landfill leakage and monitor the presence of pollutants in natural water reservoirs. Maintaining bodily fluid is also beneficial. Hyperchloremia and high blood pressure can be caused by an increase in chloride ions in the human body.[63] Cyanide is used in a variety of industries, including electroplating, mining, and the manufacture of organic materials. Excessive and surplus cyanide leakage can have serious consequences and

is exceedingly harmful to living things.[64] Nitrate ions can be found in a variety of places, including fish farms, aquaculture waste products, and agriculture.

Since both cations and anions have distinct roles to perform, developing chemosensors for trace-level detection of both cations and anions is a burgeoning field of chemistry. Chemosensors are an effective method for determining these cations and anions due to their ease of synthesis, efficient interaction with metal ions, and water solubility. The signal obtained from the chemosensor was reported using a range of traditional techniques, but in recent years, spectroscopic and voltammetry techniques have proven to be highly effective tools due to the ability to detect target metal ions with the naked eye, without the use of expensive equipment, on-site detection, and lower detection limit.

From the discussion, it can be deduced that these ions play vital roles in a variety of disciplines and can cause unintended environmental release. Recognizing and assessing distinct ions in diverse matrixes for trace levels becomes essential, as unregulated amounts will have damaging effects. As a result, many researchers are concentrating their efforts on developing simple, sensitive, and cost-effective analytical techniques that may be utilized for on-site ion monitoring.

Phenyl ether and phenyl amine-based moieties have recently been shown to be effective chemosensors for detecting metal ions and anions. Both phenyl ether and phenylamine give the receptor molecule rigidity and versatility. Keeping the cavity size constant, a good combination of ethereal oxygen, hydroxyl group, and substituted amine linkage is crucial in the selective detection of target species. It is suggested that a series of triphenylether and triphenylamine-based receptors have been investigated with varying numbers of hetero atoms in the molecules. They are well-structured ionophores with the ability to detect cations, anions, and amino acids at a trace level. It would be fascinating to describe receptor output in terms of hetero atom variance in the cavity of the receptor. The chemical sensor's efficiency was improved by improving the solvent system, allowing it to detect target ions more accurately and expand its use in environmental, biomedical, and routine sensing of heavy metal ions and toxic anions using spectroscopic and voltammetry techniques.

1.5 Triphenylether and triphenylamine molecule as receptor unit

While a large number of aryl rings with hetero atoms (O, N, S) have been published in the literature, only a few have been used for complexation with cations or anions. By properly arranging the hetero atoms and adjusting the flexibility/rigidity of the donor atoms, the ligand's behavior, such as selectivity and specificity, can be altered. Neutral macrocyclic ligands have been shown to have high sensitivity to cations and anions. The development of such chemosensors is a large and rapidly expanding field of chemistry. Pederson was the first one to prepare macrocyclic polyethers with an ether linkage.[40] Because of the oxygen atom, the receptor showed selective behavior only for alkali and alkaline earth metals. As nitrogen or sulphur are incorporated into the receptor, it becomes vulnerable to transition metal and alkali metal ions, respectively.

We have synthesized phenyl ether and phenylamine derivatives for the selective detection of cation/anions, keeping the above-described advantages of aryl ether in mind. We tried to explore the properties of aryl ethers by varying solvent media and other parameters because there hasn't been much work done on them. The ether linkage between two phenyl rings provides rigidity to the basic structure. Also, replacing one of the hetero atoms with a large aromatic ring increases the molecule's versatility. With different hetero atom environments and cavity sizes, the phenyl ether/amine would be a stronger receptor due to its combination of flexibility and rigidity. Because of the optical and electroanalytical properties of ether and amine linkages, aryl ether-based molecules have been suggested as cation and anion probes. Additional modifications to these molecules, such as increasing the number of hetero atoms and modifying the solvent system, have assisted in the entrapment of metal ions and exhibit a range of biological applications.

References

1. F. R. Simões and M. G. Xavier, *Nanoscience and its Applications*, 2017, 155-178.
2. A. Hulanicki, S. Glab and F. Ingman, *Pure and Applied Chemistry*, 1991, **63**, 1247-1250.
3. P. Gründler, *ChemTexts*, 2017, **3**, 1-24.
4. F. Scholz, *ChemTexts*, 2015, **1**, 1-24.
5. A. Brecht and G. Gauglitz, *Biosensors and Bioelectronics*, 1995, **10**, 923-936.
6. D. Wu, A. C. Sedgwick, T. Gunnlaugsson, E. U. Akkaya, J. Yoon and T. D. James, *Chemical Society Reviews*, 2017, **46**, 7105-7123.
7. L. E. Santos-Figueroa, M. E. Moragues, E. Climent, A. Agostini, R. Martínez-Máñez and F. Sancenón, *Chemical Society Reviews*, 2013, **42**, 3489-3613.
8. S. Upadhyay, A. Singh, R. Sinha, S. Omer and K. Negi, *Journal of Molecular Structure*, 2019, **1193**, 89-102.
9. D. Udhayakumari, S. Naha and S. Velmathi, *Analytical Methods*, 2017, **9**, 552-578.
10. D. Udhayakumari, *Sensors and Actuators B: Chemical*, 2018, **259**, 1022-1057.
11. A. Roy, M. Nandi and P. Roy, *TrAC Trends in Analytical Chemistry*, 2021, 116204.
12. A. Patil and S. Salunke-Gawali, *Inorganica Chimica Acta*, 2018, **482**, 99-112.
13. J. Wu, W. Liu, J. Ge, H. Zhang and P. Wang, *Chemical Society Reviews*, 2011, **40**, 3483-3495.
14. N. S. Patil, R. Dhake, M. I. Ahamed and U. Fegade, *Journal of Fluorescence*, 2020, 1-36.
15. G. Fukuhara, *Journal of Photochemistry and Photobiology C: Photochemistry Reviews*, 2020, **42**, 100340.
16. Z. Xu, J. Yoon and D. R. Spring, *Chemical Society Reviews*, 2010, **39**, 1996-2006.
17. V. G. KT and B. Meggitt, *Optical Fiber Sensor Technology*, Chapman & Hall, 1998.
18. R. Ulber, J.-G. Frerichs and S. Beutel, *Analytical and Bioanalytical Chemistry*, 2003, **376**, 342-348.
19. R. Narayanaswamy and O. S. Wolfbeis, *Optical Sensors: Industrial Environmental and Diagnostic Applications*, Springer Science & Business Media, 2013.
20. E. R. Diebold, R. J. Kordal, N. A. Surridge and C. D. Wilsey, *Journal*, 1995.
21. N. F. Carter, G. R. Chambers, G. J. Hughes, S. Scott, G. S. Sanghera and J. L. Watkin, *Journal*, 1997.
22. J. Wang, *Chemical Reviews*, 2008, **108**, 814-825.

23. D. Grieshaber, R. MacKenzie, J. Vörös and E. Reimhult, *Sensors*, 2008, **8**, 1400-1458.

24. K. Ariga and T. Kunitake, *Supramolecular Chemistry-Fundamentals and Applications: Advanced Textbook*, Springer Science & Business Media, 2006.

25. S. Stepanow, M. Lingenfelder, A. Dmitriev, H. Spillmann, E. Delvigne, N. Lin, X. Deng, C. Cai, J. V. Barth and K. Kern, *Nature Materials*, 2004, **3**, 229-233.

26. M. Zhang, D. Xu, X. Yan, J. Chen, S. Dong, B. Zheng and F. Huang, *Angewandte Chemie*, 2012, **124**, 7117-7121.

27. D. W. Christianson and J. D. Cox, *Annual Review of Biochemistry*, 1999, **68**, 33-57.

28. L.-m. Liu and Z.-y. Yang, *Inorganica Chimica Acta*, 2018, **469**, 588-592.

29. S. M. Saleh, R. Ali and I. A. Ali, *Spectrochimica Acta Part A: Molecular and Biomolecular Spectroscopy*, 2017, **183**, 225-231.

30. H. Wang, T. Kang, X. Wang and L. Feng, *Sensors and Actuators B: Chemical*, 2018, **264**, 391-397.

31. M. Shellaiah, N. Thirumalaivasan, B. Aazaad, K. Awasthi, K. W. Sun, S.-P. Wu, M.-C. Lin and N. Ohta, *Spectrochimica Acta Part A: Molecular and Biomolecular Spectroscopy*, 2020, **242**, 118757.

32. C. Liu, J.-c. Qin, J. Xue, L.-m. Tian, T.-r. Li and Z.-y. Yang, *Journal of Photochemistry and Photobiology A: Chemistry*, 2019, **385**, 112091.

33. H. Kim, S. Sarkar, M. Nandy and K. H. Ahn, *Spectrochimica Acta Part A: Molecular and Biomolecular Spectroscopy*, 2020, 119088.

34. B. Zhang, H. Liu, F. Wu, G. Hao, Y. Chen, C. Tan, Y. Tan and Y. Jiang, *Sensors and Actuators B: Chemical*, 2017, **243**, 765-774.

35. S. Qu, Q. Cao, J. Ma and Q. Jia, *Talanta*, 2020, 121280.

36. G. A. Somorjai and J. Y. Park, *Angewandte Chemie International Edition*, 2008, **47**, 9212-9228.

37. F. Faridbod, M. R. Ganjali, R. Dinarvand, P. Norouzi and S. Riahi, *Sensors*, 2008, **8**, 1645-1703.

38. J. W. Steed and J. L. Atwood, *Supramolecular Chemistry*, John Wiley & Sons, 2013.

39. D. J. Cram, *Angewandte Chemie International Edition in English*, 1988, **27**, 1009-1020.

40. C. J. Pedersen, *Journal of the American Chemical Society*, 1967, **89**, 7017-7036.

41. E. Weber and H.-P. Josel, *Journal of Inclusion Phenomena*, 1983, **1**, 79-85.

42. A. Von Zelewsky, *Stereochemistry of Coordination Compounds*, John Wiley & Sons, 1996.

43. A. Bratov, N. Abramova and A. Ipatov, *Analytica Chimica Acta*, 2010, **678**, 149-159.

44. E. Bakker, P. Bühlmann and E. Pretsch, *Chemical Reviews*, 1997, **97**, 3083-3132.

45. E. P. Arthur, *Journal*, 1969.

46. D. A. Gough, *Journal*, 1987.

47. B. H. Kim, H. Park, H. Kim, G. Kim, I. Chang, J. Lee and N. Phung, *Applied Microbiology and Biotechnology*, 2004, **63**, 672-681.

48. P. T. Kissinger and W. R. Heineman, *Journal of Chemical Education*, 1983, **60**, 702.

49. F. Winquist, P. Wide and I. Lundström, *Analytica Chimica Acta*, 1997, **357**, 21-31.

50. R. C. Larson, R. T. Iwamoto and R. N. Adams, *Analytica Chimica Acta*, 1961, **25**, 371-374.

51. N. Elgrishi, K. J. Rountree, B. D. McCarthy, E. S. Rountree, T. T. Eisenhart and J. L. Dempsey, *Journal of Chemical Education*, 2018, **95**, 197-206.

52. J. J. Van Benschoten, J. Y. Lewis, W. R. Heineman, D. A. Roston and P. T. Kissinger, *Journal of Chemical Education*, 1983, **60**, 772.

53. A. P. Brown and F. C. Anson, *Analytical Chemistry*, 1977, **49**, 1589-1595.

54. A. P. De Silva, H. N. Gunaratne, T. Gunnlaugsson, A. J. Huxley, C. P. McCoy, J. T. Rademacher and T. E. Rice, *Chemical Reviews*, 1997, **97**, 1515-1566.

55. V. Amendola, L. Fabbrizzi, C. Mangano and P. Pallavicini, *Accounts of Chemical Research*, 2001, **34**, 488-493.

56. A. P. de Silva, B. McCaughan, B. O. McKinney and M. Querol, *Dalton Transactions*, 2003, 1902-1913.

57. J. Barcelo and C. Poschenrieder, *Environmental and Experimental Botany*, 2002, **48**, 75-92.

58. Q. Diao, P. Ma, L. Lv, T. Li, Y. Sun, X. Wang and D. Song, *Sensors and Actuators B: Chemical*, 2016, **229**, 138-144.

59. J. M. Berg and Y. Shi, *Science*, 1996, **271**, 1081-1085.

60. Y. H. Hung, A. I. Bush and R. A. Cherny, *JBIC Journal of Biological Inorganic Chemistry*, 2010, **15**, 61-76.

61. N. Lombaert, D. Lison, P. Van Hummelen and M. Kirsch-Volders, *Toxicology and Applied Pharmacology*, 2008, **227**, 299-312.

62. C. R. Wade, A. E. Broomsgrove, S. Aldridge and F. P. Gabbai, *Chemical Reviews*, 2010, **110**, 3958-3984.

63. K. Berend, L. H. van Hulsteijn and R. O. Gans, *European Journal of Internal Medicine*, 2012, **23**, 203-211.

64. T. B. Hendry-Hofer, P. C. Ng, A. E. Witeof, S. B. Mahon, M. Brenner, G. R. Boss and V. S. Bebarta, *Journal of Medical Toxicology*, 2019, **15**, 128-133.

Chapter 2

Literature Survey

The identification of environmentally and biologically significant organisms has got a lot of attention because accurate detection of these analytes offers crucial details on how they should be disposed of in the ecosystem. Sensors based on small organic molecules have proven to be an effective tool in this regard due to their advantages of ease of synthesis, wide applicability, and low cost. From this perspective, current interest is based on organic sensors with high stability, excellent environmental tolerance, and emission wavelength/near-infrared excitation. The identification of analytes using a receptor molecule is done using a variety of analytical techniques. Spectrophotometric and electrochemical techniques are the most important for determining the optical and electrical changes in the receptor solution among other available techniques. This is because they are simple to manage and run, cost-effective, and provide real-time applications.[1-4] Recent publications from professional journal papers were used to determine the existing state of information.

In comparison to other approaches, fluorescence signalling is one of the primary choices because to its functional simplicity, real-time detection, and high sensitivity. Chemosensors that demonstrate fluorescence increase by interacting with the target analytes are more effective because there is less chance of erroneous signals. Hard donor sites like N and O should be preferred in the coordination sphere for developing selective fluorescence chemosensors for metal ions. As a result, the majority of reported sensors have nitrogen and oxygen donor sites. A variety of signal mechanisms, including as photo-induced electron transfer (PET), intramolecular charge transfer (ICT), electronic energy transfer (EET), and resonance energy transfer (RET), have been employed to produce efficient fluorescent systems to detect ions based on photophysical processes. To introduce the above-mentioned photophysical mechanisms, various sorts of non-covalent interactions between the chemosensor and metal ions are used. In addition, new sensing mechanisms for the detection of ions have evolved in recent years, such as aggregation-induced emission (AIE), C=N isomerization, and excited-state intramolecular proton transfer (ESIPT). Some of the mechanisms have been defined here that are used to propose sensing mechanism for both cations and anions.

PET (Photo-induced electron transfer) based interaction

The fluorophore is usually coupled by spacer to an ionophore unit with a non-bonding electron pair in PET phenomenon-based sensors. During the excitation of a fluorophore, an electron from the lowest unoccupied molecular orbital (LUMO) moves to the highest occupied molecular orbital (HOMO), undergoes charge recombination, and returns to the ground state, emitting fluorescence.

If the HOMO orbital of another component of the molecule, such as the ionophore, has energy between the energy levels of the fluorophore, then electron transfer from the ionophore's HOMO orbital to the fluorophore's half-occupied HOMO occurs, resulting in non-radiative decay and fluorescence quenching. In the bonded state with a guest molecule, however, the energy of the HOMO of the ionophore is lower than that of the fluorophore due to increased redox potentials. The electron transfer is limited by this process, which allows the fluorophore to glow (Fig. 1).

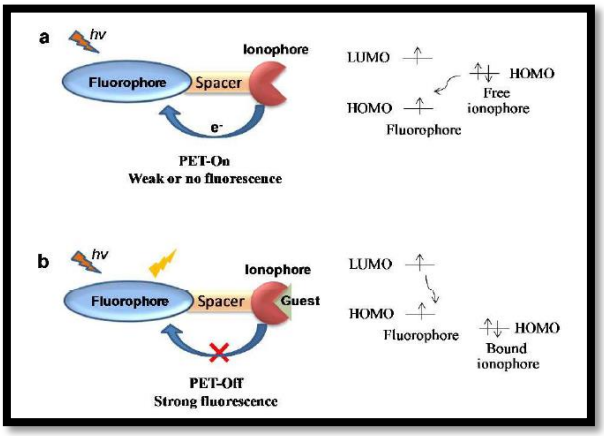

Fig. 1 PET process in chemosensor

ICT (Intra-molecular charge transfer) based interactions

Fluorophores and ionophores are directly coupled in ICT-based sensors, resulting in a single species. In ICT-based sensors, these two capabilities act as either an electron donor or an electron acceptor. In this system, the sensor's HOMO has electron density near the electron-donating group, while the sensor's LUMO has electron density near the electron-acceptor group, resulting in dipoles with ICT from the donor to the acceptor unit upon excitation. However, when a guest species is complexed with either the donor or acceptor component, the dipole strength of the donor-acceptor species changes, resulting in a change in photophysical behaviour. The interaction of the guest with the donor component causes the

donor's electron-donating character to decrease, resulting in a blue-shift in the emission spectrum. When the acceptor group interacts with the guest species, the acceptor group's electron-withdrawing nature increases, resulting in a red-shift in the emission spectrum (Fig. 2).

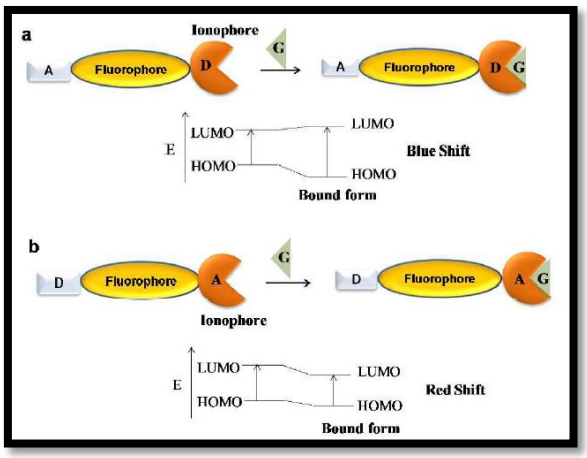

Fig. 2 ICT process in chemosensor

RET (Resonance energy transfer) based interactions

Resonance energy transfer (RET) is a photophysical process in which an excited chemical moiety transfers its excitation energy in a non-radiative manner to a nearby chemical moiety, which then releases energy in a radiative manner. An energy donor-acceptor pair is a pair of molecules that interact in such a way that RET occurs. In general, the energy transfer is determined by the distance between the donor and acceptor components, as well as the level of spectral overlap between the emission and absorption spectra of the donor and acceptor components (Fig. 3).

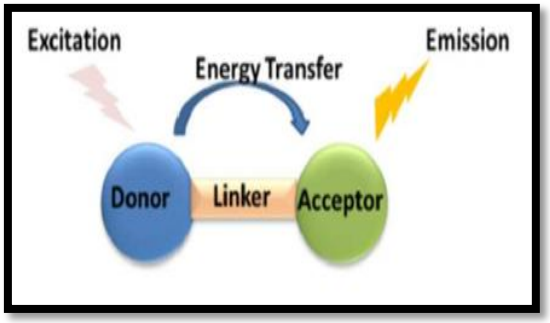

Fig. 3 RET process in chemosensor

C=N isomerization based interactions

The investigation of photophysical characteristics of conformationally constrained molecules led to the discovery of the C=N isomerization mechanism. C=N isomerization has been discovered to be a nonradiative decay process of excited states in compounds, making it non-fluorescent. The complexation of metal cations can impede this non-radiative activity, providing a means to create fluorescent-sensing molecules (Fig. 4).

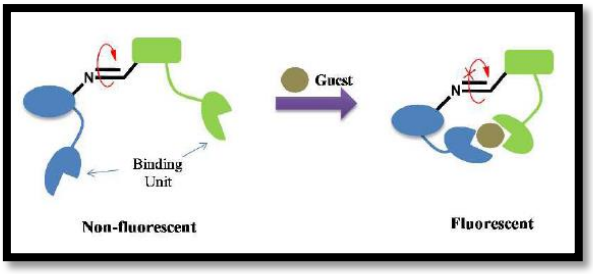

Fig. 4 ICT process in chemosensor

ESIPT (Excited-state intramolecular proton transfer) based interactions

ESIPT is a phenomena that happens in fluorophores that may transfer proton between two locations of the molecule, such as keto-enol tautomers. In such systems, the ground state tautomer differs from the excited state tautomer. Intramolecular hydrogen bonding stabilises the enol-form in its ground state. The excited enol-form is promptly transformed into the excited keto-form by the transfer of a proton after excitation, resulting in an emission band with a longer wavelength than expected without the process. After that, the keto-form decays to the ground state and reverts to the original enol form via reverse proton transfer (Fig. 5).

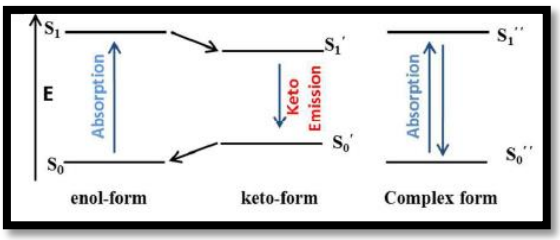

Fig. 5 ESIPT process in chemosensor

AIE (Aggregation induced emission) based interactions

AIE active sensors are propeller-shaped, with rotatable phenyl rings connected to the central core by a C-C connection with analyte-specific functional groups. In the solution phase, these rotors are active, allowing the energy of approaching photons to be dissipated via a non-radiative pathway, making the molecule non-luminescent or less luminous (Fig. 6).

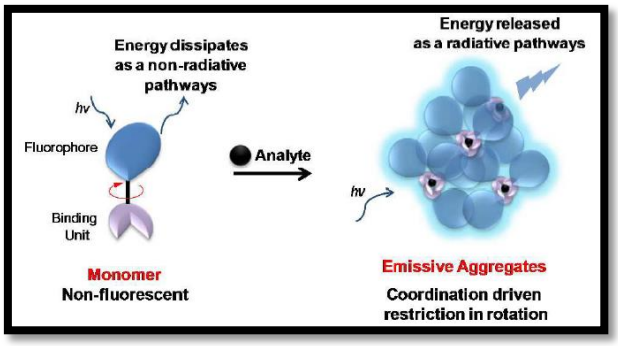

Fig. 6 AIE process in chemosensor

2.1 Cation Sensors

When it comes to cations, they can be present in the earth's crust in both their natural and composite states, with varying amounts. Some metals (Hg (II), Pb (II), Cd (II), and others) are extremely hazardous to mankind and the environment and are referred to as heavy metal ions, while others (Cu (II), Zn (II), and Mn (II)) are needed for human growth (up to a certain concentration). Metals are essential not only for human survival but also for the growth of plants and aquatic animals. Even critical metals become a pollutant to humans, soil, and the atmosphere above a certain concentration. As a result, their fast identification in various matrices is crucial.[5, 6] Selective determination of these cations by artificial receptors has attracted considerable interest. A wide variety of organic receptors are present in literature which different mechanisms or interactions to establish the selective binding between receptor and cations.

To detect alkali, alkaline earth metals, and transition metals, there is a wide body of literature that uses spectrophotometric and electrochemical techniques to detect cations.

2.1.1 Spectrophotometric method

Carbon Quantum Dots (CQDs) based sensors for metal detection

Carbon quantum dots (CQDs) have piqued the interest of many scientists around the world in recent years due to their numerous applications in (chemical/biological) sensors, energy storage, optoelectronics, biomedical applications, and photocatalysis.[7-9]

Fu *et al.* (2017)[10] have used a one-pot hydrothermal synthesis method to make rhodamine coupled CQDs. It's a dual emission ratiometric probe that can detect Hg (II) ions as well as glutathione (GSH). CQD-RhB displayed no fluorescence in the absence of metal ions, but when Hg (II) ions were added, the probe became strongly fluorescent. CQDs with an amino group have been updated by **Wang *et al.* (2017)[11]** for the precise detection of Cu (II) ions. The interaction of amino groups with Cu (II) ions allows the d-orbital of Cu (II) to break, resulting in heavy fluorescence quenching of CQDs.

Using aminosalicylic acid as a precursor, **Song *et al.* (2017)[12]** produced a new form of bright and color-tuneable CQDs. These CQDs were also doped with nitrogen to tune the photoluminescence emission. The resulting NCQDs were used to detect Fe (III) at 623 nm with a detection limit of 0.52 M using a ‘'turn off'' mechanism. NCQDs have also been identified as a fluorescent chemosensor for Fe (III) ions by **Wu and colleagues (2017)[13]** When NCQDs were bound with Fe (III) in an acidic medium, the fluorescence intensity at 436 nm was quenched with a detection limit of 0.21 nM. **Singh and colleagues (2018)**[14] used a one-step hydrothermal process to create nitrogen and phosphorus-doped CQDs. These N, P-CQDs, which were synthesized, exhibited optical properties in both sunlight and UV light. They act as “on-off” fluorescent probe that uses a static quenching mechanism[15] to detect toxic Cr (VI) ions.

Sulphur doped CQDs were synthesized by **Du *et al.* (2020)[16]** and these S-CQDs showed a selective response to Fe (III) ions compared to Fe (II) ions. Fluorescence quenching was observed in S-CQDs as the concentration of Fe (III) ions increased. The detection limit was determined to be 0.050 M, with linear behavior from 0-200 M. To boost the optical properties of the nanoparticles, **Han *et al.* (2018)[17]** added Fe (II) metal to the CQDs. On excitation at 455 nm, Fe-CQDs detected Zn (II) ions and histidine. In terms of naked eye behavior, fluorescence changes from blue-pink and pink-blue-pink for Zn (II) and histidine, respectively. For Zn (II) ions, ratiometric fluorescence behavior was observed.

Schiff base as chemical sensor for the detection of metal ions

Schiff bases are widely used chemosensors due to their unique properties such as (i) the Schiff base is synthesized with water as a by-product, which is needed for the fabrication of certain reactors and sensors, (ii) the Schiff base undergoes an n-π* transformation due to C=N bonds, which gives it auto-fluorescent properties, and (iii) they have an extraordinary property of reversibility with changing pH values. This is an important property for pH-triggered drug release. All of these characteristics contribute to the Schiff base's excellent optical/fluorescent behavior in the detection of metal ions.[6, 18]

Harathi group (2020)[19] synthesized two Schiff bases (2.1&2.2). Both probes were used to detect Fe (III) ions in solvent mediums of 10: 90:: THF: H_2O and 40: 60:: THF: H_2O, with detection limits of 0.163 M and 3.99 M, respectively. Spectrophotometric response of the receptor was supported by electrochemical technique (Differential Pulse Voltammetry). The proposed sensing mechanism was corroborated with DFT studies. **Xie *et al.* (2020)[20, 21]** developed a Schiff base for the selective detection of Cu (II) ions using the ESIPT mechanism. Under sunlight, the color of the probe changed from colorless to yellow following optical detection, indicating 1:2 stoichiometry.

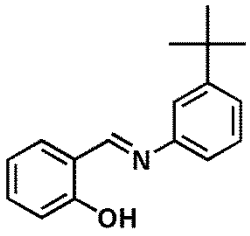

2.1

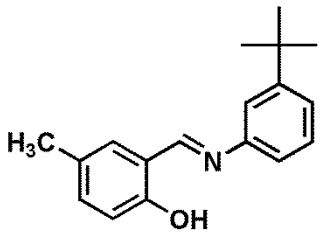

2.2

Patra *et al.* (2018)[22] used the ESPIT mechanism to synthesize a Schiff base (2.3) with fluorescence off properties. Under UV light, the probe operated as a multiple analyte detector, detecting all analytes with the naked eye. The presence of Zn (II) and Al (III) inhibits the C=N isomerization and hence both chelation enhance fluorescence and excited-state intermolecular proton transfer process play a key role in the enhancement of intensity. A single probe has detected Al (III), Zn (II), and F^- ions with a detection limit of 2.24×10^{-7} M, 4.1×10^{-8} M, and 3.7×10^{-8} M, respectively. Structural changes of both receptor and complex are determined by density functional theory and time-dependent density functional theory.

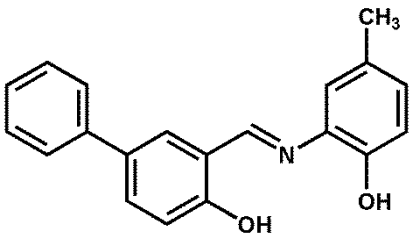

2.3

A novel optical/fluoro chemosensor has been developed for the detection of Cu (II) ions by **Suleh *et al.* (2017)**[23] Polyvinyl chloride was used to make a sensor film of the Schiff base. The CHEF mechanism was found to be responsible for the film's optical behavior, with a detection limit of $1.1x10^{-8}$ M. The EDTA solution was used to make the sensor reversible. **Kumar group (2018)**[24] synthesized a Schiff base (2.4) for the detection of Al (III) ions selectively. The probe was non-emissive before the addition of Al (III), which caused the fluorescence to turn on and was visible under UV light.

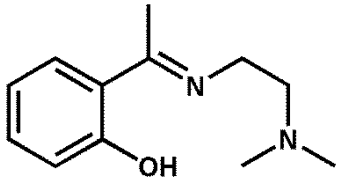

2.4

Miscellaneous compounds for the detection of metal ions

Other than CQDs and Schiff base, a large variety of chemosensors are being synthesized as well as successfully employed to detect metal ions. Some other chemosensors such as pyrazole, squaraine, quinoline, dansyl, and rhodamine, etc. are going to be discussed because of their naked eye detection, easy synthesis, and real-life applications. Also, some of these chemosensors act as multi-analyte sensors because of their simultaneous detection of cations, anions, and biomolecules.

Squaraine dye is quite suitable for designing metal ion chemosensors as they have tunable properties according to temperature, pH, solvent system, and other additives. Squaraines consist of four potential binding sites i.e. two nitrogen atoms of aniline moiety and two oxides at electron-deficient cyclobutene ring. Therefore, it can bind two metal ions and enhance its optical properties.

Squaraine-based, multi-response chemosensor 2.5 was developed by **Sun *et al.* (2017)**[25]. The sensor exhibited response for Al (III), Zn (II), and Cd (II) in ethanol-water buffer solution. Using UV–VIS, fluorescence, mass spectra, and ^{1}H NMR techniques, a mechanism of binding was established, which follows that the addition of metal ions leads to inhibition of C=N isomerization (*cis-trans*), and hence, chelation enhanced fluorescence took place. Furthermore, the probe could restore the $A\beta_{1-42}$-Al complex in Alzheimer's disease, which can ultimately, provide a better biological understanding for developing a treatment of Alzheimer's disease. Another squaraine-based molecule that showed selective detection for Cu (II) ions in acetonitrile was synthesized by **Liu *et al.* (2018)**[26] Color of the probe changes from blue to faint yellow in the presence of Cu (II) ions with a detection limit of $1.88x10^{-7}$ $molL^{-1}$. Also, paper strips were constructed which detect metal ions up to the concentration of $1x10^{-6}$ $molL^{-1}$.

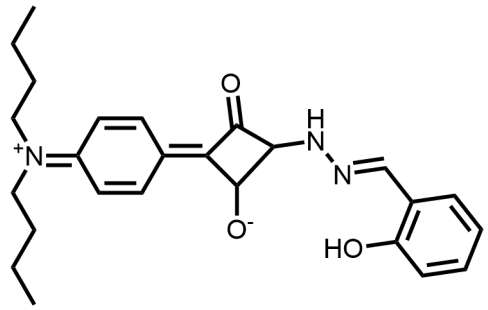

2.5

Pyrazole-based molecules exhibit excellent character among the azole family. Pyrazole, having both electron-donating and accepting character and its substituted derivatives is widely studied due to high fluorescent quantum yield, solvatochromic behavior, and optical properties.

Following the hetero atom environment of pyrazole, a new sensor 2.6 was developed by **Zhu *et al.* (2020)**[27] based on the pyrazine moiety for the selective detection of Co (II) ions. The recognition process showed color variation from colorless to blue fluorescence with the limit of detection of 0.104 μM (response time < 4 min). The mechanism of sensing was confirmed by HR-MS, FT-IR, and DFT calculations. Presence of Co (II) in the probe leads to restricting the rotation of C=N group and the pyrazine ring. Test strips were also prepared and were used for potential applications in water samples. With a good recovery of Co (II) (93 %) in water samples, it was also detected in HeLa cells by fluorescence imaging.

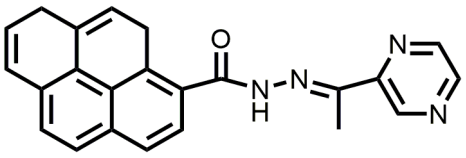

2.6

Quinoline, a nitrogen heterocycle, has emerged as a potential chemosensor due to strong polarization and Π-Π* transition. It exhibits striking coordination and strong fluorescence. Following that **Song *et al.* (2019)[28]** have developed a new probe 2.7 by inserting an amide group into the 8-aminoquinoline and propargylamine chelating site. This quinoline-based sensor was used to detect Zn (II) and Cd (II) distinctly. Zn (II) was detected in almost complete water through the amide tautomer form of the probe. Cd (II) ions were detected in an aqueous acetonitrile medium through the imidic acid tautomer form of the probe. Also, Zn (II) was detected in mung bean sprouts through bioimaging.

Due to chemical stability, large stokes shift, and high quantum yield, dansyl and its derivatives have proved to be an excellent chemosensor for metal ions. **Wang *et al.* (2019)[29]** have developed a chemosensor 2.8 based on the conjugation of dipeptide with the dansyl group. The probe was used to detect Zn (II) ions via the generation of monomer-excimer formation in aqueous solutions. This fluorescence turn-on complex was further used to detect Na_2EDTA. The limit of detection of Zn (II) was reported to be 11.2 nM with emission change from light yellow to bright green. Another dansyl-based probe was synthesized by **Li and coworkers (2019)[30]** constituting a naphthalene-1-sulfonamide/2-hydroxybenzaldehyde, for the detection of Pb (II) ions in acetonitrile medium. The probe proved to be a naked eye sensor as on addition of Pb (II) ions makes the solution yellow from colorless and under UV light emission intensity changes from green to light yellow. The limit of detection was found to be 23.2 ppb with an association constant of $7.68 \times 10^8\ M^{-1}$.

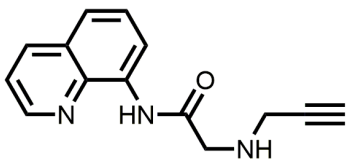

2.7

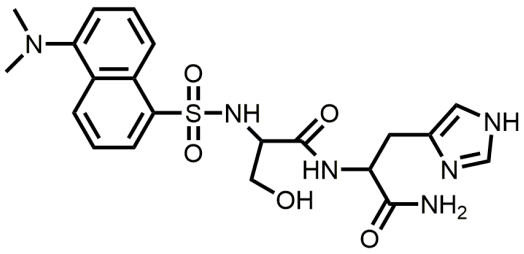

2.8

Rhodamine, a fluorophore and chromophore (i.e. a fluorochrome), has piqued the interest of chemists because of its excellent photophysical properties, availability, longer wavelength emission, and high fluorescence quantum yield. Rhodamine comes in two isomeric forms: the ring closed form, which is non-fluorescent in nature, and the ring-opened form, which has different optical properties and higher fluorescence strength.[31, 32] For the detection of metal ions, a variety of rhodamine-based sensors have been synthesized.

Probe (2.9) was synthesized by **Mondal *et al.* (2019)[33]** for the selective detection of Pb (II) ions in an organic aqueous medium. DFT studies showed that the original structure of the probe changed to amide form with the addition of Pb (II) ions. Under ambient light, the probe's color varies from colorless to pink. The color transition from colorless to orange when exposed to UV light.

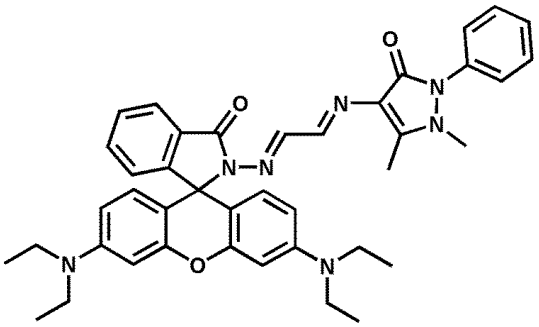

2.9

Alam and coworkers (2017)[34] developed a receptor that uses the chelation enhanced fluorescence (CHEF) mechanism to detect trivalent metal ions (2.10). In methanol/H_2O (1: 1, v/v, pH 7.2), the probe detected Al (III), Fe (III), and Cr (III) ions, Al (III) complex showed reversibility with arsenate ion. For all three metal ions, a molecular logic gate was built and for the application purpose, bioimaging was performed on live cells. **Tang and colleagues (2020)[35]** have produced two new fluorescent sensors for the selective detection of the Pd (II) ion in an aqueous medium. One probe is based on rhodamine, while the other is based on coumarin-rhodamine. Both the probes exhibit colorimetric and fluorometric responses to Pd (II) ions due to the opening of spirolactam rings of the receptors. The palladium-based sensor showed 70-fold enhancement in intensity while the rhodamine-based probe showed 1.75-fold ratiometric change.

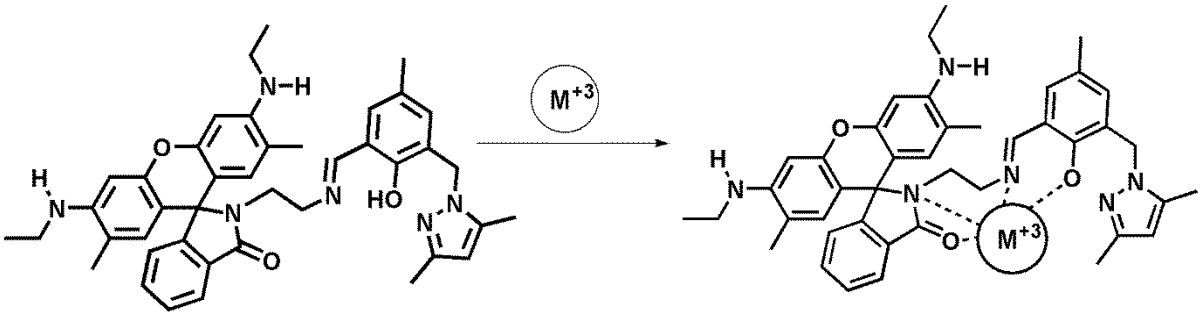

2.10

Maniyazagan *et al.* (2017)[36] developed a rhodamine-based moiety (2.11) for the selective detection of Cd (II) ions. The receptor was non-fluorescent by itself, but the addition of Cd (II) ions increased the strength of the complex at 480 nm. The color of the solution changed from deep magenta to bright orange when exposed to UV light. **Murugan and colleagues (2018)[37]** developed a probe (2.12) for the detection of two paramagnetic metal ions, Fe (III) and Cu (II). The addition of Cu (II) increased absorption at 529 nm, while the addition of Fe (III) increased fluorescence at 572 nm. Fe (III) ions were successfully detected in zebrafish embryos using the probe.

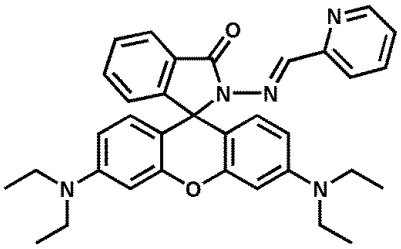

2.11

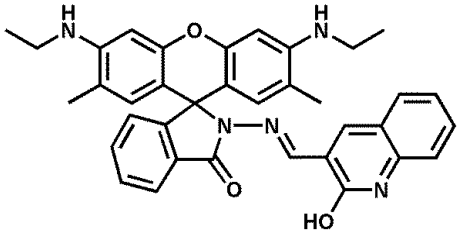

2.12

Diarylethene, a thermally stable and fast responsive chemosensor, based new photochromic sensor was developed by **Wang *et al.* (2019)[38]** for the detection of Mg (II) ion in acetonitrile solution. Addition of Mg (II) leads to enhancement in fluorescence at 522 nm, with 1: 1 stoichiometry. Fluorescent color change was observed from dark purple to green with a detection limit of 3.58×10^{-7} mol L^{-1}. Benzocoumarin and its derivatives have tunable optical properties as they have different sites for substitution. A novel benzocoumarin derivative was synthesized by **Liu and coworkers (2019)[39]**. The probe proved to be a multiple analyte detector as it senses Zn (II), Cu (II), and S^{2-}. Enhancement in fluorescence took place on the addition of Zn (II) ion in acetonitrile medium and in case of Cu (II) ions, fluorescence

quenching took place in aqueous ethanol solution. And S^{2-} ions were detected as a recovery of fluorescence of Cu (II) complex.

2.1.2 Electrochemical methods for the detection of cations

To understand the oxidative/reductive nature of the species as well as its behavior towards the target analyte, different types of electrochemical techniques are used. These are extensively used due to on-site monitoring, accuracy, cost-effective manner, simplicity, miniaturization capability, low instrumentation cost, and automation.[40-42]

Frag *et al.* (2019)[43] developed an organic molecule (2.13) namely methyl red for the detection of Al (III) ions in water and pharmaceutical samples. Electrode gave linear response in the range of $5.0x10^{-6}$-$1.0x10^{-2}$mol/L with detection limit of $5.0x10^{-6}$ mol/L. Proposed method gave a stable response for up to 14 weeks. **Kumbhat *et al.* (2018)[44]** have detected potassium ions from the solution using 4-aminobenzo-18-Crown-6 ether modified electrode. Host-guest interactions were recorded by CV, DPV, UV-VIS, and FTIR studies. Developed sensor was found to work well in the range of 1 μM-10 mM. **Pudza *et al.* (2020)[45]** have modified a glassy carbon electrode with carbon dots and gold nanoparticles for the detection of Cd (II), Pb (II), and Cu (II) ions. Electrode worked well in the concentration range of 0.01-0.27 ppm for all the heavy metal ions. The detection limit of the electrode was found to be 0.0028, 0.0042, and 0.014 ppm for Cd (II), Pb (II), and Cu (II) ions, respectively.

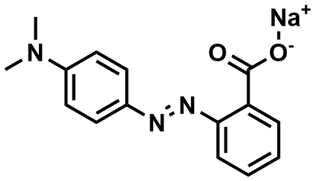

2.13

Shishtawy *et al.* (2018)[46] have developed an electrochemical sensor for the selective detection of Cd (II) ions by modifying the glassy electrode with a synthesized Schiff base (2.14). A thin film of Schiff base was fabricated on an electrode and linear response was obtained for Cd (II) ions within the range of 0.1 nM to 0.1 mM. The limit of detection and limit of quantification was found to be 1.62 pM and 106.67 pM, respectively. **Khan *et al.* (2019)[47]** have synthesized carboxyl-functionalized nanowires which were then fabricated on glassy carbon electrode for the selective detection of Ce (III) ions. The probe worked well in a linear concentration range of 0.1 nM-0.01 mM with a detection limit of 96.03 pM. For

practical application, Ce (III) was detected in environmental samples as well as from toxic chemicals.

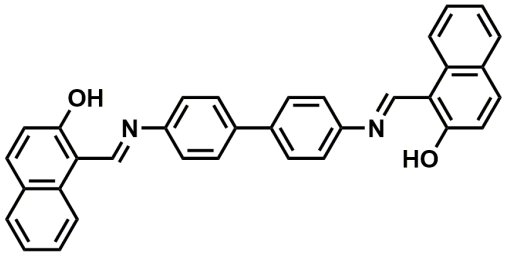

2.14

Arfin *et al.* (2019)[48] used a solution casting method to fabricate a Pb (II) ion-selective system using polyaniline-zirconium (IV) iodate (PANI-ZrI) composite. Due to the presence of negative charge on the surface of ZrI, it displayed selectivity for the Pb (II) cation. To evaluate Pb (II) from urine samples, **Frenandez *et al.* (2020)**[49] modified an electrode with high biocompatibility, excellent conducting capability, and a high surface-to-volume ratio are all achieved by the adsorption of gold nanoparticles on the electrode's surface. With a 99-107% recovery rate, the proposed method was used to assess Pb (II) from spiked urine samples. **Ali *et al.* (2017)**[50] used four Schiff base ionophores to create a plasticized carbon paste electrode. Via potentiometric and voltammetry reaction, the electrode showed a selective response to Co (II) ions. It followed the Nernstian response and could function in a broad pH range. This sensor was known to perform well over the ICP-AES process.

Baghayeri *et al.* (2019)[51] have developed a voltammetric sensor based on magnetic graphene oxide functionalized with poly (amidoamine) dendrimer for the selective recognition of Pb (II) and Cd (II) ions. The metal ion detection limit was discovered to be $6.2x10^{-10}$ M. **Aqlan *et al.* (2019)**[52] announced the use of a tetradentate Schiff base ligand in the fabrication of a Pb (II) ion sensor with a binder/GCE electrode. In real environmental samples, the electrode was used to detect Pb (II) ions. **Maleki *et al.* (2019)**[53] developed an electrochemical sensor that uses voltammetry technique to identify Cd (II) and Pb (II) ions using this sensor. Modifier amount, pH, supporting electrolyte, potential, and deposition time were all optimized. Under optimized conditions, the lower detection limits for Pb (II) and Cd (II) ions were found to be $8.21x10^{-10}$ M and $1.8x10^{-9}$ M, respectively.

Miao *et al.* (2018)[54] developed an electrode for the detection of Hg (II) ions. Performance of electrode was improved by introducing multiwalled carbon nanotubes, resulting in a high

selectivity of the electrode for Hg (II) ions. The detection limit was discovered to be $4.1x10^{-11}$ mol L^{-1}. Hg (II) ions were successfully detected in seafood using the proposed electrode. **Jeromiyas *et al.* (2019)[55]** reported a reusable electrode that was anchored with bismuth nanoparticles in order to improve its response towards the metal ions. Hg (II) ions were detected selectively using this system. Cyclic voltammetry and differential pulse voltammetry were used to investigate the relationship between Bi-nanocomposite modified SPE and Hg (II). With real-life detection in tap water, human serum, fish oil tablet, and urine samples, the limit of detection for Hg (II) was found to be 0.2 nM with a fabricated electrode.

A Fe (II) ion-selective sensor (2.15) has been developed by **Kumar *et al.* (2017)[56]** The electrode's output was enhanced after it was updated with multi-walled carbon nanotubes. For improved electrode efficiency, various factors such as the amount of ionophore, anion excluder, plasticizers, and multi-walled carbon nanotubes were optimized. It was also used to detect Fe (II) ions in real-life samples. Proposed interactions between analyte and target species were backed by DFT (2.16) studies. The same group has reported another potentiometric and voltammetric sensor for the detection of Cu (II) ions. The proposed ionophore worked well in the concentration range of $1.0x10^{-7}$–$1.0x10^{-1}$ mol/L with a detection limit of $1.0x10^{-7}$ mol/L.[57]

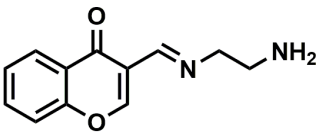

2.15

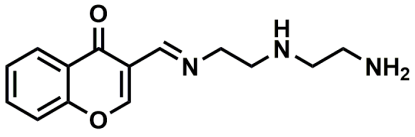

2.16

Li and colleagues (2017)[58] developed a system that favors Hg (II) ions over other cations. The proposed method was used to detect Hg (II) ions in tremella samples, with 99.8-103.4% recovery rate. The sensing mechanism was established using electrochemical response of the probe, quantum chemical computation, and X-ray photoelectron spectroscopy. A disposable voltammetric sensor for the detection of Fe (II) ions has been reported by **Rana *et al.* (2018)[59]** Modification of SPE with Schiff base (2.17) was validated with SEM and EDX spectroscopy. Detailed voltammetric discussion is carried out in order to understand the oxidative and reductive nature of the probe and its Fe (II) complex. The detection limit for Fe (II) ions was discovered to be 0.54 M.

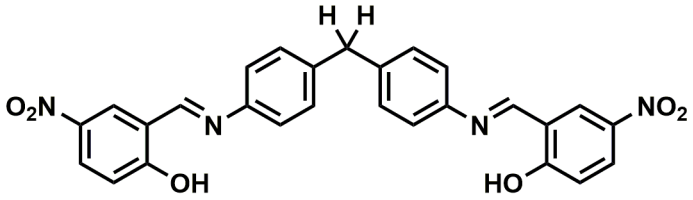

2.17

Deshmukh *et al.* (2018)[60] have demonstrated an approach to detect Ni (II) ions over other cations. They have synthesized a polyaniline nanocomposite using carbon nanotubes. Also, EDTA was used during synthesis to provide a good chelating site for Ni (II) ions. Probe worked well in the aqueous media due to ring-like structure of composite. The lower detection limit was found to be $1x10^{-3}$ mM/L for Ni ions using differential pulse voltammetry. A similar research group has modified the properties of probe by adding different chemicals to make a new receptor for the selective detection of Cu (II) ions. The probe showed selectivity without the interference of Pb (II), Cd (II), Ni (II), and Co (II) ions. Detection limit of the probe was found to be 1.4 μM with a sensitivity of 189 mA/μM.[61]

Xu *et al.* (2020)[62] have modified a glassy carbon electrode with polypyrrole nanoparticles for the detection of Pb (II) ions. The electrode has detected Pb (II) in the concentration range of 0.1-50 μM with a detection limit of 55 nM. Electrode showed a selective response to Pb (II) without interference from Hg (II) and Cu (II). For practical application, Pb (II) was detected in wastewater samples. **Ahmad *et al.* (2017)[63]** have synthesized an organic molecule and its electrochemical response was checked for various cations. Among all the cations, receptor responded selectively towards Pb (II) ions. Glassy carbon electrode was used to measure the response and it gives a linear response in the range of 0.1 nM-0.1 mM. The limit of detection and limit of quantification was found to be 3.95 μA and 0.02 nM, respectively. A prepared electrochemical system was applied on real water samples for the detection of Pb (II) ions.

Rana *et al.* (2017)[64] have modified a disposable electrode with a Schiff base (2.18) for the detection of Al (III) ions. Response of sensing was obtained by CV and DPV with a detection limit of 2.26 ng/L. Electrode worked well in the concentration range of 0.67-4.59 μg/L. Proposed experimental interactions were supported by DFT calculations. Al (III) was detected in natural water samples for practical application purposes. The same group has reported another Schiff base (2.19) modified electrode for the detection of Zn (II) ions. The probe showed a detection range of 0.47-5.56 μM with a LoD of 0.92 μM. CV and DPV

proposed interactions were supported by DFT calculations. Also, Zn (II) was detected in various food samples around the characteristic peak at -0.59 and 0.55 V.[65]

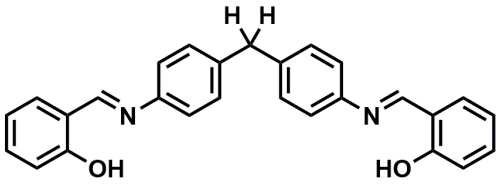

2.18

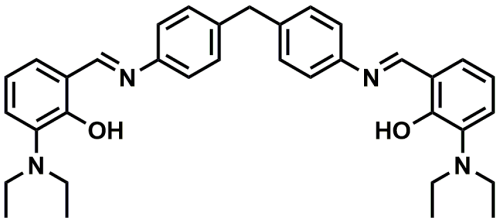

2.19

Sha *et al.* (2017)[66] have decorated an electrode with an iron-modified matrix. The probe showed a response to multiple analytes such as Cd (II), Cu (II), and Pb (II) ions. Electrochemical behavior of the probe was checked using differential pulse voltammetry. The limit of detection for Cd (II), Cu (II), Pb (II) was found to be $1.92x10^{-2}$ μM, $8.78x10^{-2}$ μM, and $0.98x10^{-2}$ μM, respectively. **Kakob *et al.* (2019)[67]** have designed a recognition layer modified with amino acids for the detection of metal ions. Probe acted as a multiple analyte detector by giving response to Zn (II), Cd (II), Cu (II), and Hg (II) ions with a detection limit of 8.29, 5.77, 3.01, and 5.89 pM respectively. Various electrochemical techniques were used to record the response of the electrode. Experimental results of the electrode were supported with theoretical calculations. **Wu *et al.* (2019)[68]** have modified a glassy carbon electrode with magnetite nanoparticles for the detection of heavy metal ions. Electrode gave a response to Cd (II), Pb (II), Hg (II), Zn (II), and Cu (II) ions and for practical application, metal ions were detected from water and rice samples.

2.2 Anion Sensor

Anions are important in our daily lives, as they are required for physiological function and a variety of industrial processes. As a result, anionic species can be harmful to the ecosystem either need for growth or pollute the environment. Anion sensor design is more difficult than metal ion sensor design due to the larger size of anions corresponding to isoelectronic cations and hence the lower charge to radius ratio of anions. Regardless of these factors, there are a large number of receptors in the literature that have been shown to recognize different types of anions. There are a lot of reports where designed probes have detected anions via optical or electrochemical methods.

2.2.1 Spectrophotometric method

Carbon Quantum Dots (CQDs) based sensors for anion detection

Zou *et al.* (2020)[69] have synthesized lanthanide-modified carbon quantum dots with tunable photoluminescence. This fluorescent probe was used to detect the MnO_4^- ion in an aqueous solution while preventing interference from other anions. CQDs modified with lanthanide could be used in photocatalytic sensors. **Baragau *et al.* (2020)[70]** used a continuous hydrothermal flow process to synthesize nitrogen-doped CQDs from citric acid. Without modifying their structure, these NCQDs showed selectivity for toxic and carcinogenic Cr (VI) ions. Chemosensor has demonstrated selectivity up to a detection limit of 0.365 ppm. **Jiang *et al.* (2020)[71]** used chitin as a source for NCQD synthesis and detected ClO^- ions among other anions in the solution. For ClO^- ions, the detection limit was found to be 1.47 M, and the particles performed well in the linear range of 0-50 M. When nanoparticles were illuminated with a UV light, their luminescence shifted from bright blue fluorescence to dark blue fluorescence.

Feng *et al.* (2020)[72] used 3-mercapto-1,2-propanediol as a bridge material to make boronic acid decorated carbon dots. The fluorescent "turn off" state was observed in the presence of F^- ions and the detection limit was determined to be 1.5 M, with a working range of 9-117 M. The logic gate was also prepared based on the response. A functional hybrid of graphene quantum dots and cobalt pyrene-derivatized phthalocyanine has been synthesized by **Achadu *et al.* (2019)[73]** These nanoprobes were found to be selective for CN^- ions, with a detection limit of 0.5 nM. In the linear range of 1-50 nM, the probe performed admirably. CN^- ions were retrieved from spiked samples using the proposed hybrid structure for real-life sampling.

For the detection of nitrite anion in aqueous media, **Jana *et al.* (2019)[74]** prepared nitrogen-doped CQDs which showed selective response to nitrite ions with fluorescence switch-off behavior. The probe's detection limit was found to be 7.9 nM, with a linear range of 2.3-7.7 M. The nitrite anion was found in various water samples as well as in HeLa cells for real-time applications. **Shahbazi *et al.* (2019)[75]** developed gold nanoparticles for evaluating sulfide ions in aqueous media. The effect of pH, temperature and time on the selective detective detection of sulfide ions was optimized. The target ion was detected by gold nanoparticles with a detection limit of 0.57 ppm.

Schiff base sensors for anion detection

The condensation reaction of 3, 5-diiodosalicyaldehyde with isoniazid was used to create a new Schiff base (2.20) by **Shree *et al.* (2020)[76]** Via colorimetric sensing, the probe demonstrated selectivity for F- ions with a detection limit of $0.1x10^{-6}$ M. For naked-eye detection, the color of the probe's solution changed from pale yellow to orange. **Li *et al.* (2018)[77]** developed a Schiff base (2.21), namely 2-hydroxy-1-naphthaldehyde-2-quinoline acylhydrazone. F^- ions were detected using this colorimetric probe that changed color from colorless to yellow. With a binding stoichiometry of 1: 2, the detection limit was found to be $8.28x10^{-6}$ M. The intermolecular proton transfer process that occurred between the hydroxyl group of ligand and F^- ion was suggested as a plausible mechanism.

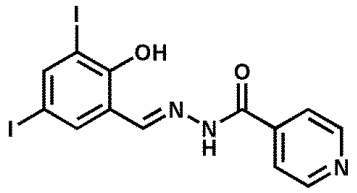

2.20

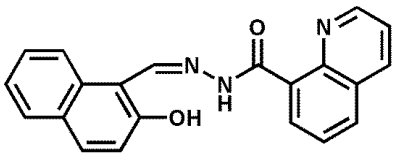

2.21

Alreja *et al.* (2018)[78] used 1, 10-phenanthroline to make Schiff base (2.22), 2-((E)-(1, 10-phenanthroline-5-ylimino) methyl) phenol. In an acetonitrile medium, the probe exhibited chromogenic activity against F^- ions. Owing to the presence of a new band in the visible field, the color of the solution changed from colorless to yellow. The probe was programmed into an INHIBIT logic gate for real-time use. **Dey *et al.* (2020)[79]** used picolinohydrazide-naphthol (2.23), a Schiff base reagent, to detect CN^- ions at the trace level. In a DMSO/Water solvent medium, the color of the solution changed from colorless to yellow. The deprotonation mechanism was suggested and confirmed by ^1H NMR titration. CN^- ions were detected in water samples for real-life application of the probe, and a paper strip system was also created.

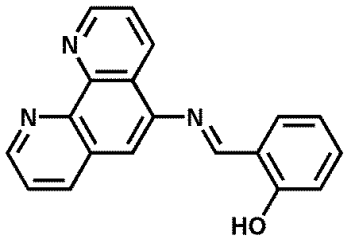

2.22

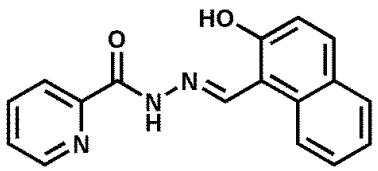

2.23

Chowdhury *et al.* (2017)[80] prepared a Schiff base chemoreceptor with hydrazine functionalization for the selective detection of F^- ions. The receptor's response was enhanced by adding more NH and C=N units to the structure. Cyclic voltammetry and ^{19}F NMR were used to confirm the receptor's chromogenic response. The binding constant was found to be $0.84x10^5$ M^- with a detection limit of $1.42x10^{-5}$ M. **Purkait *et al.* (2018)[81]** synthesized a multi responsive Schiff base for I^- ions among various anions in THF solvent. With a binding stoichiometry of 1: 1, the color of the solution changes from slightly yellow to orange-red, following the colorimetric reaction. 5 nM was discovered to be the detection limit of the probe.

Saini *et al.* (2018)[82] used a greener approach to synthesize hydrazone-based Schiff base. For both cations and anions, the probe operated as a multi-analyte detector. With detection limits of 0.073 ppm and 0.023 ppm, the probe detected both CN^- and F^- ions among various anions. Job's interpretation of the plot indicated 1: 2 stoichiometry for CN^- ions and a 1: 1 stoichiometry for F^- ions. ICT and PET processes were plausible mechanisms for anionic interactions.

Miscellaneous compounds for anion detection

Liu *et al.* (2020)[83] have synthesized a squaraine dye (2.24) for the detection of CO_3^{2-} ions using spectroscopic techniques. First Fe (III) complex was formed then sequentially CO_3^{2-} was detected. The limit of detection for both Fe (III) and CO_3^{2-} was found to be 0.14 and 0.17 μM. Following the spectroscopic response INHIBIT logic gate was constructed. **Liu *et al*. (2017)[84]** have synthesized an ether substituted squaraine dye for selective detection of CN^- ions. The probe exhibited strong absorption and intense fluorescence emission in the far-red spectral region. The probe detected CN^- ions with a detection limit of 1.7 μM.

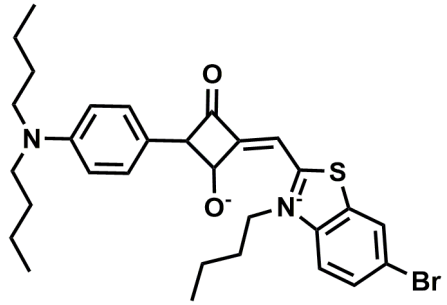

2.24

Alkis *et al.* (2017)[85] have synthesized a coumarin-pyrazole-pyridine triad for the detection of F^- ions in DMSO solvent. Probe exhibited naked eye detection following a stoichiometry of 1:1. Experimental results were supported by computational calculations. **Krishnaveni *et al.* (2021)**[86] have designed hydrazine-appended pyrazole-based moiety (2.25) for the detection of F^- ions in aqueous DMSO solvent. Naked eye response of the probe was confirmed by ^{19}FNMR and DFT calculations. From the Jobs plot, the stoichiometry was found to be 1:1 with an association constant of 0.26×10^{-4} M. **Yalcin *et al.* (2018)**[87] have synthesized a coumarin-pyrazole-pyridine triad for the selective detection of F^- ions in DMSO solvent. Probe exists in different tautomeric forms and exhibits acid chromic properties. ^{1}HNMR titrations confirmed the deprotonation mechanism with a stoichiometry value of 1:1.

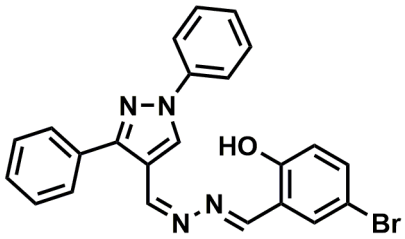

2.25

Wu *et al.* (2017)[88] have synthesized a quinolone-based chemosensor (2.26) for the sequential detection of CN^- ions using Cu (II) complex of the probe. All spectroscopic studies were carried out in an aqueous DMSO solvent system. The detection limit for CN^- ions was found to be 4.3 μM without the interference from other anions present in the same solution. **Kim *et al.* (2019)**[89] have designed a sensor (2.27) for the detection of ClO^- ions via a color variation from yellow to colorless. The detection limit of the probe was found to be 3.10 μM. Experimental results were supported with computational studies. **Bhaskar *et al.* (2019)**[90] have designed a reversible chemosensor for the selective detection of CN^- ions using an eco-friendly method. Probe gave naked eye response in the presence of CN^- ions from yellow to orange. The binding mechanism of the probe was established to be an ICT mechanism and confirmed by ^{1}HNMR titrations. The detection limit was found to be 6.88 μM with a binding stoichiometry of 1:2. Following the spectroscopic behavior, IMPLICATION logic gate was constructed.

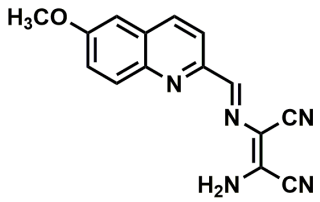

2.26

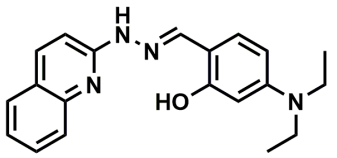

2.27

Long *et al.* (2018)[91] developed a rhodamine-based probe (2.28) for the detection of CN^- ions selectively. The presence of cyanide was observed with the naked eye, with a detection maximum of $3.54x10^{-7}$ M. Probe found cyanide in tap water, bitter almond, and germinated potato for possible use. **Long *et al.* (2019)**[92] developed a rhodamine B hydrazone-based derivative (2.29) for the detection of CN^- ions in an aqueous solution. For CN^- ions, the probe showed both colorimetric and fluorimetric responses. The suggested sensing mechanism was deprotonation and ICT. In sprouting potatoes, a chemosensor was successfully used to detect CN^- ions.

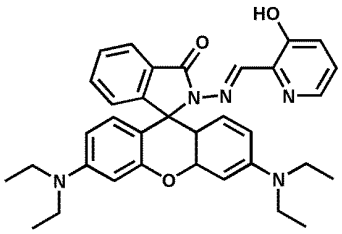

2.28

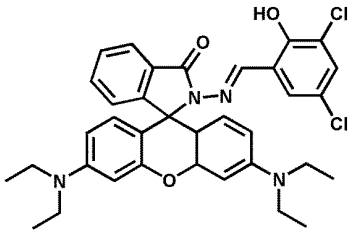

2.29

Roy *et al.* (2019)[93] developed a rhodamine-based moiety (2.30) for the detection of bisulfite anion selectively. The molecule was naturally weakly emissive, but addition of the bisulfite ion resulted in heavy probe emission with a color range of faint to pink. For the bisulfite ion, the detection limit was found to be 0.4 M. **Upadhyay *et al.* (2017)**[94] synthesized Rhodamine 6G hydrazide for the selective detection of HSO_4^- ions in an aqueous medium. The presence of an anion in the cavity of rhodamine caused the spirolactum ring to open, as shown by the color change from colorless to pink. For possible use, INHIBIT logic gate and paper strips were prepared.

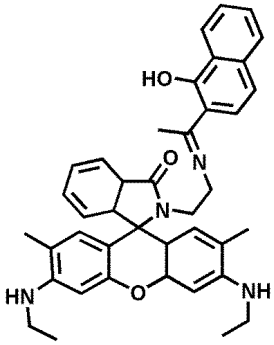

2.30

Zhu *et al.* (2020)[95] synthesized a probe (2.31) for colorimetric determination of ClO^- ions in a DMSO/PBS buffer. As ClO^- was added to the probe solution, the rhodamine moiety's ring-opened, and the color of the solution changed from blue to orange. The mechanism was demonstrated using the FRET mechanism and the probe's fluorescence ratiometric behavior towards the ClO^- ion. Chemosensor was used for cell staining purposes without interference from reactive oxygen species (ROS).

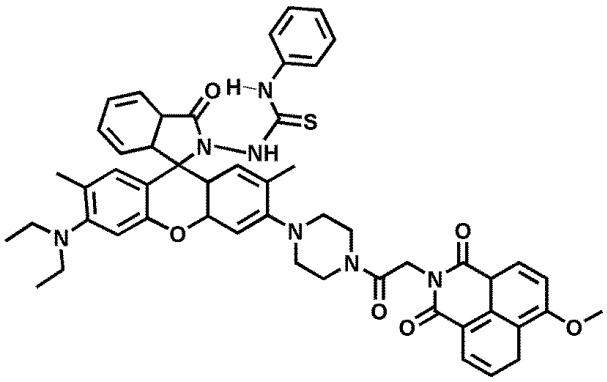

2.31

A new six-membered rhodamine-based fluorescent probe has been developed by **Wang *et al.* (2019)**[96] ClO^- ions were found in both water and HUVEC cells using the probe. Selective behavior was attributed to the twisted nature of the probe. With a detection limit of 12 nM, the probe detected ClO^- ion in tap water and swimming pool water.

2.2.2 Electrochemical methods for the detection of anions

Anions are important in a variety of environmental, industrial, and physiological activities, thus detecting and quantifying them is important. Electroanalytical sensors can be used to perform selective, sensitive, low-cost, portable, and real-time analyses of anion presence using appropriate combinations of selective (non-covalent) recognition and transduction.

Electrochemical anion sensing has gotten a lot of attention in the last two decades, due to significant advances in anion supramolecular chemistry.

Mejri *et al.* (2018)[97] have modified an electrode with curcumin (2.32) for the determination of F^- and CN^- ions. The limit of detection was found to be 17.2 nM and 28.3 nM for F^- and CN^-, respectively. For practical applications, the electrode was applied in river water, petrochemical refinery wastewater for the detection of anions. **Zhang *et al.* (2018)[98]** have developed a new ferrocenophane receptor for the detection of $H_2PO_4^-$ ions. The receptor was prepared using "click reaction" between amide and triazole donor atoms. Electrochemical behavior suggests a large potential shift in the case of complex as compared to the receptor. This large potential shift was supported with ^{1}HNMR and DFT calculations.

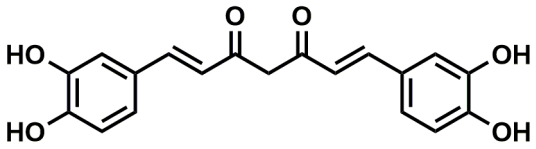

2.32

A carbon electrode was developed by **Cunha-Silva *et al.* (2019)[99]** for the determination of I^- using a single drop of sample. They compared the behaviour of electrode with and without chitosan coating modification in their research. A chitosan-coated working electrode was found to be a better iodine sensor with a detection limit of $1x10^{-8}$ M. The results of voltammetry were supported by the spectrophotometric method. The same group has reported another method of modification of electrode for the determination of Br^- ions. They have modified the electrode with rhodium nanoparticles for enhancement sensitivity. The electrode has detected Br^- ions with a detection limit of 39 μM, with a calibration plot up to 40 mM.

Liu *et al.* (2017)[100] modified an electrode with nitrogen-doped hollow mesoporous carbon spheres. With a high sensitivity of 1.49 Acm^{-2} M^{-1}, SPE has demonstrated enzyme and metal-free electrochemical detection of superoxide anions. **Bujes-Garrido *et al.* (2017)[101]** developed a disposable and wearable SPE for detecting Cl^- ions. In the presence of chloride ions, the established sensor measures the Nernestian change of the voltammetric peak potential of ferrocenemethanol. Using amide and thiourea donors, **Huang *et al.* (2018)[102]** synthesized two ferrocene-pyrene dyads. In the presence of F^-, OAc^-, and $H_2PO_4^-$, both probes showed a strong negative change in the ferrocene-based redox potential. They have

also synthesized a ferrocene-appended dansyl fluorophore for the selective detection of F^- ions using CV and DPV. An electrochemical shift in complex was investigated by ^{1}HNMR technique and DFT calculations.

Bisimidazole-based unit with naphthoquinone as a signaling unit (2.33) has been synthesized by **Lakshmi *et al.* (2019)[103]** With a color shift from yellow to brown, the probe detected CN^- ions in an aqueous HEPES buffer-DMSO medium. The probe had 1: 2 stoichiometry. DFT studies have suggested that deprotonation of the imidazole N-H proton as a sensing mechanism. **Chaudhuri *et al.* (2018)[104]** synthesized five receptors based on arylamino-naphthoquinone using the same mechanism. The electron-donating and withdrawing groups attached to receptors gave them different redox properties. Following a deprotonation process of the N-H moiety by the cyanide ions, all receptors displayed detection limits in the range of 10^{-8} M.

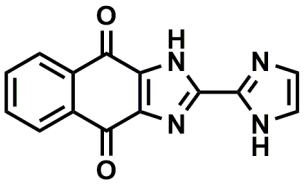

2.33

Sudha *et al.* (2018)[105] have developed an electrode for the detection of sulfite and nitrite anions. The electrochemical activity of the electrode was investigated using techniques CV and DPV. They have also modified the glassy carbon electrode with copper oxide for the detection of sulfite and nitrite anions. Electrocatalytic oxidation of both the anions was detected using CV and DPV techniques. The difference between the oxidation peak potential of sulfite and nitrite was 400 mV. The detection limit for both sulfite and nitrite was found to be 21.10 μM and 13.6 μM, respectively. A glassy carbon electrode modified with carboxyl graphene, polypyrrole, and chitosan nanocomposite has been reported by **Xiao *et al.* (2018)[106]** CV and electrochemical impedance spectroscopy was used to characterize electrochemical behavior. The DPV response of the modified electrode has detected nitrite anions up to a detection limit of 0.02 M.

Han *et al.* (2019)[107] developed a composite for nitrite anion detection. Because of the large surface area, good conductivity, and synergistic catalysis of each part, the composite had excellent electroxidative activity against nitrite ions with a detection limit of 1.0 M. **Yan *et al.* (2020)[108]** have modified an electrode on which the reduced electrochemical signal of

potassium ferricyanide was used to record the response for F^- ions on the electrode surface. The sensor that was developed was successfully used to detect F^- ions in tap water. For the selective detection of sulfate in water, **Gulebiewski *et al.* (2019)[109]** developed an electrochemical sensor consisting of a gold electrode modified by cyclopeptide and a bis (dipyrromethene) Cu (II) or Co (II) complex. In water, the sensor showed sensitivity at the picomolar level. Metal embedded in between the electrode surface and the cyclopeptide was responsible for the redox properties of the sensor.

Wu *et al.* (2019)[110] have modified an electrode with silver nanoparticles for the selective detection of superoxide anion. The probe can detect target anion with a detection limit of 2.32 fM at a working potential of -0.5 V. **Durai *et al.* (2020)[111]** have synthesized a novel hydrazone-based sensor (2.34)for the detection of F^- ions in DMSO solvent. The colorimetric response of the probe was supported with CV and DPV techniques. The detection limit was found to be 0.02 μM and ^{1}HNMR titration confirmed the electrochemical interactions. For real-life sampling, F^- was detected in environmental samples and toothpaste.

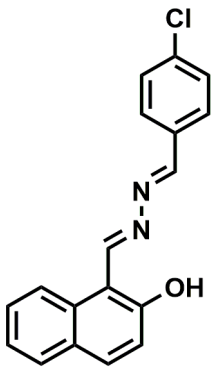

2.34

Riojas *et al.* (2019)[112] proposed a new electrochemical sensor for the detection of CN^- ions at trace levels. In this sensor, silver sulfide nanoparticles and hierarchical porous carbon were added to a carbon paste electrode. The morphology of the electrode was studied using TEM and SEM. Electrode detected CN^- ions within the linear range of $5.9x10^{-7}$ to $1.1x10^{-3}$ mol/L with a detection limit of $7x10^{-8}$ mol/L via square-wave adsorptive anodic stripping voltammetry. **Zhang *et al.* (2020)[113]** recorded the electrode response using cyclic voltammetry and amperometry techniques. 40 nM, 0.7192 A, and 0.1 to 210 M were found to be the detection maximum, sensitivity, and working range, respectively for cyanide ions.

Electrochemical findings have also been successfully applied to real-world samples such as apricot juice for the detection of cyanide ions.

Kaur *et al.* (2017)[114] have modified a gold electrode by adding a redox-active layer made of dipyrromethene complexed with Cu (II) and Co (II). The modified electrode showed electrochemical signal sensing of Cl^- ions. Apart from Cl^- ions, the probe showed selectivity for SO_4^{-2} and Br^- ions in the picomolar range, following the selectivity series $Cl^- > SO_4^{-2} > Br^-$. Higher selectivity for Cl^- ions could be attributed to the higher binding constant and stronger electronic effect. **Nguelo *et al.* (2018)[115]** have developed an electrochemical sensor for the detection of thiocyante ions. Various parameters such as accumulation time, electrolyte concentration were optimized. Electrode gave a good linear response in the concentration range of $1x10^{-6} – 1x10^{-5}$ M with a detection limit of 15 nM. Various anions such as NO_3^-, Cl^-, SO_4^{2-}, and CH_3COO^- interfered in the selective response of SCN^- ions. The sensor was applied to detect SCN^- in human saliva samples.

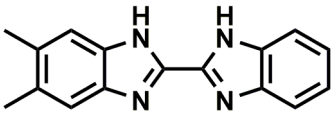

2.35

Cunha-Silva *et al.* (2019)[116] have used platinum electrode for the detection of Cl^- ions. Electrode gave reproducible results with a detection limit of 0.76 mM and worked well in the concentration range of 150 mM. **Cui *et al.* (2020)[117]** have modified an electrode for detection of O_2^- using tetraphenyl porphine and graphene oxide. Performance of electrode was recorded using cyclic voltammetry, electrochemical impedance spectroscopy. Furthermore, differential pulse voltammetry was used to analyse the performance of electrode. Electrode worked well in the concentration range of 0.0-110.0 μmol/L with a detection limit of 0.03 μmol.

Gauthama *et al.* (2020)[118] have synthesized a Schiff base (2.36) using isatin hydrazones for the selective detection of F^- ions. The probe detected anion in two different solvent media i.e. in pure acetonitrile and aqueous acetonitrile with a detection limit of 0.45 and 0.41 ppm. A potential difference of 1.06 V was observed for complex using CV and DPV techniques. The electrochemical response was supported by ^{1}HNMR titrations.

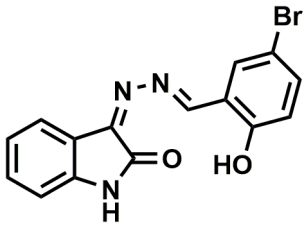

2.36

Mahmoud *et al.* (2021)[119] have modified a carbon paste electrode for the detection of CN^- ions. Performance of the electrode was recorded by CV, DPV, and electrochemical impedance spectroscopy. By observing the anodic peak behavior of the electrode towards CN^- ions, it was found that the electrode gave a linear response in the range of 1.87-25 μM with a detection limit of 0.60 μM. For real-life sampling, electrode was applied in different environmental samples. **Ling *et al.* (2019)[120]** have appended ferrocene with N-tosyl hydrazones for the sensing of F^- ions. With an increasing amount of F^- ions, oxidation peak current decreases and shifted anodically, and in presence of an excess of F^- ions, CV becomes irreversible.

From the review of literature, it can be seen that there is hardly any molecule based on triphenyl ether derivative reported as an ionophore for the sensing of small molecules like cyanide, fluoride, aluminium, and copper. A research problem was conceived to study triphenylether and triphenylamine molecules with variable hetero atom environments. Anticipating the rigidity of triphenyl ethers and the complex forming tendency of the hetero atoms, different structures of new molecules were designed. Since chemical sensing of the above-mentioned target ions using host-guest theory of ionophores depends largely on two important principles of (a) steric consideration and (b) electronic environment in the pseudo cavity. In order to study the above hypothesis, several experiments for the synthesis of new molecules, their characterization were planned. Interaction of the receptor molecules with the target species was studied using optical and voltammetric techniques as chemical sensing tools. Validation of the proposed molecules as chemical sensors was planned through real-time analysis of samples using the proposed receptors.

References

1. D. Cao, Z. Liu, P. Verwilst, S. Koo, P. Jangjili, J. S. Kim and W. Lin, *Chemical Reviews*, 2019, **119**, 10403-10519.

2. L. Mao, Y. Liu, S. Yang, Y. Li, X. Zhang and Y. Wei, *Dyes and Pigments*, 2019, **162**, 611-623.

3. H. N. Kim, Z. Guo, W. Zhu, J. Yoon and H. Tian, *Chemical Society Reviews*, 2011, **40**, 79-93.

4. Z. Xu, X. Chen, H. N. Kim and J. Yoon, *Chemical Society Reviews*, 2010, **39**, 127-137.

5. M. C.-L. Yeung and V. W.-W. Yam, *Chemical Society Reviews*, 2015, **44**, 4192-4202.

6. B. Kaur, N. Kaur and S. Kumar, *Coordination Chemistry Reviews*, 2018, **358**, 13-69.

7. S. Y. Lim, W. Shen and Z. Gao, *Chemical Society Reviews*, 2015, **44**, 362-381.

8. J. C. E. da Silva and H. M. Gonçalves, *TrAC Trends in Analytical Chemistry*, 2011, **30**, 1327-1336.

9. Y. Dong, J. Cai, X. You and Y. Chi, *Analyst*, 2015, **140**, 7468-7486.

10. H. Fu, Z. Ji, X. Chen, A. Cheng, S. Liu, P. Gong, G. Li, G. Chen, Z. Sun and X. Zhao, *Analytical and Bioanalytical Chemistry*, 2017, **409**, 2373-2382.

11. J. Wang, R. S. Li, H. Z. Zhang, N. Wang, Z. Zhang and C. Z. Huang, *Biosensors and Bioelectronics*, 2017, **97**, 157-163.

12. Y. Song, C. Zhu, J. Song, H. Li, D. Du and Y. Lin, *ACS Applied Materials & Interfaces*, 2017, **9**, 7399-7405.

13. P. Wu, W. Li, Q. Wu, Y. Liu and S. Liu, *RSC Advances*, 2017, **7**, 44144-44153.

14. V. K. Singh, V. Singh, P. K. Yadav, S. Chandra, D. Bano, V. Kumar, B. Koch, M. Talat and S. H. Hasan, *New Journal of Chemistry*, 2018, **42**, 12990-12997.

15. Y. Zhang, X. Fang, H. Zhao and Z. Li, *Talanta*, 2018, **181**, 318-325.

16. F. Du, Z. Cheng, W. Tan, L. Sun and G. Ruan, *Spectrochimica Acta Part A: Molecular and Biomolecular Spectroscopy*, 2020, **226**, 117602.

17. B. Han, T. Peng, M. Yu, C. Chi, Y. Li, X. Hu and G. He, *New Journal of Chemistry*, 2018, **42**, 13651-13659.

18. A. L. Berhanu, I. Mohiuddin, A. K. Malik, J. S. Aulakh, V. Kumar and K.-H. Kim, *TrAC Trends in Analytical Chemistry*, 2019, **116**, 74-91.

19. J. Harathi and K. Thenmozhi, *Materials Chemistry Frontiers*, 2020, **4**, 1471-1482.

20. H.-F. Xie, C.-J. Yu, Y.-L. Huang, H. Xu, Q.-L. Zhang, X.-H. Sun, X. Feng and C. Redshaw, *Materials Chemistry Frontiers*, 2020, **4**, 1500-1506.

21. J. Xiong, Z. Li, J. Tan, S. Ji, J. Sun, X. Li and Y. Huo, *Analyst*, 2018, **143**, 4870-4886.

22. L. Patra, S. Das, S. Gharami, K. Aich and T. K. Mondal, *New Journal of Chemistry*, 2018, **42**, 19076-19082.

23. S. M. Saleh, R. Ali and I. A. Ali, *Spectrochimica Acta Part A: Molecular and Biomolecular Spectroscopy*, 2017, **183**, 225-231.

24. M. Kumar, A. Kumar, M. S. H. Faizi, S. Kumar, M. K. Singh, S. K. Sahu, S. Kishor and R. P. John, *Sensors and Actuators B: Chemical*, 2018, **260**, 888-899.

25. J. Sun, B. Ye, G. Xia and H. Wang, *Sensors and Actuators B: Chemical*, 2017, **249**, 386-394.

26. Y. Liu, L. Wang, C. Guo and Y. Hou, *Tetrahedron Letters*, 2018, **59**, 3930-3933.

27. M. Zhu, W. Wang, J. Liu, R. Na, Z. Li and Y. Wang, *Journal of Molecular Liquids*, 2020, **303**, 112680.

28. H. Song and Z. Zhang, *Dyes and Pigments*, 2019, **165**, 172-181.

29. P. Wang, J. Wu, Y. An and Y. Liao, *Spectrochimica Acta Part A: Molecular and Biomolecular Spectroscopy*, 2019, **220**, 117140.

30. C.-L. Li, P.-h. Lu, S.-Y. Lin and A.-T. Wu, *Journal of Photochemistry and Photobiology A: Chemistry*, 2019, **385**, 112088.

31. H. N. Kim, M. H. Lee, H. J. Kim, J. S. Kim and J. Yoon, *Chemical Society Reviews*, 2008, **37**, 1465-1472.

32. R. Zhang, F. Yan, Y. Huang, D. Kong, Q. Ye, J. Xu and L. Chen, *Rsc Advances*, 2016, **6**, 50732-50760.

33. S. Mondal, S. K. Manna, S. Pathak, A. Al Masum and S. Mukhopadhyay, *New Journal of Chemistry*, 2019, **43**, 3513-3519.

34. R. Alam, R. Bhowmick, A. S. M. Islam, K. Chaudhuri and M. Ali, *New Journal of Chemistry*, 2017, **41**, 8359-8369.

35. F.-K. Tang, S.-M. Chan, T. Wang, C.-S. Kwan, R. Huang, Z. Cai and K. C.-F. Leung, *Talanta*, 2020, **210**, 120634.

36. M. Maniyazagan, R. Mariadasse, J. Jeyakanthan, N. Lokanath, S. Naveen, K. Premkumar, P. Muthuraja, P. Manisankar and T. Stalin, *Sensors and Actuators B: Chemical*, 2017, **238**, 565-577.

37. A. S. Murugan, N. Vidhyalakshmi, U. Ramesh and J. Annaraj, *Sensors and Actuators B: Chemical*, 2018, **274**, 22-29.

38. Z. Wang, S. Cui, S. Qiu and S. Pu, *RSC Advances*, 2019, **9**, 6021-6026.

39. C. Liu, J.-c. Qin, J. Xue, L.-m. Tian, T.-r. Li and Z.-y. Yang, *Journal of Photochemistry and Photobiology A: Chemistry*, 2019, **385**, 112091.

40. E. Zdrachek and E. Bakker, *Analytical Chemistry*, 2018, **91**, 2-26.

41. R. Hein, P. D. Beer and J. J. Davis, *Chemical Reviews*, 2020, **120**, 1888-1935.

42. G. Aragay, J. Pons and A. Merkoçi, *Chemical Reviews*, 2011, **111**, 3433-3458.

43. E. Y. Frag, M. E. Mohamed and Y. Samy, *Russian Journal of Electrochemistry*, 2019, **55**, 841-849.

44. S. Kumbhat and U. Singh, *Journal of Electroanalytical Chemistry*, 2018, **809**, 31-35.

45. M. Y. Pudza, Z. Z. Abidin, S. Abdul-Rashid, F. M. Yasin, A. S. M. Noor and J. Abdullah, *Environmental Science and Pollution Research*, 2020, 1-10.

46. R. M. El-Shishtawy, H. A. Al-Ghamdi, M. Alam, Z. M. Al-amshany, A. M. Asiri and M. M. Rahman, *Chemical Engineering Journal*, 2018, **352**, 225-231.

47. A. A. P. Khan, A. Khan, M. Alam, A. M. Asiri, J. Uddin and M. M. Rahman, *Journal of Molecular Liquids*, 2019, **279**, 392-399.

48. T. Arfin and A. Tarannum, *Journal of Environmental Chemical Engineering*, 2019, **7**, 102811.

49. E. Fernández, L. Vidal, J. Silvestre-Albero and A. Canals, *Microchimica Acta*, 2020, **187**, 1-10.

50. T. A. Ali, G. G. Mohamed, M. Omar and N. M. Hanafy, *Journal of Industrial and Engineering Chemistry*, 2017, **47**, 102-111.

51. M. Baghayeri, H. Alinezhad, M. Fayazi, M. Tarahomi, R. Ghanei-Motlagh and B. Maleki, *Electrochimica Acta*, 2019, **312**, 80-88.

52. F. M. Aqlan, M. Alam, A. M. Asiri, M. E. Zayed, D. A. Al-Eryani, F. A. Al-Zahrani, R. M. El-Shishtawy, J. Uddin and M. M. Rahman, *Journal of Molecular Liquids*, 2019, **281**, 401-406.

53. B. Maleki, M. Baghayeri, M. Ghanei-Motlagh, F. M. Zonoz, A. Amiri, F. Hajizadeh, A. Hosseinifar and E. Esmaeilnezhad, *Measurement*, 2019, **140**, 81-88.

54. J. Miao, X. Wang, Y. Fan, J. Li, L. Zhang, G. Hu, C. He and C. Jin, *Journal of Food and Drug Analysis*, 2018, **26**, 670-677.

55. N. Jeromiyas, E. Elaiyappillai, A. S. Kumar, S.-T. Huang and V. Mani, *Journal of the Taiwan Institute of Chemical Engineers*, 2019, **95**, 466-474.

56. S. Kumar, S. K. Mittal, N. Kaur and R. Kaur, *RSC Advances*, 2017, **7**, 16474-16483.

57. S. Kumar, S. K. Mittal and N. Kaur, *Analytical Methods*, 2019, **11**, 359-366.

58. X.-Q. Li, H.-Q. Liang, Z. Cao, Q. Xiao, Z.-L. Xiao, L.-B. Song, D. Chen and F.-L. Wang, *Materials Science and Engineering: C*, 2017, **72**, 26-33.

59. S. K. Mittal, S. Rana, N. Kaur and C. E. Banks, *Analyst*, 2018, **143**, 2851-2861.

60. M. A. Deshmukh, H. K. Patil, G. A. Bodkhe, M. Yasuzawa, P. Koinkar, A. Ramanavicius, S. Pandey and M. D. Shirsat, *Colloids and Surfaces A: Physicochemical and Engineering Aspects*, 2018, **537**, 303-309.

61. M. A. Deshmukh, H. K. Patil, G. A. Bodkhe, M. Yasuzawa, P. Koinkar, A. Ramanaviciene, M. D. Shirsat and A. Ramanavicius, *Sensors and Actuators B: Chemical*, 2018, **260**, 331-338.

62. T. Xu, H. Dai and Y. Jin, *Microchimica Acta*, 2020, **187**, 1-7.

63. I. Ahmad, M. N. Arshad, M. M. Rahman, A. M. Asiri, T. A. Sheikh and F. M. Aqlan, *Inorganica Chimica Acta*, 2017, **467**, 297-306.

64. S. Rana, S. K. Mittal, N. Singh, J. Singh and C. E. Banks, *Sensors and Actuators B: Chemical*, 2017, **239**, 17-27.

65. S. Rana, S. K. Mittal, N. Kaur and C. E. Banks, *Journal of The Electrochemical Society*, 2019, **166**, B464.

66. H. Sha, Y. Wu and Y. Fan, *Analytical Methods*, 2017, **9**, 5618-5631.

67. T. Kokab, A. Shah, F. J. Iftikhar, J. Nisar, M. S. Akhter and S. B. Khan, *ACS Omega*, 2019, **4**, 22057-22068.

68. W. Wu, M. Jia, Z. Wang, W. Zhang, Q. Zhang, G. Liu, Z. Zhang and P. Li, *Microchimica Acta*, 2019, **186**, 1-10.

69. F.-R. Zou, S.-N. Wang, F.-F. Wang, D. Liu and Y. Li, *Catalysts*, 2020, **10**, 833.

70. I.-A. Baragau, N. P. Power, D. J. Morgan, T. Heil, R. A. Lobo, C. S. Roberts, M.-M. Titirici, S. Dunn and S. Kellici, *Journal of Materials Chemistry A*, 2020, **8**, 3270-3279.

71. Q. Jiang, Y. Ni, R. Gao and P. Zhou, *Microchemical Journal*, 2020, **157**, 105111.

72. D.-Q. Feng, G. Liu, Z. Chen, H. Lu, Y. Gao and X. Fang, *Microchemical Journal*, 2020, **157**, 104977.

73. O. J. Achadu and T. Nyokong, *Dyes and Pigments*, 2019, **160**, 328-335.

74. J. Jana, H. J. Lee, J. S. Chung, M. H. Kim and S. H. Hur, *Analytica Chimica Acta*, 2019, **1079**, 212-219.

75. N. Shahbazi and R. Zare-Dorabei, *Microchemical Journal*, 2019, **145**, 996-1002.

76. G. J. Shree, S. Murugesan and A. Siva, *Spectrochimica Acta Part A: Molecular and Biomolecular Spectroscopy*, 2020, **226**, 117613.

77. Z. Li, S. Wang, L. Xiao, X. Li, X. Shao, X. Jing, X. Peng and L. Ren, *Inorganica Chimica Acta*, 2018, **476**, 7-11.

78. P. Alreja and N. Kaur, *Inorganica Chimica Acta*, 2018, **480**, 127-131.

79. S. Dey, C. Sen and C. Sinha, *Spectrochimica Acta Part A: Molecular and Biomolecular Spectroscopy*, 2020, **225**, 117471.

80. A. R. Chowdhury, B. G. Roy, S. Jana, T. Weyhermuller and P. Banerjee, *Sensors and Actuators B: Chemical*, 2017, **241**, 706-715.

81. R. Purkait, S. Dey and C. Sinhaa, *New Journal of Chemistry*, 2018, **42**, 16653-16665.

82. N. Saini, N. Prigyai, C. Wannasiri, V. Ervithayasuporn and S. Kiatkamjornwong, *Journal of Photochemistry and Photobiology A: Chemistry*, 2018, **358**, 215-225.

83. X. Liu, H. Yao, N. Li, M.-M. Xu, C. Jiang, Z. Chen, Y. Wang and H. Shi, *Tetrahedron*, 2020, **76**, 131626.

84. T. Liu, X. Liu, M. A. Valencia, B. Sui, Y. Zhang and K. D. Belfield, *European Journal of Organic Chemistry*, 2017, **2017**, 3957-3964.

85. M. Alkış, D. Pekyılmaz, E. Yalçın, B. Aydıner, Y. Dede and Z. Seferoğlu, *Dyes and Pigments*, 2017, **141**, 493-500.

86. K. Krishnaveni, S. Murugesan and A. Siva, *Inorganic Chemistry Communications*, 2021, 108843.

87. E. Yalçın, M. Alkış, N. Seferoğlu and Z. Seferoğlu, *Journal of Molecular Structure*, 2018, **1155**, 573-581.

88. C. Wu, J. Wang, J. Shen, C. Zhang, Z. Wu and H. Zhou, *Tetrahedron*, 2017, **73**, 5715-5719.

89. A. Kim and C. Kim, *New Journal of Chemistry*, 2019, **43**, 7320-7328.

90. R. Bhaskar and S. Sarveswari, *Sensor Letters*, 2019, **17**, 344-351.

91. C. Long, J.-H. Hu, P.-W. Ni, Z.-y. Yin and Q.-Q. Fu, *New Journal of Chemistry*, 2018, **42**, 17056-17061.

92. C. Long, J.-H. Hu, Q.-Q. Fu and P.-W. Ni, *Spectrochimica Acta Part A: Molecular and Biomolecular Spectroscopy*, 2019, **219**, 297-306.

93. S. Roy, A. Maity, N. Mudi, M. Shyamal and A. Misra, *Photochemical & Photobiological Sciences*, 2019, **18**, 1342-1349.

94. Y. Upadhyay, S. Bothra, R. Kumar, H.-J. Choi and S. K. Sahoo, *Spectrochimica Acta Part A: Molecular and Biomolecular Spectroscopy*, 2017, **180**, 44-50.

95. Z. Zhu, H. Ding, Y. Wang, C. Fan, Y. Tu, G. Liu and S. Pu, *Tetrahedron*, 2020, **76**, 131291.

96. Z. Wang, Q. Zhang, J. Liu, R. Sui, Y. Li, Y. Li, X. Zhang, H. Yu, K. Jing and M. Zhang, *Analytica chimica acta*, 2019, **1082**, 116-125.

97. A. Mejri, A. Mars, H. Elfil and A. H. Hamzaoui, *Microchimica Acta*, 2018, **185**, 1-8.

98. Y.-H. Zhang, H. Huang, S.-S. Yang and Q.-Y. Cao, *Journal of Organometallic Chemistry*, 2018, **871**, 74-78.

99. H. Cunha-Silva and M. J. Arcos-Martinez, *Talanta*, 2019, **199**, 262-269.

100. L. Liu, H. Zhao, L. Shi, M. Lan, H. Zhang and C. Yu, *Electrochimica Acta*, 2017, **227**, 69-76.

101. J. Bujes-Garrido and M. Arcos-Martínez, *Sensors and Actuators B: Chemical*, 2017, **240**, 224-228.

102. H. Huang, Z. Xin, L. Yuan, B.-Y. Wang and Q.-Y. Cao, *Inorganica Chimica Acta*, 2018, **483**, 425-430.

103. P. R. Lakshmi, P. Jayasudha and K. P. Elango, *Spectrochimica Acta Part A: Molecular and Biomolecular Spectroscopy*, 2019, **213**, 318-323.

104. T. Chaudhuri, A. Mondal and C. Mukhopadhyay, *Journal of Molecular Liquids*, 2018, **251**, 35-39.

105. V. Sudha, S. M. S. Kumar and R. Thangamuthu, *Journal of Alloys and Compounds*, 2018, **749**, 990-999.

106. Q. Xiao, M. Feng, Y. Liu, S. Lu, Y. He and S. Huang, *Ionics*, 2018, **24**, 845-859.

107. Y. Han, R. Zhang, C. Dong, F. Cheng and Y. Guo, *Biosensors and Bioelectronics*, 2019, **142**, 111529.

108. F. Yan, X. Ma, Q. Jin, Y. Tong, H. Tang, X. Lin and J. Liu, *Microchimica Acta*, 2020, **187**, 1-8.

109. P. Gołębiewski, B. Puciłowski, F. Sommer, S. Kubik, M. Daniels, W. Dehaen, U. Sivasankaran, K. G. Kumar, H. Radecka and J. Radecki, *Sensors and Actuators B: Chemical*, 2019, **285**, 536-545.

110. T. Wu, L. Li, G. Song, M. Ran, X. Lu and X. Liu, *Microchimica Acta*, 2019, **186**, 1-9.

111. W. A. Durai and A. Ramu, *Journal of Fluorescence*, 2020, **30**, 275-289.

112. A. A. C. Riojas, A. Wong, G. A. Planes, M. D. Sotomayor, A. La Rosa-Toro and A. M. Baena-Moncada, *Sensors and Actuators B: Chemical*, 2019, **287**, 544-550.

113. H. Zhang, D. Sun and T. Cao, *International Journal of Electrochem Science*, 2020, **15**, 3434-3444.

114. B. Kaur, C. A. Erdmann, M. Daniels, W. Dehaen, Z. Rafinski, H. Radecka and J. Radecki, *Analytical Chemistry*, 2017, **89**, 12756-12763.

115. B. B. Nguelo, G. K. Dedzo, I. K. Tonle, C. Detellier and E. Ngameni, *Electroanalysis*, 2018, **30**, 543-550.

116. H. Cunha-Silva and M. J. Arcos-Martinez, *Sensors and Actuators B: Chemical*, 2019, **282**, 603-608.

117. M. Cui, J. Ren, X. Wen, N. Li, Y. Xing, C. Zhang, Y. Han and X. Ji, *Chemical Research in Chinese Universities*, 2020, **36**, 774-780.

118. B. Gauthama, B. Narayana, B. Sarojini, J. Manjunatha and N. Suresh, *Inorganic Chemistry Communications*, 2020, **121**, 108216.

119. A. M. Mahmoud, M. H. Mahnashi and M. M. El-Wekil, *Talanta*, 2021, **221**, 121562.

120. L. Ling, J. Hu and H. Zhang, *Tetrahedron*, 2019, **75**, 2472-2481.

Chapter 3

Materials and Instrumentation

This chapter provides a brief description of the material and instruments used for the ion recognition behavior of triphenyl derivatives. The methodology was carried out by using spectroscopic and voltammetric techniques. Probable interactions between receptor and target species were supported by theoretical studies. Experimental details of methods and techniques are mentioned in detail in this chapter.

3.1 Chemicals

All of the starting reagents and solvents were obtained from commercial sources and used without further purification. HPLC grade acetonitrile (ACN) was used in the optical and electrochemical experiments (SD Fine, India). Over a silica gel (mesh 100–120), thin-layer chromatography (TLC) and column chromatography were performed. Hexane, ethyl acetate, dichloromethane, and methanol, among other solvents used for extraction and chromatography, were of industrial quality and were used after distillation. For cation studies, perchlorate salt of Hg^{2+}, Ni^{2+}, Co^{2+}, Fe^{2+}, Fe^{3+}, Mn^{2+}, Ca^{2+}, Pb^{2+}, Mg^{2+}, Cr^{3+}, Al^{+3}, Zn^{2+} and Cu^{2+} (Sigma Aldrich) were used, and for anion interactions, tetrabutylammonium salts of HSO_4^-, $H_2PO_4^-$, ClO_4^-, OAc^-, F^-, Cl^-, I^-, CN^- were used. Various amino acids were used in the application part, including asparagine (Asn), lysine (Lys), arginine (Arg), tryptophan (Trp), proline (Pro), glutamine (Gln), histidine (His), and cysteine (Cys). For the antibacterial activity test, non-pathogenic *E. coli* bacteria (DH5-Alpha strain) were used. Bacteria were grown using Luria Britani (Loba Chemie).

3.2 Instrumentations

The JEOL spectrometer operating at 400 MHz was used to record ^1H and ^{13}C NMR spectra in $CDCl_3$. Both chemical changes are represented in parts per million (ppm) with the TMS, which acts as an internal guide. The Agilent Carry 660 spectrophotometer was used to record FT-IR spectra. UV-Vis experiments were performed on an Analytic Jena machine with a 1.0 cm path length and matched quartz cells. Fluorescence spectra were recorded on a Perkin Elmer LS-55 fluorescence spectrometer. Gamry Potentiostat/Galvanostat/ZRA Interface 1000 was used for all electrochemical measurements. Tetrabutylammonium hexafluorophosphate ($TBAHPF_6$) (Sigma Aldrich) was used as a supporting electrolyte in all of the voltammetric

experiments. As a working electrode, a glassy carbon electrode (2.0 mm diameter, CH Instruments, USA) was used. A platinum electrode was used as the counter electrode. With Ag/AgCl as the reference electrode, all potentials were determined. Internal solutions in the Ag/AgCl electrode were $AgNO_3$ (0.01 M) and $TBAHPF_6$ (0.1 M) in acetonitrile solvent. The working GC electrode was cleaned by polishing it with alumina powder and then washing it in water and solvent. At room temperature, the electrochemical tests were performed. The test solutions were de-aerated in all experiments by moving a stream of N_2 gas through them for at least 4-5 minutes.

Dewinter fluorescence inverted microscope with violet light excitation and 20X objective was used for cell imaging studies.

3.2.1 Spectrophotometry

Spectrophotometry is a method of measuring the intensity of light as it travels through a sample solution to determine how much a chemical compound absorbs light. Each substance absorbs or transmits light over a specific wavelength range, according to the basic principle. This measurement can also be used to determine the amount of a chemical compound that is known. Spectrophotometry is a valuable tool for quantitative study in a variety of domains, including physics, chemistry, material and chemical engineering, and clinical medicine.

3.2.2 Spectrofluorimetry

Spectrofluorimetry is a type of electromagnetic spectroscopy that examines a sample's fluorescence. Molecules can exist in a variety of states, which is referred to as energy levels. The primary focus of fluorescence spectroscopy is on electronic and vibrational states. In most cases, the species under investigation has a ground electronic state of interest (a low energy state) and an excited electronic state of greater energy. There are different vibrational states inside each of these electrical states. The species is excited in fluorescence by absorbing a photon from the ground electronic state and transferring it to one of the numerous vibrational modes in the excited electronic state. When an excited molecule interacts with another molecule, it loses vibrational energy until it approaches the vibrational level of the ground state. The Jablonski diagram is frequently used to depict this procedure.

3.2.3 Voltammetry

One type of electroanalytical method used in analytical chemistry is voltammetry. Voltammetry is a technique for obtaining information about an analyte by measuring current as a function of applied voltage.[1, 2] Voltammetric investigations teach us about the oxidation-

reduction process at the electrode surface, the adsorption process on the electrode surface, and the electron transport mechanism at the modified electrode surface. The four main types of voltammetry are categorized as (i) Linear sweep voltammetry (ii) Differential pulse voltammetry (iii) Cyclic voltammetry (iv) Square wave voltammetry.
We have experimented using DPV only therefore, it is discussed in detail.

Differential pulse voltammetry

Differential pulse voltammetry (DPV) (also differential pulse polarography, DPP) is an electrochemical voltammetry method that uses a sequence of regular voltage pulses superimposed on a potential linear sweep or stair steps. It is a derivative of linear sweep voltammetry or staircase voltammetry. Differential pulse voltammetry is used to assess the number of electroactive species present at a trace level in an organic or inorganic sample. Potential is screened using this method, which uses a series of periodic pulses superimposed on a linear potential ramp. Current is measured at two points: when the pulse starts and when the pulse finishes. The actual difference between these two points is calculated and plotted against the potential. Peak-shaped voltammograms are observed due to double sampling. The distance of the peak is used to calculate electron stoichiometry. The difference between measured current and applied base potential is displayed.

The following are the key parameters for pulse techniques:

1. **Pulse period**: The time required for one potential cycle.
2. **Sample period**: Time at the end of pulse during which the current is measured.
3. **Pulse width**: The duration of the pulse period.
4. **Pulse amplitude**: The height of the potential pulse.

3.3 Stock solution for cations/anions/amino acids

For voltammetric, absorption, and emission tests, a stock solution of receptors ($1.0x10^{-3}$ M) was prepared in ACN. Metal ions and amino acid solutions ($1.0x10^{-2}$ M) were made in water, while anions ($1.0x10^{-2}$ M) were made in ACN. Throughout all of the experiments, distilled water was used. In a small cell, a sufficient volume of receptor stock solution and various cation/anion solutions were mixed, and then absorption and fluorescence spectra were reported. All of the experiments were carried out within 10 minutes of the complexes being prepared at 25° C.

3.4 Computational studies

Theoretical calculations of the receptors and their complexes were carried out on DFT (Density Functional Theory). GAUSSIAN-03 software was used for the optimization of structures using 631G basis set. HOMO-LUMO orbitals and electron density of the molecule were calculated via these calculations.[3-5]

3.5 Antibacterial activity and fluorescence imaging

Escherichia coli (*E. coli*, Gram-negative bacteria) were used to test the antibacterial efficacy of the synthetic compound (Probe 1) and its aluminium complex. Glassware and samples must be sterilized for this experiment. E. coli was incubated in Luria-Bertani broth medium at 37^0 C for 12 h by shaking in (200 rpm) in a rotary shaker. For fluorescence imaging tests, bacteria were treated separately for 60 minutes with the compound and its aluminium complex. It was then mounted on glass slides using the heat fix process. The bacterial slides were then incubated with 2 % formaldehyde for 20 minutes before being photographed using a Dewinter fluorescence inverted microscope with green light excitation.[6]

3.6 Experimental section

Triphenyl ether and triphenyl amine-based receptors were synthesized and their detailed synthetic methodology has been presented below. Electroanalytical probes based on the receptors are also developed for cations and anions as target species. A general schematic presentation of organic reaction setup is shown in fig. 1.

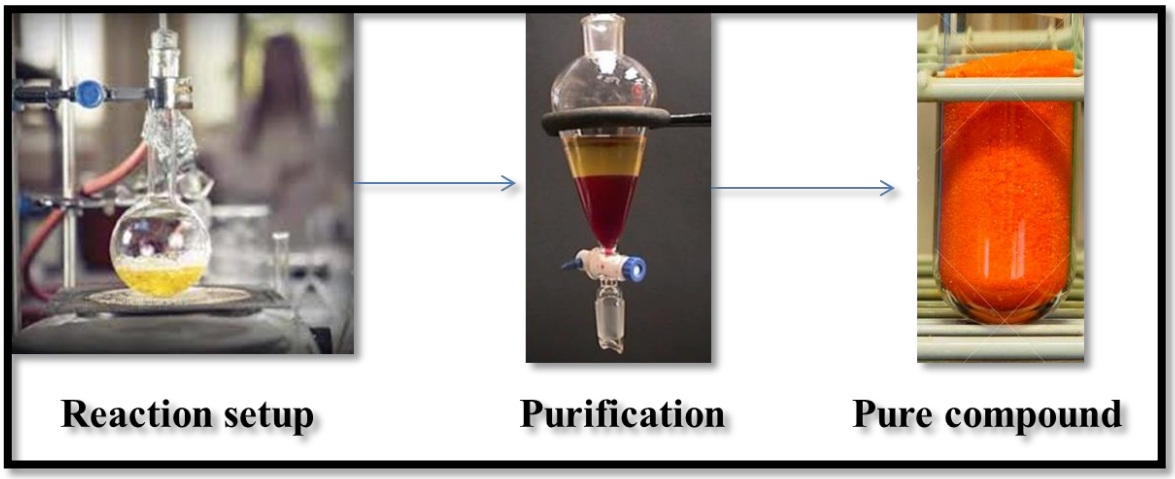

Fig. 1 General schematic presentation of organic reaction

3.6.1 Synthesis of Triphenylether derivatives

Synthesis of 1,1'-((((1,3-phenylenebis(oxy))bis(2,1-phenylene))bis(azanediyl))bis (methylene))bis(naphthalen-2-ol) (TPEA)

TPEA was synthesized from initial compound TPEI[7] (51 mg, 0.085 mmol) using sodium borohydride (12.5 mg, 0.34 mmol) in THF: Methanol (7:3) at normal temperature as shown in scheme 3.1. After completion of the reaction, the reaction mixture was partitioned between dichloromethane (15 mL) and water (15 mL) and further extracted again with dichloromethane (15 mL). The combined organic layers were dried over Na_2SO_4, filtered and separated from the solvent using a vacuum evaporator to yield a crude product that was purified by silica gel column chromatography with solvent system (ethyl acetate/hexane, 95:5, v/v) to get light yellow solid. The product yield of TPEA was obtained at 39%. **^{1}H NMR (400 MHz, $CDCl_3$) δ(ppm)** 7.7 (d, J = 7.8Hz, 2H), 7.6 (d, J = 8.72Hz, 2H), 7.5 (d, J = 8.72Hz, 2H), 7.4 (m, 2H), 7.3 (t, J = 8.72Hz, 2H), 7.2 (m, 3H), 7.0 (d, J = 8.68Hz, 2H), 6.9 (d, J = 9.16Hz, 6H), 6.7 (m, 3H), 4.8 (s, 4H); **^{13}C-NMR (100MHz, $CDCl_3$): δ(ppm)** 158.64, 151.89, 148.52, 140.96, 131.12, 130.31, 126.67, 124.88, 124.22, 123.61, 121.68, 120.99, 120.87, 118.71, 118.71, 112.55, 111.83, 107.38, 48.13. m/z calcd for $[M-H]^-.2H_2O$: 639.69; found: 639.37 (Figure 3.1, 3.2 &3.3).

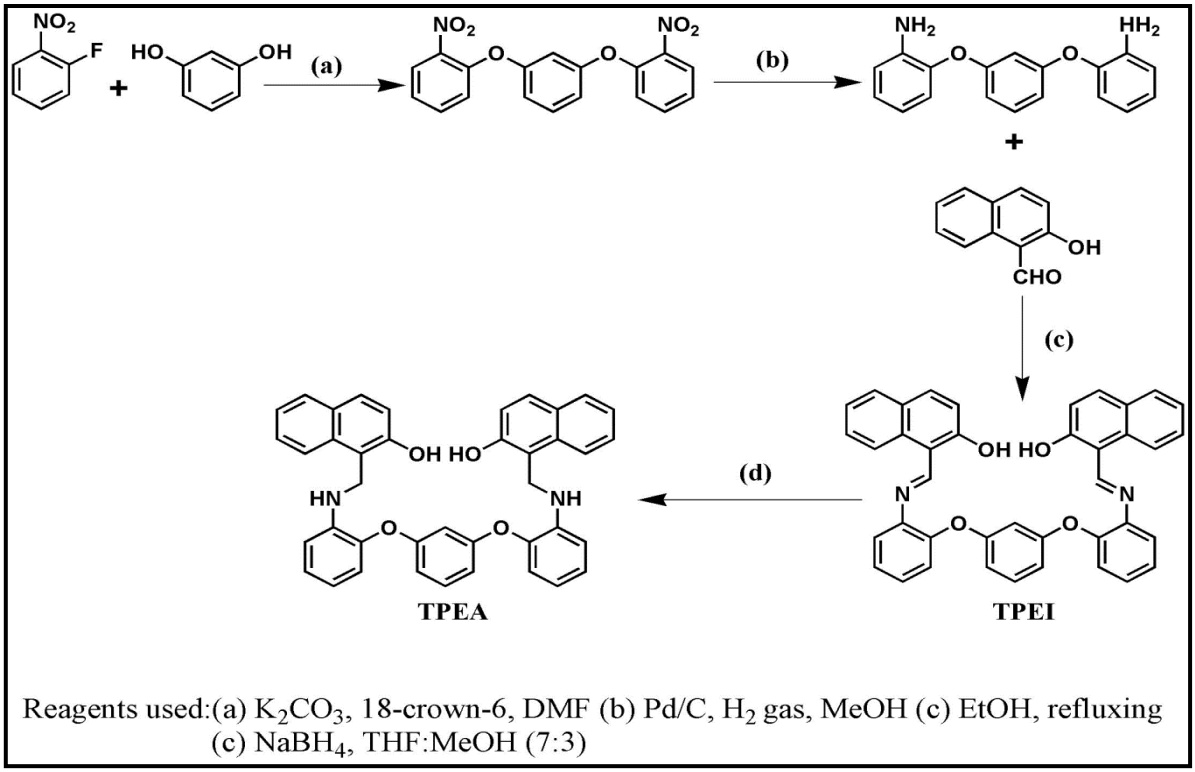

Scheme 3.1 Synthesis route of TPEA[7]

Synthesis of N,N'-((1,3-phenylenebis(oxy))bis(2,1-phenylene))bis(2-hydroxy-1-naphthamide) (TPEAM)

TPEAM was synthesized by a two-step procedure. In the first step, acid chloride was prepared from 2-hydroxy-1-naphthoic acid (1 mmol) and PCl_3 (1 mmol) by stirring and heating at 80-90^o C until the evolution of hydrochloric acid ceased. The acid chloride thus prepared was added into the solution of corresponding amine[7] (0.5 mmol) in the presence of K_2CO_3 (0.3 mmol) as a base, using dichloromethane (15 ml) as a solvent at 0^o C (Scheme 3.2). The reaction mixture was allowed to stir for 4-6 hrs. After completion of the reaction, it was quenched with water. To obtain the organic product, the reaction mixture was partitioned between dichloromethane (3×15 ml) and water (3×15 ml). The combined organic layers were dried over Na_2SO_4, filtered, and separated from the solvent using a vacuum evaporator to yield the crude product which was purified by silica gel column chromatography with a solvent system of hexane/ethyl acetate (90:10, v/v). A light yellow solid was obtained (yield = 68 %) and further characterized by using ^{1}H and ^{13}C NMR. **^{1}H NMR (400 MHz, $CDCl_3$) δ (ppm)** 12.07 (s, 1H), 8.99 (d, J = 8.68Hz, 1H), 7.99 (t, 2H), 7.90 (m, 2H), 7.83 (d, J = 8.24Hz, 1H), 7.77 (s, 1H), 7.62 (t, 1H), 7.53 (m, 2H), 7.42 (m, 2H), 7.22 (d, J = 8.68Hz, 1H); **^{13}C-NMR (100 MHz, $CDCl_3$): δ (ppm)** 171.49, 165.43, 147.47, 137.86, 133.75, 131.75, 137.72 129.75, 129.33, 128.93, 128.76, 127.89, 127.71, 126.85, 126.12, 125.42, 123.98, 121.16, 119.35, 119.03, 104.02. [M] Calculated 632.19, found: 632.79, corresponding to the deprotonated [M-H] form of the ligand (Figure 3.4, 3.5 &3.6).

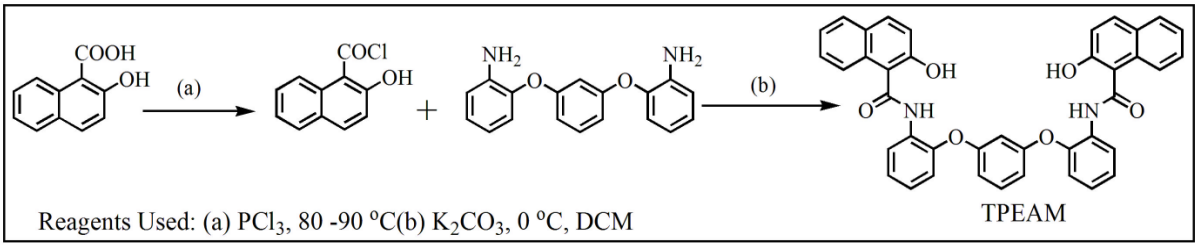

Scheme 3.2 Synthesise route of TPEAM

3.6.2 Synthesis of Triphenylamine derivatives

Synthesis of N,N-bis(2-nitrophenyl)benzene-1,3-diamine (TPAN)

To a solution of 1-fluoro-2-nitrobenzene (7.6 mmol, 736.4 µL) in ACN (5 mL) was added benzene-1, 3-diamine (5 mmol, 500 mg), potassium carbonate (10 mmol, 1.29 g). The reaction mixture was allowed to stir for 4-5 hrs as shown in scheme 3.3. After completion of the reaction, the reaction mixture was partitioned between dichloromethane (15 mL) and

water (15 mL) and further extracted again with dichloromethane (15 mL). The combined organic layers were dried over Na_2SO_4, filtered, and separated from the solvent using a vacuum evaporator to yield a crude product that was purified by silica gel column chromatography with a solvent system (ethyl acetate/hexane, 70:30, v/v) to get light red solid. The product yield of TPAN was obtained at 53%. **^{1}H NMR (400 MHz, $CDCl_3$) δ(ppm)** 9.41 (d, J = 26, 1H), 8.23 (t, 1H), 8.03 (d, J = 8.12, 1H), 7.57 (t, 2H), 7.29 (m, 3H), 7.04 (d, J = 8, 1H), 6.07 (m, 3H), 3.75 (s, 1H); **^{13}C-NMR (100MHz, $CDCl_3$): δ(ppm)** 156.91, 143.24, 142.59, 133.23, 127.34, 125.53, 122.52, 119.96, 115.78, 114.31 (Figure 3.7 & 3.8).

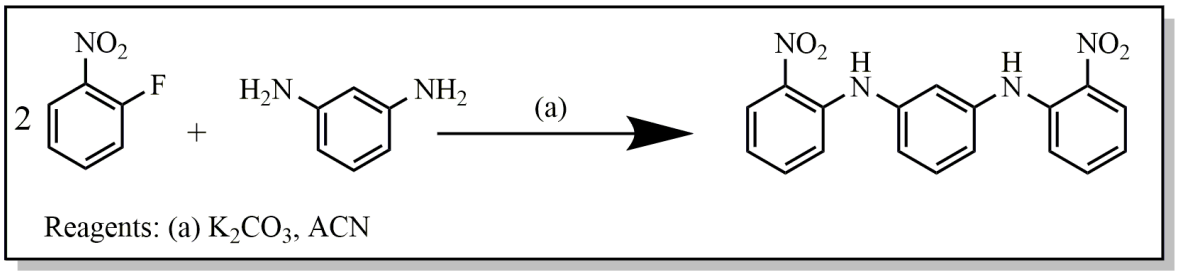

Scheme 3.3 Synthesis route of TPAN

Synthesis of N,N'-(1,3-phenylene)bis(benzene-1,2-diamine) (TPAA)

TPAN (4.1 mmol) was dissolved in 100 ml of methanol and a catalytic amount of Pd/C (10 mg) was added. The resultant solution was allowed to stir for 3-4 hrs in the presence of H_2 gas (Scheme 3.4). The color of the solution mixture changed from red to reddish-brown indicating that the reaction has taken place in forward direction. Finally, Pd/C was filtered off from the reaction mixture. The solvent was evaporated using rota-evaporated and product TPAA was obtained with a yield of 63 %. **^{1}H NMR (400 MHz, $CDCl_3$) δ(ppm)** 8.9 (d, J = 7.3Hz, 2H), 8.7 (m, 2H), 7.9 (m, 1H), 7.7 (q, 2H, J = 7.3 Hz), 7.3 (m, 3H), 7.1 (m, 2H), 4.7 (s, 4H), 4.5 (s, 2H); **^{13}C-NMR (100MHz, $CDCl_3$): δ(ppm)** 158.91, 142.24, 141.59, 130.23, 125.34, 119.53, 116.52, 110.96, 110.78, 106.31 (Figure 3.9 & 3.10).

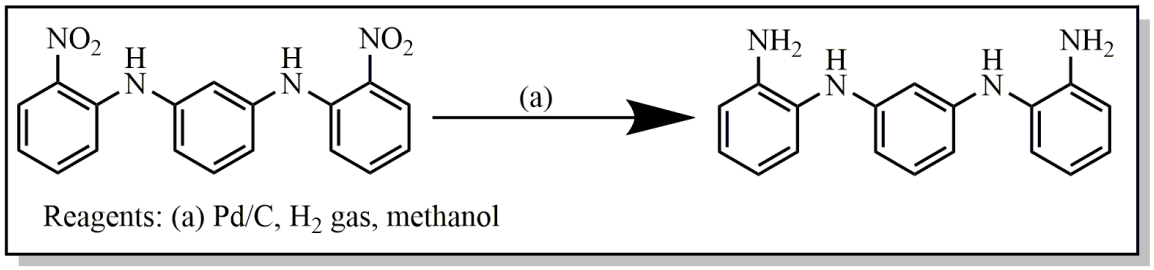

Scheme 3.4 Synthesis route of TPAA

3.6.3 Synthesis of 1,1'-((1E,1'E)-(1,2-phenylenebis(azanylylidene)) bis(methanylylidene)) bis(naphthalen-2-ol) ((Phenylene diimine) (PDI))

2-hydroxy naphthaldehyde (2.3mmol) was dissolved in ethanol (20 ml) and stirred at room temperature. To this solution, benzene-1,2-diamine (1.1 mol) was added drop-wise dissolved in ethanol (5 ml) under continuous stirring (Scheme 3.5). The resulting reaction mixture was brought to room temperature after being refluxed for 2-3 hours.[8] The stuff settled to the bottom and was filtered. Washing was done with ethanol and water, followed by vacuum drying. A yellow solid was obtained with yield of 78 %. Synthesised compound was further characterized by using ^{1}H and ^{13}C NMR.**^{1}H NMR (400 MHz, $CDCl_3$) δ (ppm)** 9.46 (s, 1H), 8.13 (d, J = 8.72Hz, 1H), 7.81 (d, J = 9.1Hz, 1H), 7.72 (d, J = 8Hz, 1H), 7.52 (t, 1H), 7.41 (m, 2H), 7.34 (t, 1H), 7.17 (d, J = 9.2Hz, 1H); **^{13}C-NMR (100 MHz, $CDCl_3$): δ (ppm)** 169.69, 155.60, 147.18, 136.93, 133.18, 130.78, 129.41, 128.29, 127.26, 123.73, 121.93, 118.93, 118.58, 112.31, 108.96 (Figure 3.11 & 3.12).

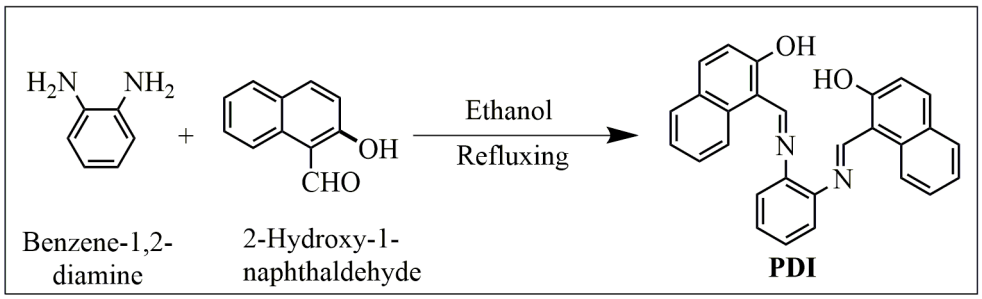

Scheme 3.5 Synthesis route of PDI

3.7 Spectroscopic measurements

Determination of the stoichiometry of complex

Job's plot method was used to evaluate the complex's stoichiometry. It is a graph of mole fraction versus absorbance. Plot between X (mole fraction) and Ab. is a common notation (absorbance).[9]

Determination of selectivity

The selectivity of the receptor is a measure of the sensor's ability to analyze the concentration of the analyte correctly in the presence of interfering ions that can impair the solution's absorbance.

Determination of stability constant

The complex stability constant (K_a) was determined from the change in fluorescence or absorbance resulting from the titration of a dilute solution of the probe against metal ions solution using the Benesi-Hildebrand equation.[10]

$$\frac{\mathbf{1}}{\boldsymbol{A - A_0}} = \frac{\mathbf{1}}{\boldsymbol{A_{max} - A_0}} + \mathbf{1}/(\boldsymbol{K}(\boldsymbol{A_{max}} - \boldsymbol{A_0})[\boldsymbol{M_n}])$$

Where A_0 is the absorbance of compound, A is the absorbance at a particular wavelength, and A_{max} is the maximum absorbance. K is the association constant in M^{-1}. M_n is the concentration of metal ion or anion added during the titration. The UV-Visible titration data provided these results. The stability constant was graphically determined by plotting 1/A against 1/[M_n], yielding a straight line. The slope and intercept of this straight line were used to calculate the K value.

Determination of limit of detection (LoD)

The detection limit was determined using emission studies. The fluorescence intensity of the probe was measured three times, and the standard deviation of blank measurements was determined to calculate the signal-to-noise ratio. The limit of detection was therefore calculated using the mathematical equation[11]:

$$\mathbf{LoD = 3\sigma/slope}$$

Where σ_{bi} is the standard deviation of blank measurements; and m is the slope of intensity vs. the sample concentration

Determination of fluorescence quantum yield (Φ_f)

To compute fluorescence quantum yield[12], the corrected integrated fluorescence spectra of the sample were compared to that of a standard (quinine in H_2SO_4; Φ_f = 0.54):

$$\boldsymbol{\Phi_f = \Phi_{f,\,std}(A_{std}/A)(n^2/n^2_{std})(D/D_{std})}$$

Where A represents absorbance, n represents the solvent's refractive index, and D represents the area under the corrected fluorescence spectrum. The sample and standard solutions were prepared with the absorbance at a maximum of roughly 0.5, followed by dilutions. The correction factors for the fluorescence spectra used to determine Φ_f were derived by measuring the spectra with known emission of the compound.

References

1. C. G. Zoski, *Handbook of electrochemistry*, Elsevier, 2006.

2. N. Aristov and A. Habekost, *World J. Chem. Educ*, 2015, **3**, 115-119.

3. S. Gunasekaran, R. A. Balaji, S. Kumeresan, G. Anand and S. Srinivasan, *Can. J. Anal. Sci. Spectrosc*, 2008, **53**, 149-162.

4. I. Fleming, *Frontier orbitals and organic chemical reactions*, Wiley, 1977.

5. I. Fleming, *Molecular orbitals and organic chemical reactions*, John Wiley & Sons, 2011.

6. S. Datta, D. Choudhury, A. Das, D. Das Mukherjee, N. Das, S. S. Roy and G. Chakrabarti, *Tumor Biology*, 2017, **39**, 1010428317694314.

7. R. Sharma, M. Chhibber and S. K. Mittal, *RSC Advances*, 2016, **6**, 51153-51160.

8. S. Samanta, B. Nath and J. B. Baruah, *Inorganic Chemistry Communications*, 2012, **22**, 98-100.

9. J. S. Renny, L. L. Tomasevich, E. H. Tallmadge and D. B. Collum, *Angewandte Chemie International Edition*, 2013, **52**, 11998-12013.

10. H. A. Benesi and J. Hildebrand, *Journal of the American Chemical Society*, 1949, **71**, 2703-2707.

11. Aanalytical Methods Committee, *Analyst*, 1987, **112**, 199-204.

12. R. Rusakowicz and A. Testa, *The Journal of Physical Chemistry*, 1968, **72**, 2680-2681.

Chapter 4

Naked eye detection of cyanide ions using amine derivative of triphenyl ether as a novel receptor in aprotic solvent: spectrofluorimetry supported with voltammetric and DFT studies

Triphenyl ether based moiety containing amine linkage between triphenyl ether basic unit and naphthyl groups have exhibited selective detection towards CN^- ions in CH_3CN: H_2O (99: 1; v/v) as a solvent medium. Probe exhibited great naked eye response as color of the receptor solution changes from yellow to orange. This response was confirmed by various analytical techniques such as UV-VIS, fluorescence technique and electrochemical technique. Furthermore, for practical application, paper strips were prepared for onsite detection of cyanide ions. Cyanide complex of receptor was also used to detect water from pure acetonitrile solvent. For real-life sample analysis, CN^- was detected from different samples such as cassava root and Indian almond.

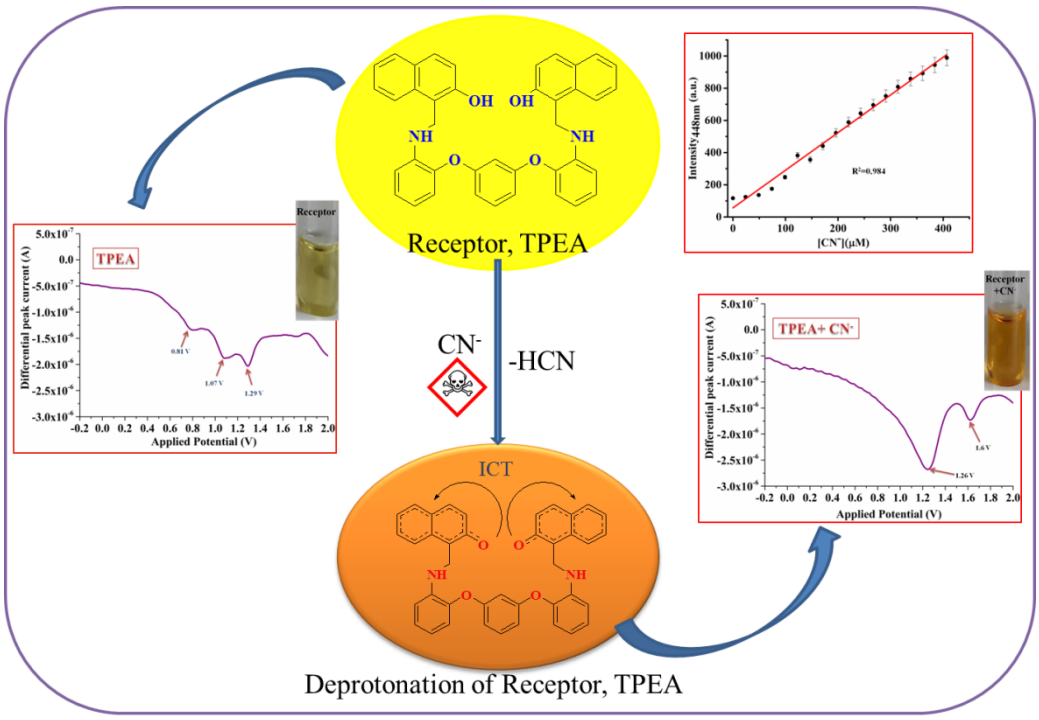

Schematic presentation of sensing behaviour of TPEA

4.1 Introduction

Improvement of chemosensors for the trace level detection of anions is a vibrant area of research because of their widespread use in our daily life. Amongst various anions, cyanide is one of the most venomous species as well as deadly to mankind because it affects many functions in an individual body such as the nervous system, metabolic system, cardiac, infringement up the electron transport chain in the mitochondria membrane and prevents respiration.[1, 2] Nonetheless, cyanide is widely used in many fields such as plastic manufacturing, gold extraction, tanning, electroplating, petrochemical, cinematography, and steel industry. All of these industries are responsible for cyanide pollution.[3] According to World Health Organisation (WHO), the specified limit of cyanide concentration is 1.9 µM (70 ppb) in drinking[4] and also by US EPA, the utmost impurity level for cyanide in ingestion water is set to be 200 ppb. Therefore, the fast determination of cyanide content in altered matrices such as urine, foodstuff, soil, water, living cells, blood and in agricultural products is extremely important.

Various kinds of traditional methods are available for the quantitative determination of cyanide ions such as cyanide selective electrode[5], polarography[6], flow injection amperometry[7], potentiometry[8] and titrimetry[9]. These methods endure various disadvantages such as poor detection limit, time-consuming, expensive and complicated procedures. Therefore, fast, reliable and more sensitive techniques are required for direct measurement of cyanide at µg/L level in altered matrices of life.

In this concern, fluorescence chemosensors with elevated specificity and selectivity, ease and safe handling have grabbed substantial awareness and have become a promising tool for the recognition of cyanide ions.[10] Most of the sensors for cyanide ions are based on emission intensity and could be notably subjective by excitation power and detector sensitivity. For the fluorescent sensor to be an effective tool for sensing, there must be color change on sensing of ions, which can be calculated directly with colorimetry or can be observed by the naked eye.[11] Other than fluorescence spectroscopy, cyclic voltammetry (CV) and differential pulse polarography (DPV) are important tools to characterize electrochemical behavior of the receptor. Electrochemical techniques have various advantages such as lower detection limits, less affected by interfering ions present in solution and use of lesser amounts of chemicals and solvents.

A great variety of fluorescent receptors have been developed for sensing cyanide ions such as derivatives of calixarene,[12, 13] rhodamine[14] and triphenylamine,[1, 15, 16] etc., but most of these molecules suffer from complicated synthesis procedures, cross-reactivity of molecules, purification by different separation techniques and interference from other present anions in solution such as acetate and fluoride ions.

Here, in this chapter we report a novel triphenylether derivative as a dual sensor for the selective detection of cyanide ions and water in trace amounts in acetonitrile. Synthesized ionophore does not require complicated synthesis procedure and it also acts as a "naked eye" optical sensor for cyanide ions. Differential Pulse Voltammetric studies of synthesized receptor and its complex with cyanide ions are also in accordance with the optical results. Mechanisms for the detection of cyanide ions have been proposed on the basis of deprotonation and intramolecular charge transfer (ICT) principles.[17, 18] Finally, in order to support the deprotonation mechanism, theoretical calculations were carried out and it confirms the ICT mechanism.

4.2 Preparation of real life samples and analysis

4.2.1 Determination of CN^- from Indian almonds

Unripe Indian almonds (5 g) were collected, dried and bleached to give fine powder. This fine powder was degreased with n-hexane for about 24 h. The filtrate thus obtained was then extracted with aqueous sodium bicarbonate (0.02 M, 100 mL) for 24 h. The extract was filtered, evaporated and used for the detection of endogenous cyanide.[19]

4.2.2 Determination of CN^- in cassava root

Part of the freshly peeled cassava roots was grounded and homogenized with a pestle and mortar. In order to hydrolytically cleave the linamarin with endogenous enzymes, the extract of cassava root was stored in a sealed tube for 1hr at room temperature. 2 g of delicately ground material was diluted with 10 mL of water and centrifuged for 15 min. Aliquots of 10-100 μL of the supernatant liquid were used for further analysis [20].

To confirm the presence of cyanide in unripe almond and cassava root, common qualitative analysis was done on the samples. The aqueous solutions of both almond and cassava were added separately into the solution of sodium thiosulfate. Both solutions were further treated with a solution of ferric chloride. Presence of intense brownish yellow colour confirmed the presence of cyanide in both almond and cassava samples.

4.3 Results and discussion

4.3.1 Design of ionophore

Triphenyl ether imine (TPEI), previously reported by our group, was a conjugated structure and had shown interactions for F^-, CN^-, and Co^{2+} in 5% aqueous acetonitrile medium. It was envisaged to observe the effect on the selectivity of the molecule by imparting flexibility when imine bond is reduced. Thus, TPEI was synthesized as reported earlier using a three-step reaction sequence.[21] The reduction of the imine group in TPEI proceeded smoothly with sodium borohydride in a mixture of THF: methanol (7:3) to afford triphenyl ether amine (TPEA). Characterization of the compound using ^1H and ^{13}C NMR confirmed the formation of a product due to the appearance of methylene protons at 4.8 ppm and carbon at 48.1 ppm and simultaneous disappearance of imine signals at 9.3 and 160 ppm, respectively.

4.3.2 Absorption studies

Absorption spectra of TPEA (1mM) in pure acetonitrile medium exhibited two peaks at 442 nm and 463 nm. In presence of cyanide ions, the two maxima merged to appear as a single peak at 465 nm, while with all other anions, separate peaks were observed at 442 nm and 463 nm with different peak maxima values (Fig. 4.1).

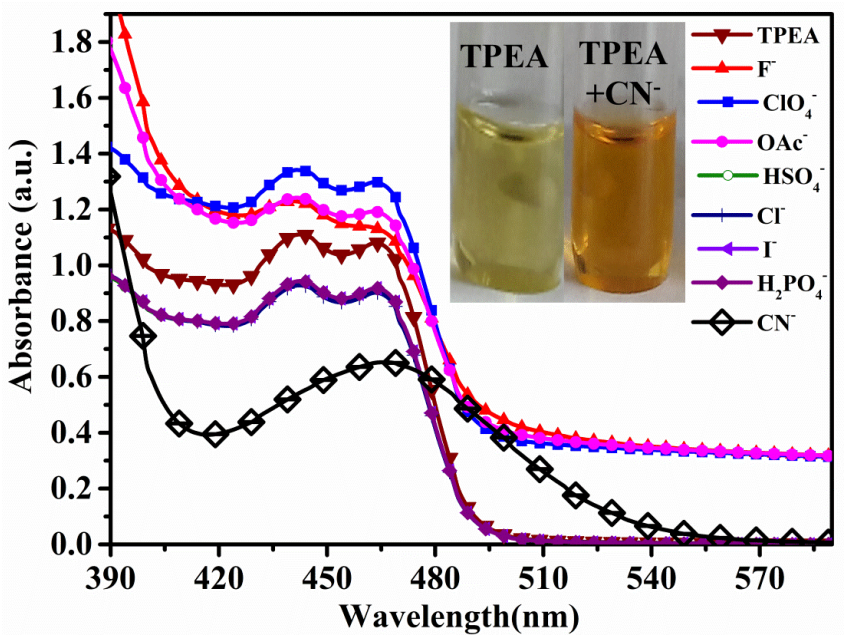

Fig. 4.1 UV-Vis spectra of TPEA receptor alone (1 mM) and upon addition of various anions (50 µM) using CH_3CN: H_2O (99: 1; v/v) as a solvent medium

No change in the absorption properties of TPEA was observed in case of any anion other than CN^- ion. All anions studied were obtained using tetra-n-butylammonium (TBA) salts. The solvent system used in above screening was a mixture of acetonitrile: water as 99:1 (v/v %) medium in order to avoid interferences due to acetate and fluoride anions, as discussed in the next section.

The disappearance of the peaks at 442 nm and 463 nm due to receptor accompanied by the appearance of absorption maxima at 465 nm indicated the formation of a new species in the presence of cyanide ions. This was also confirmed by the change in the color of TPEA from light yellow to light orange after addition of the cyanide ions (Fig. 4.1 (inset)).

4.3.3 Spectrofluorimetric studies

The emission spectrum of TPEA gave two major peaks at 363 nm and 498 nm, respectively upon excitation at 300 nm (Fig. 4.3a) which can be attributed to naphthyl (π^* to π) and hydroxyl (π^* to n) groups. Alteration in the emission properties of the receptor (TPEA) was observed only in case of CN^-, OAc^- and F^- ions, when an equivalent amount of HSO_4^-, $H_2PO_4^-$, ClO_4^-, CN^-, OAc^-, F^-, Cl^- and I^- anions were added in pure acetonitrile medium (Fig. 4.2). However, the use of an aqueous (1%) acetonitrile medium increased the selectivity of TPEA for CN^- ions, exclusively. This can be attributed to the hydration of F^- and OAc^- ions in the aqueous medium due to their high hydration energy[22-25] as compared to CN^- ions.[26]

The obtained selectivity for CN^- ions can be probably explained by taking two factors into the account, viz.; basicity of the anion and hydrogen bond formation capacity of the anion. In case of basicity, the followed trend is $CN^->AcO^->F^-$ and the reverse order is followed for hydrogen bonding capacity i.e. $F^->AcO^->CN^-$ in polar aprotic solvent. But in case of aqueous-organic solvent mixture CH_3CN: H_2O (99:1; v/v), water molecules present in the solvent system would form strong hydrogen bonding with the AcO^- and F^- ions because of the high hydration energy as compared to CN^- ions (Table 4.1).

Table 4.1 Comparison of hydration energy of various anions

S. No.	Ions	Hydration Energy ($kJmol^-$)
1.	F^-	-505
2.	AcO^-	-375
3.	CN^-	-67

Following the above-mentioned hydration energy trend, AcO^- and F^- will become incapable in terms of abstraction of proton from hydroxyl group of the receptor TPEA. Therefore, selectivity of TPEA becomes feasible for CN^- ions only in CH_3CN: H_2O (99:1; v/v) among the presence of various competing anions.

Fig. 4.3(a) shows a single emission peak at 448 nm in the presence of CN^- ions due to TPEA-CN^- system with simultaneous disappearance of peaks at 362 nm and 498 nm observed in acetonitrile: water as 99:1 (v/v %) medium. We hypothecate that the peak at 448 nm is due to charged conjugated structure II of TPEA, via intermediate I, after its interaction with the cyanide ions (Scheme 4.1).

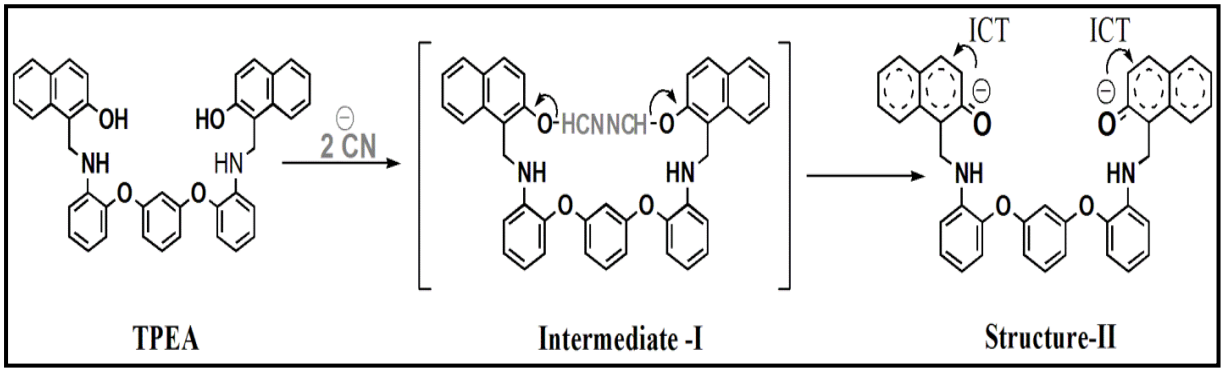

Scheme 4.1 Proposed mechanism of TPEA sensing cyanide ions

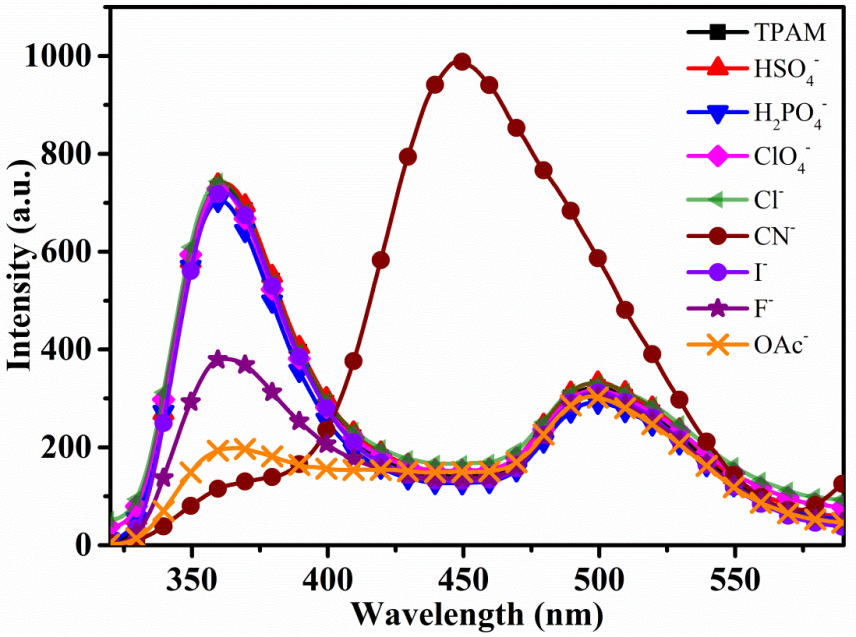

Fig 4.2 Fluorescence emission spectra of TPEA (1 mM) upon the addition of various anions (400 µM) (TBA salts) in pure acetonitrile medium

Further, titration of TPEA (Fig. 4.3(b)) with increasing concentration of cyanide ions up to an equivalent range of 0-2.3 gave a linear plot as shown in Fig. 4.3(c). It shows that the proposed spectrofluorimetric method can be used up to a concentration of 400 µM for CN^- ions with a relative standard deviation of 1.5%. Along with this, fluorescence titration suggests one isosbestic point at nearly 401 nm, which suggests that there is formation of one new species with the simultaneous addition of CN^- ions into the receptor's solution.

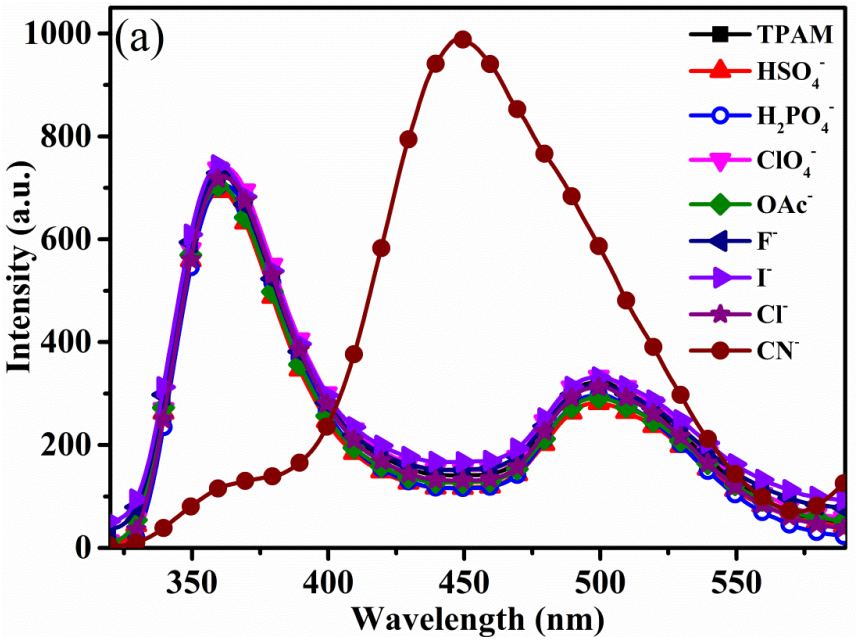

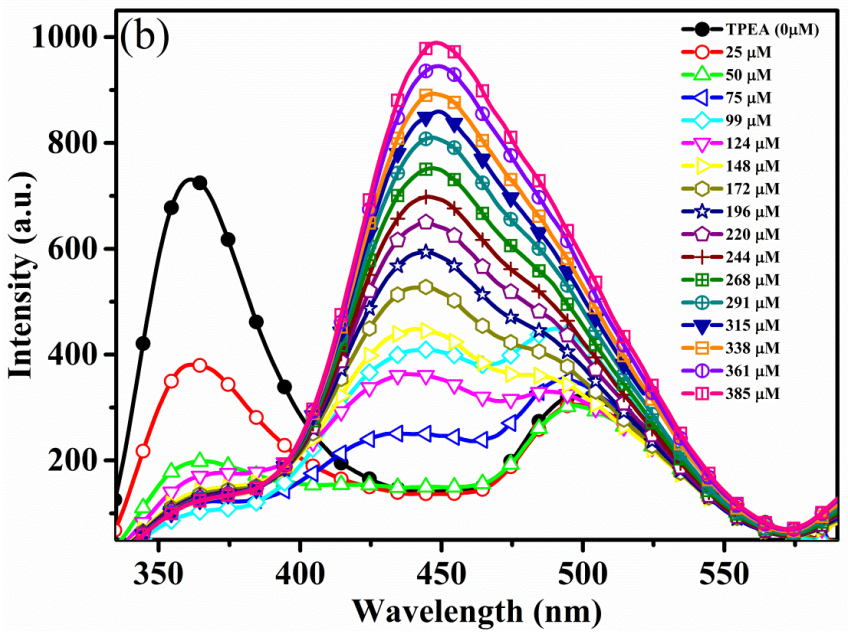

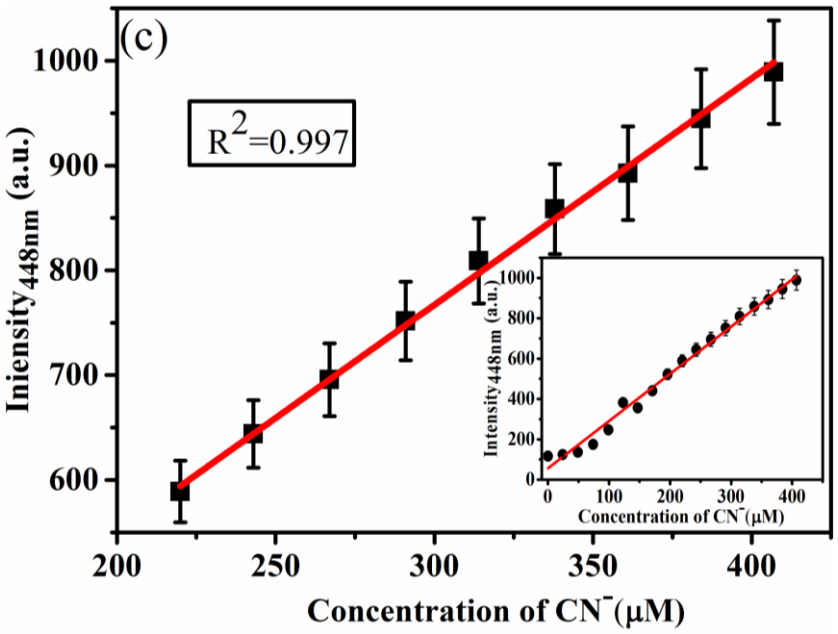

Fig. 4.3 (a) Fluorescence emission spectra of TPEA (1 mM) upon the addition of various anions (400 μM) (TBA salts) (b) fluorescence emission spectra of TPEA upon progressive addition of CN^- in CH_3CN: H_2O (99:1; v/v) medium (c) linear response of TPEA at 448 nm vs. concentration of CN^-

4.4 Job's plot and interference studies

In order to understand the stoichiometry ratio between receptor TPEA and CN ions, Job's plot analysis was carried out. Job's plots for the binding between TPEA and CN^- gave 1:2 stoichiometry as maximum absorbance value comes at mole fraction value of 0.6. The data was confirmed by repeating the experiment three times[27](Fig. 4.4). Binding constant (K) using the Benesi-Hildebrand equation (1)[28] was found to be 4.16×10^7 M^{-1}.

$$\frac{1}{I-I_0} = \frac{1}{I_{max}-I_0} + 1/(K(I_{max} - I_0)[CN^-]) \qquad \text{----------(1)}$$

Where "I_0" is the emission intensity of compound TPEA at360 nm, "I" is the intensity at a particular wavelength, "I_{max}" is the maximum intensity, [CN^-] is the concentration of CN^- added during titration and K is the association constant in M^{-1}.

From the fluorimetric calibration plot (Fig. 4.3(c)), the limit of detection for the CN^- ions using TPEA as receptor was found to be 0.4 μM, which is much below the permissible limit of 1.9 μM for CN^- ions in drinking water as set by world health organization (WHO)[4], using equation 3σ/slope (where σ is the standard deviation obtained from the intensity value of 10 blank samples and m is the slope obtained from the calibration curve) (where, slope= 10.2) through standard deviation and linear fittings.[29]

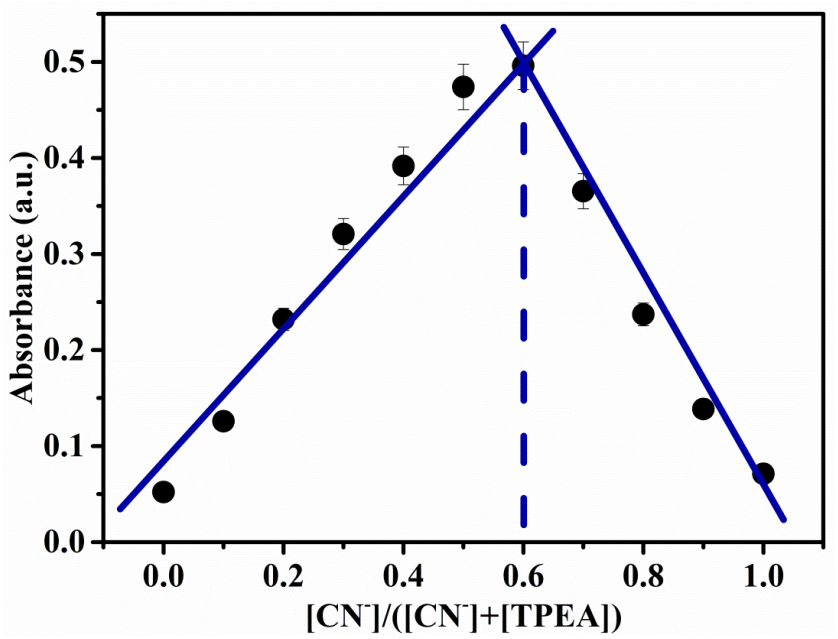

Fig 4.4 Job's plot of TPEA

No alteration in the emission properties of TPEA was observed when an equivalent amount of competitive anions (OAc^-, ClO_4^-, F^-, Cl^-, I^-, $H_2PO_4^-$ and HSO_4^-) were added. Similarly, addition of CN^- ions with an equivalent amount supposedly interfering anion did not show any difference in the intensity or emission wavelength of the TPEA-CN^- system (Fig. 4.5). Thus, none of the above-mentioned anions interfered in the selective detection of CN^- ions for the TPEA receptor in CH_3CN: H_2O (99:1; v/v) medium.

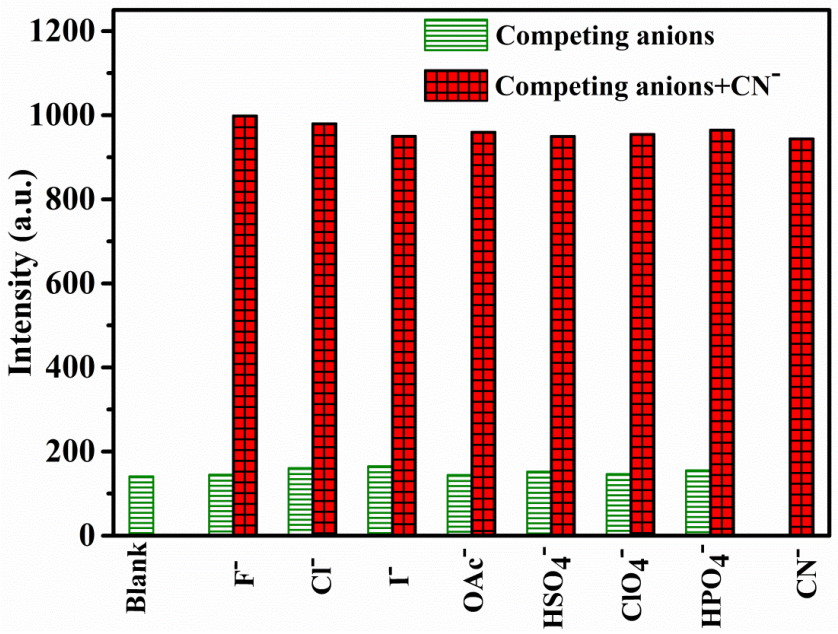

Fig. 4.5 Fluorescence intensity of TPEA (1 mM) in CH_3CN: H_2O (99: 1; v/v) in the presence of competing anions (λ_{ex} = 300 nm, λ_{em} = 498 nm)

Comparison of the proposed sensor with the previously reported literature for CN^- ions have been summarized in Table 4.2.

Table 4.2 Comparison of the present work with existing state of art

S. No.	Signaling unit	Media	Mechanistic approach	Detection limit	Stoichiometry	Ref.
1	Phenothiazine	CH_3CN-H_2O	ICT	3.39 µM	1:1	[30]
2.	Terpyridine	DMSO-H_2O	AIE	1.09 µM	-	[31]
3.	Naphthoquinone	HEPES Buffer-DMSO	Deprotonation	1 µM	1:2	[32]
4.	Oligothiophene	THF-H_2O	-	31.3 nM	-	[33]
5.	Benzothiadiazole	DMF-PBF	Nucleophilic addition	0.35 µM	-	[34]
6.	Naphthopyran	DMSO-H_2O	ICT	0.7 µM	1:1	[35]
7.	Phenothiazine	CH_3CN-H_2O	Nucleophilic addition	3.2 nM	-	[36]
8.	Naphthoquinone	HEPES Buffer-DMSO	Nucleophilic addition	69 nM	1:2	[37]
9.	Oligothiophene	THF-H_2O	Nucleophilic addition	0.2 µM	1:1	[38]
10.	Triphenylether	CH_3CN-H_2O	ICT	0.4 µM	1:2	This work

4.5 TPEA-CN^- system for the detection of water in acetonitrile

The observed selectivity of TPEA for CN^- ions in an aqueous medium as compared to those of F^- and OAc^- ions (as discussed above) encouraged us to investigate the behavior of former in the presence of water. Therefore, the fluorescence emission spectrum of TPEA-CN^- system was observed with a successively increasing ratio of water in ACN. Fig. 4.6 (a) shows a regular decrease in intensity of the TPEA-CN^- complex peak at 448 nm with simultaneous emergence of a new peak at 375 nm having isosbestic point at 425 nm. The blue shift in the presence of water can be attributed to the transfer of ionic equilibria of the cyanide ions towards partially aqueous ACN medium from pure ACN medium. The isosbestic point at 425 nm indicates a clear change in the mechanism of fluorescence emission for TPEA-CN^- system when highly polar CN^- ions move from relatively less polar ACN (dielectric constant 37.5) to highly polar aqueous medium (dielectric constant 80.1).

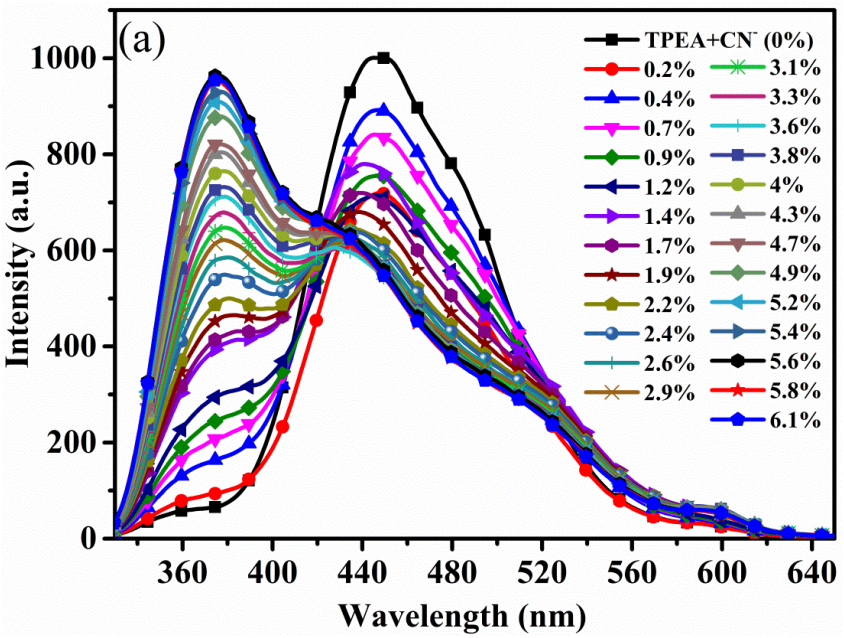

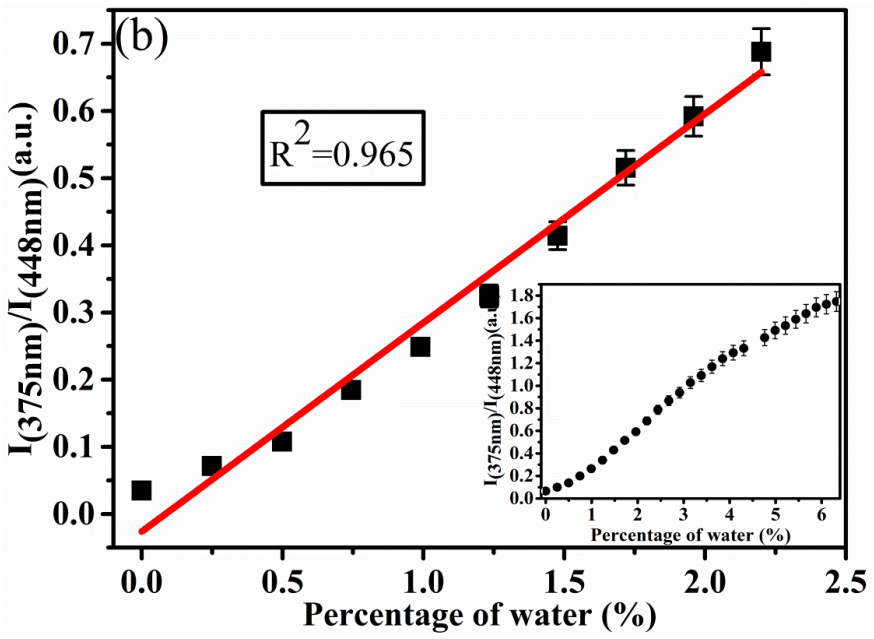

Fig. 4.6 (a) Effect of water volume fraction on the TPEA-CN^- complex in CH_3CN (b) Ratiometric response of the complex with added water (λ_{ex} = 300 nm)

We, therefore, envisioned using TPEA-CN^- system for the detection of water, as an impurity, in ACN. This is important for many applications due to the complete miscibility of water in ACN.[39] Using data obtained from the above titrations (Fig. 4.6 (a)), a linear increase in fluorescence intensity was observed as shown in Fig. 4.6 (b), when peak intensity was plotted as a function of amount of water in ACN. Using equation 3σ / *slope*, the detection limit was found to be 0.05% (V/V). Reproducible results with RSD = 1.1% were obtained in a set of five readings.

4.6 Detection and quantification of cyanide from real life samples using TPEA

The high toxicity of cyanide, as well as environmental worries about its continuous industrial usage, has sparked interest in simple and sensitive cyanide detection technologies. Cyanogenic glycosides are found in over 2000 plant species, including fruits and vegetables, and produce cyanide when acid is hydrolyzed (e.g., as occurs when ingested). Cassava (tapioca, manioc), and sorghum are stapled foods for hundreds of millions of people in tropical nations. Therefore, selective detection of cyanide in such food products is of much importance.

By using probe the TPEA, we subsequently investigated its ability to detect endogenous CN^- ions in the seeds of Indian almonds and cassava roots. The Standard Addition Method [40] was used to measure cyanide in real-life samples. Based on the calibration curve of TPEA with

spiked increasing concentration of tetrabutylammonium cyanide, the unknown concentration of cyanide in real-life samples solution of Indian almonds and cassava roots were determined to be 49.78(±2%) µM and 81.79(±3%) µM respectively as shown in Fig. 4.7 (a) and Fig. 4.7 (b).

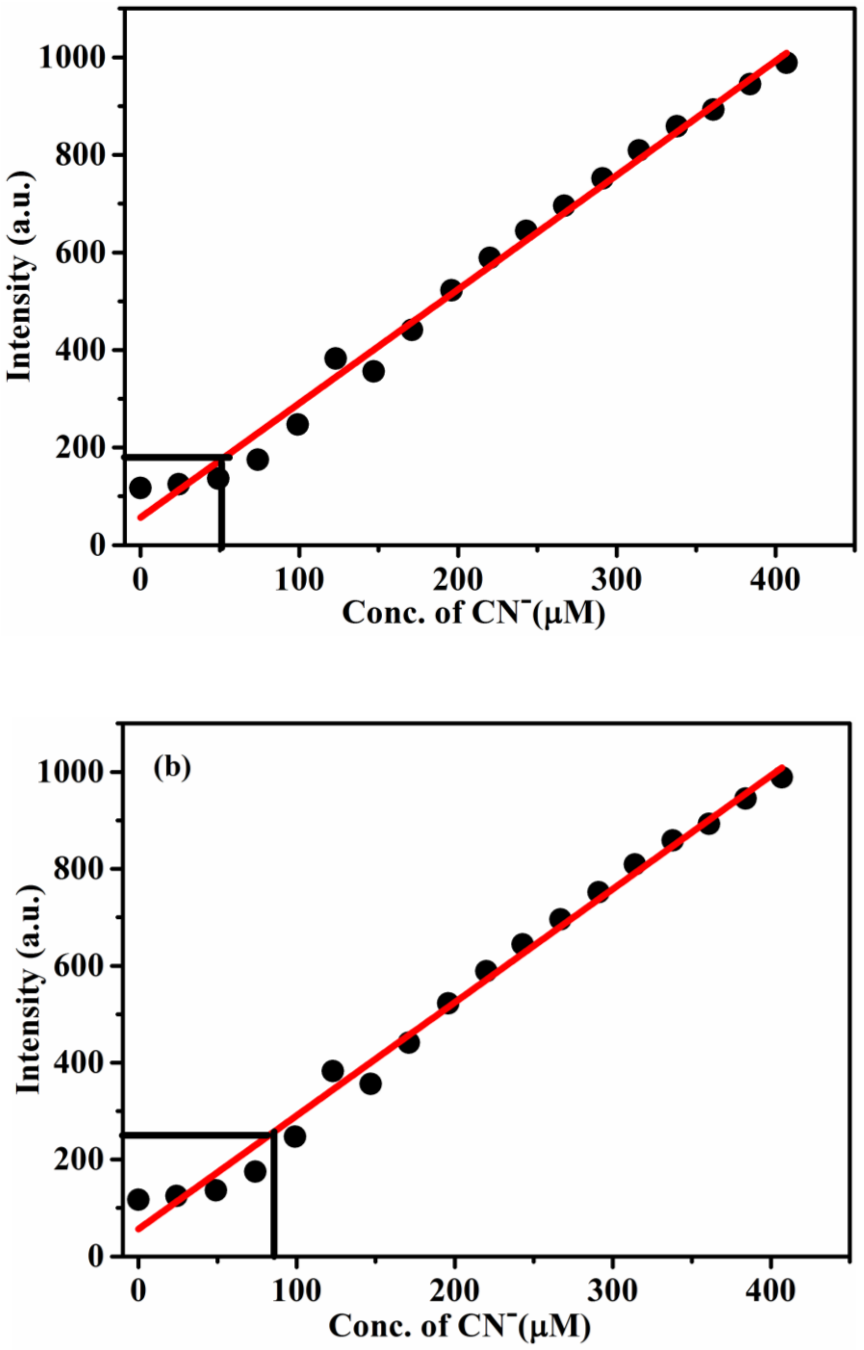

Fig. 4.7 Calibration curve for cyanide ions using probe TPEA for the determination of CN^- in (a) unripe almond (b) cassava root, (R^2= 0.984)

4.7 Electrochemical studies

Voltammograms of TPEA were recorded in pure acetonitrile and acetonitrile: water (95:5, v/v) media. Since, presence of water is likely to solvate TPEA, leading to stabilization of the functional groups in primary amines, a detailed voltammetric study is reported only in acetonitrile as a medium.

Experiments were conducted to investigate the oxidative power of the lone pair on imine nitrogen with that of nitrogen of amine group. As expected the lone pair in the latter case shows more prominent oxidative peaks in comparison to the lone pair of nitrogen of an imine group. DPV of TPEA with saturated nitrogen shows three prominent anodic peaks at 0.8, 1.07, and 1.29 V whereas TPEI, due to unsaturated nitrogen, shows broad bands with peak maxima at 0.81, 1.2, and 1.5 V (Fig. 4.8 (a)). The voltammograms as detailed above are very good examples of shifting of peak maxima along with the refinement of their respective shapes. This proves enhanced oxidative nature of primary amine (TPEA) as compared to the secondary amine (TPEI). The cathodic DPV of the two amine molecules also supports the above discussion although the current magnitude and shapes of the bands are much poorer than the anodic DPV voltammograms (Fig. 4(b)).

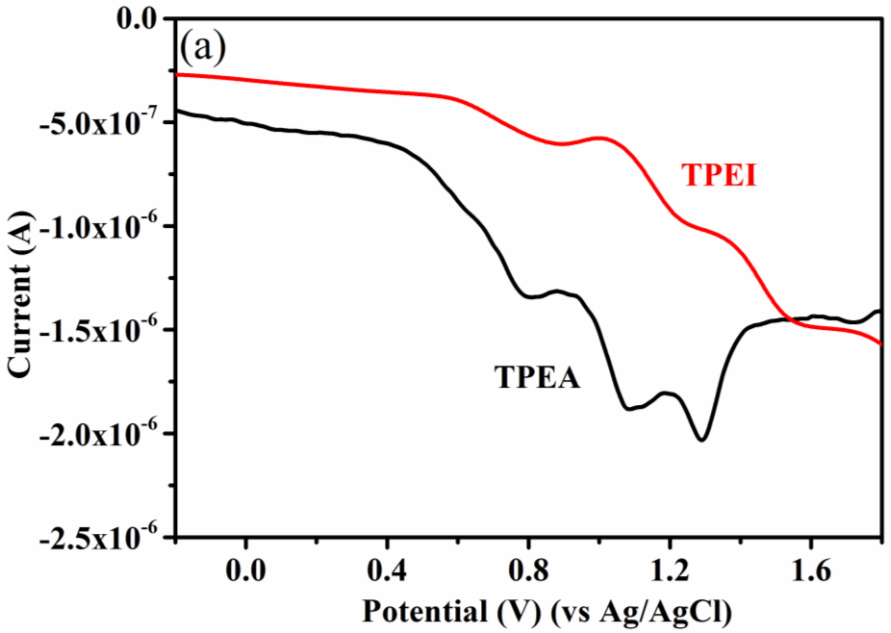

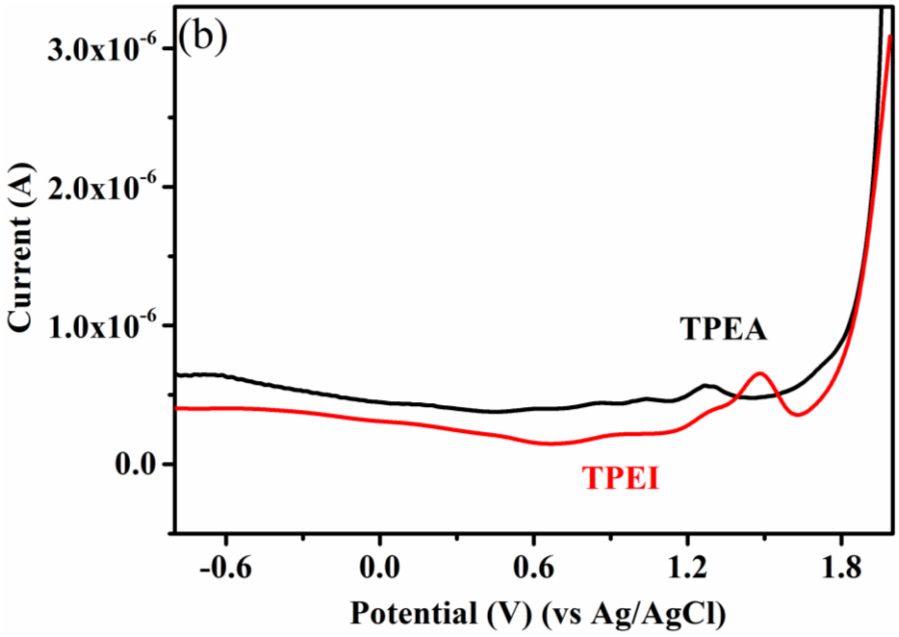

Fig. 4.8 (a) Anodic (scan in the forward direction from 0.0 to 1.7 V) (b) Cathodic (scan in the reverse direction from 1.9 to -0.7 V) differential pulse voltammograms of TPEI (1 mM) and TPEA (1 mM) in CH_3CN, 0.1 M $TBAPF_6$, scan rate: 20 mV/sec, working electrode:GC

The practical applicability of triphenyl ether amine derivative (TPEA) was studied for chemical sensing of anions of environmental importance. DPV spectra were recorded for the receptor in the presence of anionic species like OAc^-, ClO_4^-, F^-, Cl^-, I^-, $H_2PO_4^-$, HSO_4^- and CN^-, separately for each anion.

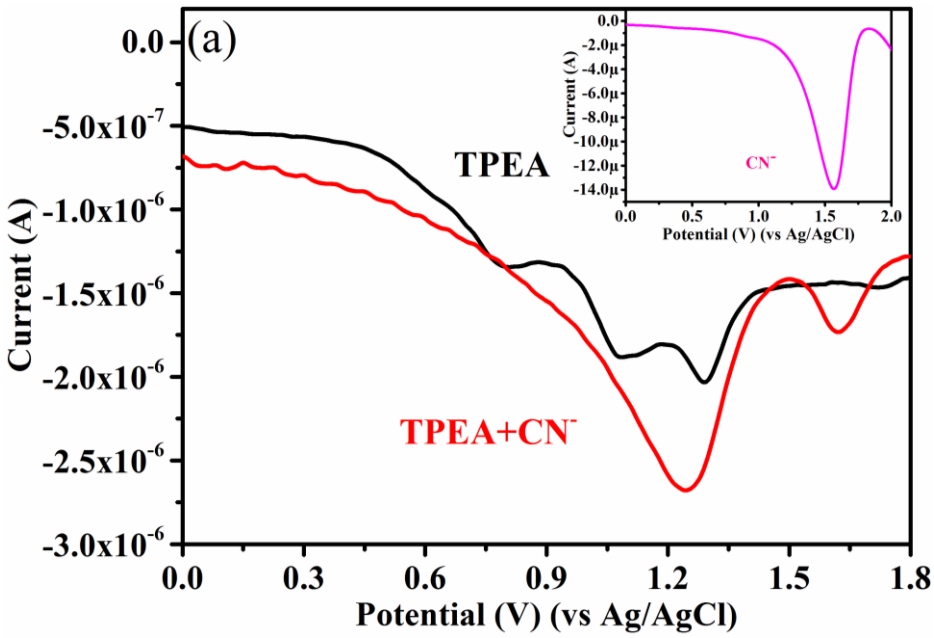

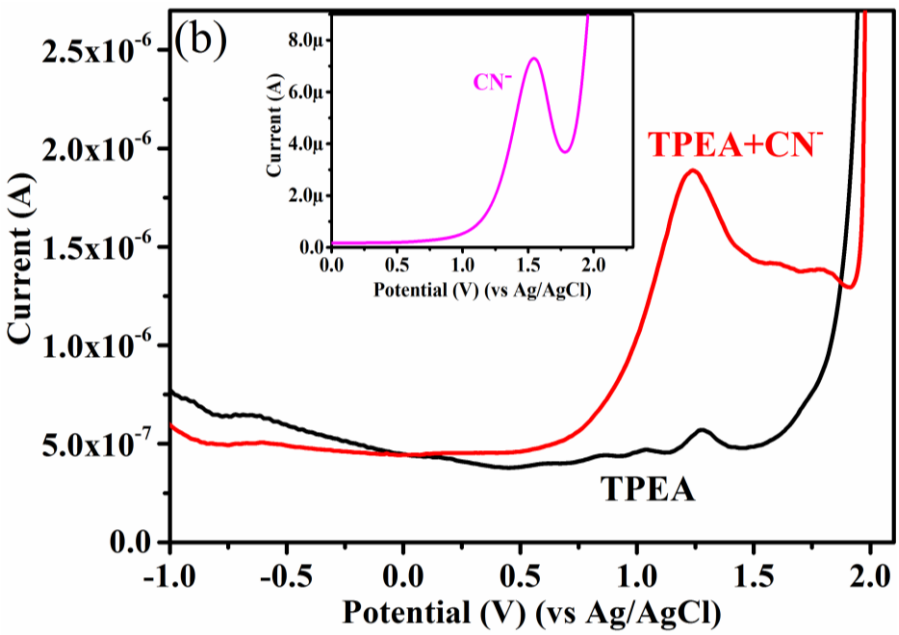

Fig. 4.9 (a) Anodic (scan in the forward direction from 0.0 to 1.8 V) (b) Cathodic (scan in the reverse direction from 2 to -1 V) differential pulse voltammograms of TPEA (1 mM) solution with and without the addition of CN^- (50 µM) ions in CH_3CN, 0.1 M $TBAPF_6$, scan rate:20 mV/sec, working electrode:GC

The most prominent shift in the anodic peak of TPEA was observed for cyanide ions as shown in Fig. 4.9 (a), where anodic peak maxima at 0.8 V, 1.07 V, and 1.29 V merged into one strong anodic peak maxima at 1.26 V. To differentiate the peak maxima of TPEA from that of CN^- ion, a DPV plot of tetrabutylammonium cyanide was recorded in ACN medium and is shown in the inset of Fig. 4.9. The anodic DPV maxima of CN^- ion appeared at 1.58 V while those of TPEA appeared in the range of 1.29 V to 1.35 V. The reorganization of anodic peak maxima as mentioned above can be explained by accepting the theory of proton abstraction (deprotonation) from hydroxyl substituent on naphthalene moiety of TPEA. As expected, the cyanide substrate, which is tetrabutylammonium cyanide would take away the acidic proton from –OH group of phenyl group, leaving behind the phenolate anion which stabilizes itself through conjugation with the naphthalene ring via intramolecular charge transfer process.[41-43] The bulky conjugate acid of tetrabutylammonium cyanide is bound electrostatically to the conjugated phenolate anion. The hydrogen of -OH group is abstracted by cyanide to form HCN which is likely to escape in the environment being a gaseous product. The presence of anodic peak maxima at 1.6 V supports the proposed hypothesis. Cathodic peak maxima corresponding to the anodic peak (at 1.6 V) could not be captured in the cathodic DPV, probably because of poor electrode kinetics of the reduction cycle of the

redox reaction. However, a broad cathodic peak of medium height was observed in the DPV spectrum of TPEA at 1.23 V on complexation with CN^- ions as shown in Fig. 4.9 (b).

For quantitative measurement of CN^- ions, calibration curve of the host TPEA on the addition of CN^- ions was plotted. The spectra include the anodic current values at the applied potential of 1.26 V (Fig. 4.9 (a)). The calibration curve for the binding of the CN^- ions with the host was plotted and the regression coefficient was found to be 0.975 as shown in fig. 4.10. Hence, it is established that TPEA can be used for chemical sensing of cyanide ions in biological and environmental samples using ACN as a medium with glassy carbon as a working electrode and potential is applied at a scan rate of 20 mV/s.

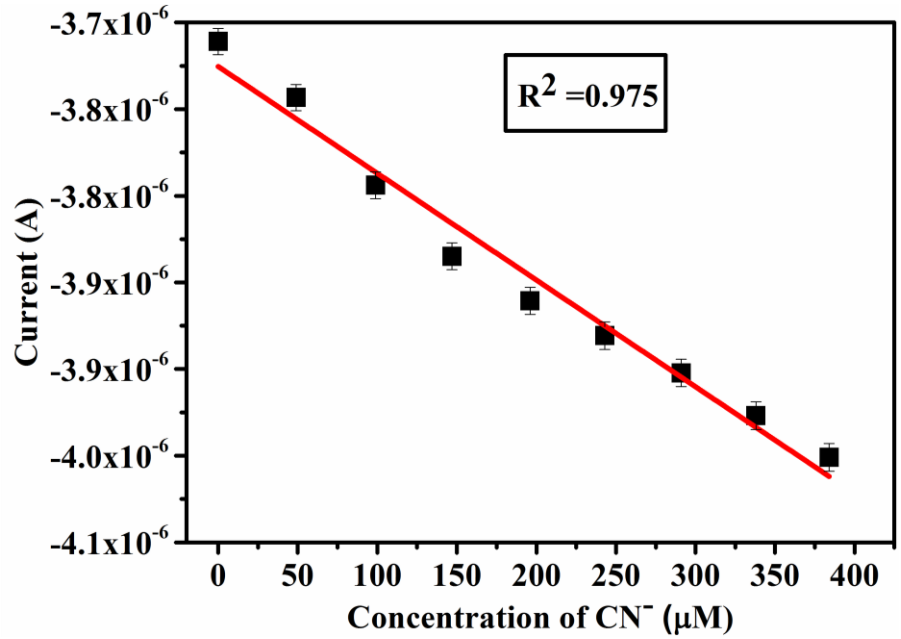

Fig. 4.10 Calibration curve between peak current and conc. of CN^- ions for quantitative measurement of CN^- using TPEA (1 mM), 0.1 M $TBAPF_6$, scan rate: 20 mV/sec, working electrode: GC

4.8 Quantum mechanical calculations

Proposed interactions between TPEA and CN^- were validated by density functional theory (DFT) calculations using the Gaussian 03W program by means of B3LYP function and 6-31G basis set. Fig. 4.11 shows the minimum energy configuration of TPEA that undergoes rotation after interaction with two CN^- ions to acquire stability. It also shows that the basic CN^- ions interact with acidic hydrogen of the hydroxyl groups leading to the stabilization of the TPEA-CN^- system. Table 4.3 shows the gap between highest occupied molecular orbital

(HOMO) and lowest unoccupied molecular orbital (LUMO) of native TPEA decreasing from 0.355 a.u to 0.141 a.u upon interaction with CN^- ions. Binding energies of TPEA and TPEA-CN^- system also show a decrease in their respective values.

Table 4.3 Energy values (in a.u) of HOMO and LUMO for TPEA and its complex with CN^- using DFT calculations

Receptor / Receptor-CN^- System	Energy in a.u		
	E_{HOMO}	E_{LUMO}	E_{gap}
TPEA	-0.266	0.089	0.355
TPEA+CN^-	-0.091	0.049	0.141

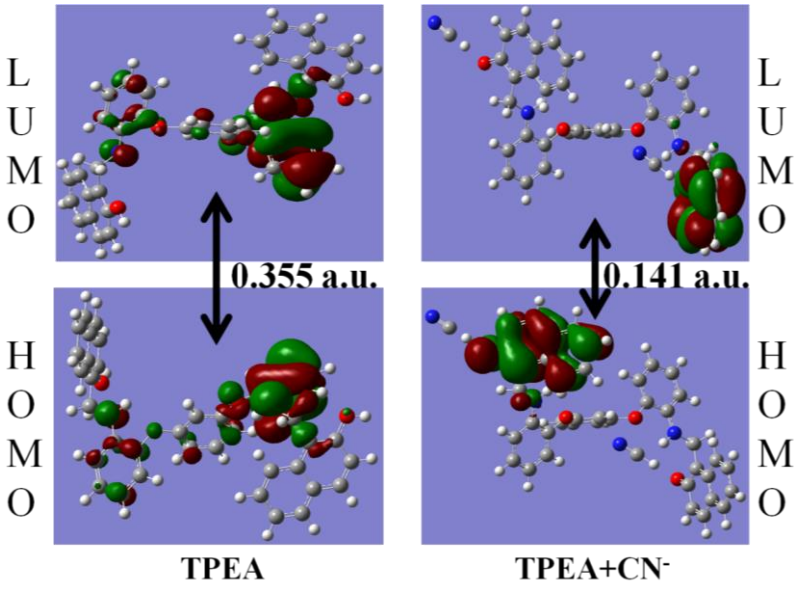

Fig. 4.11 Quantum mechanical calculations of HOMO and LUMO of TPEA and TPEA-CN^- using B3LYP/6-31G basis set

4.9 Qualitative detection method of cyanide ions using TPEA

A dip strip test was performed to assess the practical applicability of the proposed sensor for CN^- ions. Some paper strips (5 cm x 2 cm of whatman no. 1filter paper) were cut and dipped in the receptor solution (1 x 10^{-3}M) made in acetonitrile medium. These strips were dried in an air oven at 50º C. These yellow-colored strips were then immersed in cyanide solution (1 x 10^{-2} M) for 5 minutes and then dried in air. The color of the strip changed from yellow to orange as shown in Fig. 4.12. This change in color indicated the detection of cyanide ions.

Hence, the receptor TPEA can be used for naked-eye detection of cyanide ions. Similar experiment was repeated in aqueous medium also. Obtained results are shown in Fig. 4.12, which clearly indicated that the receptor TPEA shows naked eye results towards cyanide ions but not as clear as were obtained in pure acetonitrile solution. The plausible reason is that cyanide ions are highly polar in nature and have high hydration energy in aqueous medium which leads to weaken the interaction of cyanide ion towards TPEA. Therefore, synthesized probe can be used for analytical applications in acetonitrile medium.

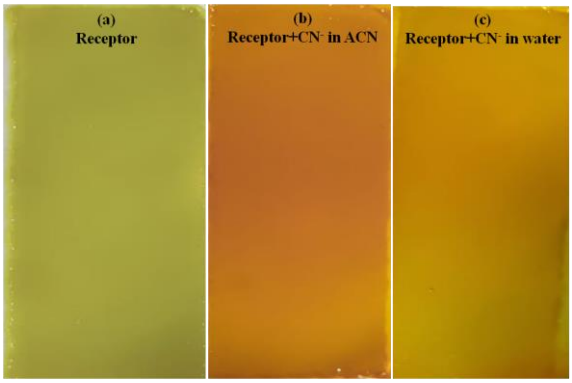

Fig 4.12 Paper strips coated with receptor (TPEA) (a) before and (b) after dipping in cyanide solution (ACN medium) (c) after dipping in cyanide solution (water medium)

Conclusions

A triphenyl ether amine (TPEA) derivative has been developed as a voltammetric and fluorimetric dual sensor for cyanide ions and water in acetonitrile medium. TPEA is also a naked eye colorimetric sensor which works on the mechanism of deprotonation and intramolecular charge transfer processes. The proposed receptor works well upto a concentration range of 400 µM with a detection limit of 0.4 µM and binding constant of 4.16×10^{7} M^{-1}. Common anions like HSO_4^-, $H_2PO_4^-$, ClO_4^-, OAc^- and halides do not interfere in the working of the proposed probe. The synthesized probe has been validated on real-life samples like almonds and cassava roots for the detection of cyanide ions. The results were comparable with the reported colorimetric methods.

References

1. A. J. Beneto and A. Siva, *Photochemical & Photobiological Sciences*, 2017, **16**, 255-261.
2. S. Paul, P. Ghosh, S. Bhuyan, S. K. Mukhopadhyay and P. Banerjee, *Dalton Transactions*, 2018, **47**, 1082-1091.
3. Z. Xu, X. Chen, H. N. Kim and J. Yoon, *Chemical Society Reviews*, 2010, **39**, 127-137.
4. W. H. Organization, *Guidelines for drinking-water quality*, World Health Organization, 2004.
5. I. G. Casella and M. Gatta, *Electroanalysis: An International Journal Devoted to Fundamental and Practical Aspects of Electroanalysis*, 2001, **13**, 549-554.
6. D. Bohrer, P. Do Nascimento, S. G. Pomblum, E. Seibert and L. M. de Carvalho, *Fresenius' Journal of Analytical Chemistry*, 1998, **361**, 780-783.
7. S. Dadfarnia, A. M. H. Shabani, F. Tamadon and M. Rezaei, *Microchimica Acta*, 2007, **158**, 159-163.
8. D. Shan, C. Mousty and S. Cosnier, *Analytical Chemistry*, 2004, **76**, 178-183.
9. D. Recalde-Ruiz, E. Andres-Garcia and M. Diaz-Garcia, *Analyst*, 2000, **125**, 2100-2105.
10. Q. Niu, L. Lan, T. Li, Z. Guo, T. Jiang, Z. Zhao, Z. Feng and J. Xi, *Sensors and Actuators B: Chemical*, 2018, **276**, 13-22.
11. R. Hu, J. Feng, D. Hu, S. Wang, S. Li, Y. Li and G. Yang, *Angewandte Chemie International Edition*, 2010, **49**, 4915-4918.
12. H. M. Chawla, R. Shukla and P. Goel, *New Journal of Chemistry*, 2014, **38**, 5264-5267.
13. D. Maity, G. Vyas, M. Bhatt and P. Paul, *RSC Advances*, 2015, **5**, 6151-6159.
14. C. Long, J.-H. Hu, P.-W. Ni, Z.-y. Yin and Q.-Q. Fu, *New Journal of Chemistry*, 2018, **42**, 17056-17061.
15. J. Chao, Z. Li, Y. Zhang, F. Huo, C. Yin, H. Tong and Y. Liu, *Sensors and Actuators B: Chemical*, 2016, **228**, 192-199.
16. Q. Zhang, J. Zhang, H. Zuo, C. Wang and Y. Shen, *Tetrahedron*, 2016, **72**, 1244-1248.
17. M. Chemchem, I. Yahaya, B. Aydıner, N. Seferoğlu, O. Doluca, N. Merabet and Z. Seferoğlu, *Tetrahedron*, 2018, **74**, 6897-6906.
18. A. Sheykhi-Estalkhjani, N. O. Mahmoodi, A. Yahyazadeh and M. P. Nadamani, *Tetrahedron*, 2018, **74**, 4868-4874.

19. B. H. Shankar, D. T. Jayaram and D. Ramaiah, *Chemistry–An Asian Journal*, 2014, **9**, 1636-1642.

20. C. Männel-Croisé, B. Probst and F. Zelder, *Analytical Chemistry*, 2009, **81**, 9493-9498.

21. R. Sharma, M. Chhibber and S. K. Mittal, *RSC Advances*, 2016, **6**, 51153-51160.

22. Y. Ding, T. Li, W. Zhu and Y. Xie, *Organic & Biomolecular Chemistry*, 2012, **10**, 4201-4207.

23. T. W. Hudnall and F. P. Gabbaï, *Journal of the American Chemical Society*, 2007, **129**, 11978-11986.

24. Y. Sun, G. Wang and W. Guo, *Tetrahedron*, 2009, **65**, 3480-3485.

25. S. Saha, A. Ghosh, P. Mahato, S. Mishra, S. K. Mishra, E. Suresh, S. Das and A. Das, *Organic Letters*, 2010, **12**, 3406-3409.

26. K. Keshav, P. Torawane, M. K. Kumawat, K. Tayade, S. K. Sahoo, R. Srivastava and A. Kuwar, *Biosensors and Bioelectronics*, 2017, **92**, 95-100.

27. J. S. Renny, L. L. Tomasevich, E. H. Tallmadge and D. B. Collum, *Angewandte Chemie International Edition*, 2013, **52**, 11998-12013.

28. H. A. Benesi and J. Hildebrand, *Journal of the American Chemical Society*, 1949, **71**, 2703-2707.

29. Analytical Methods Committee, *Analyst*, 1987, **112**, 199-204.

30. F. A. Al-Zahrani, R. M. El-Shishtawy, A. M. Asiri, A. M. Al-Soliemy, K. A. Mellah, N. S. Ahmed and A. Jedidi, *BMC Chemistry*, 2020, **14**, 1-11.

31. A. Sebastian and E. Prasad, *Langmuir*, 2020, **36**, 10537-10547.

32. P. R. Lakshmi, P. Jayasudha and K. P. Elango, *Spectrochimica Acta Part A: Molecular and Biomolecular Spectroscopy*, 2019, **213**, 318-323.

33. Z. Guo, T. Hu, T. Sun, T. Li, H. Chi and Q. Niu, *Dyes and Pigments*, 2019, **163**, 667-674.

34. K. Deng, L. Wang, Q. Xia, R. Liu and J. Qu, *Sensors and Actuators B: Chemical*, 2019, **296**, 126645.

35. Z. M. Dong, H. Ren, J. N. Wang, J. B. Chao and Y. Wang, *Spectrochimica Acta Part A: Molecular and Biomolecular Spectroscopy*, 2019, **217**, 27-34.

36. A. M. Al-Soliemy, *Journal of Molecular Structure*, 2019, **1179**, 525-531.

37. P. S. Kumar, P. R. Lakshmi and K. P. Elango, *Spectrochimica Acta Part A: Molecular and Biomolecular Spectroscopy*, 2019, **221**, 117172.

38. Z. Guo, Q. Niu, Q. Yang, T. Li and H. Chi, *Analytica Chimica Acta*, 2019, **1065**, 113-123.

39. S. Goswami, A. K. Das, A. Manna, A. K. Maity, H.-K. Fun, C. K. Quah and P. Saha, *Tetrahedron Letters*, 2014, **55**, 2633-2638.

40. W. R. Kelly, K. W. Pratt, W. F. Guthrie and K. R. Martin, *Analytical and Bioanalytical Chemistry*, 2011, **400**, 1805-1812.

41. T. B. Wei, G. T. Yan, H. Li, Y. R. Zhu, B. B. Shi, Q. Lin, H. Yao and Y. M. Zhang, *Supramolecular Chemistry*, 2016, **28**, 720-726.

42. N. Kumari, S. Jha and S. Bhattacharya, *The Journal of Organic Chemistry*, 2011, **76**, 8215-8222.

43. K. Yu, N. He, N. Kumar, N. Wang, J. Bobacka and A. Ivaska, *Electrochimica Acta*, 2017, **228**, 66-75.

Chapter 5

Electrochemical Trisensor for copper, cyanide and arginine supported with optical techniques

This study demonstrated that synthesised receptor i.e. triphenyl ether amide have selectively responded to Cu(II) and CN^- ions in the presence of various cations and anions. Cu(II) ions were detected via host guest interaction mechanism and CN^- ions were detected using deprotonation mechanism as confirmed by ^{1}HNMR titrations. Furthermore, Copper complex has detected argine among various amino acids using metal ion desplacement approach. For practical application, synthesized probe TPEAM have detected Cu(II) ions in different food samples. Interactions based on experimental results were in good agreement with the theoratical calculations.

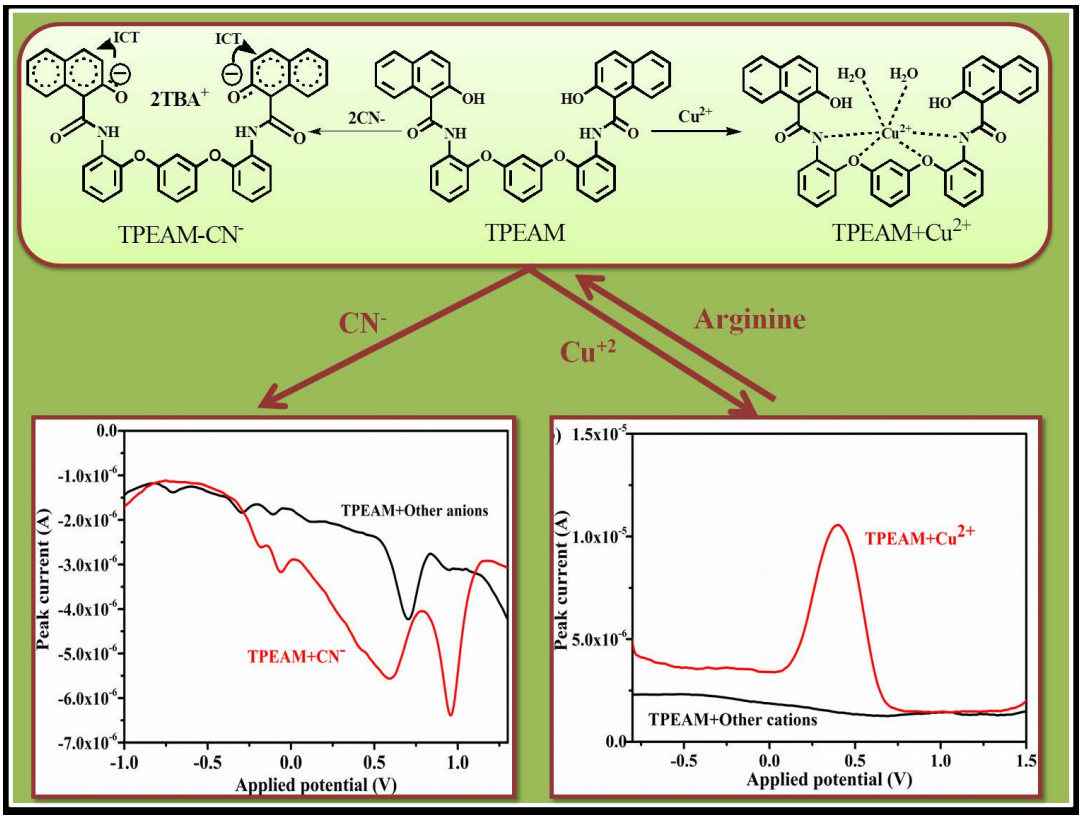

Schematic presentation of sensing behaviour of TPEA

5.1 Introduction

Copper is the third most abundant transition metal after Fe(III) and Zn(II) in a human body.[1] It is recommended to take the proper dose of it in food every day. Many of proteins in the human body use copper ions in electron transport processes, or for normal functioning of the brain and nervous system. Yet, excess of copper ions in living cells can damage lipids, catalyze the production of reactive oxygen species (ROS) and cause several diseases such as Alzheimer's disease, Indian childhood cirrhosis, and Wilson disease.[2-4] According to the World Health Organisation (WHO), the maximum limit of copper in drinking water should be 1.3 ppm.[5] The toxicity of copper is not only a concern to human species but has a great effect on the ambient environment too. An increased copper level has proven to be detrimental to the growth of stream insects, aquatic biota, and certain vegetation also. Therefore, the practical monitoring of Cu^{2+} is highly required.

Cyanide is one of the most toxic species as well as deadly to mankind. Yet, it is extensively used in many industrial processes, such as electroplating, gold mining, plastic manufacturing, herbicide, synthetic fibers, and resin industry. Because of its extensive use, it has been discarded to the environment as industrial wastewater in a huge amount of nearly 140,000 tons per year worldwide.[6] The toxicity of cyanide to mankind is due to its efficient binding to the active site of cytochrome oxidase which leads to interference in the electron transport chain in mitochondria.[7-9] In addition to this, the presence of cyanide also causes vomiting, loss of consciousness, and ultimately to death.[10, 11] According to the World Health Organisation (WHO), the concentration of cyanide in drinking water should not exceed 70 µg/L.[12] Also, the maximum contamination level of cyanide in drinking water is set to be 200 µg/L by US EPA. Therefore, trace level detection of cyanide from different matrices such as food, water, soil, living cells, and blood is very much required.

Arginine is a semi-essential amino acid that exists for tRNA, plays an important role in the synthesis of protein, wound healing, and cell replication. Reduced levels of arginine have been reported in various clinical conditions such as asthma, psoriasis, and reperfusion injury. Therefore, the detection of arginine in biological fluids has become an important goal.[13]

Various kinds of analytical techniques are available for the detection of both copper and cyanide ions, but most of these techniques require tedious sample preparation procedure, skilled labour, costly and sophisticated instruments. To overcome these problems, differential pulse voltammetry (DPV) has become an important tool to characterize electrochemical

behaviour of the receptor and have various advantages such as lower detection limit, high selectivity, and less power requirement. Other than this, fluorescence spectroscopy is a promising tool for the trace level detection of cations and anions. This is because, spectroscopic techniques are easy to handle, operate, and are also cost-effective.

There are a large number of receptors reported in literature which sense copper and cyanide ions, simultaneously. However, most of these sensors are sequential as the first sense copper ions and then cyanide ions. This is because of the high affinity of cyanide ions toward copper ions.[8, 14-18] Very few reports are available where Cu^{2+} and CN^- ions are recognized by the receptor using different mechanisms and also in a non-sequential manner.[19, 20] To this context, simple, facile, and efficient chemosensors are required for selective recognition of Cu^{2+} ions and CN^- ions using different approaches/mechanisms following the non-sequential pattern of sensing. Despite these studies, still there is a need to prepare metal-organic complex sensors for the sequential detection of amino acids.

Herein, a novel triphenylether derivative with amide linkages is described as a trisensor for the selective detection of Cu^{2+}, CN^- ions and arginine. The receptor ionophore TPEAM shows "*ON-OFF"* fluorescent selectivity for Cu^{2+} ions, which is a desirable result as Cu^{2+} ions are paramagnetic and are strong fluorescence quencher. On the other hand, CN^- ions are detected quantitatively via an intramolecular charge transfer (ICT) process. The ICT process takes place due to the abstraction of the proton (deprotonation) from hydroxyl moieties of the naphthyl groups. Voltammetric results of Cu^{2+} and CN^- ions are corroborated with spectroscopic methods and ^{1}H NMR titrations. Furthermore, the "*ON-OFF"* response of receptor TPEAM towards Cu^{2+} ions leads us to use this complex for the detection of arginine following the "*ON-OFF-ON"* pattern based on metal displacement approach.

5.2 Real-life sample preparation and determination

5.2.1 Determination of Cu^{2+} ions in a multivitamin tablet

Each tablet of a multivitamin was weighed precisely and crushed finely in a pestle mortar. One milliliter of concentrated nitric acid was added to the powder taken in a beaker and heated to near dryness under cover of a fuming hood. After cooling, the residue was again dissolved in another one milliliter of concentrated nitric acid and the solution was gently evaporated till it became colourless. The residue was again heated with 50 mL of distilled water, filtered off and diluted to 100 mL using a volumetric flask. An aliquot of this sample was taken and analyzed with the proposed method and Atomic Absorption Spectroscopy

(AAS).[21] The procedure was repeated three times and measurements were made with each sample.

5.2.2 Determination of Cu^{2+} ions in black tea

Three samples of 1g each of dry black tea was weighed accurately and taken in a 100 mL beaker. Then 10 mL of nitric acid (8 mol/L) and 4 mL of perchloric acid were added to the tea sample followed by digestion on a hot plate kept in a fuming hood. The samples were oxidized completely until it became a clear solution. After filtration, each sample was diluted to 100 mL water using a calibrated volumetric flask. The copper content in black tea was determined with the proposed method and Atomic Absorption Spectroscopy (AAS).[21]

5.3 Results and discussion

5.3.1 Design of ionophore

TPEAM receptor ionophore was designed following the strategy: the triphenyl ether group provides a suitable cavity for the target species and the amide linkages provide a suitable hetero atom environment along with the ethereal oxygen atoms to offer a good chance for chelation of the metal ion. Also, the presence of a naphthyl group provides fluorescence to the synthesized molecule. Therefore, we expected that the combination of triphenyl ether, amide linkage, and naphthyl group would show good chelation to metal ions and endow a unique photophysical and electrochemical properties. Thus, a novel receptor triphenyl ether amide (TPEAM) was synthesized using a two-step reaction sequence as described in chapter 3. Characterization of the compound using ^{1}H and ^{13}C NMR confirmed formation of the product due to the appearance of an amidic proton at 12.3 ppm and carbon at 171.5 ppm.

5.3.2 Electrochemical studies of TPEAM

Differential Pulse Voltammetry (DPV) was performed to study the electrochemical behaviour of TPEAM (1.0×10^{-4} M) alone and in the presence of various metal ions such as Hg^{2+}, Ni^{2+}, Co^{2+}, Fe^{2+}, Fe^{3+}, Mn^{2+}, Ca^{2+}, Pb^{2+}, Mg^{2+}, Cr^{3+}, Zn^{2+}, Cu^{2+} in ACN-Water (90:10, v/v) medium. For TPEAM, a weak anodic DPV curve was observed at 0.89 V while no corresponding peak was observed in the cathodic DPV (Fig. 5.1). This voltammetric behaviour is expected from TPEAM, as there is no easily reducible functional group present in the molecule; a poorly defined anodic peak can be due to the oxidative tendency of lone pair on the nitrogen atom of the amide linkage. The anodic peak is very weak because of the –ve inductive effect of –C=O group, adjacent to the secondary amine in the molecule.

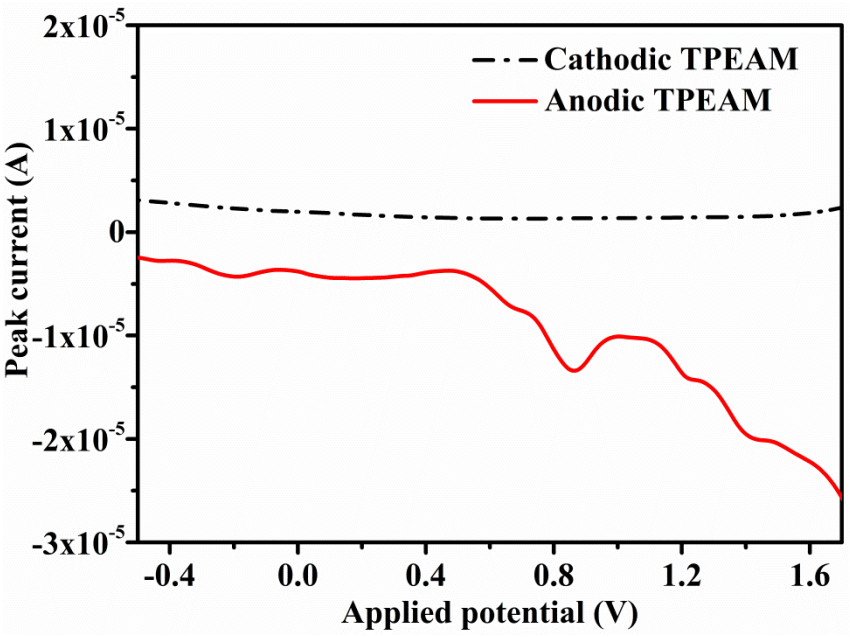

Fig. 5.1 Anodic and cathodic behaviour of TPEAM (1.0×10^{-4} M) in ACN-Water (90:10, v/v) medium, 0.1 M $TBAPF_6$, scan rate of 50 mV/sec using GC electrode against Ag/Ag^+

Among various metal ions, it is interesting to find well-established maxima in both anodic and cathodic voltammograms of TPEAM-Cu^{2+} complex (Fig. 5.2). This change in pattern provides evidence for the active interaction of Cu^{2+} ions as a guest species in the pseudo cavity of TPEAM. The presence of Cu^{2+} ions in the cavity is likely to attract electron donation (although weak) from the amidic nitrogen. The appearance of peak current maxima at 0.41 V and 0.75 V (Fig. 5.2(a)) in the anodic DPV may be due to oxidation of lone pair on nitrogen into two consecutive steps. During the reverse cycle, this oxidative lone pair of electrons is restored as observed by the cathodic peak current maxima at 0.41 V (Fig. 5.2(b)).

It is very interesting to observe that a strong cathodic peak maximum is observed in the TPEAM-Cu^{2+} complex which was missing in the DPV of TPEAM. The reason for this observed change is the electropositive character of Cu^{2+} species, which enhances the reductive tendency of the nitrogen in the reverse half cycle of the voltammogram To differentiate the peak maxima of TPEA from that of Cu^{+2} ion, a DPV plot of copper perchlorate was recorded and is shown in the inset of Fig. 5.2. To differentiate the peak maxima of TPEAM-Cu(II) complex from that of Cu(II) ion, a DPV plot of copper perchlorate was recorded in ACN medium and is shown in the inset of Fig. 5.2. The anodic DPV maxima

of Cu (II) ion appeared at -1.35 V and -0.9 V (Fig. 5.2 inset) while those of TPEAM-Cu(II) appeared in the range of 0.41 V to 0.75 V.

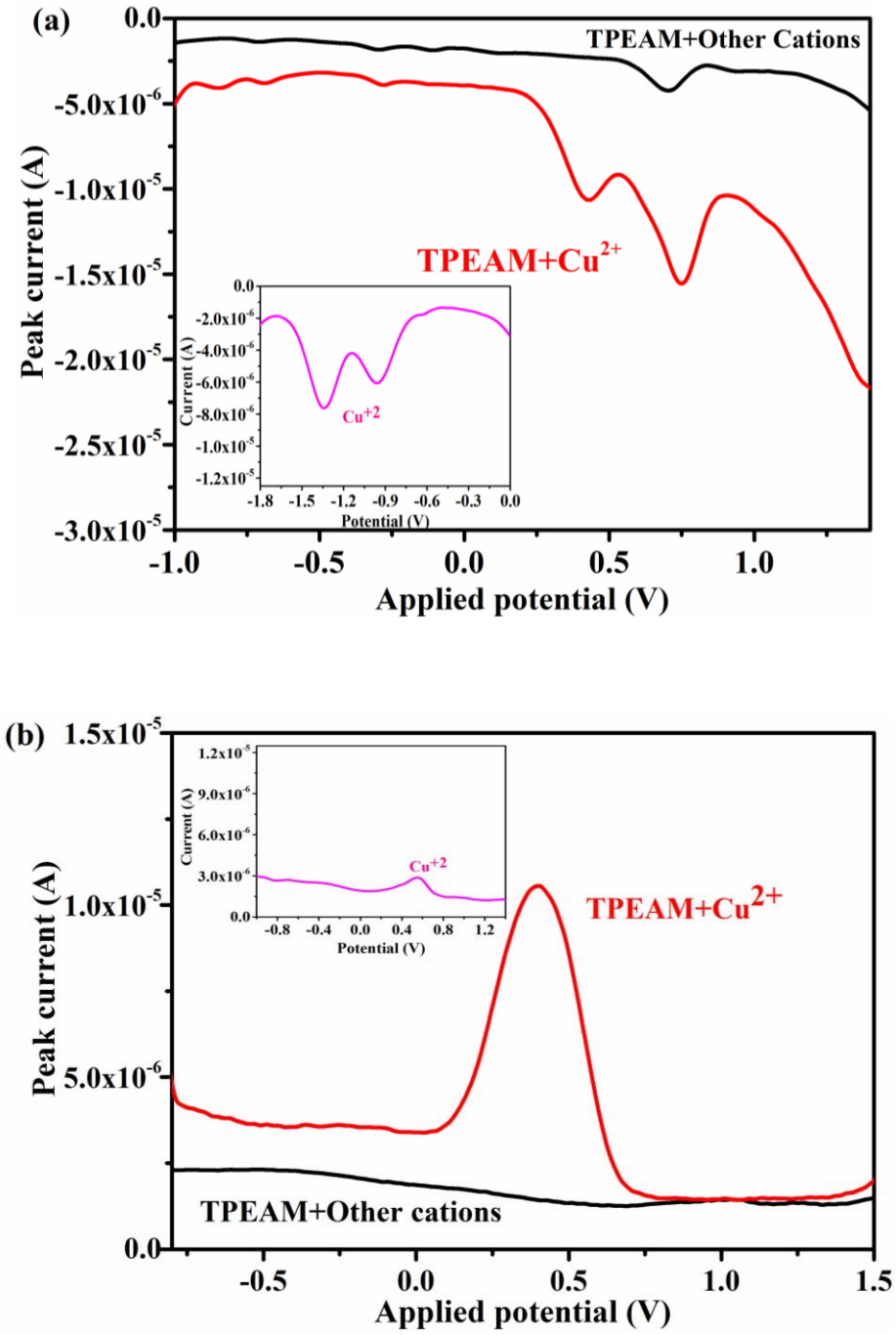

Fig. 5.2 (a) Anodic and (b) cathodic DPV of TPEAM (1.0×10^{-4} M) in the presence of various metal ions (20 µM) in ACN-Water medium at a scan rate of 50 mV/sec using GC electrode against Ag/Ag^{+} (Inset (a) anodic and (b) cathodic DPV of Cu(II) only)

For the quantitative measurement of Cu^{2+} ions, a cathodic peak current of TPEAM at 0.41 V was plotted against the concentration of Cu^{2+} ions, a straight line trend indicated the application potential of TPEAM as a voltammetric sensor. The calibration curve for the binding of the Cu^{+2} ions with the host was plotted and the regression coefficient was found to be 0.99 as shown in fig. 5.3. Hence, it is established that TPEAM can be used for chemical sensing of copper ions in environmental and biological samples using ACN as a medium with glassy carbon as a working electrode and potential is applied at a scan rate of 50 mV/s.

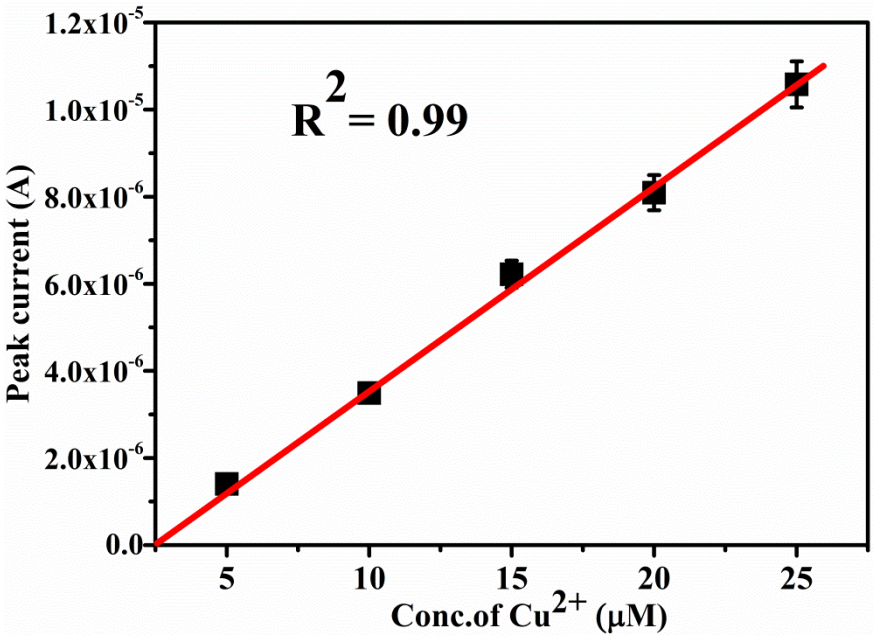

Fig. 5.3 Calibration curve between peak current and concentration of Cu(II) ions for quantitative measurement of Cu^{2+} using TPEAM (1.0×10^{-4} M); GC electrode against Ag/Ag^{+} in ACN:H_2O medium at a scan rate of 50 mV/sec

5.3.3 Photophysical behaviour of TPEAM towards Cu^{2+} ions

Metal ion sensing ability of the receptor TPEAM (1.0×10^{-4} M) was also studied by UV-vis absorption spectroscopy for various metal ions such as Hg^{2+}, Ni^{2+}, Co^{2+}, Fe^{2+}, Fe^{3+}, Mn^{2+}, Ca^{2+}, Pb^{2+}, Mg^{2+}, Cr^{3+}, Zn^{2+}, Cu^{2+} in ACN-Water (90:10, v/v) medium. As shown in Fig. 5.4, TPEAM shows absorption bands at 277 nm, 288 nm, 304 nm due to $\Pi\rightarrow\Pi^{*}$ and a weak band at 334 nm due to $n\rightarrow\Pi^{*}$ transitions. Among all the cations, Cu^{2+} ions displayed high sensitivity towards TPEAM, as the addition of copper ions leads to the disappearance of receptor bands at 277 nm and 288 nm and the appearance of a single band with high absorption at 308 nm. However, no such spectral changes were observed with any other competitive metal ion, leading to the selectivity of TPEAM towards Cu^{2+} ions. As all the

absorption changes occurred in the UV region i.e., below 400 nm, therefore no colour variation was observed with naked eyes.

Formation of the Cu^{2+} complex with TPEAM takes place via the coordination of Cu^{2+} ions with the –NH groups of the amide linkage, ethereal oxygen atoms of TPEAM and water molecules present in the solvent system, as shown in Scheme 5.1. By using UV-vis spectroscopy, the binding property of TPEAM towards Cu^{2+} ions were examined. Upon gradual addition of Cu^{2+} ions into the TPEAM solution, the absorbance value at 308 nm started increasing and finally merged into a single band (Fig. 5.5) within the equivalent range of 0-1.6. The molar extinction coefficient (ε) was found to be 1.05×10^{3} M^{-1} cm^{-1}, which suggests that metal to ligand charge transfer based transitions are taking place in the complex as this molar extinction coefficient value is too large to be Cu-based d-d transitions.[22]

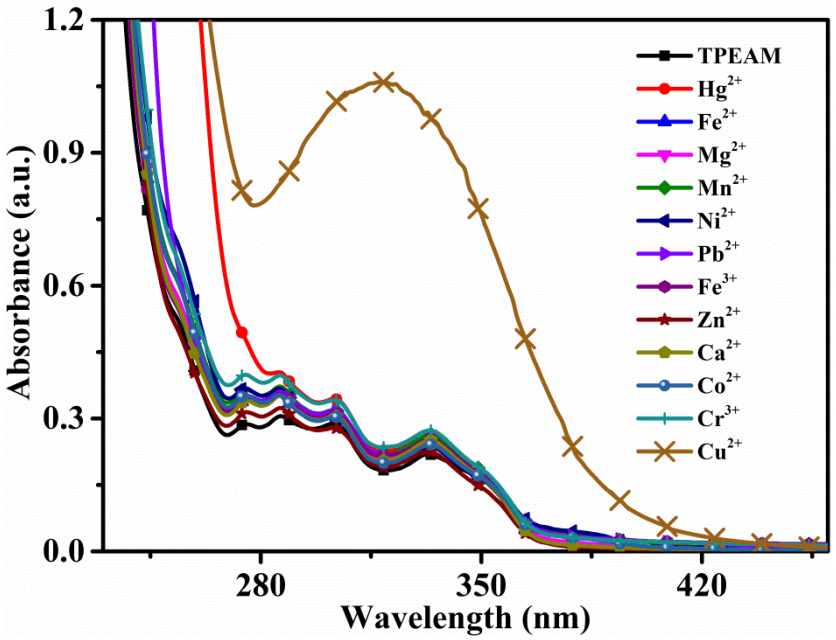

Fig. 5.4 Absorption spectral changes of TPEAM (1.0×10^{-4} M) in the presence of various metal ions (150 µM) in ACN-Water (90:10, v/v) system

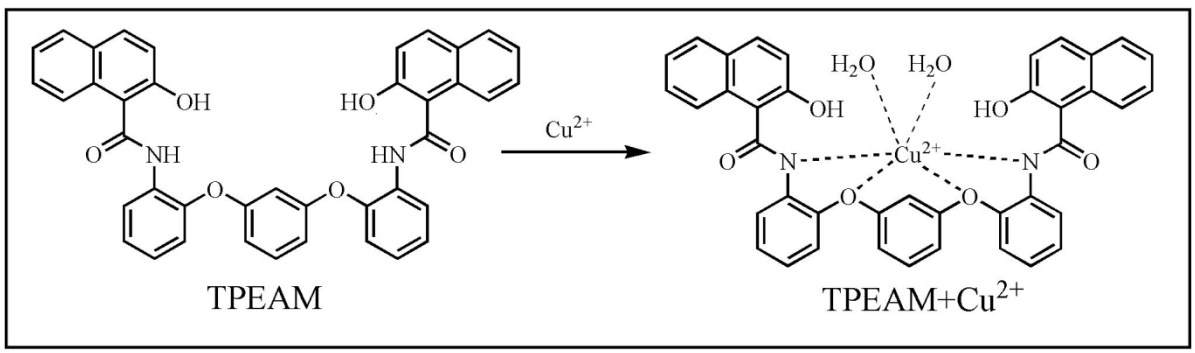

Scheme 5.1 The proposed sensing mechanism of TPEAM with Cu^{2+} ions

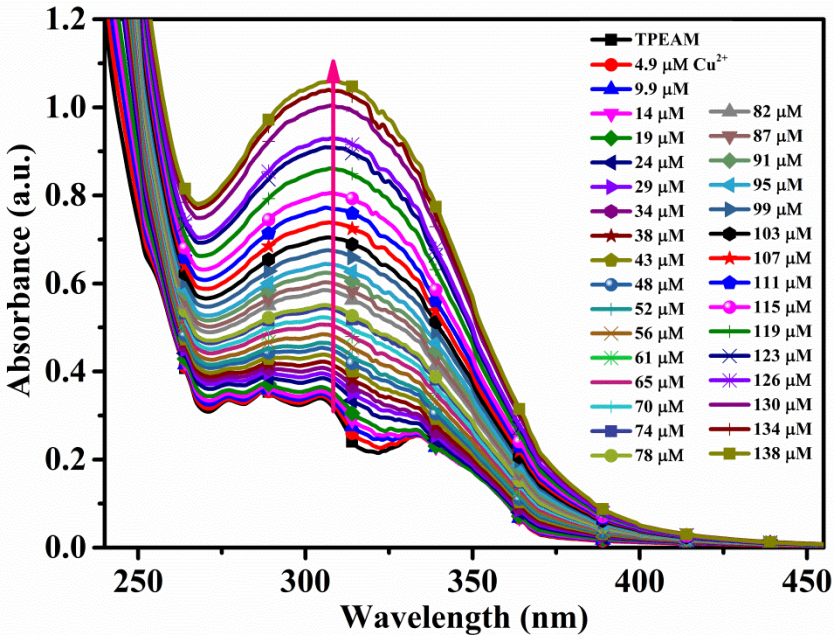

Fig. 5.5 Absorption spectral changes of TPEAM (1.0×10^{-4} M) with the incremental addition Cu^{2+} ions in ACN-Water (90:10, v/v) medium

To determine the binding stoichiometry of TPEAM with Cu^{2+} ions, Job's plot[23] studies were carried out and maximum absorption was observed when a mole fraction reached at 0.5, which signifies 1:1 stoichiometry between TPEAM and Cu^{2+} ions and mole fraction was varied from 0 to1 (Fig. 5.6).

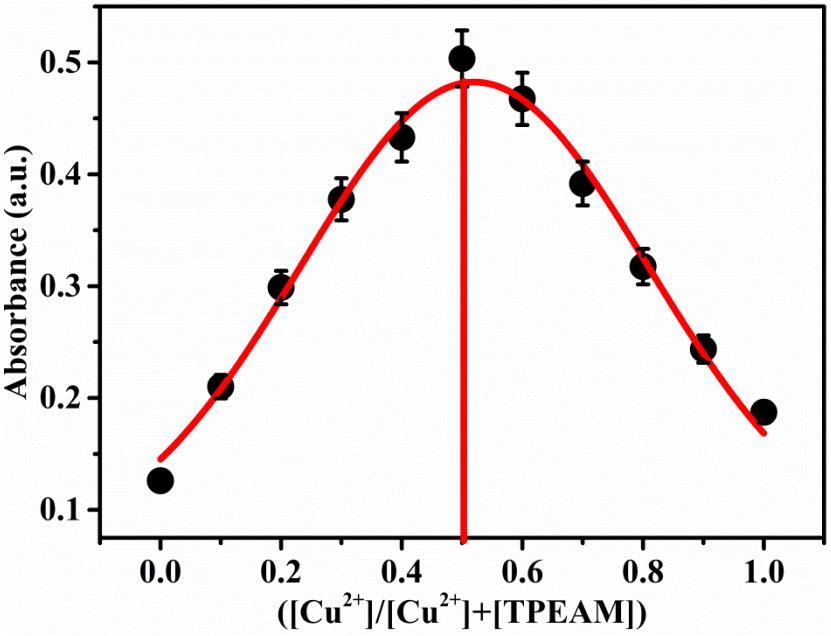

Fig 5.6 Job's plot between TPEAM and Cu^{2+} ions in ACN-Water (90:10, v/v) medium

Further, fluorescence emission titration of TPEAM (50 µM) was conceded out with different concentrations of Cu^{2+} ions when the excitation wavelength was fixed at 340 nm. Upon the progressive addition of Cu^{2+} ions, fluorescence quenching started taking place at 390 nm (Fig. 5.7). Quenching was observed because of the paramagnetic nature of Cu^{2+} ions which ultimately takes away electron (and hence energy) from the excited state of TPEAM, resulting in a fluorescence signal *"turn off"*.[24] This quenching phenomenon was also confirmed by the change in the colour of TPEAM under UV light (365 nm) from weakly fluorescent (light blue) to non-fluorescent (colourless) after the addition of the copper ions (Fig. 5.7 (inset)). From the calibration curve of emission titration (Fig. 5.8), the detection limit[25] of TPEAM for Cu^{2+} ions was found to be 40 nM. The association constant (K_a) for TPEAM, calculated using the Benesi-Hildebrand equation, was 1.5×10^4 M^{-1}. Also, the quenching degree was calculated to be 88% using the formula: $\eta = (I_o\text{-}I)/I_o$.

To study the potential of the receptor (TPEAM), for Cu^{2+} ions, an interference study was conducted. For this, fluorescence spectra were recorded in the presence of an equivalent amount of various coexisting cations such as Ni^{2+}, Co^{2+}, Fe^{2+}, Fe^{3+}, Mn^{2+}, Ca^{2+}, Pb^{2+}, Mg^{2+}, Cr^{3+} and Zn^{2+} (Fig 5.9). Different metal ions do not show any significant change in fluorescence intensity, which shows the selective and specific behaviour of TPEAM for Cu^{2+} ions.

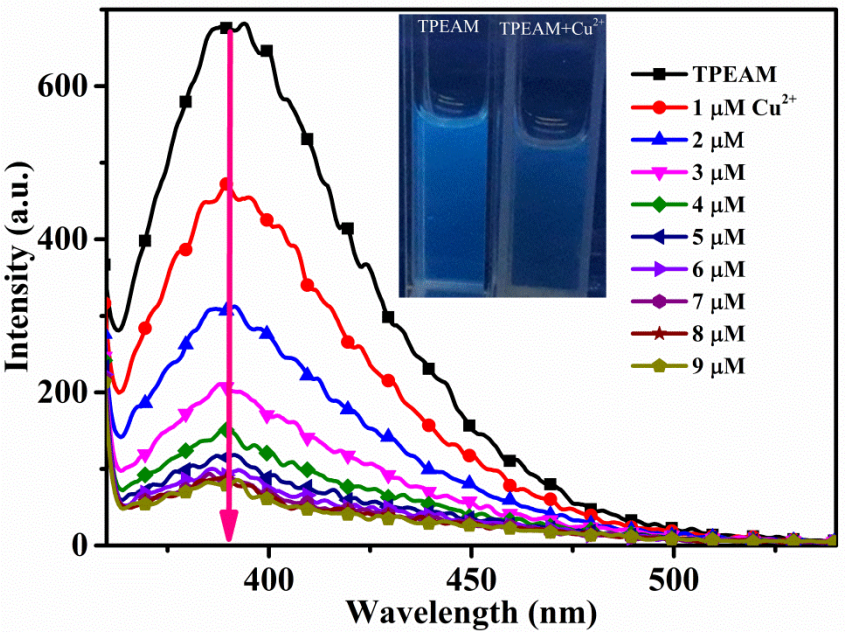

Fig. 5.7 Fluorescence emission titration of TPEAM (50 µM) on addition of incremental amount of Cu^{2+} ions in ACN-Water (90:10, v/v) medium (λ_{ex} = 340 nm)

To validate the practical applicability of TPEAM towards Cu^{2+}, real-life sample analysis was carried out on multivitamin capsules and black tea samples. Results of Cu^{2+} concentration, determined with the proposed fluorescence method were compared with Atomic Absorption Spectroscopy (AAS) method. The results obtained from three replicate measurements are given in Table 5.1 that shows concentrations of Cu^{2+} in samples with the AAS technique (Figure A5.1) agree with the proposed method.

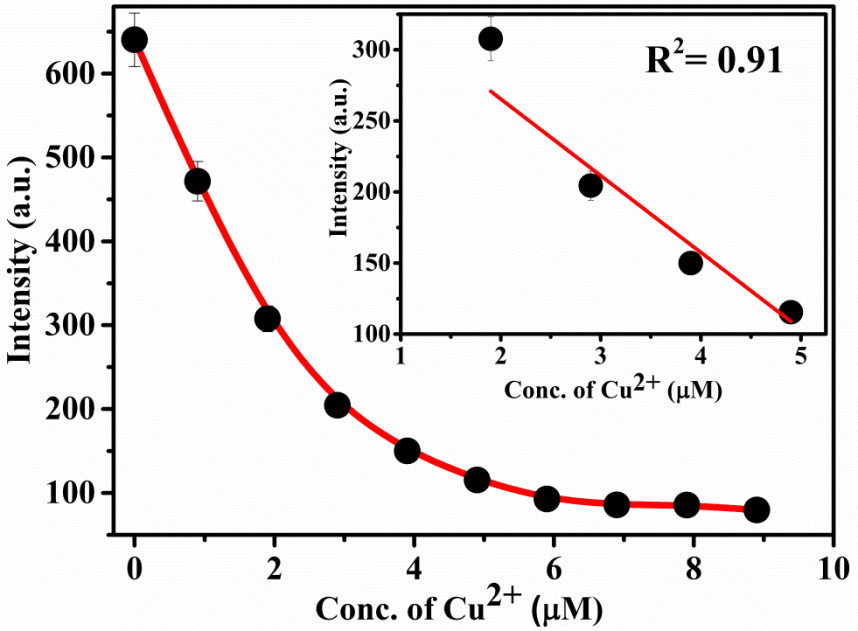

Fig. 5.8 Fluorescence emission intensity of TPEAM at 390 nm versus the conc. of Cu^{2+} ions in ACN-Water (90:10, v/v) medium

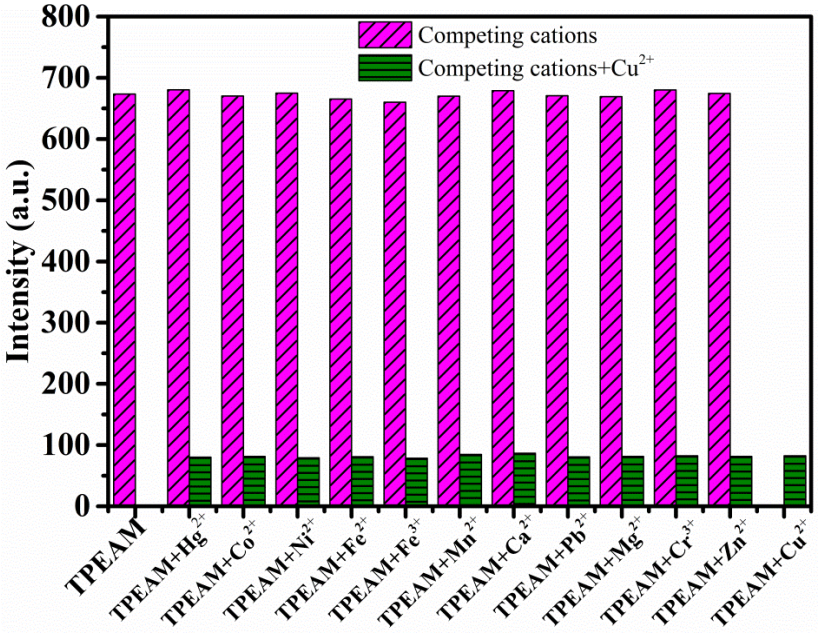

Fig. 5.9 Fluorescence emission intensity of TPEAM at 390 nm in presence of different co-existing cations (λ_{ex} = 340 nm) in ACN-Water (90:10, v/v) medium

Table 5.1 Results of three replicate determination of Cu^{2+} in real-life samples

Sample	Concentration (ppm)	
	Proposed method (Fluorescence)	**AAS method**
Multivitamin tablet	6.32	6.40
	6.28	6.33
	6.44	6.47
Black tea	0.12	0.17
	0.11	0.14
	0.13	0.13

5.3.4 Electrochemical behaviour of TPEAM towards CN^- ions

Since the recognition units of a sensor behave distinctively towards cations and anions, therefore, developing such sensors that detect both cation and anion is a challenging task. To study the complexation behaviour of TPEAM (1.0×10^{-4} M) towards various anions (equivalent amount) such as HSO_4^-, $H_2PO_4^-$, ClO_4^-, OAc^-, F^-, Cl^-, I^-, CN^-, differential pulse voltammograms (DPV) were recorded in ACN-Water (90:10, v/v). Besides weak anodic peaks in the applied potential range of -0.5 V to 0.0 V, a major anodic peak was observed at 0.71 V for TPEAM. The appearance of a weak anodic peak can be assigned to the poor basic character of the lone pair of electrons on ethereal oxygen. These anodic peaks do not show any change in their appearance even in the presence of various anions except cyanide ions. The strong anodic peak of TPEAM (due to lone pair of electrons on N atom of amide group) at 0.71 V move to higher applied potential in the presence of CN^- ions, because CN^- ions are bonded to the lone pair of nitrogen atoms of amide linkages. Hence, the lone pair electrons on nitrogen atoms lose their basic character leading to a shift of anodic peak from 0.71 V to 0.95 V (Fig. 5.10).

It is interesting to note the appearance of a new peak in the DPV of TPEAM-CN^- complex with maxima at 0.95 V unless TPEAM: CN^- stoichiometry becomes greater than 1:2. Successive additions of cyanide to the TPEAM solution do not show any further change in anodic voltammogram of TPEAM until the stoichiometry reaches to a particular ratio

(receptor: CN^-::1:2). The chemistry of complexation between ligand and guest ion can be understood as following:

1) As the guest species (CN^-) is added to a solution of the host receptor (TPEAM) it faces two competitive chemical processes.
   a) the abstraction of a proton from –OH group of hydroxyl of naphthyl moiety
   b) binding with the –NH of amide group through H-bonding

It is hypothesised that the process (b) starts only after the process (a) has reached the 1:2 stoichiometric value. It is furthered explained that the new anodic peak does not appear till the cyanide addition keeps on abstracting a proton from the hydroxyl of naphthyl groups. After the stoichiometric addition of cyanide, further addition results in hydrogen bonding with proton on the amide –NH group. This H-bonded cyanide leads to a shift anodic peak at 0.95 V.

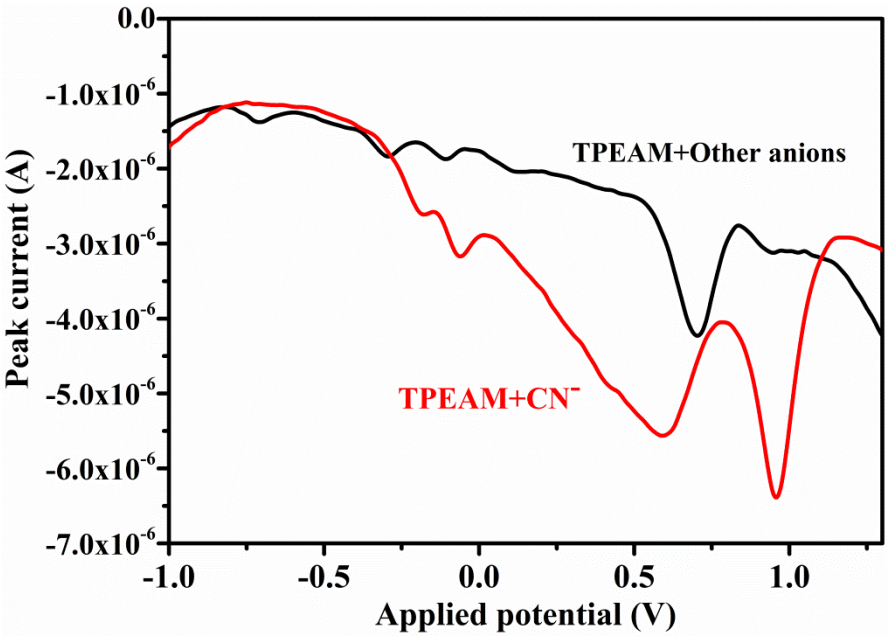

Fig. 5.10 Anodic DPV of TPEAM (1.0×10^{-4} M) in the presence of CN^- ions (20 µM)

Cathodic DPV spectrum of TPEAM in presence of CN^- ions: It has been hypothesised in the above paras that the addition of CN^- ions lead to hydrogen-bonded interactions with –NH groups of the amides, thereby making the oxidation of lone pair more difficult. This proposed electrochemical process gets support from the appearance of a weak cathodic peak at 0.99 V (Fig. 5.11). Hence, the small broad peak in the cathodic DPV spectrum is due to the reduction

cycle of the lone pair oxidation. It also indicates the very slow kinetics of the redox process of the TPEAM molecule.

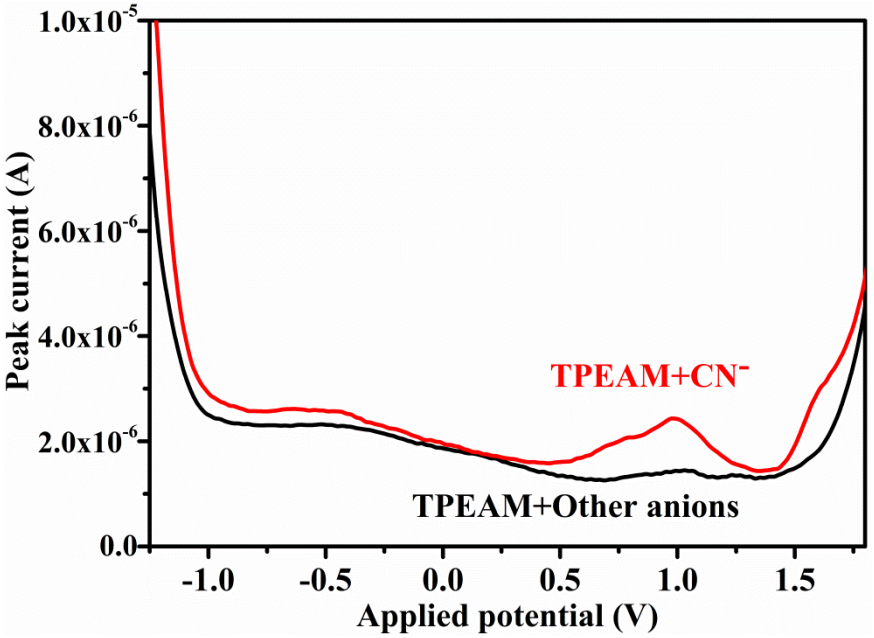

Fig. 5.11 Cathodic DPV of TPEAM (1.0×10^{-4} M) in the presence of CN^- ions

5.3.5 Photophysical behaviour of TPEAM towards CN^- ions

The selectivity of TPEAM (1.0×10^{-4} M) was checked for various anions such as HSO_4^-, $H_2PO_4^-$, ClO_4^-, OAc^-, F^-, Cl^-, I^-, CN^- in ACN-Water (90:10, v/v) medium by UV-vis spectroscopy. The receptor, TPEAM displayed absorption bands at 277 nm, 288 nm, 304 nm and at 334 nm. Among all the anions, only CN^- ions brought prominent changes in the spectrum, which defined selectivity of TPEAM (Fig. 5.12).

Upon addition of CN^- to the receptor solution, the absorbance at 277 nm, 288 nm, and 304 nm got enhanced significantly with a little redshift. The absorption band at 334 nm disappeared and a new band appeared at 376 nm. This pattern of the shift in bands was completely different from all other anions. To study the binding behaviour of TPEAM for CN^- ions, a titration experiment was conducted in ACN-Water (90:10, v/v) medium. Upon gradual addition of CN^- ions into the TPEAM solution, absorption intensity at 376 nm increased and reached the saturation value following the addition of 1.9 equivalents of CN^- ions (Fig. 14). Bathochromic shift in UV-vis studies leads us to propose the mechanism as: removal of the proton (deprotonation) of hydroxyl groups of naphthyl moiety takes place which leads to the enhancement in the intramolecular charge transfer process and hence increases in absorption intensity.

The deprotonation [26] mechanism proposed for the sensing of CN^- ions by receptor TPEAM is shown in Scheme 5.2. From literature, it was observed that during intramolecular charge transfer processes, electron cloud of the organic moiety would likely to get shifted and reorganise itself in the presence of target species. Due to this shifting in cloud either redshift or blue shift would takes place in UV-vis spectra. In case of TPEAM also, red shift was observed in the presence of CN^- ions, which suggest that ICT process has taken place.

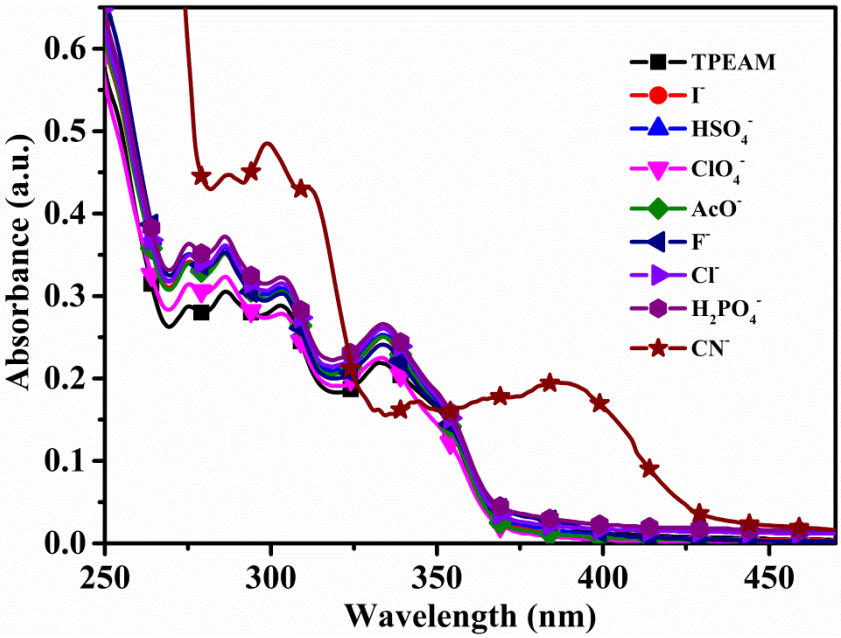

Fig. 5.12 Absorption spectral changes of TPEAM (1.0×10^{-4} M) in the presence of an of various anions (200 µM) in ACN-Water (90:10, v/v)

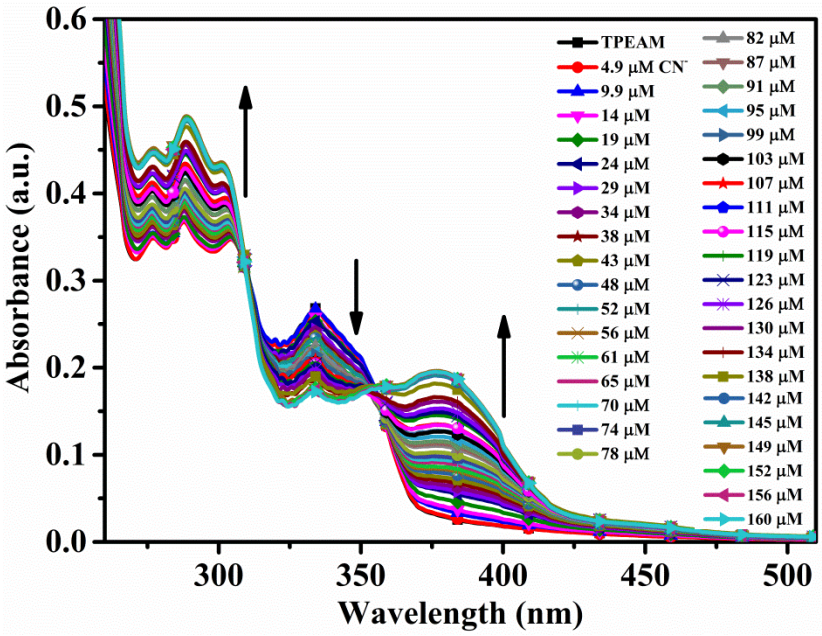

Fig. 5.13 Absorption spectral changes of TPEAM (1.0×10^{-4} M) after addition of incremental amounts of CN^- ions in ACN-Water (90:10, v/v) medium

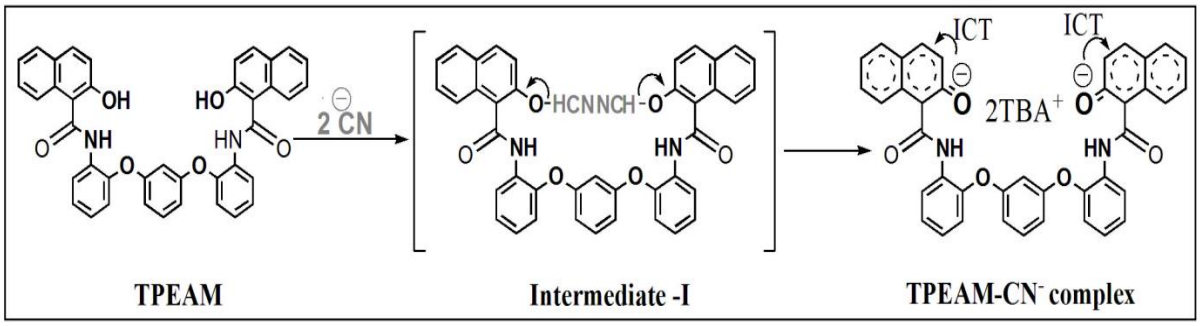

Scheme 5.2 The proposed sensing mechanism of TPEAM towards CN^- ions

To confirm the stoichiometry of binding between TPEAM and CN^-, Job's plot analysis was performed in ACN-Water (90:10, v/v) medium. The maximum absorbance was found to be at a 0.6-mole fraction, which suggests 1:2 stoichiometry between TPEAM and CN^- (Fig. 5.14). The stoichiometry obtained from Job's plot data is in good agreement with the UV-vis titration data of TPEAM with CN^- ions.

Fluorescence emission spectroscopy was used to check the complexation behaviour of TPEAM towards CN^- ions in ACN-Water (90:10, v/v) medium. Following the excitation at 340 nm, TPEAM shows only one emission band at 390 nm. But on the incremental additions of CN^- ions, the band (390 nm) started decreasing and it is accompanied by the appearance of a new band at 443 nm with a redshift of 54 nm (Fig. 5.15). From the titration experiment, it was observed that the enhancement in the peak intensity at 443 nm is accompanied by a simultaneous decrease in intensity at 390 nm. Hence, this simultaneous behaviour indicates that the receptor TPEAM behaves ratiometrically towards CN^- ions. This ratiometric behaviour of probe TPEAM towards CN^- is quite useful as it gives fluorescence behaviour at two different wavelengths. This redshift phenomenon was also supported by the change in the colour of TPEAM under UV light (365 nm) from weakly fluorescent (light blue) to highly fluorescent (bright blue) after the addition of the cyanide ions (Fig. 5.15 (inset)).

The optical dilution method was used to quantify the fluorescence quantum yields of TPEAM free ligand and CN^- complex based on a standard reference solution of quinine sulphate in 0.05 M sulfuric acid. At 298°K, this standard solution yields 54% quantum yield. In a quartz cell with a 1 cm path length, all sample solutions were measured. This cell has an absorbance value of less than 0.1 for all wavelengths of excitation and emission, allowing light to pass through the sample uniformly and cancelling the effect of the inner-filter. The value was determined to be 15 % and 25 % for TPEAM and TPEAM-CN^- complex respectively. The

values are in accordance with fluorescence spectra and the inset picture of the receptor and complex.

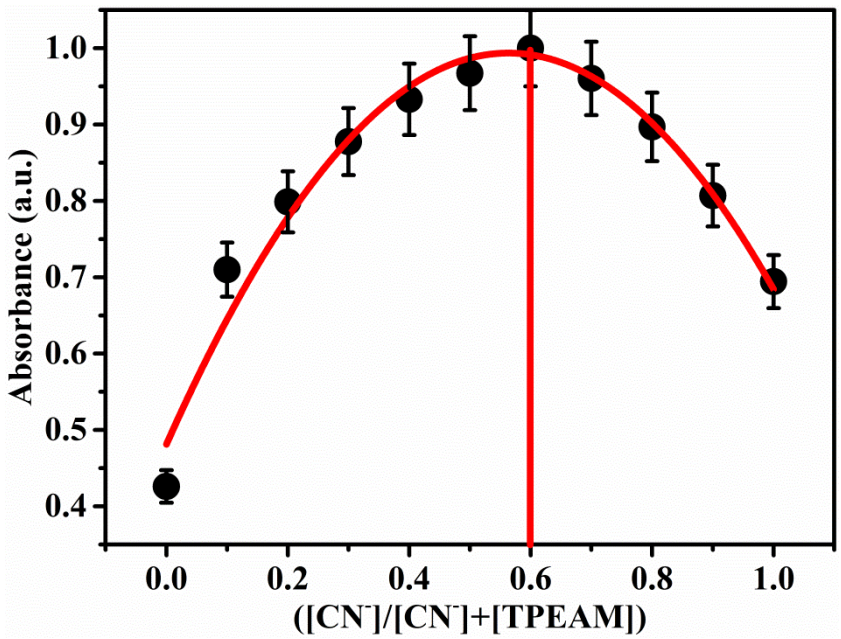

Fig. 5.14 Job's plot between TPEAM and CN^- ions in ACN-Water (90:10, v/v) medium

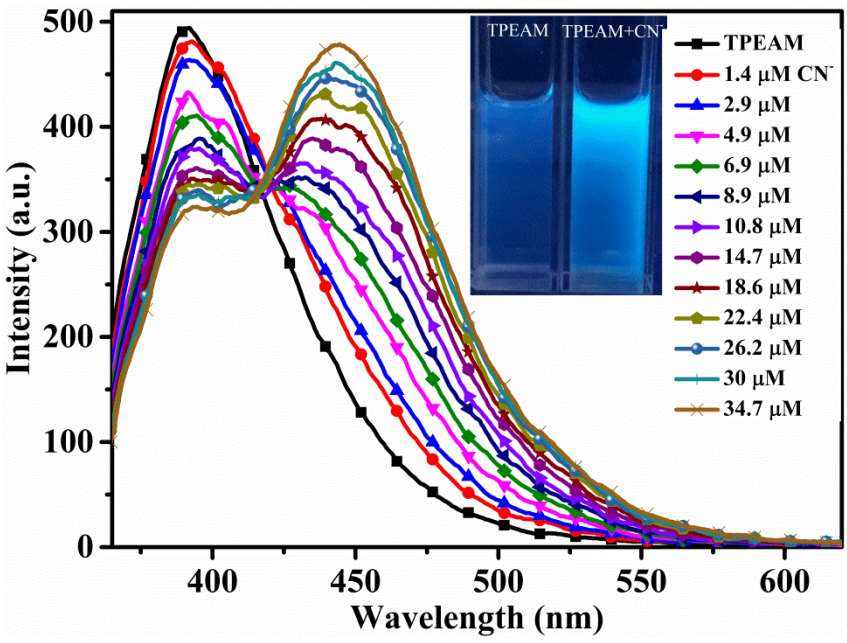

Fig. 5.15 Fluorescence emission titration of TPEAM (100 μM) with incremental addition of CN^- ions in ACN-Water (90:10, v/v) (λ_{ex} = 340 nm)

A calibration curve was plotted and used to understand the binding behaviour of TPEAM for CN^- ions. From fig. 5.16, it can be observed that the receptor-ligand complexation process can be split into two parts i.e., from 0.0 to 15.0 µM, a non-linear trend is observed while from 15.0 to 35.0 µM, the intensity of emission peak increases linearly with $R^2 = 0.98$. Hence, the latter part of the curve is proposed as a working concentration range. The calibration curve for the CN^- ions was repeated 3 times to confirm its reproducibility. From this curve, the detection limit[25] for CN^- ions was found to be 0.4 µM.

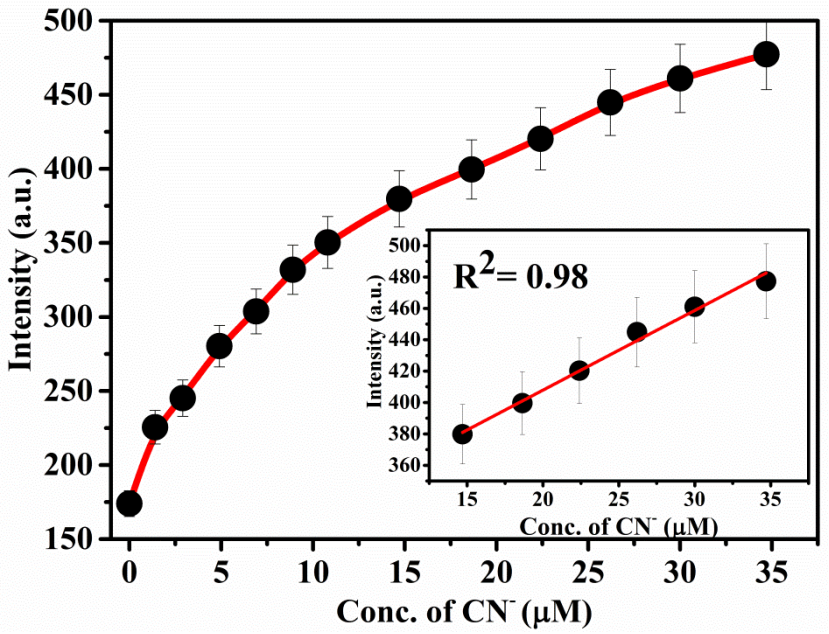

Fig. 5.16 Fluorescence emission intensity of TPEAM at 443 nm versus the conc. of CN^- ions in ACN-Water (90:10, v/v) (λ_{ex} = 340 nm)

Another important feature of a potential receptor is its selectivity towards the particular target ion in the presence of other co-existing anions. Therefore, competitive experiments were carried out by adding an equivalent amount of CN^- ions, as that of other anions to the solution of TPEAM in ACN-Water (90:10, v/v) medium (Fig. 5.17). Various other co-existing anions do not show any significant change in fluorescent intensity at 443nm (λ_{ex} = 340nm) for CN^- ions, which describes the selective and specific behaviour of TPEAM for CN^- ions.

5.3.6 ^{1}H NMR titrations

To support the hypothecated mechanism (Scheme 5.2) as described in spectroscopic and electrochemical studies of the receptor TPEAM with CN^- ion in section 5.3.4 & 5.43.5, ^{1}H NMR titration was carried out in solvent $CDCl_3$. In the case of pure TPEAM, ^{1}H NMR chemical shift (δ) for –OH proton is located at 12.3 ppm. After the addition of 2.0 equivalents

of CN^- ions to the TPEAM solution, the characteristic -OH signal disappeared which confirmed the deprotonation of the -OH proton from the naphthyl ring (Fig. 5.18). This deprotonation of -OH group was also supported by the up field shift of protons of the receptor due to the negative charge developed after the deprotonation of the hydroxyl group leading to the delocalization of the charge through naphthyl rings.[27]

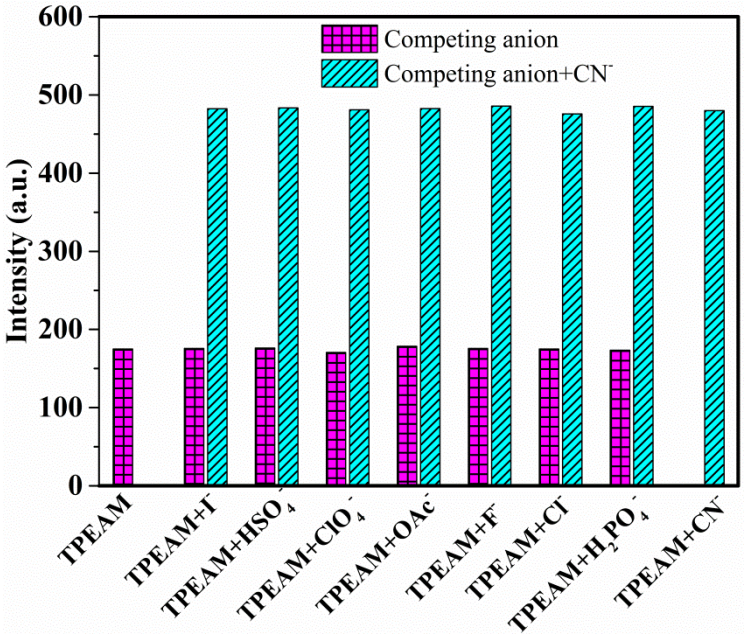

Fig. 5.17 Fluorescence emission response of TPEAM (100 µM) at 443 nm in presence of different co-existing anions (λ_{ex} = 340 nm)

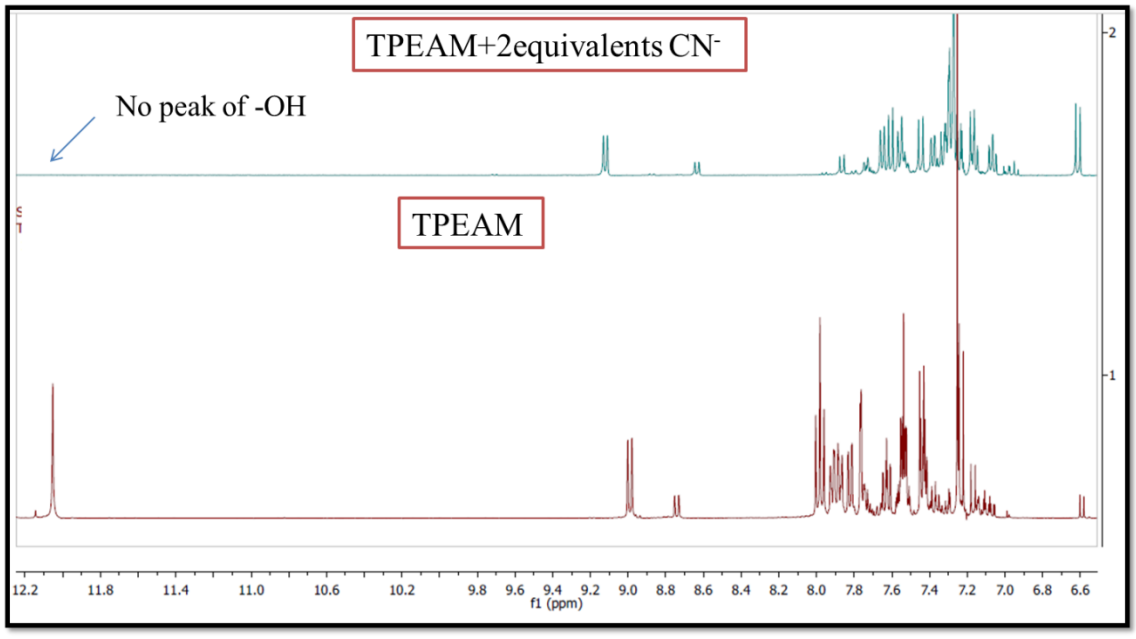

Fig. 5.18 ^{1}H NMR titrations of TPEAM with 2equivalents of CN^- ions in $CDCl_3$

5.3.7 Interference study

On one hand, TPEAM exhibits selectivity for Cu^{2+} ions among various cations and on the other hand, it also shows selectivity for CN^- ions among various anions. But from literature, it is observed that CN^- ions, being highly basic, tend to bind with metal cations in a sequential manner[8, 17, 18] (Table 5.2). Therefore, inspired by the sequential sensing behaviour of CN^- ions, we further studied the role of CN^- ions on TPEAM-Cu^{2+} complex and vice-versa.

Table 5.2 Literature reports following sequential sensing of anions

S. No	Chromophore unit	Ions	Pathway followed	Media	Ref
1.	Pyrimidine	Cu^{+2}/CN^-	Metal-ion displacement	DMSO-H_2O	28
2.	Carbazole	Cu^{+2}/CN^-	Complexation	DMSO-Buffer	22
3.	Spirobifluorene	Cu^{+2}/CN^-	Metal-ligand displacement	ACN-Buffer	29
4.	Rhodamine	Al^{+3}/F^- &AcO^-	Metal-complex dissociation	MeOH-DMSO	30
5.	Coumarin	Al^{+3}/F^-	-	DMSO-H_2O	31
6.	Pyrimidine	Cu^{+2}/S^{2-}	Demetallation	DMSO-Buffer	32
7.	Imidazole	Al^{+3}/PPi	Metal-complex displacement	Buffer	33
8.	Polyethyleneimine	Cu^{+2}/PPi	Metal-complex dissociation	H_2O	34
9.	Pyrenemethylamine	$Zn^{+2}/H_2PO_4^-$	Demetallation	DMSO	35
10.	Benzildihydrazone	Cu^{+2}/CN^-	Displacement	MeOH- H_2O	18

To study the behaviour of CN^- ions towards TPEAM-Cu^{2+} complex, a competitive experiment was conducted in the presence of five equivalents of cyanide ions as that of one equivalent of TPEAM-Cu^{2+} complex (Fig. 5.19), no spectral changes were observed in the absorption band of TPEAM-Cu^{2+} complex.

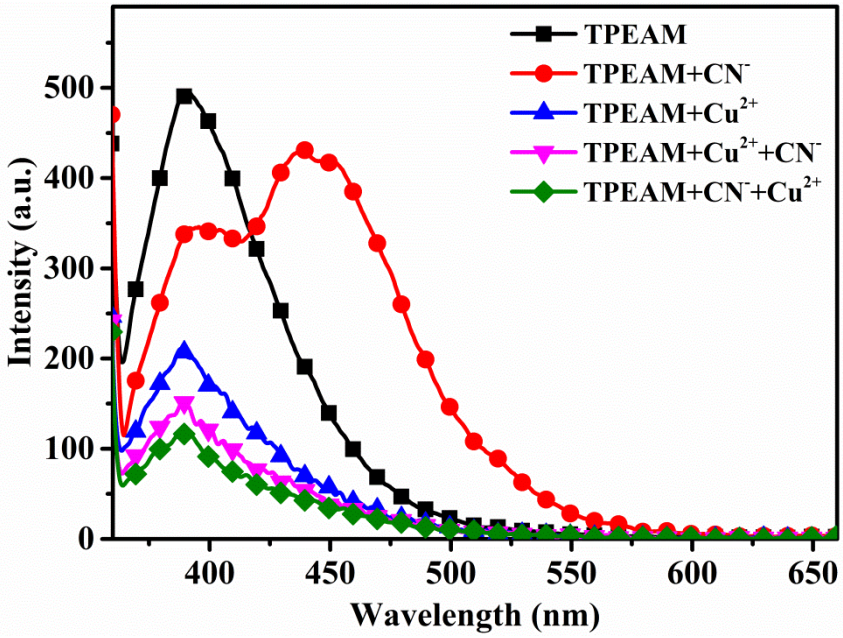

Fig. 5.19 Fluorescence response of TPEAM (10 µM) in the presence and absence of Cu^{2+} and CN^- ions in ACN-Water (90:10, v/v)

It is well known in the literature that highly basic CN^- ions can coordinate with Cu^{2+} ions to form complex as $[Cu(CN)_x]^{n-}$. However, in the case of TPEAM, CN^- ions were unable to impact the TPEAM-Cu^{2+} complex, which lead us to propose that TPEAM is extremely selective for Cu^{2+} ions over CN^- ions. To confirm the above-mentioned statement, a reverse experiment was also conducted and it was observed that in the presence of both Cu^{2+} ions and CN^- ions in the receptor solution, TPEAM selectively choose Cu^{2+} ions over CN^- ions for sensing. Therefore, obtained data confirm the selectivity of TPEAM for Cu^{2+} ions over CN^- ions and rules out the possibility of sequential sensing.

5.3.8 Fluorescence spectroscopic study of TPEAM-Cu^{2+} complex towards arginine

Since it has been reported that amino acids and peptides interact with Cu^{2+} ions very strongly[13, 36] therefore, we wish to check the selectivity of the TPEAM-Cu^{2+} complex towards various amino acids. The fluorescence study of TPEAM-Cu^{2+} complex (10 µM) with various amino acids (10 equivalents) such as asparagine, lysine, arginine, tryptophan, proline,

glutamine, histidine and cysteine were carried out in ACN-Water (90:10, v/v) medium. As shown in Fig. 5.20, among various amino acids, the only arginine showed spectral changes at λ_{max}=390 nm (λ_{ex} = 340 nm). The binding properties of TPEAM-Cu^{2+} complex towards arginine were studied by fluorescence titration experiment.

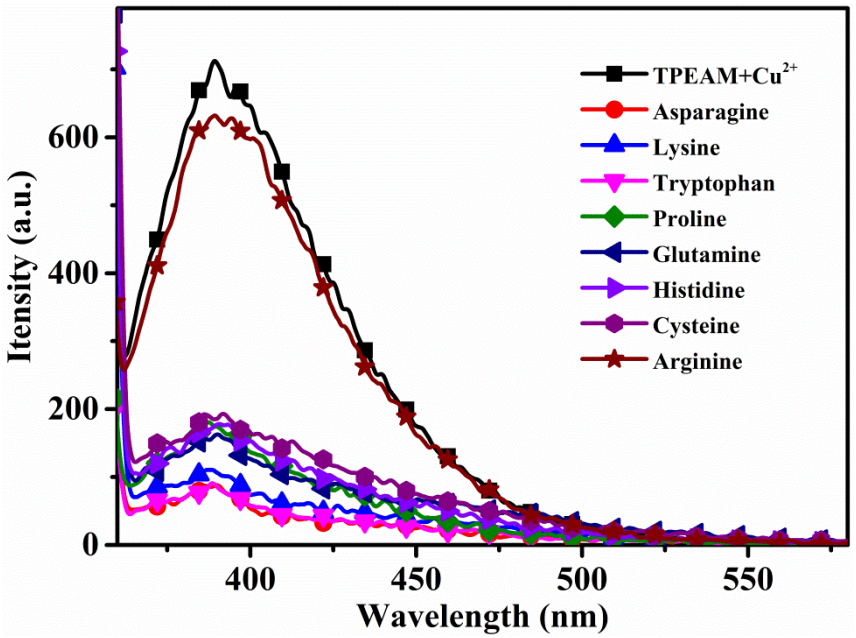

Fig. 5.20 Fluorescence spectral changes of TPEAM (1x10^{-4} M) in the presence of various amino acids (200 µM) in ACN-Water (90:10, v/v)

On incremental addition of arginine to the solution of TPEAM-Cu^{2+} complex, the spectral band at 390 nm started rising and reached to the maxima nearly at 8 equivalents concentration of the amino acid (Fig. 5.21). This regular increase in band intensity at λ_{max}=390 nm (λ_{ex} = 340 nm) demonstrated that Cu^{2+} ion slowly started coming out of the cavity of the receptor and the TPEAM regenerated itself. After the addition of nearly 8 equivalents, a clear band at 390 nm, of similar height as that of TPEAM was seen, which means that TPEAM has completely revived in the solution. From the observed data, we propose that the TPEAM-Cu^{2+} complex might have followed the metal ion displacement approach, due to stronger metal-amino acid linkage[37, 38] (Scheme 5.3).

The binding mode between the TPEAM-Cu^{2+} complex with arginine was revealed by using Job's plot analysis. The job's plot exhibited the 1:1 stoichiometry of TPEAM-Cu^{2+} complex and arginine (Fig. 5.22). From titration, the lower detection limit of arginine was found to be 4 µM, based on 3σ method.[25] Also, using the Benesi-Hildebrand equation, the binding

constant of the TPEAM-Cu^{2+} complex for arginine was determined to be 0.3×10^{3} M^{-1}. Hence, this proposal of the complexation of arginine with Cu^{2+} from the TPEAM-Cu^{2+} complex can be used as a method for the determination of arginine concentration.

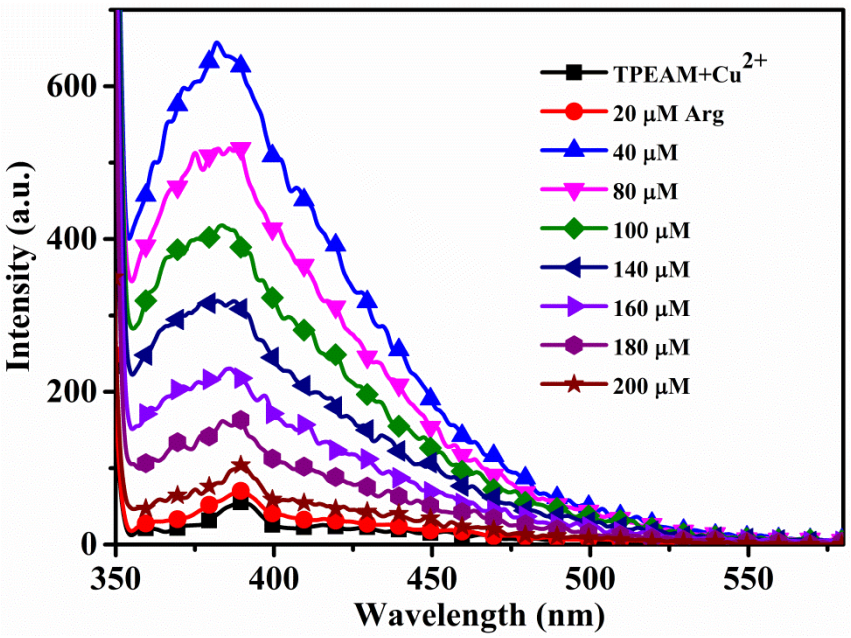

Fig. 5.21 Fluorescence response of TPEAM-Cu^{2+} complex ($1x10^{-4}$ M) after the addition of incremental amount of arginine in ACN-Water (90:10, v/v) medium

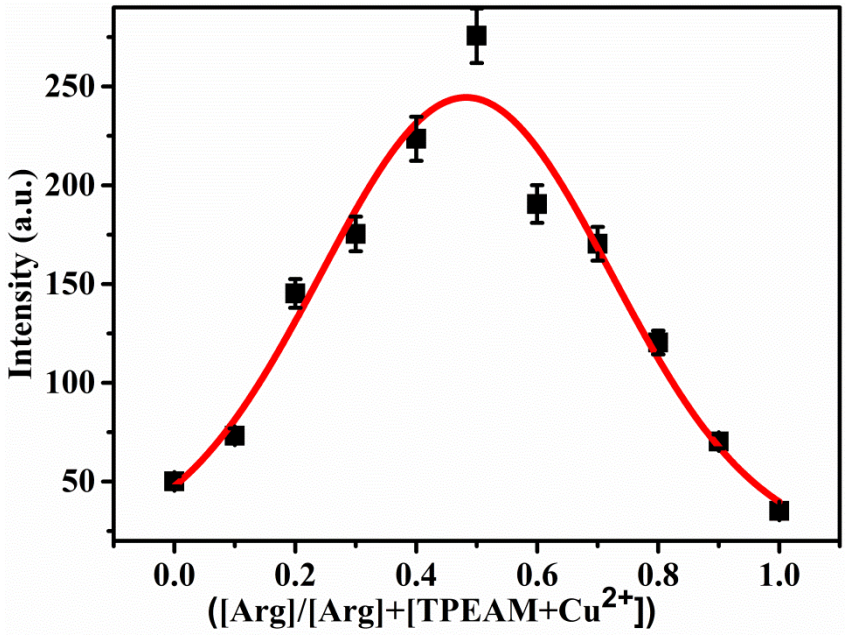

Fig. 5.22 Job's plot between TPEAM-Cu^{2+} complex and arginine ions in ACN-Water (90:10, v/v) medium

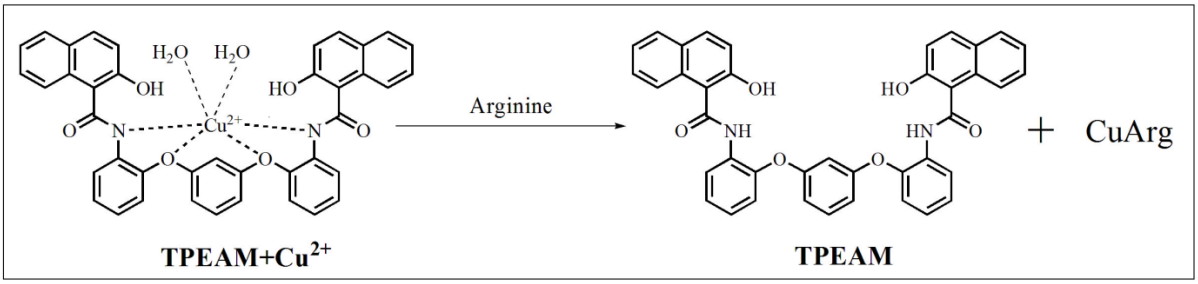

Scheme 5.3 The proposed sensing mechanism of TPEAM-Cu^{2+} complex with arginine

To further study the ability of the TPEAM-Cu^{2+} complex for arginine, interference study was performed in the presence of the above-mentioned amino acids. When the TPEAM-Cu^{2+} complex was treated with 8 equivalents of arginine in the presence of other amino acids of the same concentration, no interference was observed (Fig. 5.23).

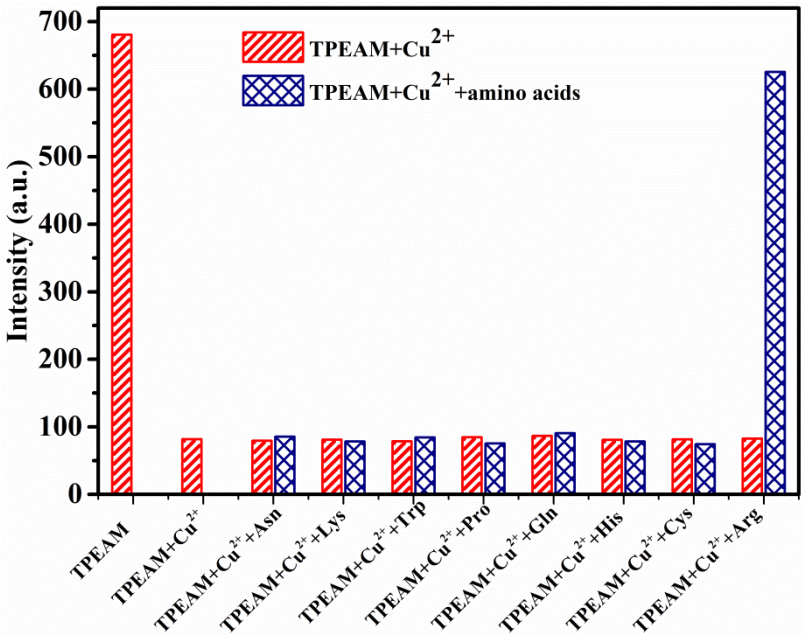

Fig. 5.23 Fluorescence emission response of TPEAM-Cu^{2+} complex in the presence of various amino acids at 390 nm (λ_{ex} =340 nm)

Hence, the TPEAM-Cu^{2+} complex method can be used for the selective detection of arginine in the ACN-Water (90:10, v/v) medium. The selectivity of TPEAM-Cu^{2+} complex for arginine over other amino acids could be due to the conformational flexibility of its long side chain and the presence of large guanidinium moiety which delocalizes its positive charge over many atoms that are involved in the conjugated Y-Π system[36]. These results demonstrate that the TPEAM-Cu^{2+} complex could be an excellent fluorogenic sensor for arginine with high selectivity over other amino acids.

5.3.9 Molecular logic gate preparation

From the differential behavior of receptor TPAM towards Cu (II) ions and CN^- ions, we realized that that the present work can serve as a potential for the molecular logic gate system. Molecular logic gates transfer input stimulations into output signals using intrinsic protocol. With the help of a binary logic system, two chemical inputs (10 equiv. of Cu (II) and CN^-) are provided to chemosensor TPAM for molecular switching behavior. From 0 and 1, we can have the information of the presence or absence of particular species at a particular wavelength (threshold) in receptor solution. There are two input signals, viz. In1 (Cu (II)) and In2 (CN^-), whereas the output signals are Out1 (E 390 nm) and out2 (E 443.5 nm). With two different inputs, different emission spectra were observed as shown in fig.5.24. Monitoring the emission changes at 390 nm and 443.5 nm i.e. the addition of Cu (II) and CN^- and an equimolar mixture of Cu (II) and CN^-, logic gates are represented in a truth table (Table 5.3). Upon addition of Cu (II) into TPAM solution, fluorescence quenching takes place at 390 nm, which is represented by the binary digit 0 (*off*) and upon addition of CN^-, there is s a new peak at 443.5 nm with valuable intensity, therefore, represented by the binary digit 1 (*on*).

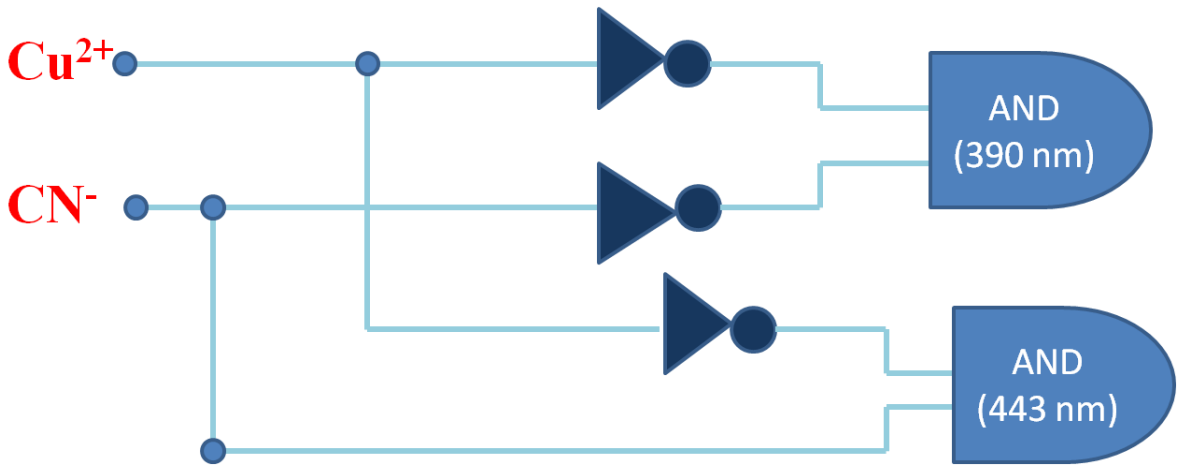

Fig. 5.24 Design of molecular logic gate for the detection of Cu (II) ions and CN^- ions

Table 5.3 Logic gate represented in a truth table

In1 (Cu (II))	In2 (CN^-)	Out1 (E 390)	Out2 (E 443.5)
0	**0**	**1**	**0**
1	**0**	**0**	**0**
0	**1**	**0**	**1**
1	**1**	**0**	**0**

5.3.10 Quantum mechanical calculations

Proposed interactions of TPEAM towards Cu (II) and CN^- were validated by density functional theory (DFT) calculations using the Gaussian 03W program by means of B3LYP function and 6-31G basis set. Fig. 5.25 shows the minimum energy configuration of TPEAM that undergoes rotation after interaction with guest ions to acquire stability. It also shows that both Cu (II) and CN^- interact well with the coordinating sites of the receptor molecule (TPEAM). Table 5.4 shows the gap between highest occupied molecular orbital (HOMO) and lowest unoccupied molecular orbital (LUMO) of native TPEAM decreases from 0.152 a.u to 0.146 and 0.018 a.u for CN^- and Cu (II), respectively. Apart from this, shift in electron density can be clearly seen in case of complex as compared to the probe TPEAM.

Table 5.4 Energy values (in a.u) of HOMO and LUMO for TPEA and its complex with CN^- using DFT calculations

Receptor / Complex System	Energy in a.u		
	E_{HOMO}	E_{LUMO}	E_{gap}
TPEAM	-0.216	-0.064	0.152
TPEA+ CN^-	-0.036	0.109	0.146
TPEA+ Cu (II)	-0.355	-0.336	0.018

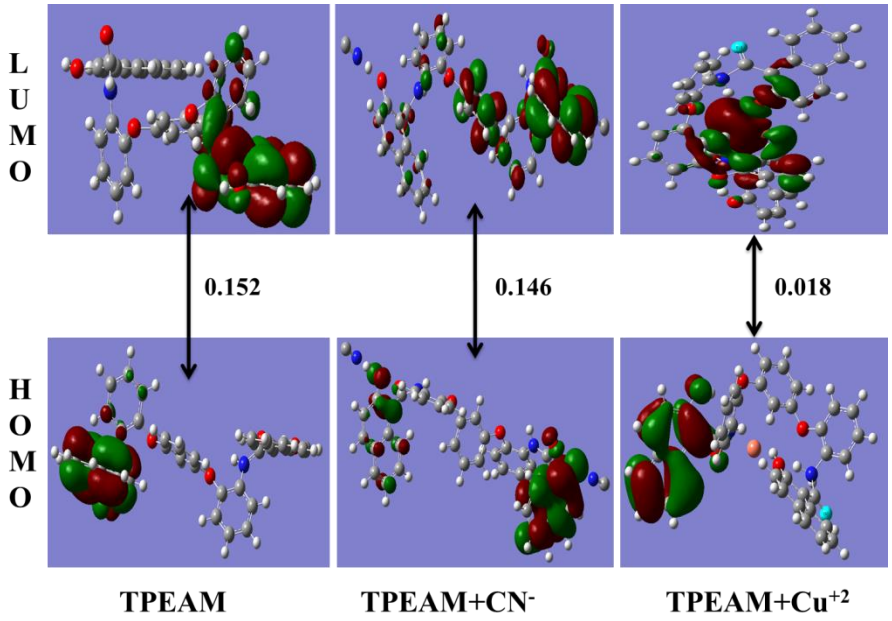

Fig. 5.25 Quantum mechanical calculations of HOMO and LUMO of TPEAM, TPEAM-CN^- and TPEAM-Cu (II), using B3LYP/6-31G basis set

Conclusions

Triphenyl ether-based receptor has proven to be an efficient voltammetric and optical sensor for Cu^{2+} and CN^- ions via host-guest and intramolecular charge transfer based interactions, respectively. The TPEAM-Cu^{2+} complex did not follow sequential sensing for the detection of CN^- ions as observed from interference studies. The voltammetric performance of the novel receptor TPEAM for Cu^{2+} and CN^- ions has been validated with spectroscopic studies and ^1H NMR titrations. The synthesized receptor has been used to determine Cu^{2+} ions from real-life samples such as multivitamin tablets and black tea. Furthermore, the TPEAM-Cu^{2+} complex has been successfully used to sense arginine over other amino acids from aqueous acetonitrile medium.

References

1. K. Fan, X. Wang, H. Yang, L.-J. Gao, G. Han, L. Zhou and S. Fang, *Analytical Methods*, 2020.
2. F. Shi, S. Cui, H. Liu and S. Pu, *Dyes and Pigments*, 2020, **173**, 107914.
3. A. Mohammadi, B. Khalili and A. S. Haghayegh, *Spectrochimica Acta Part A: Molecular and Biomolecular Spectroscopy*, 2019, **222**, 117193.
4. S. Kiran, R. Khatik and R. Schirhagl, *Analytical and bioanalytical chemistry*, 2019, **411**, 6475-6485.
5. F. Edition, *WHO chronicle*, 2011, **38**, 104-108.
6. S. Erdemir and S. Malkondu, *Talanta*, 2020, **207**, 120278.
7. F. Wang, L. Wang, X. Chen and J. Yoon, *Chemical Society Reviews*, 2014, **43**, 4312-4324.
8. N. Assadollahnejad, M. Kargar, H. R. Darabi, N. Abouali, S. Jamshidi, A. Sharifi, K. Aghapoor and H. Sayahi, *New Journal of Chemistry*, 2019, **43**, 13001-13009.
9. B. Rani, S. Swami, A. Agarwala, D. Behera and R. Shrivastava, *RSC Advances*, 2019, **9**, 30599-30614.
10. J. Li, X. Qi, W. Wei, Y. Liu, X. Xu, Q. Lin and W. Dong, *Sensors and Actuators B: Chemical*, 2015, **220**, 986-991.
11. Y.-K. Yang and J. Tae, *Organic letters*, 2006, **8**, 5721-5723.
12. W. H. Organisation and W. H. O. Staff, *Guidelines for drinking-water quality*, World Health Organization, 2004.
13. S. Wang, H. Ding, Y. Wang, C. Fan, G. Liu and S. Pu, *RSC advances*, 2019, **9**, 6643-6649.
14. K. Y. Ryu, S. Y. Lee, J. H. Kang, D. Y. Park and C. Kim, *Sensor Letters*, 2017, **15**, 837-850.
15. N. Maurya and A. K. Singh, *Dyes and Pigments*, 2017, **147**, 484-490.
16. S. Khoshsoroor, A. Mohammadi, B. Khalili and S. Mohammadi, *Journal of Photochemistry and Photobiology A: Chemistry*, 2020, **388**, 112208.
17. A. Mohammadi and Z. Ghasemi, *Spectrochimica Acta Part A: Molecular and Biomolecular Spectroscopy*, 2019, 117730.
18. R. Chandra, A. Ghorai and G. K. Patra, *Sensors and Actuators B: Chemical*, 2018, **255**, 701-711.
19. A. Mohammadi and M. Kianfar, *Journal of Photochemistry and Photobiology A: Chemistry*, 2018, **367**, 22-31.

20. T. G. Jo, Y. J. Na, J. J. Lee, M. M. Lee, S. Y. Lee and C. Kim, *Sensors and Actuators B: Chemical*, 2015, **211**, 498-506.

21. S. Kumar, S. K. Mittal, J. Singh and N. Kaur, *Analytical methods*, 2016, **8**, 7472-7481.

22. G. J. Park, G. R. You, Y. W. Choi and C. Kim, *Sensors and Actuators B: Chemical*, 2016, **229**, 257-271.

23. J. S. Renny, L. L. Tomasevich, E. H. Tallmadge and D. B. Collum, *Angewandte Chemie International Edition*, 2013, **52**, 11998-12013.

24. Z. Huang, J. Du, J. Zhang, X.-Q. Yu and L. Pu, *Chemical Communications*, 2012, **48**, 3412-3414.

25. A. M. Committee, *Analyst*, 1987, **112**, 199-204.

26. S. Gupta, M. Chhibber and S. K. Mittal, *Journal of Applied Electrochemistry*, 2020, **50**, 185-195.

27. P. M. Reddy, S.-R. Hsieh, C.-J. Chang and J.-Y. Kang, *Journal of hazardous materials*, 2017, **334**, 93-103.

28. A. Mohammadi and Z. Ghasemi, *Spectrochimica Acta Part A: Molecular and Biomolecular Spectroscopy*, 2020, **228**, 117730.

29. K. Silpcharu, S. Soonthonhut, M. Sukwattanasinitt and P. Rashatasakhon, *ACS Omega*, 2021.

30. V. K. Gupta, N. Mergu, L. K. Kumawat and A. K. Singh, *Talanta*, 2015, **144**, 80-89.

31. D. Sarkar, P. Ghosh, S. Gharami, T. K. Mondal and N. Murmu, *Sensors and Actuators B: Chemical*, 2017, **242**, 338-346.

32. M. S. Kim, S. Y. Lee, J. M. Jung and C. Kim, *Photochemical & Photobiological Sciences*, 2017, **16**, 1677-1689.

33. T. G. Jo, K. H. Bok, J. Han, M. H. Lim and C. Kim, *Dyes and Pigments*, 2017, **139**, 136-147.

34. F. Wang, C. Zhang, Q. Xue, H. Li and Y. Xian, *Biosensors and Bioelectronics*, 2017, **95**, 21-26.

35. Y. Upadhyay, T. Anand, L. T. Babu, P. Paira, G. Crisponi, R. Kumar and S. K. Sahoo, *Dalton Transactions*, 2018, **47**, 742-749.

36. H. Tavallali, G. Deilamy-Rad and N. Mosallanejad, *Applied biochemistry and biotechnology*, 2019, **187**, 913-937.

37. Y. S. Kim, G. J. Park, S. A. Lee and C. Kim, *RSC Advances*, 2015, **5**, 31179-31188.

38. K. Yu, N. He, N. Kumar, N. Wang, J. Bobacka and A. Ivaska, *Electrochimica Acta*, 2017, **228**, 66-75.

Chapter 6

A highly selective Schiff base for recognition of Al^{+3} and CN^- and its antibacterial activity against *E. coli*

Herein, a Schiff base receptor was prepared for the selective detection of cations and anions. Al^{+3} and CN^- were two ions which were selectively detected by the receptor in ACN: Water (90:10, v/v) solvent medium. Naked eye response of the receptor and its complex was captured under UV lamp (365 nm). Apart from analytical studies, antibacterial activity of the probe and its aluminium complex was carried out. Via fluorescence imaging, and SEM analysis interaction between the organic moiety and bacteria was established.

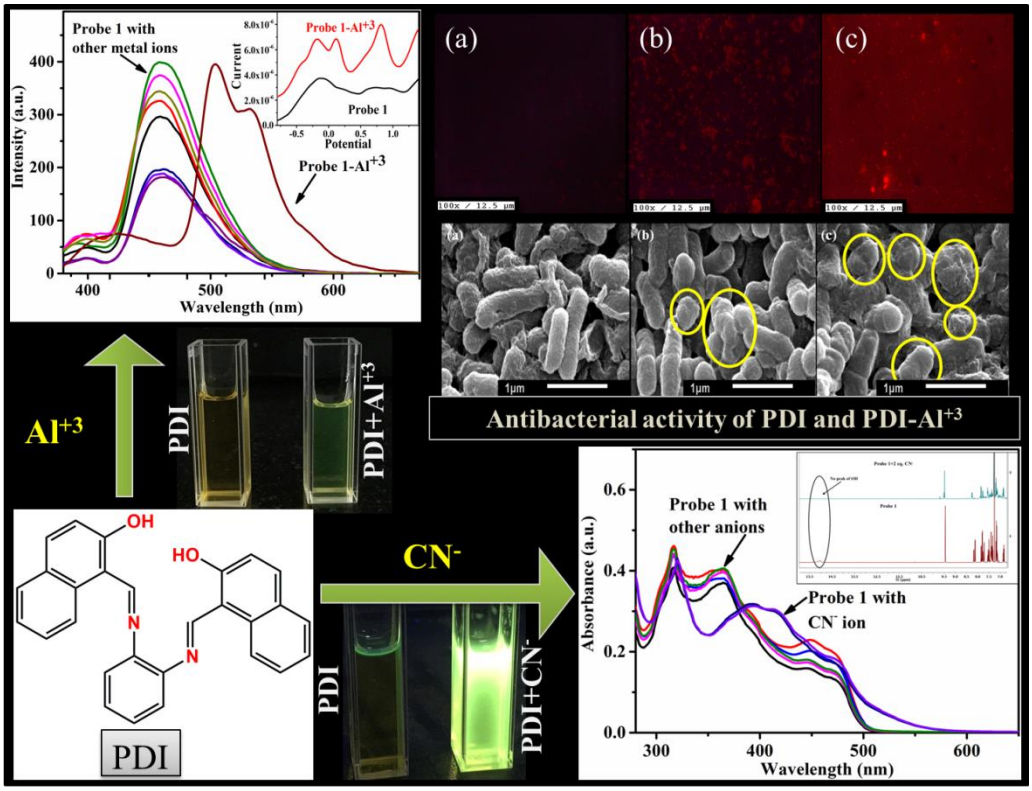

Schematic presentation of sensing behaviour of probe PDI

6.1 Introduction

Al^{3+} has been, by far, the most abundant metallic element (8.3 % by weight) in the earth's crust and the third most abundant element after oxygen and silicon.[1] It has been widely used in our routine life for various purposes such as electrical transmission, cookies sheets, medicines, paper industry, and food additives. Even being so useful, aluminium has various harmful effects not only to environment but also to biological systems as well. An increased level of aluminium in soil and water is harmful to growing plants as well as for aquatic ecosystem. In human body, increased level of aluminium is a matter of great concern because it damages the central nervous system and induces various disorders such as dementia, rickets, kidney failure, memory loss, and neuronal disorder. In addition to this, aluminium can stay inside the human cells and tissues for long time which causes diseases like Parkinson's, amyotrophic lateral sclerosis, and Alzheimer's. According to the World Health Organisation (WHO), weekly intake amount of aluminium should not be more than 7 mg/kg of the body weight. Therefore, detection of aluminium ions is of major concern so as to control its impact not only on environment but also on mankind.[2-5]

Among various anions, cyanide is considered as one of the deadliest poisons to mankind. This nature of cyanide ion is because of its interference in electron transport chain in mitochondria as it binds well with the active site of cytochrome oxidase. Also, its presence can cause loss of consciousness, vomiting, and ultimately death.[6-10] According to the World Health Organisation (WHO), in drinking water, concentration of cyanide should not exceed from 70 µg/L.[11] Also, maximum contamination level of cyanide in drinking water is set to be 200 µg/L by US EPA. Despite it being a well-known poison yet it has been extensively used in many industrial processes such as electroplating, gold mining, plastic manufacturing, herbicide, synthetic fibers, and resin industry. Because of its extreme use, it has been discarded to the environment in a huge amount nearly 140,000 tons per year worldwide. Due to its widespread presence in the environment, trace level detection of poisonous cyanide from different matrices such as food, water, soil, living cells, and blood is very much required.

Various conventional analytical techniques have been used for the detection of cations and anions but fluorescent sensors have turned out to be a promising tool because they are easy to handle as well as operate and are cost-effective also. On the other hand, conventional techniques require tedious sample preparation procedures, skilled labor, high cost, and sophisticated instruments. Other than spectroscopic techniques, differential pulse

voltammetry (DPV) is an important tool to understand the electrochemical behavior of the compound and its complexation behavior towards cations and anions.

There are few reports in literature where synthesized probes have detected Al^{+3} and CN^- ions using different mechanisms.[12-15] But, effect of water on selective detection of these probes has not much explored. To this context, simple and efficient chemosensors are required for the selective detection of Al^{+3} and CN^- ions in aqueous environment and the role of water should be explored well as both Al^{+3} and CN^- ions have high hydration energy.

Hereby, in this chapter we report imine linkage based moiety as a dual sensor for the naked eye detection of Al^{+3} and CN^- ions in aqueous acetonitrile solvent mixture. Synthesis of the receptor ionophore, phenylene diimine (PDI), has already been reported in literature,[16] while it has not been used as a probe in analytical chemistry. The PDI showed selective behavior for Al^{+3} ions following the combination of PET-CHEF (photoinduced electron transfer - chelation induced enhanced fluorescence) mechanism. PDI has also detected CN^-/F^- ions through deprotonation mechanism. PDI showed "Turn On" behavior for anions and its mechanism has been confirmed by ^1H NMR titrations. Results obtained from photophysical techniques are confirmed by electrochemical techniques and DFT studies. PDI exhibited real-life application by detecting Al^{+3} from environmental water samples. We have also demonstrated the efficient antibacterial activity of the synthesized probe and its aluminium complex against *E. coli* bacteria using ampicillin as a standard drug.

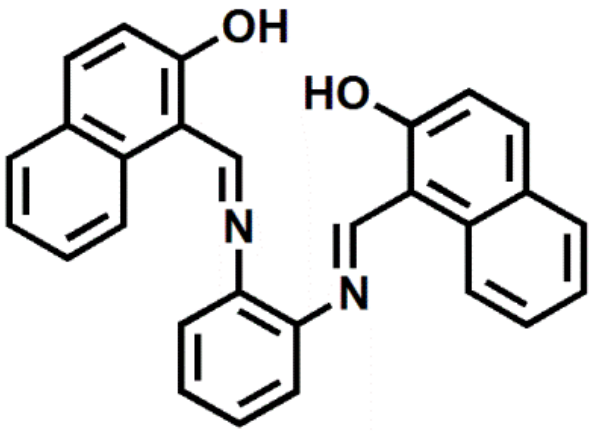

Phenylene diimine (PDI)

Fig. 6.1 Structure of PDI[16]

6.2 Results and discussion

6.2.1 Behaviour of PDI towards Al^{+3} ions

The UV-Vis spectroscopic properties of PDI (1 mM) were investigated in ACN: Water (90:10, v/v). PDI was yellow in color and exhibited spectral bands at 317 and 363 nm. On addition of different metal ions, viz., Hg^{2+}, Ni^{2+}, Co^{2+}, Fe^{2+}, Fe^{3+}, Pb^{2+}, Cr^{3+}, Zn^{2+}, Cu^{2+}, Al^{3+} to the solution of PDI, only Al^{+3} ions made prominent changes in the spectra and no other cation registered their presence in the solution of PDI (Fig. 6.2). Spectral changes were also confirmed by the change in the color of PDI from light yellow to light green after addition of the aluminium ions (Fig. 6.2 (inset)).

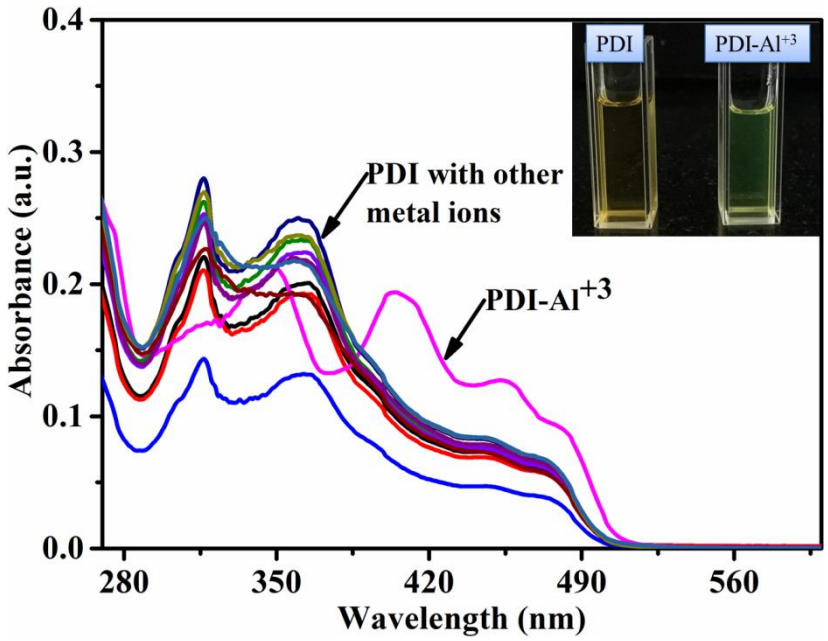

Fig. 6.2 Effect of various metal ions on absorption spectrum of PDI (1 mM) in ACN: Water (90:10, v/v)

On gradual addition of Al^{+3} ions to the solution of PDI, absorption intensity at 363 nm decreased and concomitantly a new absorption band appeared at 406 nm 454 nm and 483 nm. Absorption band intensity at 317 nm shifted to 351 nm progressively on the addition of Al^{+3} ions to the solution of PDI (Fig. 6.3). Thus, PDI can detect Al^{+3} ions within the equivalent range of 0.0 - 2.5 through UV-Vis absorption spectroscopy. From Job's plot,[17] the binding stoichiometry of PDI was found to be 1: 1 for Al^{+3} as absorption maxima was found at 0.5 mole fraction when mole fraction was varied from 0 to 1 (Fig.6.4).

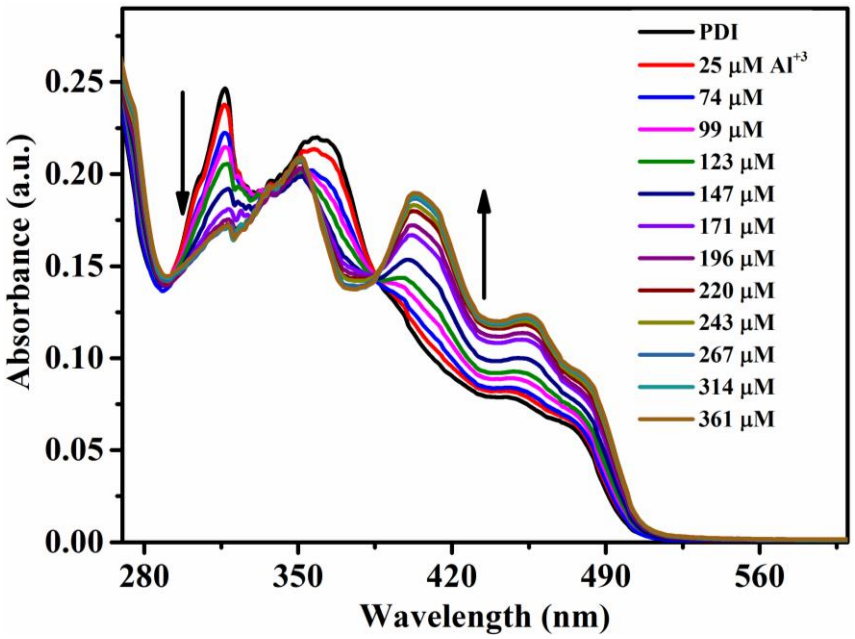

Fig. 6.3 Effect of addition of Al^{+3} (0-360 μM) ions on absorption spectrum of PDI (1 mM) in ACN: Water (90:10, v/v)

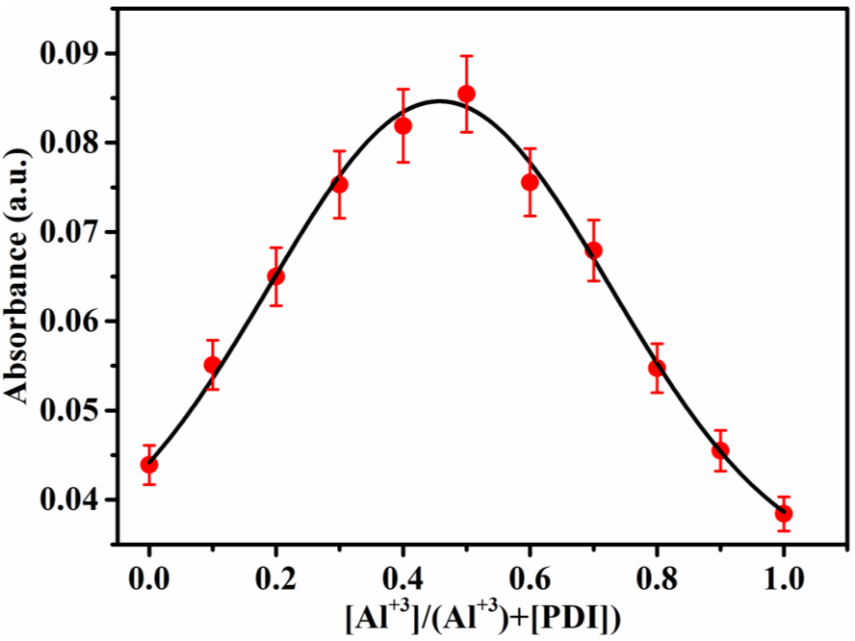

Fig. 6.4 Job's plot diagram of PDI with Al^{+3} ions

Even though receptor PDI responded best towards Al^{+3} in pure ACN as observed from fig 6.5. Yet considering the application of the probe for Al^{+3} detection in real-time samples it was desirable to check the performance of the probe for Al^{+3} in the presence of a mixture of solvents. Hence, experiment was conducted to check the response of probe for Al^{+3} detection in ACN mixed with different ratios of water, as water is undisputedly present in ACN

solvent. Since the performance of probe in mixed solvent medium was best with the ratio of ACN: Water as 90:10, v/v, therefore, chosen to work upon. The probe detected Al^{+3} selectively even in the presence of Fe^{+3} and Cr^{+3} ions which are likely to accompany Al^{+3} in the wastewater samples (Fig. 6.6).

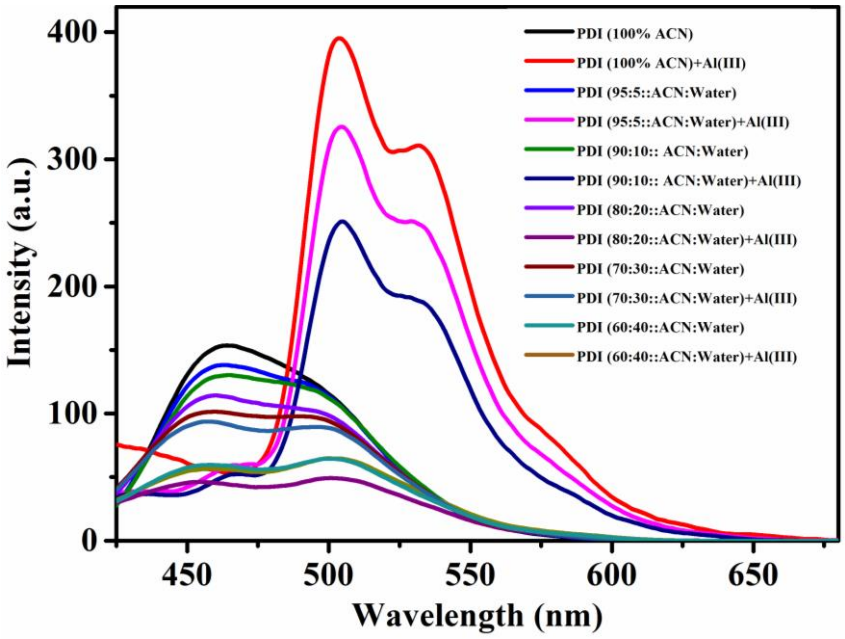

Fig. 6.5 Optimization of water ratio for the selective detection of Al^{+3} ions

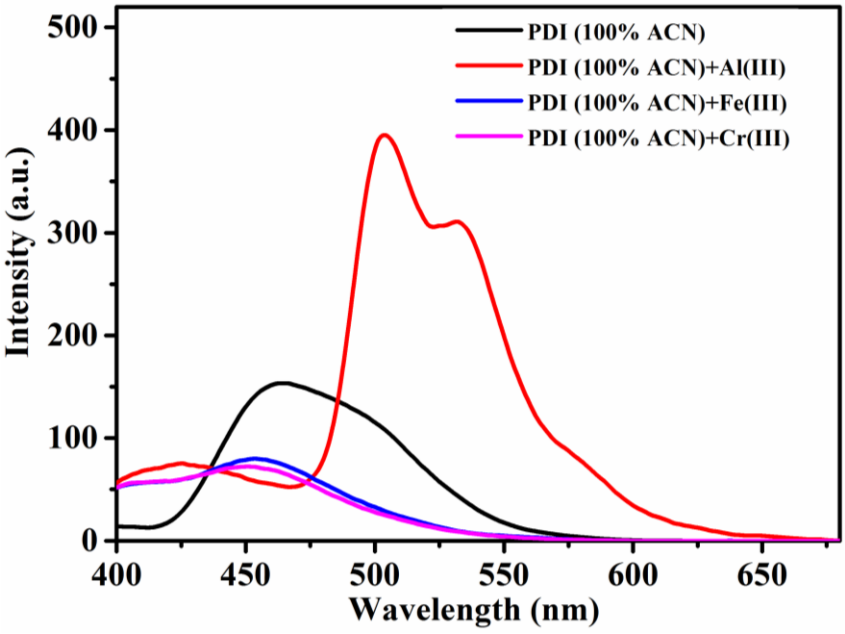

Fig. 6.6 Selectivity of Probe 1 in 100% ACN solvent

Afterwards, to gain better understanding of the interaction of PDI (50 μM) with various metal ions viz., Hg^{2+}, Ni^{2+}, Co^{2+}, Fe^{2+}, Fe^{3+}, Pb^{2+}, Cr^{3+}, Zn^{2+}, Cu^{2+}, Al^{3+} ions (5 μM), fluorescent spectral responses were recorded in ACN: Water (90:10, v/v) solvent medium. On excitation at 360 nm, receptor was weakly fluorescent with a band position at 460 nm but on addition of Al^{+3} ions (perchlorate salt), receptor band got shifted to 504 nm with increase in intensity and no other cation brought such prominent change in the emission spectra of PDI (Fig. 6.7).

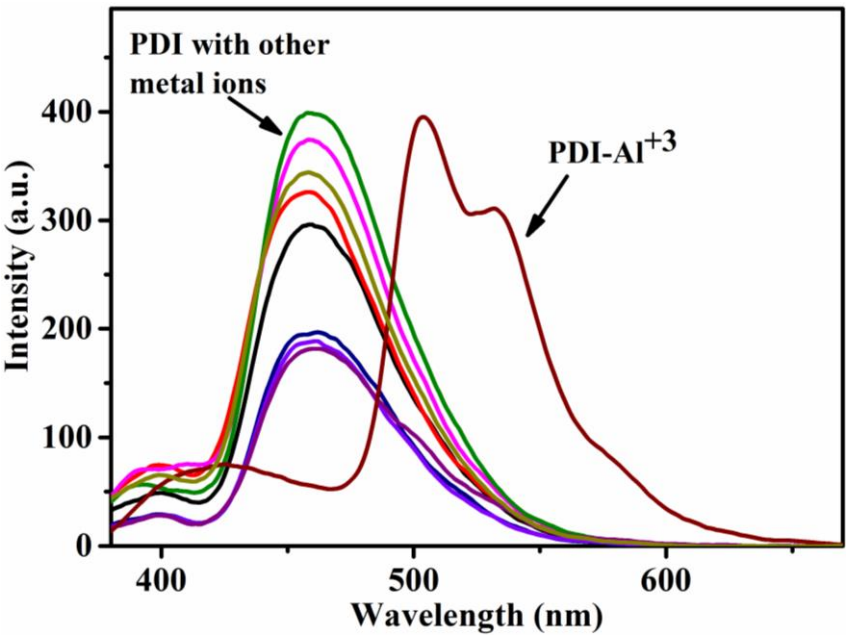

Fig. 6.7 Effect of various metal ions (5 μM) on emission spectrum of PDI (50 μM) in ACN: Water (90:10, v/v)

Upon titration of PDI with Al^{+3} ions, ratiometric behavior of probe was observed with shifting in band position from 460 to 504 nm. Not only shifting in band position but enhancement in intensity was also observed (Fig. 6.8). The intensity ratio at 460 and 504 nm varied from 0.3 to 7.24, indicating 24-fold emission intensity ratio change. From the ratiometric calibration curve of emission titration, detection limit of the PDI was found to be 6.7×10^{-7} M using 3σ method (Fig. 6.9) [18]. The binding constant was calculated by using Benesi-Hildebrand[19] equation and the value found to be 0.314×10^{4} M^{-1}. Thus, the PDI can be used to estimate Al^{+3} ions within the equivalent range of 0-4 through fluorescence spectroscopy.

To check practical ability of the PDI towards Al^{+3} ions, interference studies were conducted in ACN: Water (90:10, v/v) solvent medium. In the competitive experiment concentration of

interfering ions was equal to that of Al^{+3} ions. As seen from Fig. 6.10, no significant interference was observed in the selective detection of Al^{+3} ions in the presence of other metal ions.

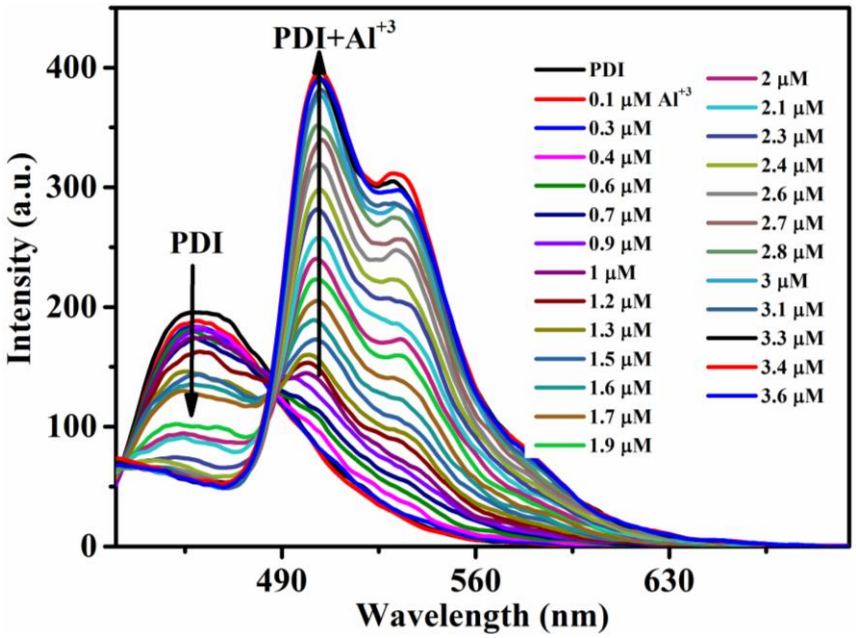

Fig. 6.8 Effect of addition of Al^{+3} (0-3.6 µM)ions on absorption spectrum of PDI (50 µM) in ACN: Water (90:10, v/v)

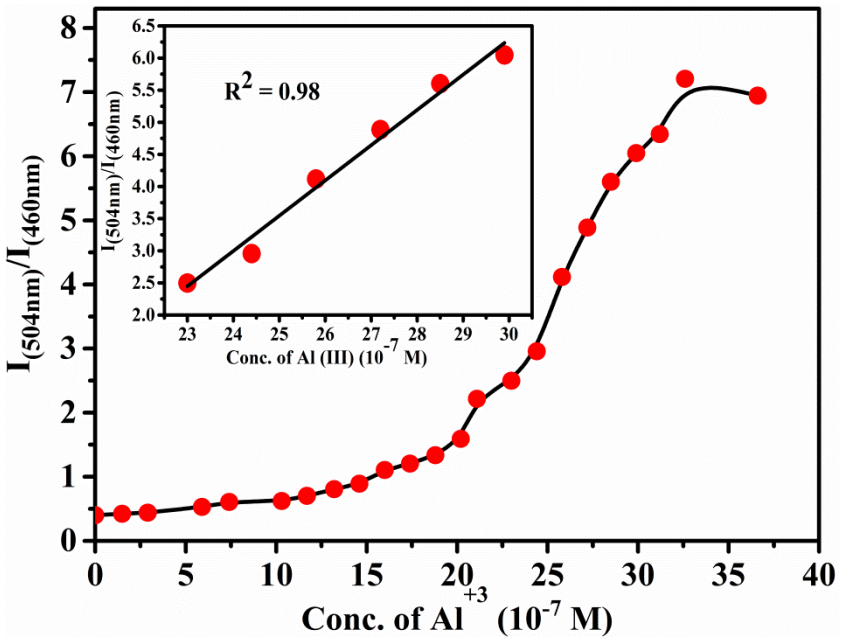

Fig. 6.9 Ratiometric calibration plot between intensity ($I_{504/460}$) and conc. of Al^{+3} ions

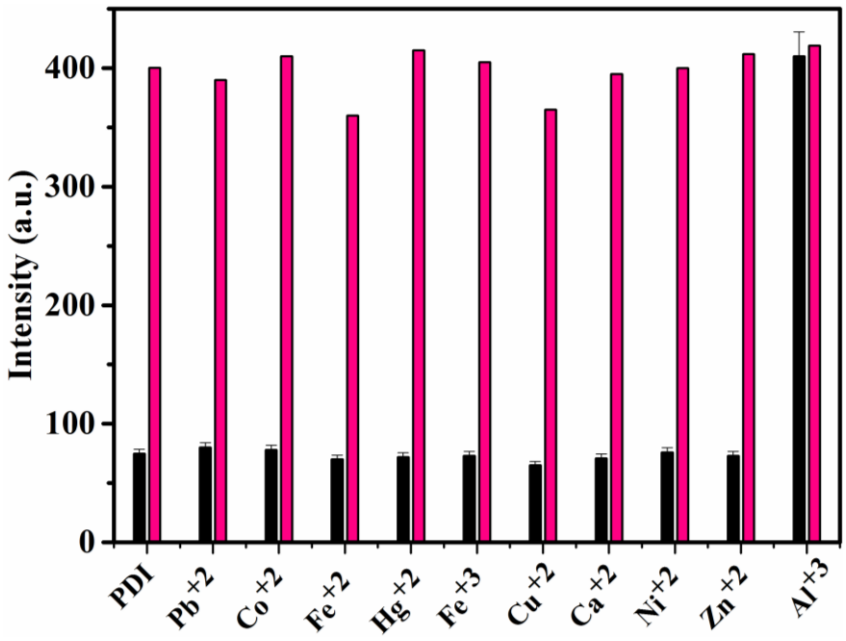

Fig. 6.10 Black bars represents selectivity of PDI (50 µM) in presence of different metal ions in ACN: Water (90:10, v/v) medium and pink bars show the competitive selectivity of PDI in the presence of Al^{+3}

Determination of Al^{+3} in water samples

To study potential analytical applications of PDI for the detection of aluminium in water samples, experiments were conducted on the samples drawn from ground water of Thapar Institute Campus. From different locations of Thapar Institute of Engineering and Technology, Patiala, two water samples were collected and used for the detection of Al^{+3} ions. After spiking the water samples with aluminium, the content was found to be 11-13 ppm using Atomic Absorption Spectroscopy (Fig. A6.1) and the proposed method. Satisfactory results were obtained in a set of triplicate (Table 6.1) experiments. Thus, PDI can be applied successfully for the determination of Al^{+3} ions in environmental water samples. The method of detection of Al^{+3} ions has been validated by government approved laboratory.

Table 6.1 Results of three replicate determinations of Al^{+3} in water samples

Sample	Concentration (ppm)	
	Proposed method (Fluorescence)	**AAS method**
Water sample 1	12.34	12.61
	12.37	12.82
	12.31	12.74
Water sample 2	11.78	12.38
	11.83	12.35
	11.85	12.45

Electrochemical behavior of PDI towards Al^{+3} ions

A diimine derivative of benzene (PDI) has been explored as a voltammetric probe for the detection of Al^{+3} ions. Its selectivity for Al^{+3} ions is based on the exploratory work carried out using UV spectroscopy and spectrofluorimetry techniques. Voltammograms of PDI was recorded in both ACN and ACN: water (90:10, v/v) media using glassy carbon as working electrode, platinum as a counter, and Ag/AgCl as a reference electrode at an optimized scan rate of 50 mV/sec (Fig. 6.11). In ACN, anodic DPV has two major current maxima at -0.25 V and 0.62 V with weak maxima at 0.9 V. It was interesting to observe the relatively sharpened current maxima with enhanced current magnitude when the voltammogram of PDI was recorded in solvent mixture of ACN and water in the ratio of 90:10. Sharpening of peak is proposed to be due to transition of intramolecular H-bonding to intermolecular H-bonding as the medium is changed from pure ACN to ACN: H_2O (90:10, v/v) mixture. In the absence of water in the medium, there exists H-bonding between each nitrogen atom of imine group with hydrogen of –OH group attached at ortho position to each naphthyl group. In presence of water in the medium, this intramolecular H-bonding is lost in favor of intermolecular H-bonding between the two hydroxyl groups through a chain of water molecules in the solvent. Sharpening of the peaks in aqueous ACN medium is because of the better oxidative environment for the lone pair of electrons on nitrogen of each imine group, hence, leading to better defined anodic peak maxima.[20]

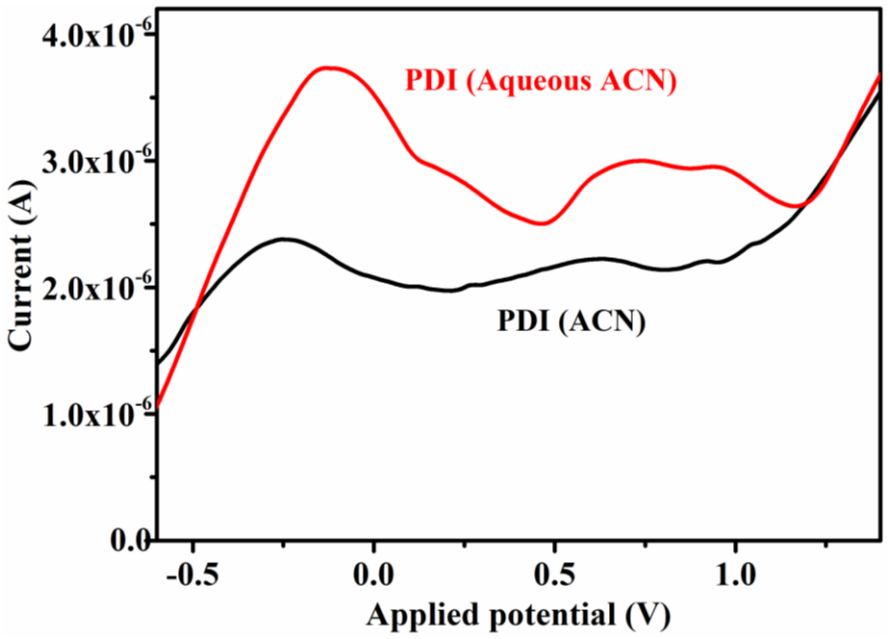

Fig. 6.11 Voltammetric response of PDI (1 mM) in ACN and ACN: H_2O (90:10, v/v) system, 0.1 M $TBAPF_6$, scan rate: 50 mV/sec, working electrode:GC

Anodic voltammogram of receptor PDI was also recorded in the presence of Al^{+3} ions to know about its complexing ability with the metal with the receptor. Inspired from the effect of water on the selective detection of Al^{+3} ions, metal complexation study was carried out in both ACN and ACN: H_2O (90: 10, v/v) media. In the absence of water, anodic voltammogram of PDI showed broad peak at -0.25 V and 0.62 V while in the case of its complex with Al^{+3} ions, well-defined respective peaks were observed at -0.05 V and 0.79 V (Fig. 6.12). Anodic voltammogram of PDI in the presence of Al^{+3} was also recorded in ACN solvent medium containing 10 % water. The voltammogram showed a sharp splitting of the peak at -0.25 V into two maxima at -0.17 V and 0.12 V, while the broad peak maxima at 0.62 V and 0.9 V merged to a well-defined current maximum at 0.81 V (Fig. 6.13).

Following the above mentioned results, two hypotheses are proposed based on the behavior of PDI and its aluminium complex in ACN and ACN: H_2O (90:10, v/v) system.

(a) Sharpness of peaks, as observed in the presence of Al^{+3}, is due to the shift in electronic environment in the pseudo cavity near imine N atoms from metal complexation to the lewis base character, as indicated by the strong and sharp anodic peaks in the voltammograms. Al^{+3} gets preferably engaged with hydroxyl species and water molecules than with the lone pair of N atoms of the imine group.

(b) In the absence of water in the medium, relatively broader peaks were observed which might be due to the complexation of Al^{+3} with two nitrogen of imine group as well as ACN solvent, thereby lone pair of electrons on imine nitrogen atoms do not fully exercise their Lewis basic character.

Application of the voltammetric method in quantitative determination of Al^{+3}

Inspired from the observed sharp anodic peak maxima at 0.81 V, a calibration curve of the host PDI was drawn between anodic current values recorded at successively increased amounts of Al^{+3} in a partially non-aqueous medium of ACN: H_2O (90:10, v/v). The calibration curve for the binding of the Al^{+3} ions with the host PDI was plotted and regression coefficient was found to be 0.985. It implies the linear binding with the Al^{+3} is taking place. A linear response of the plot between the anodic current and Al^{+3} content was repeated at least five times to confirm its reproducibility (Fig. 6.14). A relative standard deviation of calibration curve was observed as 1.3 %.

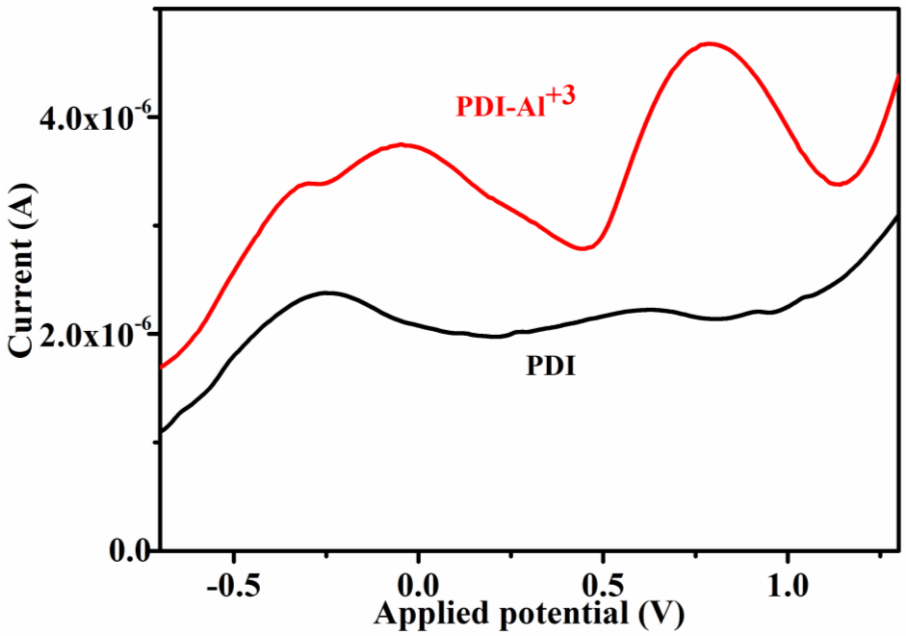

Fig. 6.12 Response of PDI (1 mM) and PDI-Al^{+3} complex in ACN solvent, 0.1 M $TBAPF_6$, scan rate: 50 mV/sec, working electrode:GC

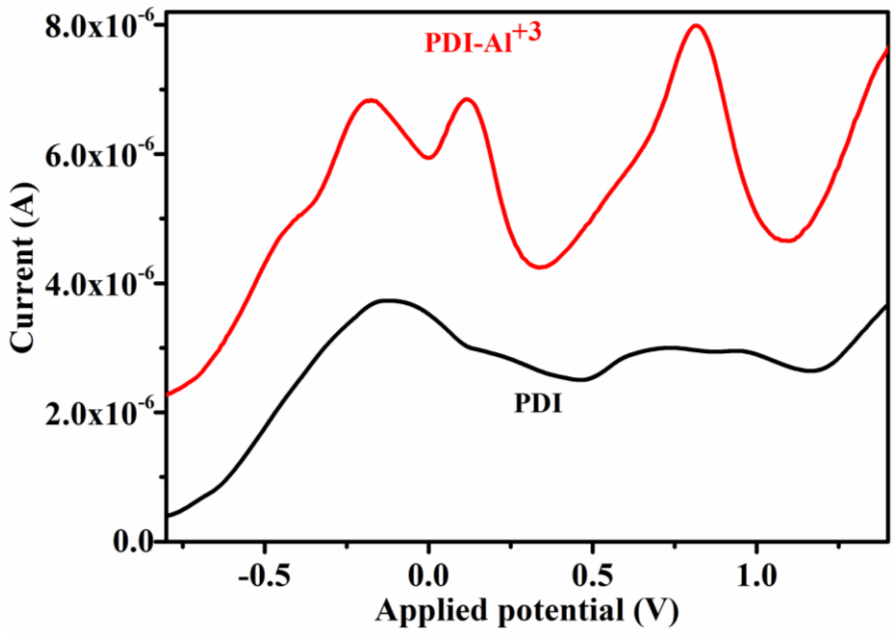

Fig. 6.13 Anodic DPV of PDI (1 mM) and PDI-Al^{+3} in ACN: H_2O (90:10, v/v) system, 0.1 M $TBAPF_6$, scan rate: 50 mV/sec, working electrode:GC

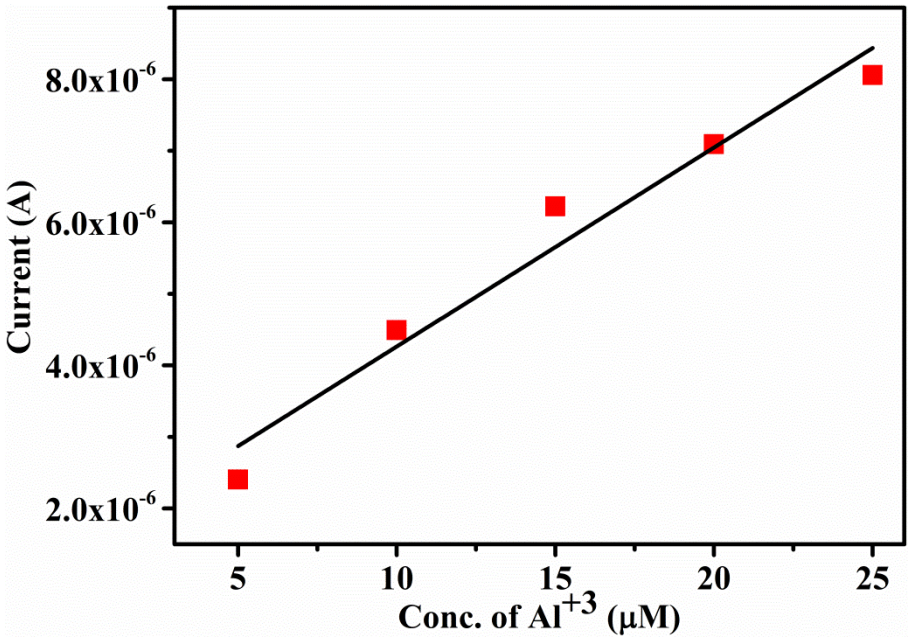

Fig. 6.14 Calibration plots of peak current of PDI versus the conc. of Al^{+3} ions, 0.1 M $TBAPF_6$, scan rate: 50 mV/sec, working electrode:GC

6.2.2 Behaviour of PDI towards CN^-/F^-

Sensing properties of PDI ($1x10^{-4}$ M) were examined for various anions like HSO_4^-, $H_2PO_4^-$, ClO_4^-, OAc^-, F^-, Cl^-, CN^- using their respective tetrabutylammonium salts in ACN: Water (90:10, v/v).

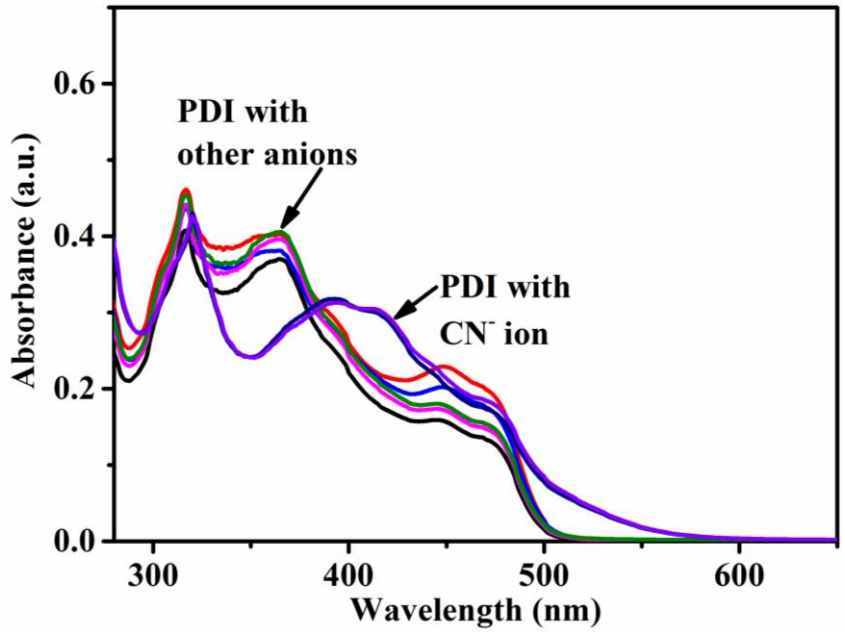

Fig. 6.15 Effect of various anions (400 µM) on absorption spectrum of PDI (1 mM) in ACN: H_2O (90:10, v/v)

Upon addition of various anions, only CN^- and F^- brought significant changes in absorption spectra of PDI and no other anion showed any shift in the absorption spectra (Fig. 6.15). Upon addition of CN^- and F^- ions, absorption bands at 369 nm diminished with simultaneous appearance of a new band at 412 nm. To gain better understanding, titration of PDI was conducted with CN^- ions and it was observed that the band at 369 nm got shifted to 412 nm with a bathochromic shift of 43 nm. Using UV-Vis spectroscopy, the PDI has been successfully used to determine CN^-/F^- ions over a wide range of 0 - 360 µM (Fig. 6.16).

From the Job's plot,[17] the binding stoichiometry of the probe was found to be 1: 2 for CN^-/F^- ions as absorption maxima was found at 0.6 mole fraction when mole fraction was varied from 0 to 1 (Fig. 6.17.)

Emission properties of PDI were checked for various anions such as HSO_4^-, $H_2PO_4^-$, ClO_4^-, OAc^-, F^-, Cl^-, CN^- in ACN: Water (90:10, v/v). On excitation at 360 nm, PDI was weakly fluorescent at 460 nm and showed "turn on" behavior for CN^- and F^- ions at the same

wavelength while no other anion showed any prominent change in the emission intensity of the PDI (Fig. 6.18). Titration experiment was conducted for PDI with CN^- ions and it was found that with the addition of 20 μM CN^-, there was enhancement in intensity at 460 nm indicating fluorescence "turn on" behavior of PDI (Fig. 6.19).

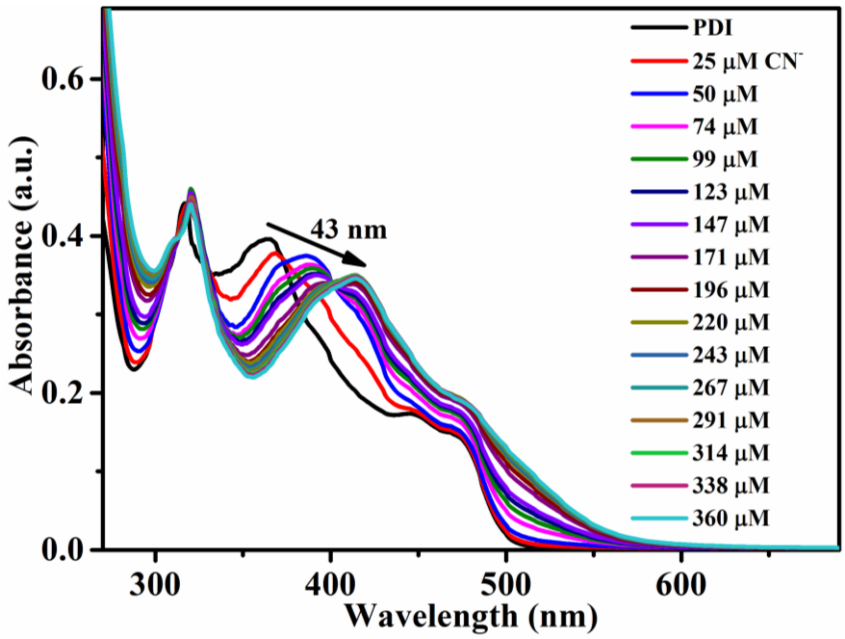

Fig. 6.16 Effect of addition of CN^- ions on absorption spectrum of PDI (1 mM) in ACN: H_2O (90:10, v/v)

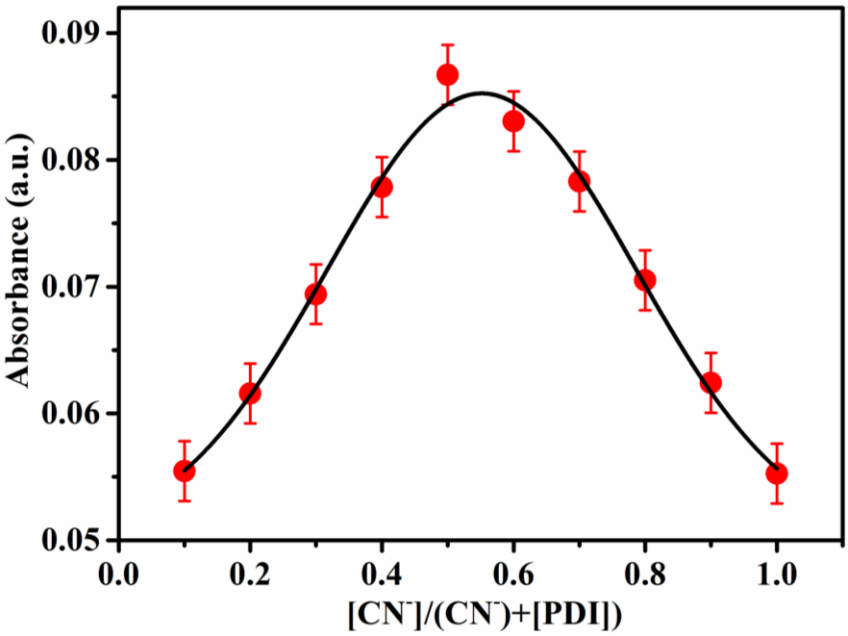

Fig. 6.17 Job's plot diagram of PDI with CN^- ions

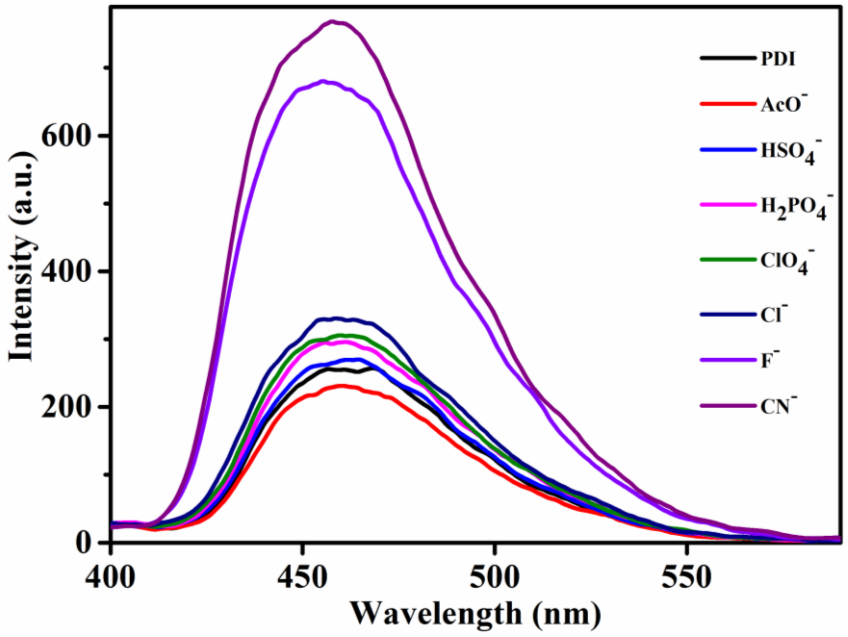

Fig. 6.18 Effect of various anions (20 µM) on emission spectrum of PDI (50 µM) in ACN: H_2O (90:10, v/v)

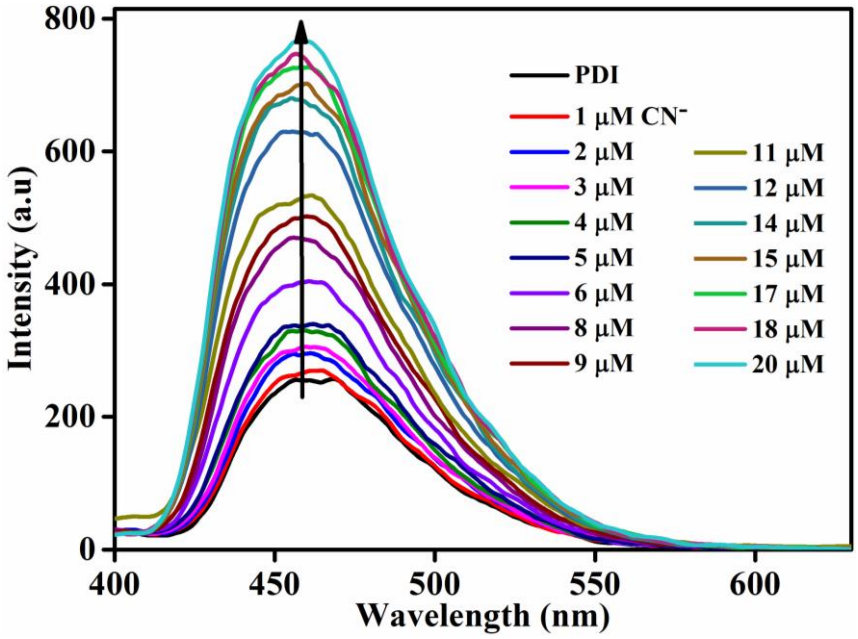

Fig. 6.19 Effect of addition of CN^- ions on emission spectrum of PDI (50 µM) in ACN: water (90:10, v/v)

Using Benesi-Hildebrand equation[19] the binding constant was calculated to be 0.143×10^3 M^{-1} with the lowest detection limit[18] of 0.1 µM (Fig. 6.20). The limit of quantification was found to be 0.56 µM. For successfully applying the sensor on to real samples, knowledge about the enhancement in intensity is of great importance. The emission intensity at 504 nm varied

from 257.06 a.u. to 771.42 a.u. indicating 3-folds enhancement in intensity. Similar changes were observed for F^- ions which indicated that both anions follow the same mechanism.

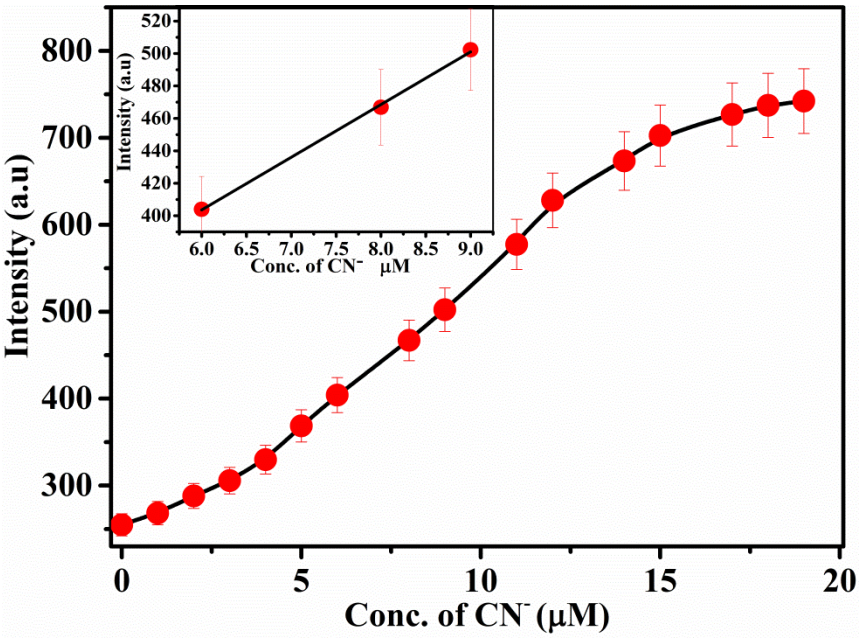

Fig. 6.20 Plots of emission intensity at 460 nm vs [CN^-] ions of PDI

To check the practical applicability of PDI-CN^- complex towards various anions, competitive experiment was conducted. In this experiment, concentration of the competitive anions such as HSO_4^-, $H_2PO_4^-$, ClO_4^-, OAc^-, F^-, Cl^- was equal to the concentration of the CN^- ions. No significant variation was observed in the emission spectra of the PDI-CN^- complex when comparing the results with or without the presence of competitive ions. These results clearly indicate that the probe PDI is selective in nature and is able discriminate CN^- and F^- ions from various other anions present in the same solution of receptor. As already discussed in the above paragraph, probe PDI does not differentiate between CN^- and F^- ions. Therefore, the proposed probe works for both CN^- and F^- ions in a similar way. Even little amount of water could not differentiate between the two target ions. Black bar represents selectivity of PDI (5 μM) upon addition of different anions in ACN: Water (90:10, v/v) and pink bars show the competitive selectivity of the probe in presence of CN^- (Fig. 6.21).

^{1}H NMR titrations of PDI with CN^- ions

To get further insight into the mechanism of interaction ^{1}H NMR titration was conducted between PDI and CN^- ions. Upon addition of 2 equivalents of CN^- ions, ^{1}H NMR spectrum of the PDI showed shifting in various signals. Signal at 10.79 ppm disappeared completely in

the presence of cyanide ions (Fig. 6.22), which demonstrates that deprotonation of hydroxyl group took place. In addition to this, protons of naphthyl group of PDI got upfield shifted due to the delocalization of negative charge that developed after deprotonation of hydroxyl group.[21]

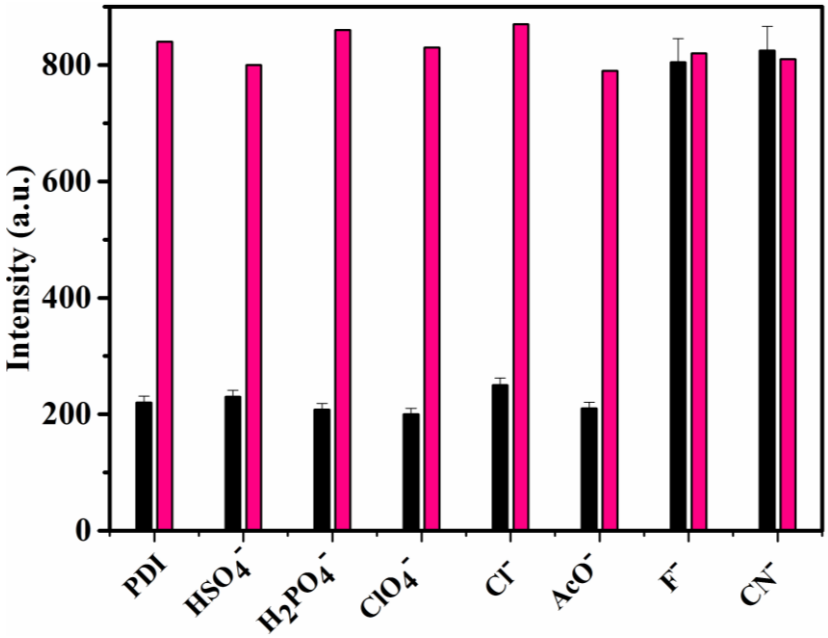

Fig. 6.21 Emission intensity profile of PDI-CN^- complex in presence of interfering ions

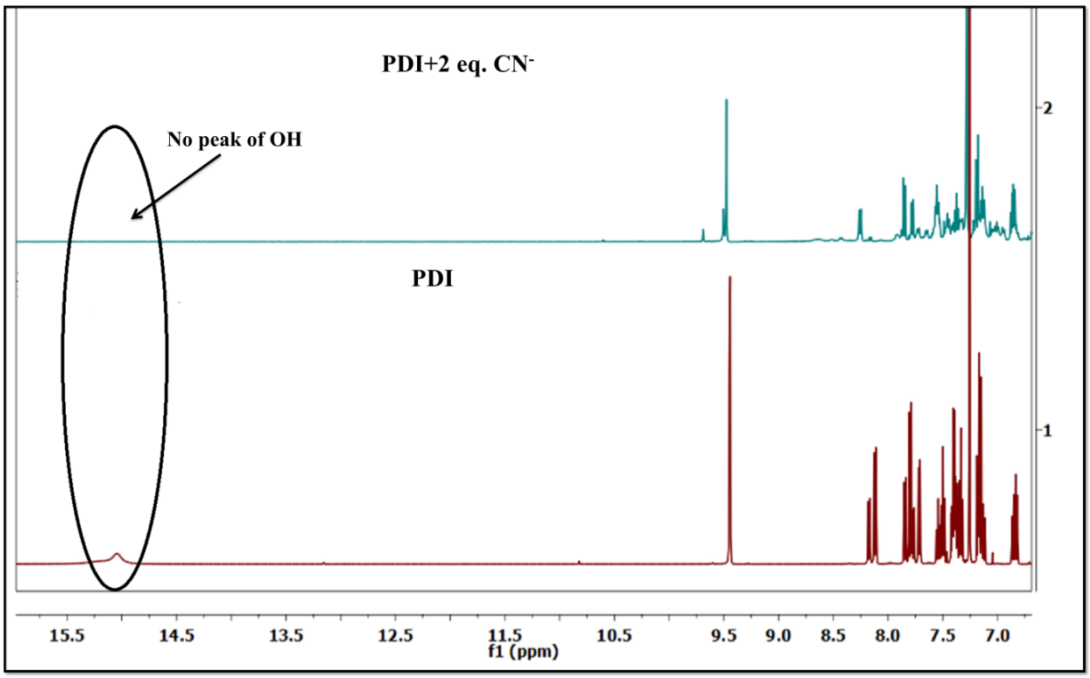

Fig. 6.22 Partial ^1H NMR spectral (10.9-6.7 ppm region) changes of PDI in the presence of 2equivalents of cyanide ions in $CDCl_3$

6.2.3 Proposed binding approach of PDI towards Al^{+3}/CN^-

The imine linkage in PDI provides a suitable electronic environment in the molecule. The unrestricted torsional rotation for imine linkage will deactivate the excited state. Deactivation took place via utilizing the energy in molecular motions which leads to weak fluorescence of the probe and hence resulted in a photoinduced electron transfer (PET) process. Presence of lone pair of electrons on nitrogen atom of the imine linkage is likely to undergo the PET process through its electron donation tendency, while presence of Al^{+3} in the vicinity of PDI suggested coordination of Al^{+3} with nitrogen atom of imine linkage and hydroxyl molecule of naphthyl moiety. Thus, electron transfer process from nitrogen to naphthyl group got stopped and hence PET process got blocked and triggered the strong emission of PDI in the presence of Al^{+3} ions. Moreover, PDI- Al^{+3} complex gained structural rigidity which lead to fluorescent enhancement through CHEF-PET phenomena (Scheme 6.1).

Likewise, the optimization of PDI-CN^- complex resulted in deprotonation of hydroxyl proton as confirmed by ^1H NMR titrations and stabilization of complex by 0.078 kcal/mol energy,[22,23] which clearly predicts the resistance in PET process and ultimately triggered the emission intensity.

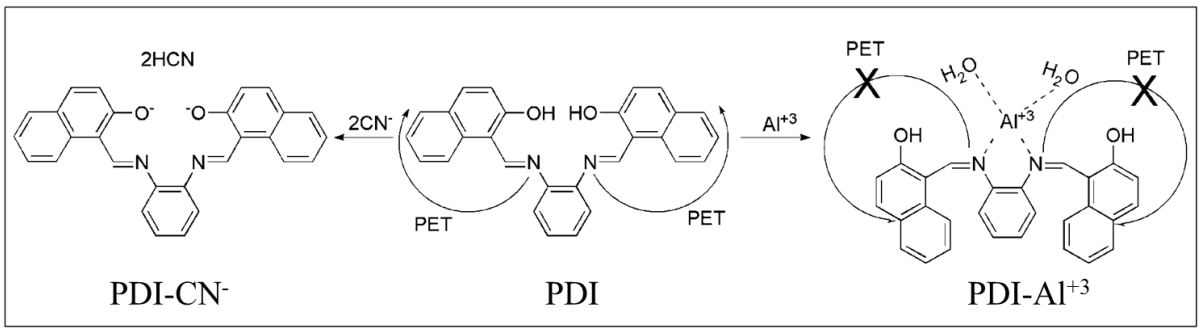

Scheme 6.1 Proposed sensing mechanism of PDI with Al^{+3} and CN^- ions

6.2.4 PDI- Al^{+3} system for the detection of water in acetonitrile

The selectivity of PDI for Al^{+3} ions in ACN: Water (90: 10, v/v) encouraged us to investigate the behavior of PDI-Al^{+3} complex in the presence of increasing amount of water in ACN solvent. Fig. 6.23 shows a regular decrease in intensity of the complex peak at 504 nm. This decrease in intensity indicates that the complex is getting stabilized in the ACN: water medium with an increased ratio of water in ACN medium. Also, it has been optimized that an

increased amount of water provides greater number of ion-dipole bonds which lead to greater solvation of complex in partially aqueous media with enhanced ionic environment.

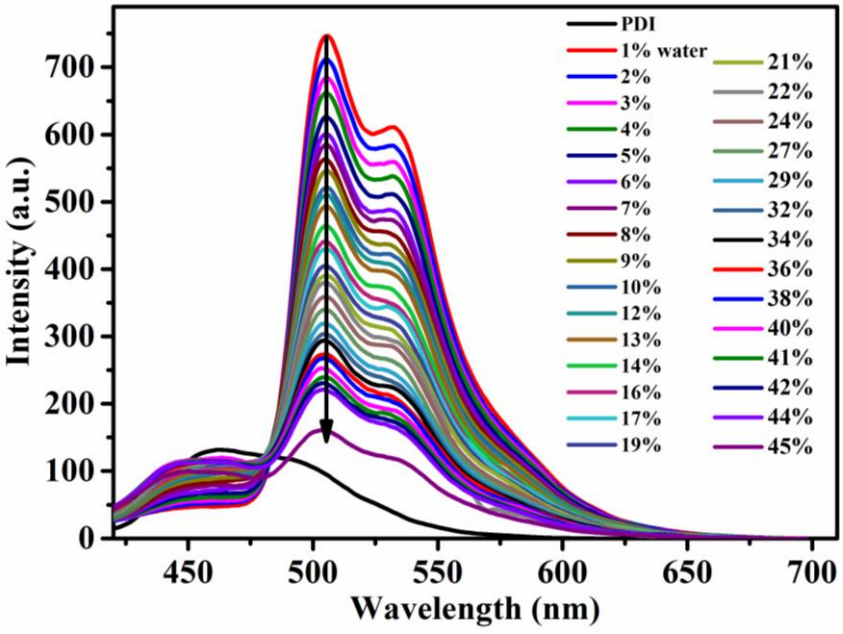

Fig. 6.23 Effect of addition of water on emission spectra of PDI-Al^{+3} complex

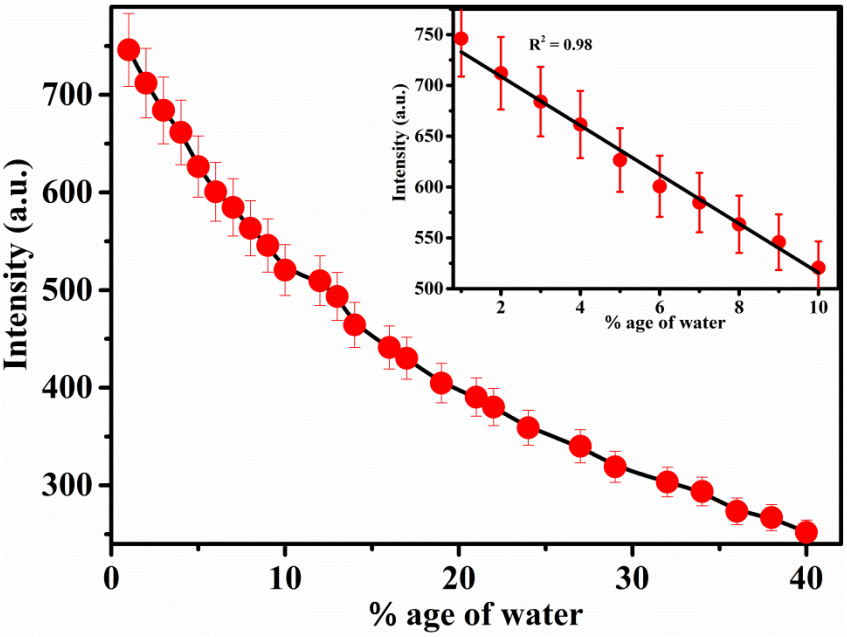

Fig. 6.24 Plot of emission intensity at 504 nm vs % age of water

We, therefore, envisioned using PDI-Al^{+3} system for the detection of water, as an impurity, in ACN. This is important for many applications due to the complete miscibility of water in ACN.[22] Using data obtained from the above titrations (Fig. 6.24), a linear decrease in fluorescence intensity was observed when peak intensity was plotted as a function of percentage of water in ACN. Using equation $3\sigma / slope$,[18] the lower detection limit of water in ACN was found to be 0.4%. Reproducible results with RSD = 1.1% were obtained in a set of five readings.

6.2.5 Antibacterial activity and cell imaging

The antibacterial activity of PDI and its complex with Al^{+3} was carried out against non-pathogenic bacterial strain, namely *E. coli*, using broth dilution method. At first, various parameters such as growth period of bacteria, concentration of organic moieties, and inhibition time scale were optimized. Concentration of both organic moieties i.e. PDI and PDI-Al^{+3} was optimized to be 40 µg/ml. The antibacterial activity was found to be increasing sequentially with an increasing concentration of both PDI and PDI-Al^{+3}. This shows that both organic moieties can inhibit the growth of bacteria more effectively in a concentration-dependent manner.[24] While optimizing time scale it was found that PDI is quite effective within 60 minutes of its addition into the bacteria solution (Fig. 6.25).

Broth dilution method was used to study the antibacterial activity of the PDI and PDI-Al^{+3} complex towards *E. coli* bacteria in 60 minutes with same concentration of compound and complex against standard drug ampicillin. ACN solvent was taken as a negative control. Bar graph (Fig. 6.26) demonstrates that both compound and its metal complex exhibited effective percentage activity against *E. coli* bacteria, whereas, ampicillin was not very much effective within the said time span. PDI exhibited 89 % activity and complex exhibited 94 % activity but there was no inhibition in bacterial growth in case of ampicillin drug. The reason for increases in antibacterial activity of complex can be explained based on Tweedy's chelation theory [25] and Overtone's concept [26]. According to overtone's concept, liposolubility is one of the most important factors to control the antibacterial activity of the compound. This is because lipid membrane around the cell wall favors the passage of only lipid soluble materials. According to chelation theory, polarity of the metal reduces on coordination, principally because of the partial sharing of its cations with the donor group. Moreover,

delocalization of pi-electron took place over the whole chelate ring, which results into the increase in lipophilicity of the chelate, which in turn favor the easy permeability of the complex through the lipid layer of bacterial membrane than the corresponding ligand. This process, in turn, may block the enzymatic activity of the bacteria by stopping the respiration process of the microorganism.

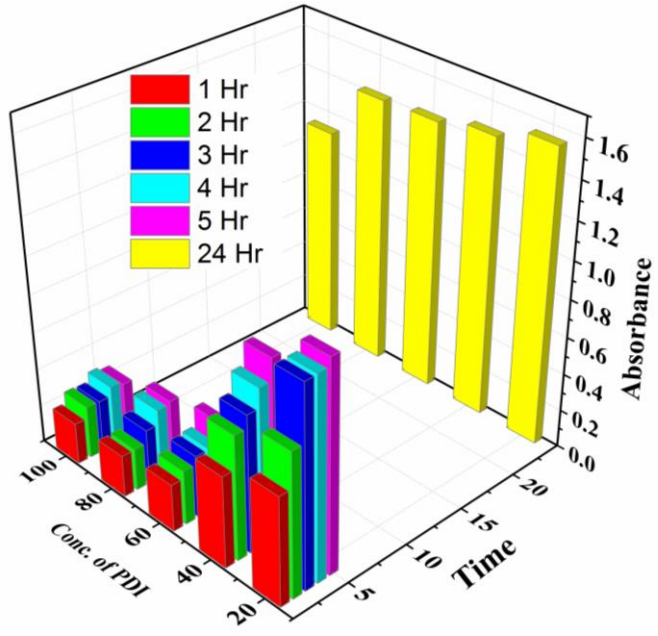

Fig. 6.25 Bar graph presenting optimization of concentration and time

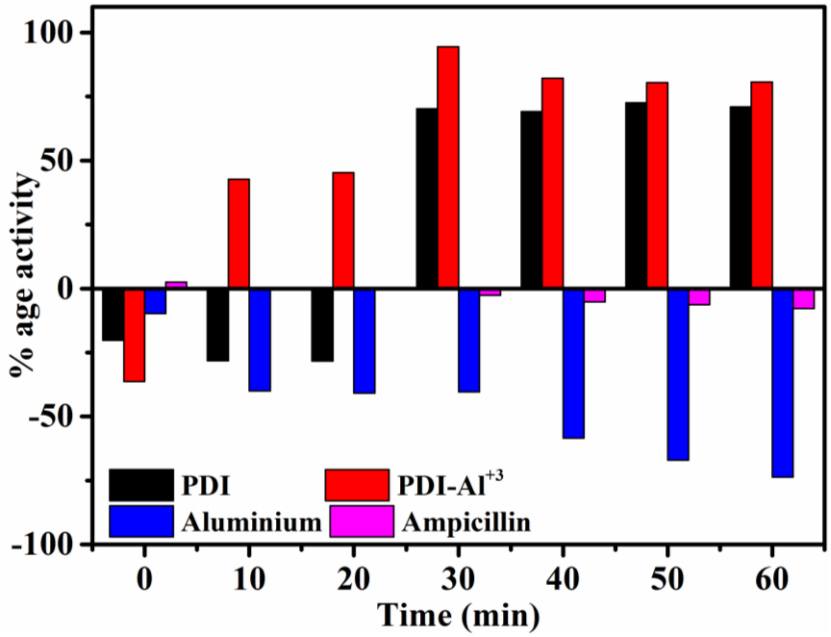

Fig. 6.26 Comparative study of inhibition of PDI, PDI-Al^{+3} complex, aluminium and ampicillin drug against time intervals

For practical biological application, fluorescence imaging experiment was carried out. Since both PDI and its aluminium complex showed excellent fluorescence properties, therefore employed to check their behavior with the *E. coli* bacteria. Bacteria itself was non-fluorescent therefore, no fluorescence was observed in case of pure bacteria (Fig. 6.27 (a)), but when bacteria were incubated with PDI and its aluminium complex separately then red color fluorescence was observed under the excitation in green light lamp (Fig. 6.27 (b, c)). Fluorescent images have demonstrated that both organic moieties have interacted well with the bacteria. Moieties can interact with the cell wall leading to its disruption or can enter the bacteria through permeable channels. Presence of organic moieties on the cell wall of bacteria was confirmed by bacteriolysis using bead beating method. Absorbance spectra of the probe and its aluminium complex after bacteriolysis was similar to as that of pure probe and PDI-Al^{+3} complex[27] (Fig. 6.28).

For more information, SEM analysis was carried out to check the morphology of *E. coli* before and after treatment with PDI and its aluminium complex. Untreated bacteria had rod-shaped structure with smooth surface (Fig. 29(a)). In case of treated *E. coli* with organic moieties showed disoriented pattern of bacterial cells, multiple depression and indentation indicating damage of the cell wall or cell membrane of the bacteria (Fig. 29 (b, c)) [28]. SEM images support the fluorescence imaging experiment.

6.2.6 Theoretical studies

In order to provide insight into the mode of complexation, structure of PDI and its complex with Al^{+3}/CN^{-} were optimized by B3LYP functional in combination with 6-31G basis set. Presence of cyanide ions caused deprotonation of hydroxyl group as proposed and confirmed by ^{1}H NMR titration of PDI with cyanide ions. And in other case, Al^{+3} lies in close proximity of the probe and showed strong interaction with hetero atoms. Table 6.2 shows the gap between highest occupied molecular orbital (HOMO) and lowest unoccupied molecular orbital (LUMO) of native PDI and upon its complexation with Al^{+3} and CN^{-} ions. Obtained values clearly indicate that gap between HOMO and LUMO has decreased when Al^{+3} and CN^{-} came into the picture which states that stable complexation has taken place (Fig. 6.30).

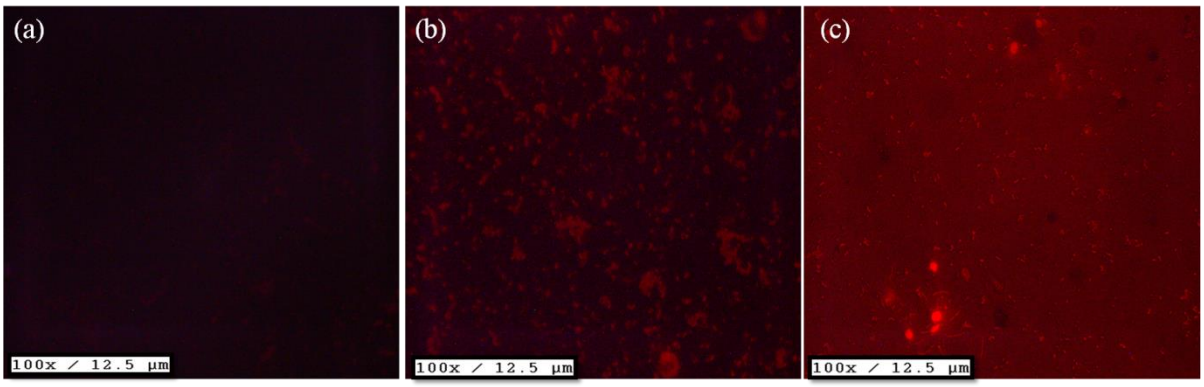

Fig. 6.27 Fluorescence microscopic images of (a) untreated bacteria (b) treated bacteria with PDI (40 µg/ml) (c) treated with PDI-Al^{+3} complex (40 µg/ml)

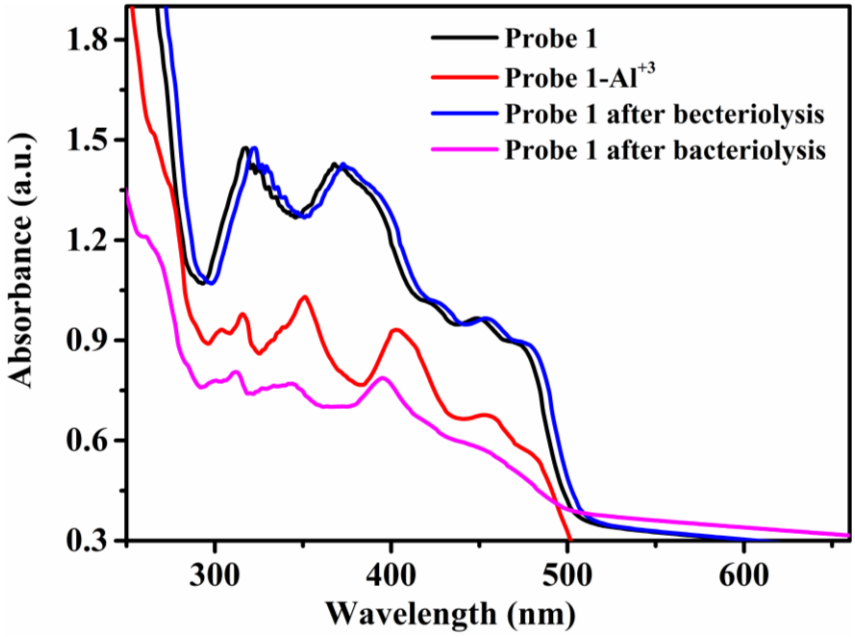

Fig. 6.28 Absorbance spectra of PDI and PDI-Al^{+3} complex before and after bacteriolysis

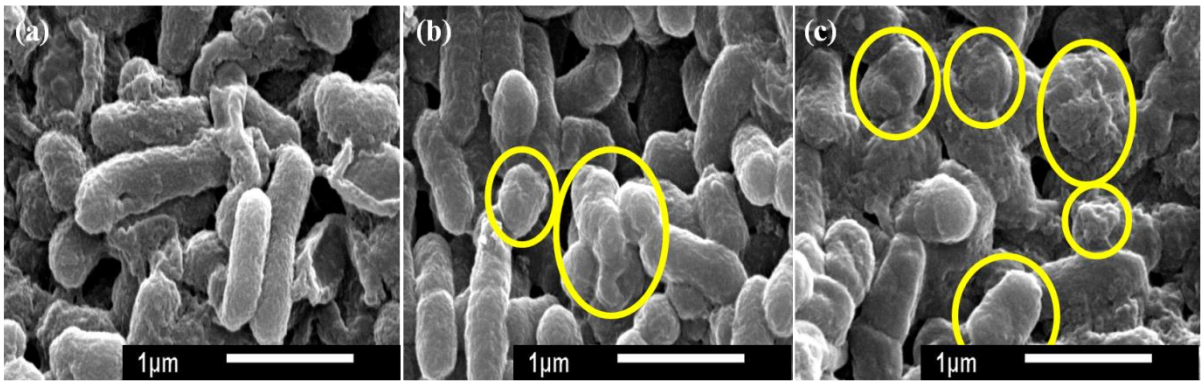

Fig. 6.29 SEM images of (a) untreated bacteria (b) treated bacteria with PDI (40 µg/ml) (c) treated with PDI-Al^{+3} complex (40 µg/ml)

Table 6.2 Energy values (in a.u.) of HOMO and LUMO for PDI and its complex with Al^{+3}/ CN^- using DFT calculations

Receptor / Complex System	Energy in a.u		
	E_{HOMO}	E_{LUMO}	E_{gap}
PDI	-0.190	-0.063	0.127
PDI-Al^{+3}	-0.542	-0.515	0.027
PDI-CN^-	0.066	0.144	0.078

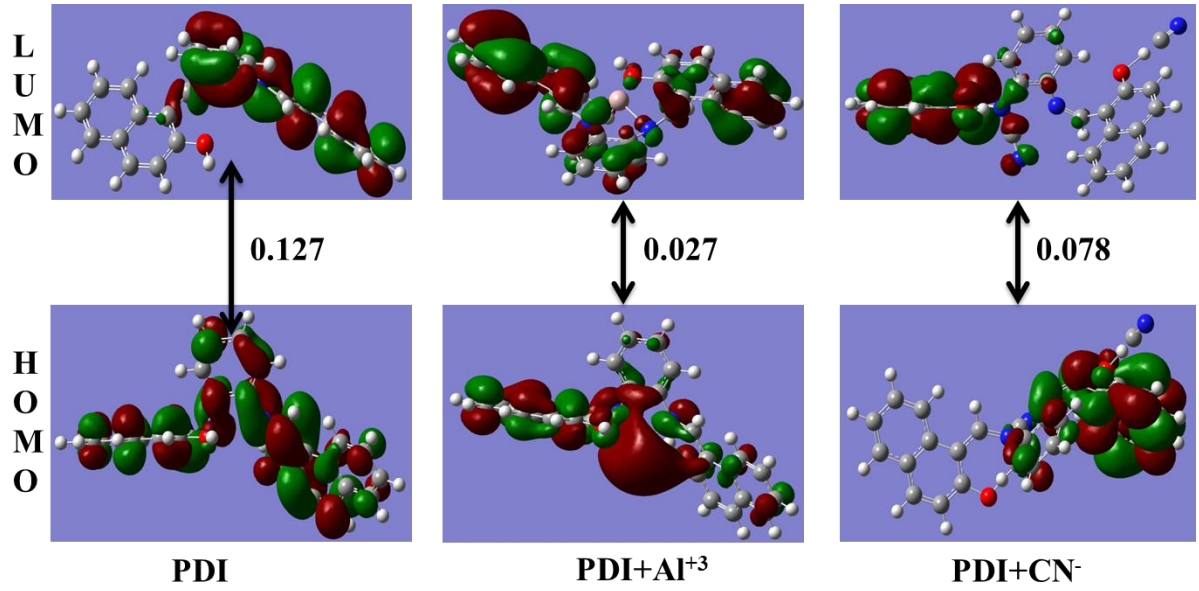

Fig. 6.30 Optimized structure of PDI, PDI-Al^{+3} and PDI-CN^-

Conclusions

A diimine derivative of benzene (PDI) showed selective behavior towards Al^{+3} and CN^-/F^- ions among various cations and anions in ACN: H_2O (90:10, v/v) medium. Al^{+3} ions were detected via restriction in the PET process and the results were corroborated with electrochemical studies. A mechanism based on deprotonation of the hydroxyl groups of the ionophore explained the selective behavior for CN^-/F^- ion detection, which was confirmed by ^1H NMR titrations. PDI was successfully tested for Al^{+3} detection in spiked water samples as real-time application, through fluorescence technique. Also, the PDI- Al^{+3} complex has been developed as a new method for the detection of water in acetonitrile solvent. All the results for cation as well as anion were in good agreement with theoretical studies. PDI and its

aluminium complex have shown excellent antibacterial activity against *E. coli* bacteria using ampicillin as a standard drug.

References

1. K. Baljeet, K. Navneet and K. Subodh, *Coordination Chemistry Reviews*, 2018, **358**, 13-69.
2. T. Das, A. Roy, H. Uyama, P. Roy and M. Nandi, *Dalton Transactions*, 2017, **46**, 7317-7326.
3. S. l. Vallejos, A. n. Muñoz, S. Ibeas, F. Serna, F. l. C. García and J. M. García, *ACS Applied Materials & Interfaces*, 2015, **7**, 921-928.
4. M.-H. Yu, T.-L. Hu and X.-H. Bu, *Inorganic Chemistry Frontiers*, 2017, **4**, 256-260.
5. J. Fu, Y. Chang, B. Li, H. Mei, L. Yang and K. Xu, *Analyst*, 2019, **144**, 5706-5716.
6. F. Wang, L. Wang, X. Chen and J. Yoon, *Chemical Society Reviews*, 2014, **43**, 4312-4324.
7. N. Assadollahnejad, M. Kargar, H. R. Darabi, N. Abouali, S. Jamshidi, A. Sharifi, K. Aghapoor and H. Sayahi, *New Journal of Chemistry*, 2019, **43**, 13001-13009.
8. B. Rani, S. Swami, A. Agarwala, D. Behera and R. Shrivastava, *RSC Advances*, 2019, **9**, 30599-30614.
9. J. Li, X. Qi, W. Wei, Y. Liu, X. Xu, Q. Lin and W. Dong, *Sensors and Actuators B: Chemical*, 2015, **220**, 986-991.
10. Y.-K. Yang and J. Tae, *Organic Letters*, 2006, **8**, 5721-5723.
11. G. WHO, *World Health Organization*, 2011, **216**, 303-304.
12. E. Feng, C. Fan, N. Wang, G. Liu and S. Pu, *Dyes and Pigments*, 2018, **151**, 22-27.
13. N. Ahfad, G. Mohammadnezhad, S. Meghdadi and H. Farrokhpour, *Spectrochimica Acta Part A: Molecular and Biomolecular Spectroscopy*, 2020, **228**, 117753.
14. A. S. Gupta, K. Paul and V. Luxami, *Analytical Methods*, 2018, **10**, 983-990.
15. T. G. Jo, J. J. Lee, E. Nam, K. H. Bok, M. H. Lim and C. Kim, *New Journal of Chemistry*, 2016, **40**, 8918-8927.
16. S. Samanta, B. Nath and J. B. Baruah, *Inorganic Chemistry Communications*, 2012, **22**, 98-100.
17. J. S. Renny, L. L. Tomasevich, E. H. Tallmadge and D. B. Collum, *Angewandte Chemie International Edition*, 2013, **52**, 11998-12013.

18. Analytical Methods Committee, *Analyst*, 1987, **112**, 199-204.

19. H. A. Benesi and J. Hildebrand, *Journal of the American Chemical Society*, 1949, **71**, 2703-2707.

20. P. Gili, M. M. Reyes, P. M. Zarza, I. Machado, M. G. Da Silva, M. Lemos and A. Pombiero, *Inorganica chimica acta*, 1996, **244**, 25-36.

21. P. M. Reddy, S.-R. Hsieh, C.-J. Chang and J.-Y. Kang, *Journal of Hazardous Materials*, 2017, **334**, 93-103.

22. S. Gupta, M. Chhibber and S. K. Mittal, *Journal of Applied Electrochemistry*, 2020, **50**, 185-195.

23. S. Gupta, S. K. Mittal and M. Chhibber, *Journal of the Electrochemical Society*, 2020, **167**, 167506.

24. T. Boobalan, M. Sethupathi, N. Sengottuvelan, P. Kumar, B. Zoltán Gulyás, P. Padmanabhan, S. Tamil Selvan and A. Arun, *ACS Applied Nano Materials*, 2020.

25. B. Tweedy, *Phytopathology*, 1964, **55**, 910-914.

26. N. Dharmaraj, P. Viswanathamurthi and K. Natarajan, *Transition Metal Chemistry*, 2001, **26**, 105-109.

27. A. Salonen, J. Nikkilä, J. Jalanka-Tuovinen, O. Immonen, M. Rajilić-Stojanović, R. A. Kekkonen, A. Palva and W. M. de Vos, *Journal of Microbiological Methods*, 2010, **81**, 127-134.

28. T. Saha, P. Kumar, N. Sepay, D. Ganguly, K. Tiwari, K. Mukhopadhyay and S. Das, *ACS Omega*, 2020, **5**, 16342-16357.

Brief summary

In summary, the work done in this thesis demonstrates the synthesis procedure of triphenylether and triphenylamine based moieties. Sensing behaviour of the synthesised moieties was checked for various anions and cations. Different kind of parameters such as solvents system, concentration of analyte and properties of hetero atoms were discussed in detail. Novel structure design of these triphenyl derivatives has given them a specific environment, cavity size and proper hetero atom arrangement for the detection of target species. Various kinds of techniques such as UV-VIS spectrometer, fluorescence spectrometer, differential pulse voltammetry and DFT were used to understand the mechanism of interaction between receptor and target species. For real life application, selected metal cations and anions were detected from various food samples and the results obtained with these food samples were in good agreement with the atomic absorption spectroscopy.

Receptor TPEA have detected CN^- ions with a detection limit of 0.4 μM in aqueous acetonitrile solvent medium. A paper strip based tool kit was also fabricated for onsite detection of target ions. Probe TPEAM have detected Cu (II) and CN^- ions with a detection limit of 40 nM and 0.4 μM respectively. Cu (II) complex of probe have detected amino acid using metal ion displacement approach. Other than this, molecular logic gate was designed for the detection of target species using their emission wavelength. Water being non polar has pronounced effect on sensing, therefore, role of water on the selective detection of metal ion as well as detection of organic solvent was also explored.

Apart from this, one molecule having Schiff base linkage was explored for detection of Al (III), CN^- and F^- ions. Limit of detection was found to be $6.7x10^{-7}$M for Al (III) ions and $1x10^{-7}$M for CN^- and F^- ions. Furthermore, the role of receptor and its metal ion complex was explored towards the antibacterial activity of the nan-pathogenic bacteria *E. coli*. Mechanism of interaction between organic moieties and bacteria was established via fluorescence imaging and SEM technique. Percentage inhibition of both the organic moieties has proved to be efficient antibacterial agents.

These findings demonstrate detailed sensing behaviour of triphenyl derivatives towards cations, anions and amino acids. Synthesised probes have proven to be excellent chromogenic and voltammetric sensors that can be used for various biological applications.

Appendix

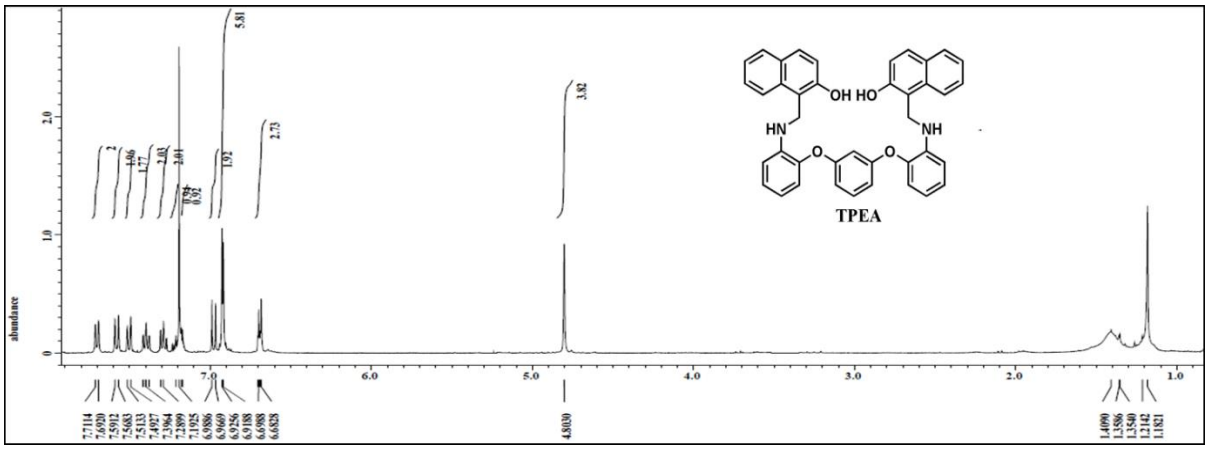

Figure A3.1 [1]HNMR data of TPEA

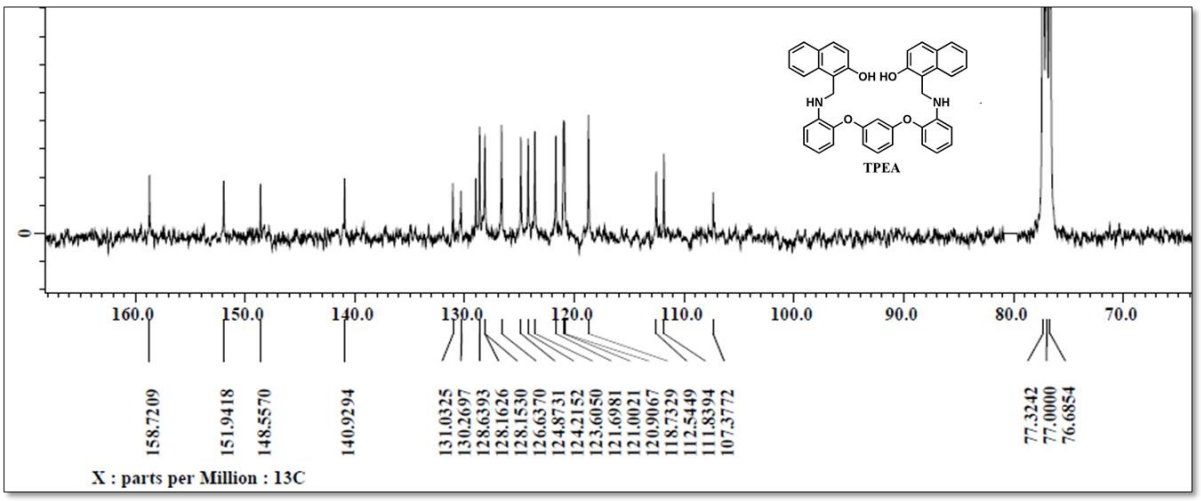

Figure A3.2 [13]CNMR data of TPEA

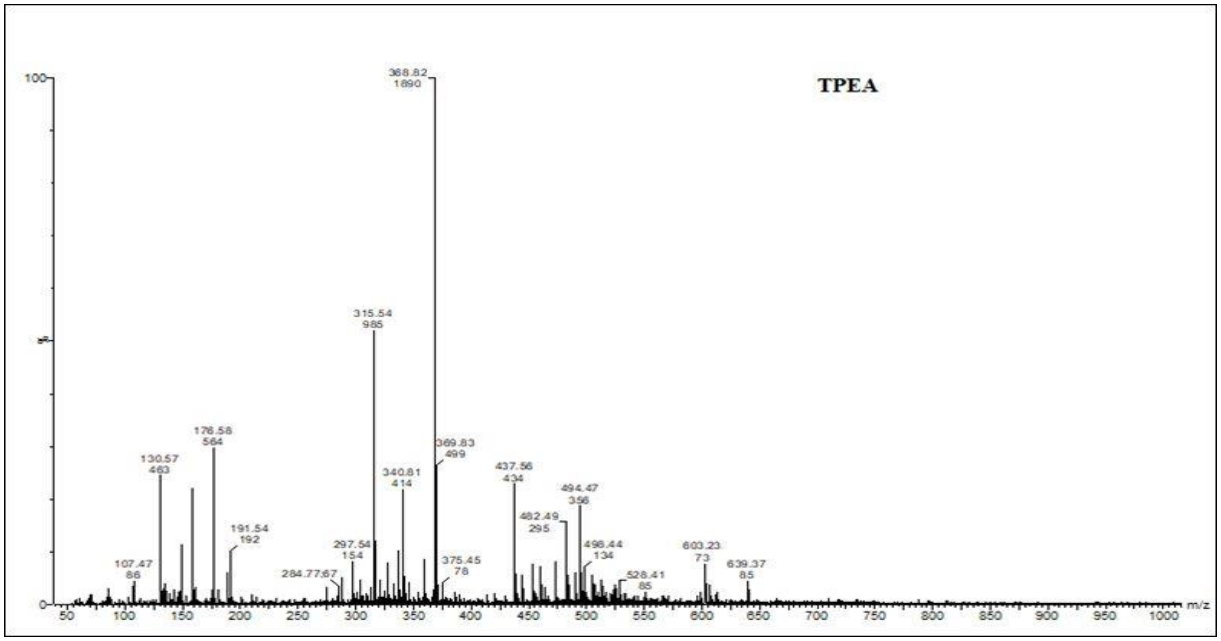

Figure A3.3 Mass spectra of TPEA

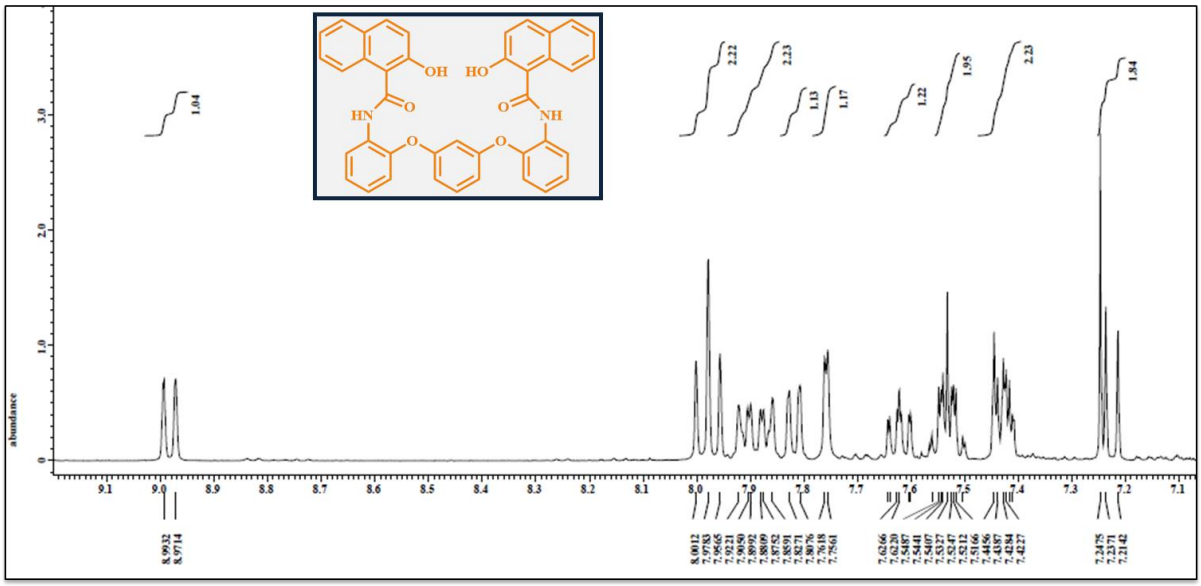

Figure A3.4 ^{1}HNMR data of TPEAM

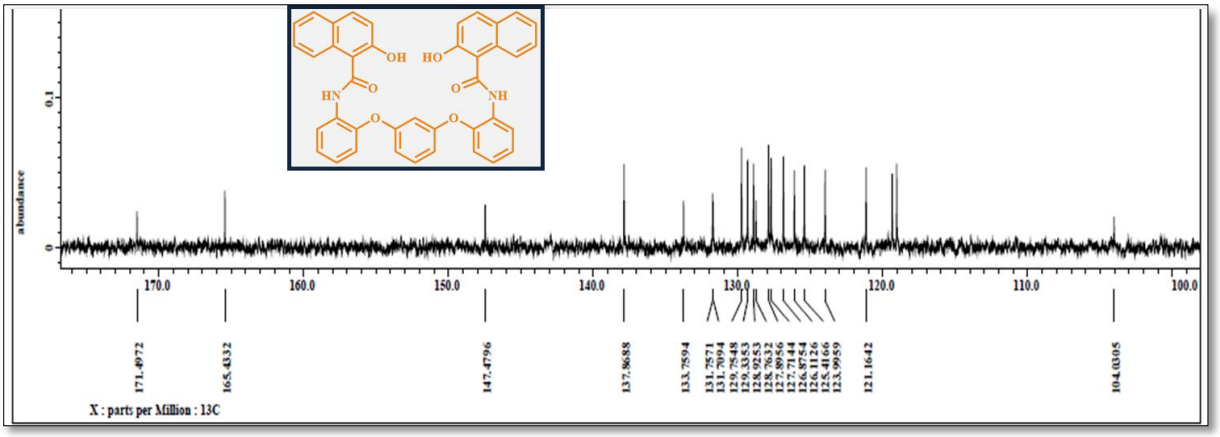

Figure A3.5 ^{13}CNMR data of TPEAM

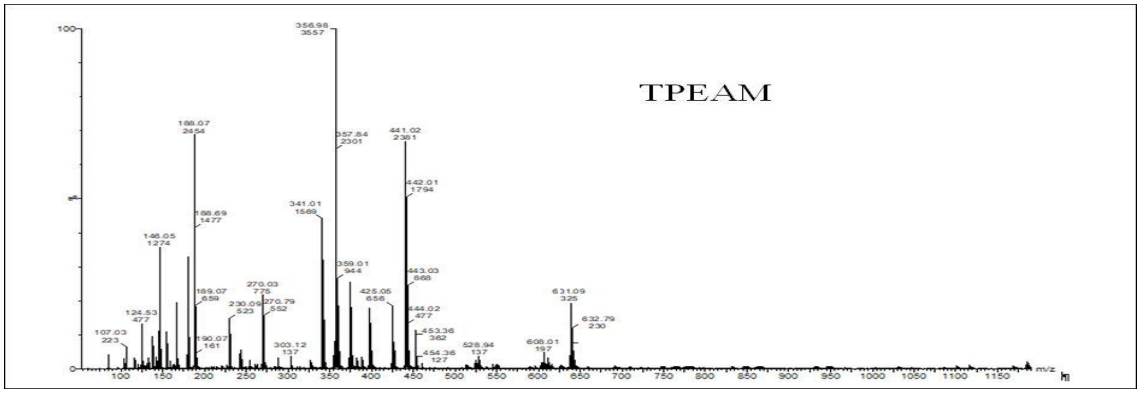

Figure A3.6 Mass Spectrum (ESI-MS) of TPEAM

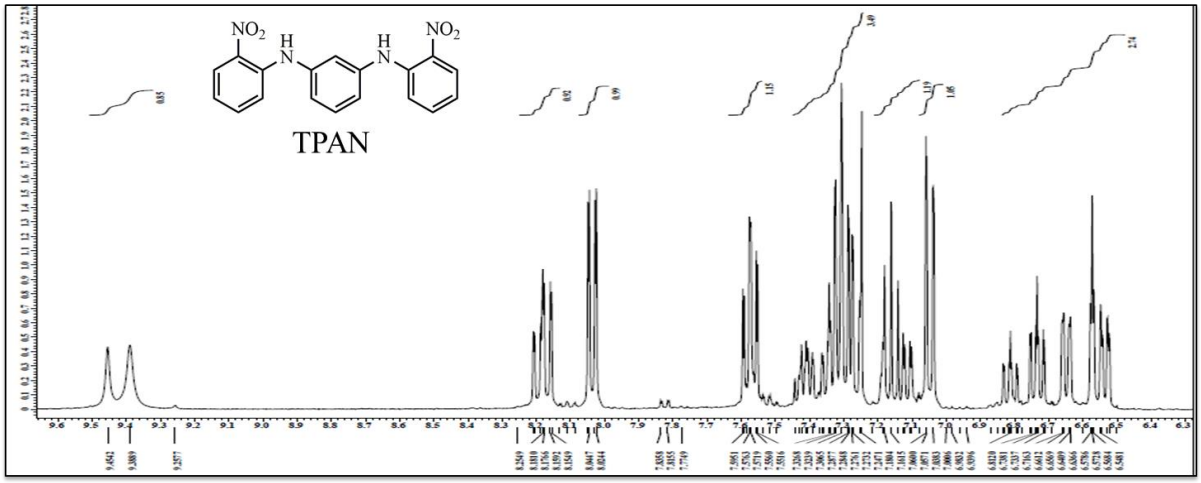

Figure A3.7 ^{1}HNMR data of TPAN

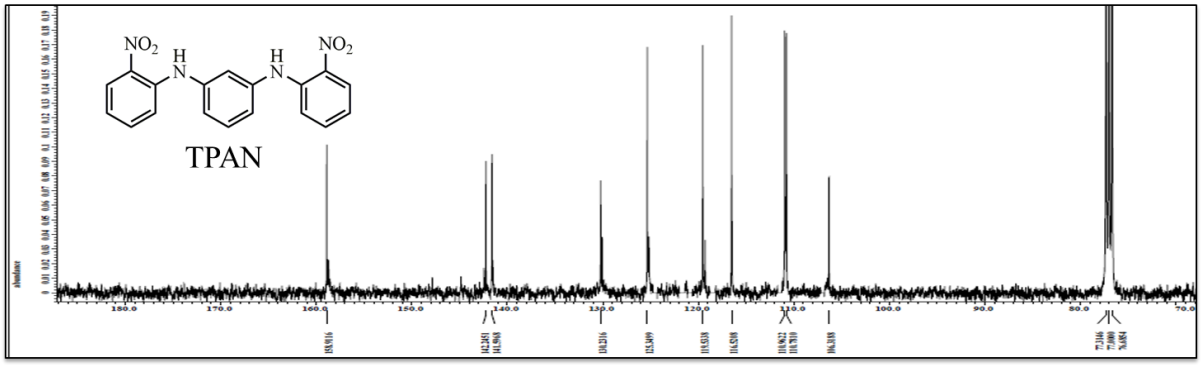

Figure A3.8 ^{13}CNMR data of TPAN

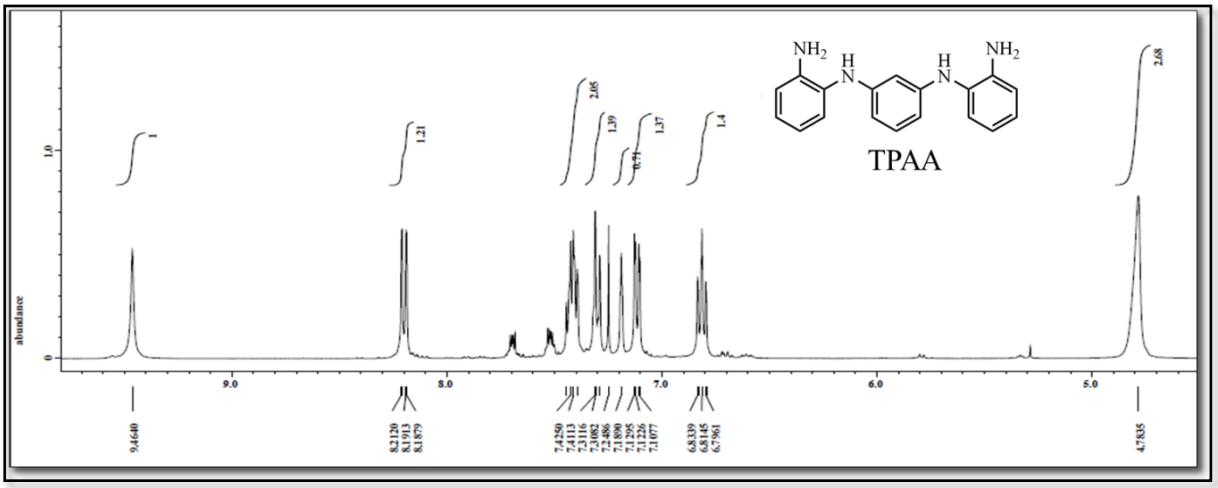

Figure A3.9 ^{1}HNMR data of TPAA

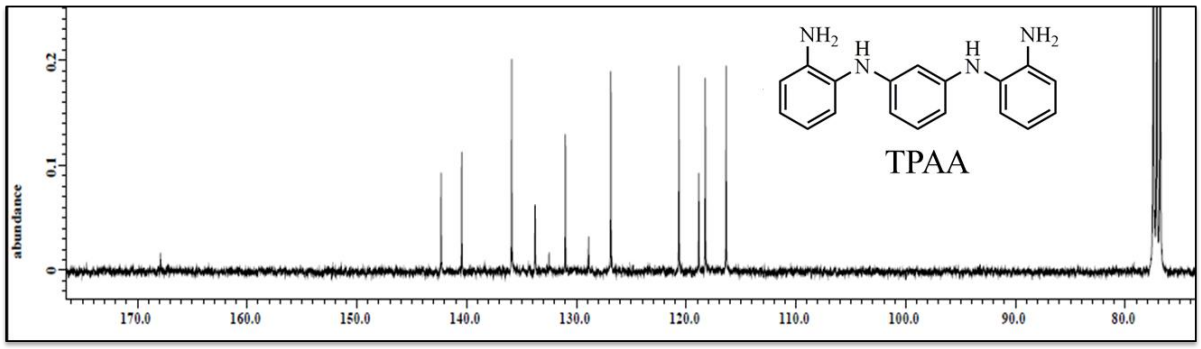

Figure A3.10 ^{13}CNMR data of TPAA

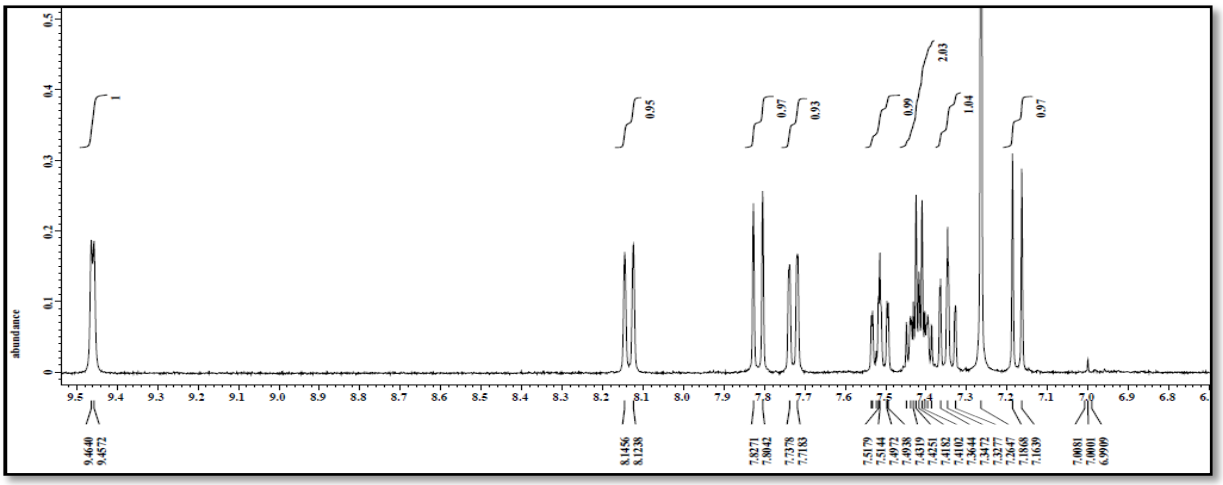

Figure A3.11 ^{1}HNMR data of PDI

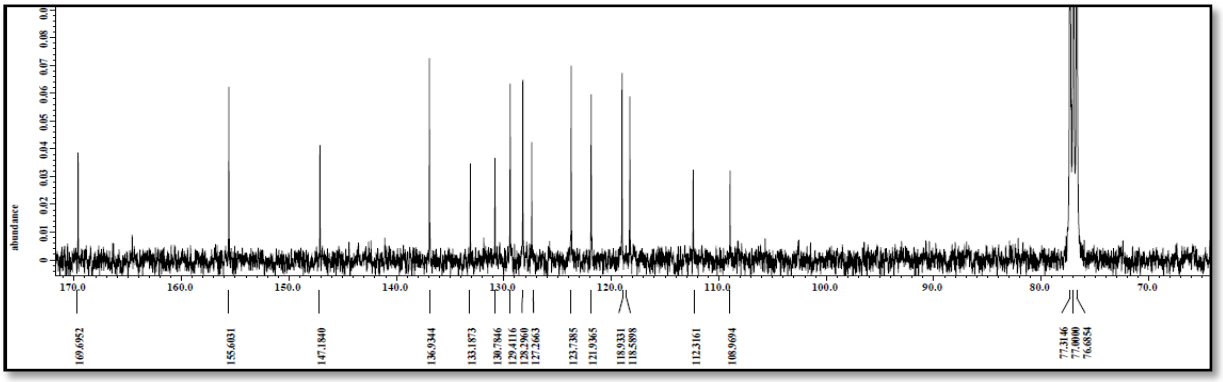

Figure A3.12 ^{13}CNMR data of PDI

Sophisticated Analytical Instruments Laboratories Society (Registered as Society with Registrar of Firms & Societies, Punjab, Chandigarh)
Thapar Technology Campus, Bhadson Road, Patiala-147 004 (India)

TEST REPORT

Test Report No.:	NN/19-20/133	Date:	26.06.2019
Service No.	NN/19-20/133 (01-02)	Customer's Ref.	Sample submitted by Ms. Sonia on dtd. 25.06.2019

Customer's name and address:
School of Chemistry and Biochemistry
Thapar Institute of Engineering & Technology
Patiala
Kind attn.: Dr. Susheel Mittal

Sample Description	Liquid Samples
Condition of the sample received	O.K.
Customer's sample identification No. (if any)	As described below
Quantity/number of samples	50 ml each / Two
Sampling Procedure (if any)	--
Test parameters	Copper
Standard/Specification/Method followed	Atomic Absorption Spectrometer
Deviations (if any)	--
Documents constituting this report (if any)	--

Date of Receipt of Job	Date of Completion of Job	Total Number of Pages
25.06.2019	26.06.2019	1

TEST RESULTS

S. No.	Parameters	Test Method	Unit	Results	
				01 (CUBT)	02 (CUT)
1	Copper as Cu	Atomic Absorption Spectrometer	mg/l	0.14	6.40

.....end of report.....

Dr. S. Mittal
Professor In-charge, SAI Labs
(Authorized Signatory)

Note: 1. The results listed refer only to the tested samples and applicable parameters. [illegible]ment of products is neither inferred nor implied.
2. Samples will be destroyed after one month from the date of issue of the test report unless otherwise specified.
3. This report is not to be reproduced wholly or in part and cannot be used as an evidence in the products is neither inferred nor implied. court of law and should not be used in any advertising media without special permission in writing.
4. In case any reconfirmation of contents of the test report is required, please contact the authorized signatory of the test report within 15 days of the issue of test report.

SAI/FM/CSC-11

Phone: +91(175) 2393552 Fax : +91(175) 2393548 Email: office.sailabs@thapar.edu, info@sailabs.org
URL: www.sailabs.org

Figure A5.1 Detection of Cu^{+2} by standard AAS method

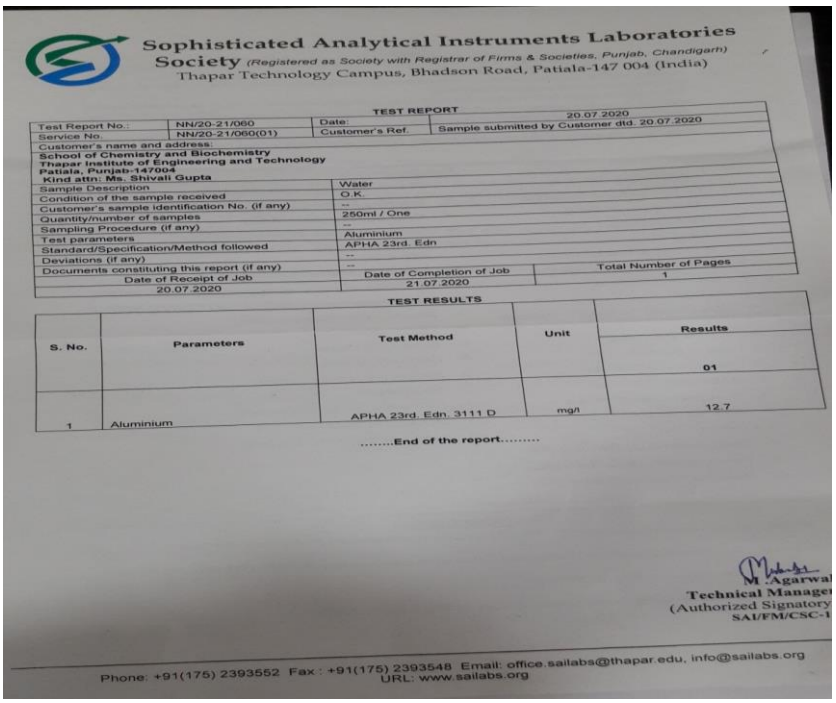

Sophisticated Analytical Instruments Laboratories Society (Registered as Society with Registrar of Firms & Societies, Punjab, Chandigarh)
Thapar Technology Campus, Bhadson Road, Patiala-147 004 (India)

TEST REPORT

Test Report No.:	NN/20-21/060	Date:	20.07.2020
Service No.	NN/20-21/060(01)	Customer's Ref.	Sample submitted by Customer dtd. 20.07.2020

Customer's name and address:
School of Chemistry and Biochemistry
Thapar Institute of Engineering and Technology
Patiala, Punjab-147004
Kind attn: Ms. Shivali Gupta

Sample Description	Water
Condition of the sample received	O.K.
Customer's sample identification No. (if any)	--
Quantity/number of samples	250ml / One
Sampling Procedure (if any)	--
Test parameters	Aluminium
Standard/Specification/Method followed	APHA 23rd. Edn
Deviations (if any)	--
Documents constituting this report (if any)	--

Date of Receipt of Job	Date of Completion of Job	Total Number of Pages
20.07.2020	21.07.2020	1

TEST RESULTS

S. No.	Parameters	Test Method	Unit	Results
				01
1	Aluminium	APHA 23rd. Edn. 3111 D	mg/l	12.7

.....End of the report.....

Technical Manager
(Authorized Signatory)
SAI/FM/CSC-1

Phone: +91(175) 2393552 Fax : +91(175) 2393548 Email: office.sailabs@thapar.edu, info@sailabs.org
URL: www.sailabs.org

Figure A6.1 Detection of Al^{+3} by standard AAS method

List of publications

- **Shivali Gupta**, Manmohan Chhibber*, Susheel K. Mittal, Amine derivative of triphenyl ether as an optical sensor for the detection of cyanide ions and traces of water in acetonitrile supported with voltammetric studies, Journal of Applied Electrochemistry (2020) 50 (2):185-195 **(IF=2.8)**

- **Shivali Gupta**, Susheel K. Mittal*, Manmohan Chhibber, Triphenyl Ether Amide as a Probe for Electrochemical and Optical Sensing of Copper, Cyanide and Arginine, Journal of the Electrochemical Society (2020) 167 (16):167506 **(IF=4.3)**

- Susheel K. Mittal*, Manmohan Chhibber, **Shivali Gupta**, Imine derivative as an analytical probe for Al^{+3}, F-and CN^- sensing with antibacterial activity against E. coli-an application of electrochemical and spectrofluorimetric techniques, Microchemical Journal (2021) 168: 106500 **(IF=4.8)**

- **Shivali Gupta**, Susheel K. Mittal*, Manmohan Chhibber, Solvent and substituent effect on selectivity of triphenylether based ionophores: A voltammetric study (Communicated)

Publications in national and international conferences

1. **Poster Presentation** in "8th National Symposium on Advances in Chemical Sciences" held on February 15-16, 2019 at Guru Nanak Dev University, Amritsar.

2. **Poster presentation** in "Professor Ram Chand Paul National Symposium on Emerging Chemical Innovations for Swachh, Swasth & Sarvatra Bharat" held on February 27-28, 2020 at Punjab University, Chandigarh.

3. **Certificate of participation** in "National Virtual Conference on Recent Advances in Analytical Techniques-2020" held on August 16-17, 2020 via online mode.

4. **Certificate of participation** in "International Workshop on "Supporting Chemistry Research with modern DFT (Density Functional Theory): Software, Techniques, and Applications" held on February 5-16, 2021 via online mode.

5. **Oral presentation** in International Scientific Conference "Current Problems of Chemistry, Materials Science and Ecology" held on May 12-14, 2021 in Lutsk, Ukraine via online mode.